

Development of Dual Setting Cement Systems as Composite Biomaterials with Ductile Properties

Dissertation zur Erlangung des naturwissenschaftlichen Doktorgrades
der Julius-Maximilians-Universität Würzburg

vorgelegt von

Michaela Rödel

aus Bayreuth

Würzburg 2019

Eingereicht bei der Fakultät für Chemie und Pharmazie am

Gutachter der schriftlichen Arbeit

1. Gutachter: _____

2. Gutachter: _____

Prüfer des öffentlichen Promotionskolloquiums

1. Prüfer: _____

2. Prüfer: _____

3. Prüfer: _____

Datum des öffentlichen Promotionskolloquiums

Doktorurkunde ausgehändigt am

Für meine lieben Eltern und die beste Schwester der Welt

Table of contents

Chapter 1 Introduction	1
1.1 Motivation and aim	2
1.2 Challenges by combining organic and inorganic phases.....	5
Chapter 2 Literature overview	9
2.1 Calcium phosphate bioceramics.....	10
2.2 Calcium phosphate cements	14
2.2.1 Setting mechanisms and kinetics.....	15
2.2.2 Apatite cements	16
2.2.3 Brushite cements.....	18
2.2.4 Calcium phosphate cements as drug delivery materials.....	20
2.3 Hydrogels	35
2.3.1 Definition and classification.....	35
2.3.2 Polymerization reactions and cross-linking of hydrogels	43
2.3.3 Hydrogels as drug delivery systems	45
2.4 Established dual setting systems and their comparison	48
2.4.1 Variation in cross-linking reaction mechanisms	53
2.4.2 Variation in organic and inorganic phase.....	56
Chapter 3 Tough and elastic α-tricalcium phosphate cement composites with degradable PEG-based cross-linker	59
3.1 Abstract	60
3.2 Introduction.....	61
3.3 Results	63
3.3.1 Cross-linker and hydrogel characterization.....	63
3.3.2 Inorganic reference and composite characterization	69
3.4 Discussion	80
3.5 Conclusion and outlook	83
Chapter 4 Degradable dual setting systems based on PEG-hydrogels and brushite cement as composite material for biomedical applications	85
4.1 Abstract	86
4.2 Introduction.....	87

Table of contents

4.3	Results.....	90
4.3.1	Polymer characterization.....	90
4.3.2	Analysis of dual set composites	92
4.4	Discussion	110
4.5	Conclusion and outlook.....	117
Chapter 5 Dual setting system based on brushite cement and genipin cross-linked gelatin with increased ductility and sustained drug release.....		119
5.1	Abstract.....	120
5.2	Introduction	121
5.3	Results.....	124
5.3.1	Characterization of gelatin-brushite composite formulations in comparison to brushite cement as inorganic reference and pure gelatin hydrogel as organic reference	124
5.3.2	Cytocompatibility testing	130
5.3.3	Mechanical advantages of gelatin-brushite composites compared to pure brushite cement	133
5.3.4	Porosity measurements and drug release of antibiotics	137
5.3.5	Release of vancomycin and rifampicin.....	140
5.4	Discussion	143
5.5	Conclusion and outlook.....	151
Chapter 6 Integral discussion and future directions		153
Chapter 7 Summary / Zusammenfassung		161
Chapter 8 Experimental section		169
8.1	Synthesis and characterization of polymers.....	170
8.1.1	Synthesis of PEG-based polymers.....	170
8.1.2	¹ H Nuclear magnetic resonance spectroscopy.....	172
8.1.3	Gel permeation chromatography.....	172
8.1.4	Matrix-assisted laser desorption and ionization/Time-of-flight mass spectrometer	173
8.1.5	Fourier transform infrared spectroscopy	173
8.2	Preparation and characterization of hydrogels.....	174
8.2.1	Pure hydrogel production and characterization of HEMA hydrogels, PEG-PLLA-DMA hydrogels and their combination	174
8.2.2	Preparation of pure PEG-based hydrogels as organic reference	177

8.2.3	Production of organic reference – gelatin hydrogels.....	178
8.2.4	Mechanical characterization of pure hydrogels.....	178
8.3	Physicochemical characterization of inorganic references and dual set composites.....	180
8.3.1	α -/ β -Tricalcium phosphate preparation	180
8.3.2	Measurement of pH-value and temperature during initial setting reaction.....	180
8.3.3	Initial setting time determination <i>via</i> Gillmore needle test	180
8.3.4	X-ray diffraction and Rietveld refinement.....	181
8.3.5	(Cryo-) Scanning electron microscopy.....	181
8.3.6	Energy-dispersive X-ray spectroscopy	182
8.3.7	Fourier Transform Infrared spectroscopy.....	182
8.3.8	Mercury porosimetry	182
8.4	Preparation procedures of pure inorganic references and dual set composites	183
8.4.1	Dual setting system based on apatite cement	183
8.4.2	Dual setting system based on PEG-hydrogels and brushite cement	184
8.4.3	Dual setting system based on gelatin and brushite cement.....	187
8.5	Mechanical characterization of inorganic references and dual set composites	189
8.5.1	Compressive strength testing	189
8.5.2	Evaluation of compressive strength upon degradation of PEG-brushite composite materials.....	189
8.5.3	Evaluation of 3-point bending strength and toughness of PEG-brushite composite materials.....	190
8.5.4	Mechanical characterization <i>via</i> 4-point bending testing of HEMA-apatite composite materials.....	191
8.6	Biological testing	192
8.7	Drug release study	194
8.8	Statistical analysis	196
	References	197
	Acknowledgements / Danksagung.....	215

List of abbreviations

3D	Three-dimensional
AA	Acrylamide
ACN	Acetonitrile
ACP	Amorphous calcium phosphate
Ala	Alanine
ANOVA	Analysis of variance
API	Active pharmaceutical ingredient
APS	Ammonium persulfate
Arg	Arginine
Asp	Aspartate
ATP	Adenosine triphosphate
BP	Bisphosphonate
Ca/P ratio	Calcium-to-phosphate ratio
CaP	Calcium phosphate
CDHA	Calcium-deficient hydroxyapatite
COX	Cyclooxygenase
CPC	Calcium phosphate cement
DCM	Dichloromethane
DCPA	Dicalcium phosphate anhydrous
DCPD	Dicalcium phosphate dihydrate
DCTB	<i>trans</i> -2-[3-(4- <i>tert</i> -Butylphenyl)-2-methyl-2-propenylidene]malononitrile
Dex-MA	Glycidyl methacrylated dextran

DMF	<i>N,N</i> -Dimethylformamide
DNA	Deoxyribonucleic acid
dsDNA	Double stranded deoxyribonucleic acid
ECM	Extracellular matrix
EDTA	Ethylenediaminetetraacetic acid
EDX	Energy dispersive X-ray spectroscopy
EO	Ethylene oxide
EWC	Equilibrium water content
FPP	Farnesyl diphosphate
FRP	Free radical polymerization
FTIR	Fourier transform infrared spectroscopy
Gly	Glycine
GPC	Gel permeation chromatography
H40	40 wt% HEMA
H40P10	40 wt% HEMA and 10 wt% polymer (cross-linker)
HA	Hydroxyapatite
HEMA	2-Hydroxyethyl methacrylate
HEPES	4-(2-Hydroxyethyl)-1-piperazineethanesulfonic acid
hFOB	Human fetal osteoblast cell line 1.19
HPLC	High performance liquid chromatography
Hyl	Hydroxylysine
Hyp	Hydroxyproline
JCPDS	The Joint Committee on Powder Diffraction Standards
K_{sp}	Solubility product constant
LCST	Lower critical solution temperature

List of abbreviations

Lys	Lysine
MALDI-TOF	Matrix-assisted laser desorption/ionization-time of flight
MALS	Multi-angle light scattering
MBAM	<i>N,N'</i> -Methylene bisacrylamide
M_c	Molecular weight of two neighboring cross-linkers
MCPA	Monocalcium phosphate anhydrous
MCPM	Monocalcium phosphate monohydrate
MG-63	Human osteosarcoma cancer cells
M_n	Number-averaged molar mass
MPC	Magnesium phosphate cement
MRSA	Methicillin-resistant <i>Staphylococcus aureus</i>
MTX	Methotrexate
M_w	Weight-averaged molar mass
NMR	Nuclear magnetic resonance
NSAID	Nonsteroidal anti-inflammatory drug
OCP	Octacalcium phosphate
P10/25	10 wt% or 25 wt% Polymer (cross-linker)
PA	Poly(acrylamide)
PAA	Poly(acrylic acid)
PAMPS	Poly(2-acrylamido-2-methylpropanesulfonic acid)
PBS	Phosphate buffered saline
PCL	ϵ -Polycaprolactone
PEG	Poly(ethylene glycol)
PEG-DMA	Dimethacrylated poly(ethylene glycol)

PEG-DMA _{hmw}	Dimethacrylated poly(ethylene glycol) based on high molecular weight backbone
PEG-DMA _{lmw}	Dimethacrylated poly(ethylene glycol) based on low molecular weight backbone
PEG-PLLA-DMA	Dimethacrylated poly(ethylene glycol) based on high molecular weight backbone with poly(lactic acid)-spacer units
PEO	Poly(ethylene oxide)
PG	Prostaglandin
PGA	Poly(glycolic acid)
PHBV	Poly(3-hydroxybutyrate-co-3-hydroxyvalerate)
Phe	Phenylalanine
PLA	Poly(lactic acid)
PLGA	Poly(lactic-co-glycolic acid)
PLR	Powder-to-liquid ratio
PMMA	Poly(methyl methacrylate)
PO	Propylene oxide
polyHEMA	Polymerized 2-hydroxyethyl methacrylate network
POX	Poly(oxazolines)
PPGL-DMA	Poly(propylene glycol-co-lactide) dimethacrylates
Pro	Proline
PS	Polystyrene
PVA	Poly(vinyl alcohol)
PVC	Poly(vinyl chloride)
Q _v	Swelling ratio
rhBMP-2	Recombinant human bone morphogenetic protein

List of abbreviations

RNA	Ribonucleic acid
R_t	Retention time
SEM	Scanning electron microscopy
Ser	Serine
TCP	Tricalcium phosphate
TEMED	<i>N-N-N'-N'</i> -Tetramethyl ethylene diamine
TEOS	Tetraethyl orthosilicate
TTCP	Tetracalcium phosphate
TX	Thromboxane
UV	Ultraviolet
VEGF	Vascular endothelial growth factor
W_d	Weight of dry hydrogel specimen
W_s	Weight of swollen hydrogel specimen
WST	Water-soluble tetrazolium salt
XRD	X-ray diffraction
α -/ β -TCP	α -/ β -Tricalcium phosphate

Chapter 1

Introduction

1.1 Motivation and aim

Throughout the whole life of a human being, the bony skeleton carries and protects all parts of our body (inner organs, skin as well as essential circulation systems) and fulfills many different requirements regarding mechanical and biological properties [1, 2]. Thanks to its complex, nanostructured components, a fascinating and exceptional composite material is formed. In general, two different types of bone are distinguished: (i) compact or cortical bone and (ii) cancellous or trabecular bone, which is often also called spongy bone [3]. These structural differences, on a macroscopic level, are depicted in **Figure 1 A**. For the majority of all bones, cortical bone has the function of a very dense outer shell which protects the inner core structures [4]. This inner part is then filled by cancellous bone, which is described as a highly porous and connected network of rods or plates [5]. Compared to dense cortical bone, it allows faster cell ingrowth, vascularization and consequently fracture healing [6]. Both bone types' microstructure with arranged lamellae is based on mineralized collagen fibers [7] as well as distinct configurations on a nano-structural level composed of several collagen fibrils (see **Figure 1 B**).

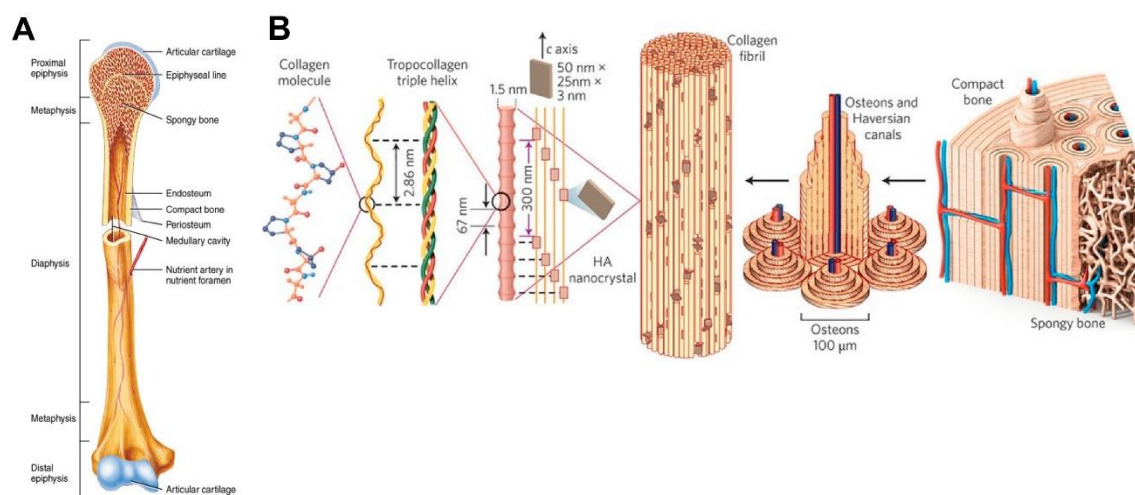


Figure 1:

Structure of long bone (A) as well as hierarchical orientation from collagen molecules as smallest building block up to the whole compact and spongy bone construct (B), reproduced from [4] as open access article distributed under the Creative Commons Attribution License which permits unrestricted use, distribution and reproduction in any medium.

These elemental building blocks of an organic collagen phase and apatite crystals as inorganic component are often ideal prototypes for bone replacement materials. From a chemical perspective, the overall composition of bone can be divided in an inorganic phase consisting of about 60 wt% hydroxyapatite (HA), 9 wt% water and other components like carbonate, citrate or related ions like magnesium (Mg^{2+}) or sodium (Na^+) [4]. Collagen (20 wt%) on the other hand is the main structural protein of the organic phase. Furthermore, traces of non-collagenous proteins like osteocalcin, osteonectin or morphogenetic and serum proteins as well as polysaccharides, lipids and finally primary bone cells (osteoblasts, osteocytes and osteoclasts) are also incorporated [4].

Both phases together provide a mechanical stiffness with compressive strength up to 193 MPa for cortical bone [8] and an elasticity with 1-3 % elongation at fracture [9]. Accordingly, the development of newly engineered replacement materials is always targeted towards combination of mechanically strong materials with a certain degree of ductility [10].

Bone replacement materials used today can be categorized in different types of transplants or synthetic materials. The first class contains autografts that are harvested and transferred within the same individual and are still the most promising and best graft option. However, they have some major limitations due to donor site morbidity, high treatment costs or availability limitations and especially an additional trauma for the patient [11]. Other alternative transplants are allografts, donated by another individual of the same species, or xenografts, derived from non-human species like for example porcine tissue. Besides that, several non-biogenic materials have been developed as alternative systems for a bone replacement in non-load bearing defects. Metallic implants [12] as well as ceramic [13], polymer [14] or composite [15] biomaterials are widely used and can be subsumed as synthetic materials or alloplasts to (re-)construct or augment bony tissue defects. Among ceramic implants, calcium phosphate cements (CPCs) are promising candidates due to their excellent biological properties, like biocompatibility, resorbability, osteoconductivity or even osteoinduction [16]. They are used as pure bone cements or in combination with other inorganic fillers like bioactive glasses [17]. To overcome risks of natural transplants as well as high

brittleness and fragility of pure inorganic matrixes, several approaches were already established to improve their mechanical properties and increase deformability and flexibility: (i) fiber reinforced constructs, (ii) nanocomposites with carbon nanotubes or (iii) dual setting systems, which are created by combining different organic hydrogel systems with an incorporated inorganic matrix. Based on the fact, that bone itself is a composite material, which mostly consists of a fibrous collagen matrix enriched with platelet-shaped nanocrystals of carbonated apatite [18], several studies were already published concerning dual setting principles, which actually try to imitate the natural structure of bone. This design allows a higher polymer content, which enhances the final functional properties and also enables the incorporation of drugs with a better control over release kinetics. The difference between a powder filled hydrogel and an *in situ* generated composite material is the missing interconnectivity of the inorganic network in case of the dispersed individual particles. In case of the hybrid material, the nucleation processes of the cement crystals *via* dissolution-precipitation reaction instead create an inorganic network parallel to the gelation reaction. Consequently, dual setting systems combine both, strength as well as flexibility and are therefore a promising class of biomaterials that have a high potential as bone replacement materials.

Among these established systems of hydrogel and CPC reported in literature, the innovation and focus of this thesis is directed towards an improved degradability and the development of new strategies for this material class in order to overcome brittleness of pure inorganic systems and to shift their behavior towards higher elasticity and ductility.

1.2 Challenges by combining organic and inorganic phases

The development of dual setting systems implicates some challenges that have to be taken into account by a careful selection of the single components involved in the complex process of an interpenetrating network formation. With respect to the simultaneous initiation of cement setting as well as gelation and their complete and successful run, there are several points that have to be considered in this field of biomedical research. A general overview is listed in **Table 1**.

Table 1:

List of different challenges, which have to be addressed by combining an inorganic and organic phase in the formulation development of dual setting systems.

Challenge	Required condition
Similar time frame for both reactions	Guarantee of successful proceeding of cement setting and hydrogel formation
Homogenous, incorporated network	Improvement in mechanical properties
Interface compatibility	Effort in maximization
Competition for free water molecules	Formation of desired end products
Similar essential reaction conditions	Same pH-range for parallel reactions, hardening as well as gelation

First of all, there is the need for a similar reaction time frame of both, the cement setting and the hydrogel formation. If the latter one takes too long, there is no chance of gelation in an already set cement matrix due to far distances and missing reaction spaces between the different molecules like hydrogel precursors or initiators. This fact avoids the creation of a homogenous, incorporated network distribution of both, organic and inorganic phase, which is required for an improvement in elasticity and flexibility. Quite the contrary, agglomerates will be formed and thus a decrease in mechanical strength will be the consequence by

inducing many potential defect points in the construct. Ideally, one should achieve a congruent gel network penetrating through the cement crystals. The interfaces of both phases should be compatible and not influence compressive or bending strength. Another important issue is a certain competition for free water molecules. They are required as reaction component for both phases, either during cement setting as well as hydrogel formation. Brushite cements, for example, bind two crystal waters according to their stoichiometric composition ($\text{CaHPO}_4 \cdot 2 \text{H}_2\text{O}$). If only low amounts of water are present, the formation of the water-free form monetite (CaHPO_4) would be favored, which is not desired in the end product. This increased need for water as well as the swelling capacity of the hydrogel challenge the simultaneous course of both reactions. Thus, an appropriate water content is only one requirement condition for the successful development of a dual setting system. Another challenge that has to be taken into account are the essential reaction conditions for each component. Setting of the inorganic matrix can occur at either acidic or basic conditions. Hence, there are certain prerequisites for solubility, stability and reaction course of hydrogel precursors with other components like radical initiators or cross-linkers. A pH-value higher or lower than 4.2, which was given in consideration of the setting conditions for the inorganic matrix, could have an enormous influence on the polymerization kinetics and the subsequent gelling behavior.

In this thesis, **Chapter 2** gives an overview of the relevant literature dealing with the chemistry of CPCs, different types of hydrogels with their variation in polymerization and cross-linking principles as well as a closer analysis of already established dual setting systems.

In a first approach, circumvention of all the above mentioned challenges aims to achieve an improved composite by advancing an already existing dual setting system based on HA and a polymerized 2-hydroxyethyl methacrylate (polyHEMA) gel with the addition of a degradable, linear and high molecular weight cross-linker (see **Chapter 3**). Increased elasticity and higher toughness values in comparison to pure inorganic matrices should be reached in conjugation with an improvement of the previous compositions towards higher bending strength.

Focusing on the development of completely new formulations, the inorganic matrix was exchanged from HA, with a low *in vivo* solubility, to brushite cement emphasizing the degradability of the inorganic part also in combination with a degradable and highly flexible poly(ethylene glycol) (PEG) organic hydrogel system (see **Chapter 4**). The advantages of this newly developed dual setting system are based on material degradability as well as flexibility, which can be a promising tool for bone regeneration applications in non-load bearing craniomaxillofacial defects.

A third approach should be established by replacing the synthetic hydrogel phase by gelatin derived from natural sources. With this organic network, in addition to the mechanical characterization, also drug release profiles of two antibiotic compounds are analyzed with the main goal of a sustained drug release in combination with increased ductility in contrast to pure inorganic matrix (see **Chapter 5**).

Finally, the overall and integral conclusion of all three established systems with a closer look on promising future perspectives is outlined in **Chapter 6**.

Chapter 2

Literature overview

Section **2.2.4** was published as book chapter (Michaela Rödel, Susanne Meininger, Jürgen Groll, Uwe Gbureck, Bioceramics as drug delivery systems, in *Fundamental Biomaterials: Ceramics*, Woodhead, 2018, pp. 153-194) and reproduced from [19] with permission from Elsevier to include it in this thesis with adapted layout.

This part was thoroughly written by the author of this thesis Michaela Rödel, who also did literature research, conceptualization and implementation of the figures.

2.1 Calcium phosphate bioceramics

Calcium phosphates (CaPs) are materials and minerals that can be found on earth in different modifications and consist of the three major elements calcium (Ca), phosphorus (P) and oxygen (O) [20]. Overall, they belong to the group of calcium ortho phosphates that are distinguished from meta (PO_3^-), pyro ($\text{P}_2\text{O}_7^{4-}$) or poly (PO_3) $_n^{n-}$ structures. From a more detailed chemical point of view, these kind of bioceramics can be described as salt-like structures based on primary (H_2PO_4^-), secondary (HPO_4^{2-}) or tertiary (PO_4^{3-}) phosphate ions [21] with the counter ion calcium (Ca^{2+}). The most common compounds are as follows:

- Tricalcium phosphates (TCPs) that occur in two different modifications (polymorphs α -TCP and β -TCP; $\text{Ca}_3(\text{PO}_4)_2$)
- Dicalcium phosphate dihydrate (DCPD; $\text{CaHPO}_4 \cdot 2 \text{H}_2\text{O}$)
- Octacalcium phosphate (OCP; $\text{Ca}_8(\text{HPO}_4)_2(\text{PO}_4)_4 \cdot 5 \text{H}_2\text{O}$)
- Monocalcium phosphate monohydrate (MCPM, $\text{Ca}(\text{H}_2\text{PO}_4)_2 \cdot \text{H}_2\text{O}$).

Furthermore, the group of CaPs with an amorphous character is represented by amorphous calcium phosphate (ACP; $\text{Ca}_x(\text{PO}_4)_y \cdot n \text{H}_2\text{O}$) with various existing stoichiometric combinations.

The most prominent candidate among CaPs is HA. Its appearance is not only limited to bone in form of carbonated HA [22]. With the main functions of strength, stability as well as functionality, this mineral is also part of teeth and tendons.

CaPs can be mainly categorized according to their formation procedure. The first group contains CaPs that are formed at high temperatures, typically above 1000 °C [23, 24] *via* green body sintering [25]. The second category is obtained at low temperatures (room temperature) by precipitation from an aqueous solution or preparation by hydrolysis of more soluble CaPs [26]. Depending on supersaturation, solution-pH as well as precipitation rate [20], typically the formation of ACP, DCPD, HA or OCP is favored [27].

A prediction of the pH-dependent stability of CaP compounds can be given by using a solubility phase diagram (see **Figure 2**).

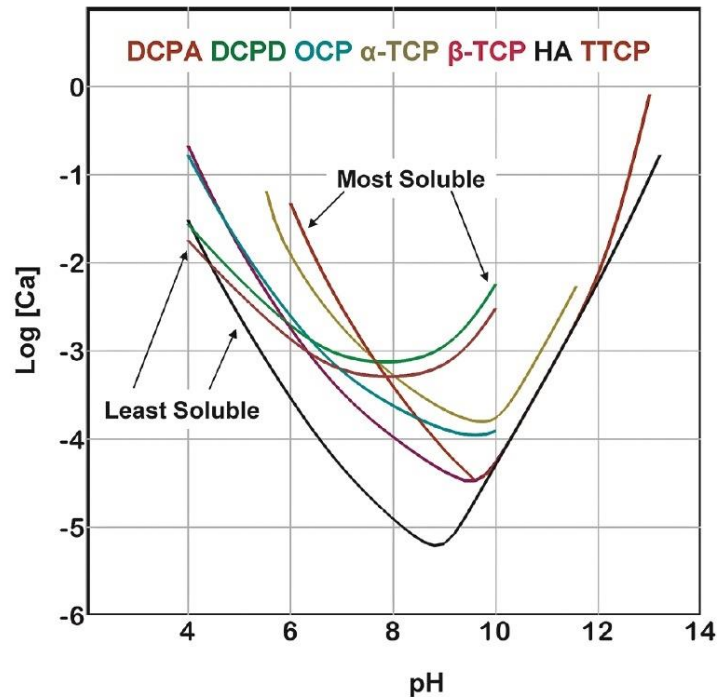


Figure 2:

Solubility isotherms of different CaP compounds in water (37 °C) whereas a high content of calcium ions (Ca^{2+}) in solution reveals a high solubility. The following compounds are depicted in this phase diagram: dicalcium phosphate anhydrous (DCPA), dicalcium phosphate dihydrate (DCPD), octacalcium phosphate (OCP), α - β -tricalcium phosphate (α - β -TCP), hydroxyapatite (HA) and tetracalcium phosphate (TTCP).

This image was reproduced from [28] with permission from Copyright 2009 The Japanese Society for Dental Materials and Devices.

In 1999, Chow [29] published a paper dealing with studies on self-setting CPCs that shed light on chemistry, properties and applications of this fascinating material class. Based on Gibbs phase rule, he described CPCs as a ternary system with two phases, a solid and a liquid one, that is in a certain equilibrium state at constant pressure and temperature and has one degree of freedom. This can be indicated by defined lines in phase diagrams. These isotherms are plotted in a coordinate system with the logarithm of calcium ion concentration ($\log [\text{Ca}^{2+}]$) and the logarithm of hydrogen ion activity ($\text{pH} = \log [\text{H}^+]$). At a certain pH-value, an isotherm with lower calcium concentration is less soluble than another salt, whose curve lies above the chosen one. As example, at a pH lower than 4.2, DCPA has the least solubility whereas HA is the most soluble compound. Changing the parameters to neutral conditions, the concentration of free calcium ions for HA decreases with a resulting increase in stability [29]. In basic environment, DCPD is

the most soluble salt. Having a prediction about stability in aqueous solutions at 37 °C, a conclusion about direction for all chemical reactions like dissolution, precipitation as well as phase transformation can be drawn additionally [30]. In general, the lower the value of calcium-to-phosphate ratio (Ca/P ratio), the more acidic and soluble are those compounds in water (see **Table 2**) [22]. Under neutral conditions, a prediction of CaP degradation rate can be drawn with respect to the phase diagram. Hereby, MCPM is the most soluble compound whereas HA can be categorized as least soluble [23]. Tetracalcium phosphate (TTCP; $\text{Ca}_4(\text{PO}_4)_2\text{O}$) as well as calcium-deficient hydroxyapatite (CDHA; $\text{Ca}_{10-x}(\text{HPO}_4)_x(\text{PO}_4)_{6-x}(\text{OH})_{2-x}$) form the frame for the two polymorphs α - and β -TCP as well as the water containing and free form of dicalcium phosphates (DCPD and DCPA) and OCP. Regarding rate of solubility, the main CaPs are arranged as follows:



Generally, degradation of calcium orthophosphates *in vivo* is based on two different mechanism. The first route is driven by cellular processes of macrophages, osteoclasts or other kind of cells like multinucleated giant cells [31]. This active resorption is induced by attachment of these cells to the surface of the mineral, the formation of lacunas, decrease of pH-value and finally dissolution of the CaP bioceramics reaching values below the solubility product constant K_{sp} . The material volume is decreased from the periphery to an inner core with disintegration in particles by phagocytosis. A second way is called passive resorption and occurs with respect to solubility processes of the material, for example brushite cements. In most cases, biodegradation is more or less a combination of several processes. Liu *et al.* [32] reported on (i) physically based resorption *via* abrasion as well as fracture or (ii) chemical procedures like dissolution or local increases in Ca/P ratio. Furthermore, the previously described (iii) biological effects contribute to biodegradation with a reduction in pH. Several parameters like chemical composition, crystal properties like size and perfection are related to these dissolution characteristics.

Table 2:

Calcium phosphate compounds and their major properties ordered by increasing Ca/P ratio [22-24, 29, 30].

CaP compound incl. abbreviation	Chemical formula	Ca/P ratio	Solubility at 25 °C, -log (K _s)	Solubility at 25 °C / mg*L ⁻¹
Monocalcium phosphate monohydrate (MCPM)	CaHPO ₄ ·H ₂ O	0.5	1.14	~ 18,000
Dicalcium phosphate anhydrous (DCPA)	CaHPO ₄	1.0	6.9	~ 48
Dicalcium phosphate dihydrate (DCPD)	CaHPO ₄ ·2 H ₂ O	1.0	6.59	~ 88
Octacalcium phosphate (OCP)	Ca ₈ (H ₂ PO ₄) ₂ (PO ₄) ₄ ·5 H ₂ O	1.33	96.6	~ 8.1
Amorphous calcium phosphate (ACP)	Ca ₃ (PO ₄) ₂ ·n H ₂ O with n = 3-4.5	1.5	–	35.6-32.8
α-Tricalcium phosphate (α-TCP)	α-Ca ₃ (PO ₄) ₂	1.5	25.5	~ 2.5
β-Tricalcium phosphate (β-TCP)	β-Ca ₃ (PO ₄) ₂	1.5	28.9	~ 0.5
Calcium-deficient hydroxyapatite (CDHA)	Ca _{10-x} (HPO ₄) _x (PO ₄) _{6-x} (OH) _{2-x}	1.5-1.67	~ 85	~ 9.4
Hydroxyapatite (HA)	Ca ₅ (PO ₄) ₃ OH	1.67	116.8	~ 0.3
Tetracalcium phosphate (TTCP)	Ca ₄ (PO ₄) ₂ O	2.0	38-44	~ 0.7

2.2 Calcium phosphate cements

Almost 40 years ago, Brown and Chow developed in the early 1980s a new class of materials based on CaPs that could be used as cements, so called CPCs. These materials are made of a single- or poly-phase system of CaP raw powders in an aqueous solution [33]. By mixing all components, a paste is formed that sets in a very short time frame within a few minutes. Thus, both scientists introduced a synthetic, self-setting bone substitute material with several advantages like moldability, injectability and complete *in situ* filling of defects during surgery [34]. Due to the fact that CPCs belong to the category of non-Newtonian fluids, they form the required shape at implantation side. After setting, the dimensionally stable, solid product stays in its specific shape.

Another big selling point is their osteoclastic and osteoblastic activation, which affects bone regeneration and consequently the stimulation of new bone formation. Their excellent biocompatibility in combination with harden mechanical properties offers the possibility to use these materials in a wide range in biomedical applications. Most commercial products set to HA and are forming the major inorganic component of natural bone. One exemplary product is Calcibon[®] which represents a two-component system based on a powder mixture of α -TCP, DCPA, calcium carbonate (CaCO_3) and CDHA with a liquid solution of H_2O and disodium hydrogen phosphate (Na_2HPO_4) [35]. Another injectable kit is called Cementek[®] that is composed of α -TCP, TTCP and sodium glycerophosphate as solid phase and a liquid phase prepared of lime and phosphoric acid (H_3PO_4) [36].

Over the last few years, CPCs are under rapid progress and have demonstrated a great potential to be used as bone replacement materials in many clinical applications. Modification and further improvements of degradation and its kinetic or even bioactivity were improved by incorporation of different ions. Always with respect to the composition of natural bone, a substitution with for example Mg^{2+} [37], strontium (Sr^{2+}) [38], copper (Cu^{2+}) [39] or iron ($\text{Fe}^{2+/3+}$) [40] was performed.

2.2.1 Setting mechanisms and kinetics

Setting of CPCs is an hydration reaction that always starts with dissolution of different components in the solid phase [41]. Therefore, a two-phase system is based on liquid and solid parts that are mixed together. Both phases can consist of different components, which means several powder-fractions like the combination of the firstly developed formulations with TTCP and DCPA or DCPD, respectively. Liquid solutions are vehicles for the reactants' dissolution and the products' precipitation. They are mainly (i) water-based with dissolved setting retardants like citric acid as well as setting accelerators like Na_2HPO_4 or non-aqueous, water-miscible liquids like glycerin or PEG. The formation of one or more CPCs is therefore induced. Furthermore, also (ii) organic acids like H_3PO_4 can be used as liquid for hardening by complexation of Ca^{2+} . A combination of both reaction types is expected by using aqueous, (iii) polymeric solutions [42]. Further descriptions regarding cement hardening are referred to the first water-based mechanism. After dissolution of all powder components, the dissolution-precipitation reaction is initiated. In general, there is the formation of a super-saturated gel with afterwards crystal entanglement starting from nucleation clusters by forming a solid and interlocked crystal network [43, 44]. However, the mechanism is always depending on the kind of solid phase composition and reaction partners. With respect to processing and microstructure of reactants and products, **Figure 3** illustrates the hydraulic reaction.

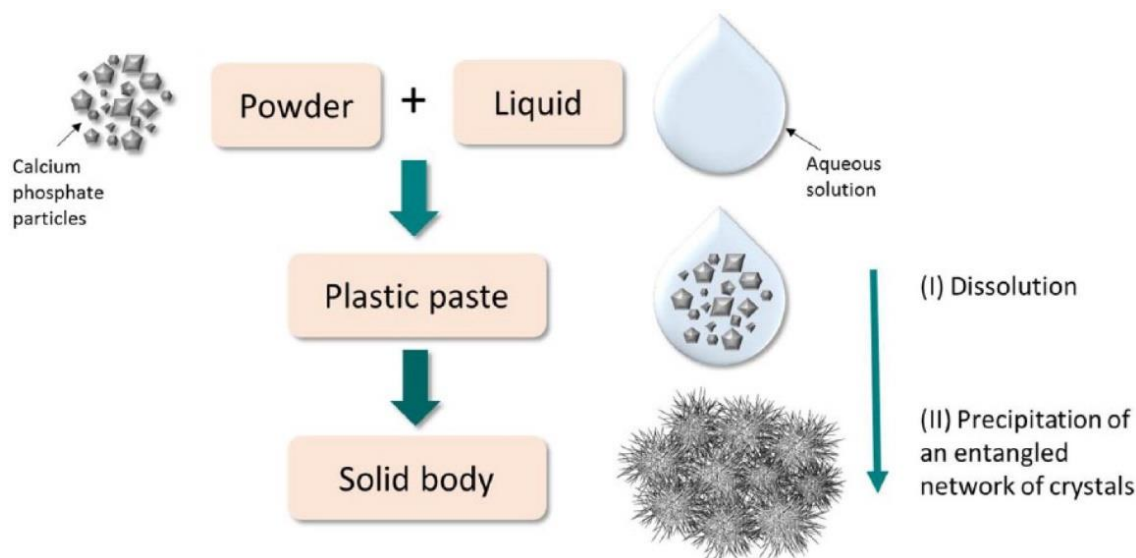


Figure 3:

Schematic overview and description of dissolution-precipitation reaction of CPCs with processing and microstructure reproduced from [45] as open access article distributed under the Creative Commons Attribution License which permits unrestricted use, distribution and reproduction in any medium.

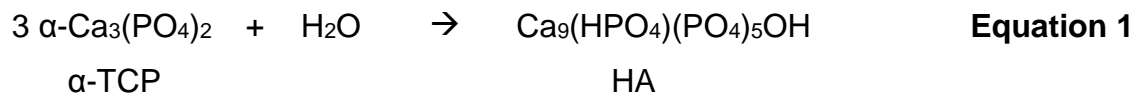
Different factors can influence the setting reaction of CPCs. An important key variable is the present pH-level during the reaction whereas pH-values ≥ 4.2 result in apatite cements. In contrast, values ≤ 4.2 favor the formation of brushite cements. This is also correlated to the solubility of the products (see **Figure 2**). Furthermore, the chosen powder-to-liquid ratio (PLR) affects the setting and also the percental conversion to stoichiometrically different compositions, crystal size and their distribution as well as shape and possible interactions [46].

A main categorization of CPC formulations is performed by division into (i) apatite and (ii) brushite forming cements.

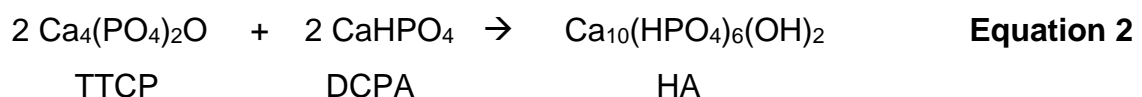
2.2.2 Apatite cements

The most prominent class of CPCs are apatite forming compounds like HA ($\text{Ca}_{10}(\text{PO}_4)_6(\text{OH})_2$) or CDHA. The latter one has a very high similarity to mineral phase in bone and teeth and shows a poorly crystalline structure [21]. Apatite cements degrade much faster in comparison to mineral bone HA though, overall, they still have a relatively slow degradation [47]. *In vivo*, recrystallization of other CaPs like ACP, DCPA or TTCP can occur and result in the formation of HA. With

respect to a synthetic route, there are two different possibilities for the formation of HA. Thus, precursors for calcium and phosphate are used in the preparation process under a certain pH-control [48]. The first is based on α -TCP by reaction with water (see **Equation 1**). Here, a single component system favors CPC formation where one component (in this case α -TCP) [49] undergoes hydrolysis by formation of HA at this given and constant Ca/P ratio.



A second option for production of this self-hardening CPC is an equimolar mixture composed of ground TTCP and DCPA or DCPD, respectively [50] (see **Equation 2**). This reaction can be classified as multicomponent system whereas two or more compounds with different properties (acidic or basic) are combined [51]. In this case, TTCP has the function of a basic reaction partner in combination with the acidic reactant DCPA. The final stoichiometric composition as well as Ca/P ratio are depending on the relative amounts of both educts. The second option is based on natural sources like extraction of HA from mammalian bones, egg-shells or even plants by chemical transformation of native woods through thermal and hydrothermal processes [48, 52].



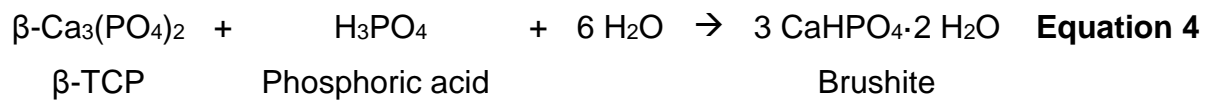
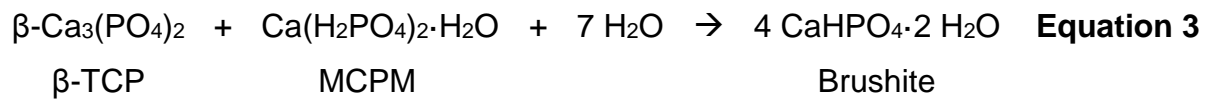
With respect to moldability as well as injectability, reaction rate and thus setting of the cement plays an important role. It should not take too long time on the one hand or instead harden too fast on the other hand. In case of apatite cements, this can take several minutes to hours [53-55], even with addition of accelerators like Na_2HPO_4 . Synthetic apatite has a high similarity to biological apatite. Also the stoichiometric composition with a certain percental amount of calcium (39.6 %) and phosphate (18.5 %) are close to the ratio of biological apatite like bone (1.65), dentin (1.67) or enamel (1.59) [56]. It has been found that synthetically produced

HA has properties that stand out for this material: it is biocompatible, osteoconductive and has a high affinity to peptides or growth factors [57]. In this context, the terminus “osteoconductivity” should be defined. These CaPs allow all relevant steps leading to bone formation: attachment, proliferation, migration and differentiation of bone cells [56]. Consequently, osteoblasts are attracted after adsorption of circulating proteins, migrate and differentiate with formation of a mineralized matrix. Even though, synthetic HA does not show osteoinductive characteristics (= process by which osteogenesis is induced [4]) in comparison to natural sourced HA, the improvement and advancement in mechanical properties enormously increases its attractivity for the application as bone replacement material.

2.2.3 Brushite cements

Regarding the category of low-temperature CaPs, DCPD or brushite cement is the most soluble among them. The water free form or anhydride is monetite (CaHPO_4) which can be formed by modifying precipitation conditions with focus on DCPA crystallization or by dehydration of the water containing compound [43]. Brushite cements have the big advantage combining both properties, bioresorption as well as biocompatibility. After different diffusion and resorption processes, DCPD shows osteoconductive effects and is replaced by new bone [58]. Crystallization occurs from aqueous solutions in the range of $\sim 2 < \text{pH} < \sim 6.5$ [22]. The final product is metastable under physiological conditions and thus faster resorbable with higher degradation rate in comparison to HA [59]. Though some might argue, that HA is a more suitable bone replacement material due to its (i) affinity to natural bone, (ii) higher mechanical strength or even (iii) setting conditions at neutral pH-values, the big advantage of resorbability that could be modified by reinforcement processes turns brushite cement to another excellent candidate.

There are two different processes based on β -TCP and either MCPM or H_3PO_4 as acidic components that both favor the formation of brushite cement (see **Equation 3** and **Equation 4**).



A comparison of the most prominent CPC candidates, apatite and brushite cement with respect to their components for the setting reaction as well as crystal morphology and setting mechanism, is depicted in **Figure 4**. Contrary to HA, brushite cement hardens relatively fast in a few seconds to minutes [60] whereas it is elucidated that additives like citrates ($\text{C}_6\text{H}_5\text{O}_7^{3-}$) or pyrophosphates ($\text{P}_2\text{O}_7^{4-}$) retard crystal growth by Ca^{2+} complexation [61]. The setting time correlates to the solubility of the alkaline phase. The faster the dissolution, the faster the initiation of crystal growth and the higher the reaction rate in a given time frame [21]. A comparison in mechanical strength reveals higher values with perspective for use in load bearing applications for HA. These higher levels also correlate to crystal morphology after setting. As shown in **Figure 4**, brushite cements favor the formation of platelet structures that are more stacked interlocked crystals. HA, however, shows rosette-like shapes with higher entanglement degree.

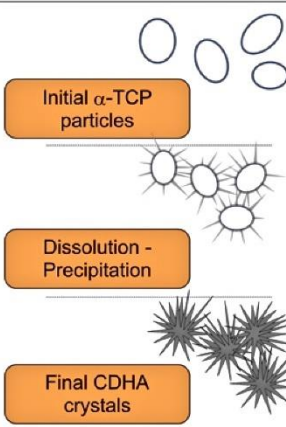
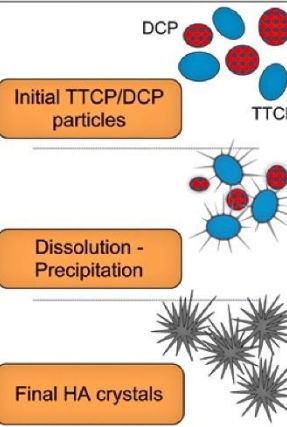
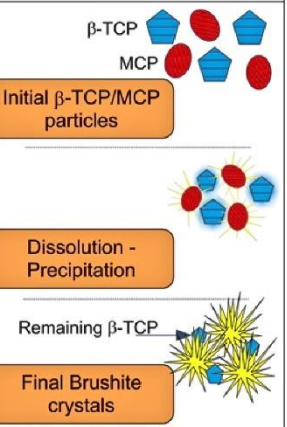
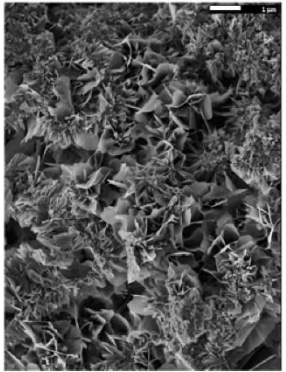
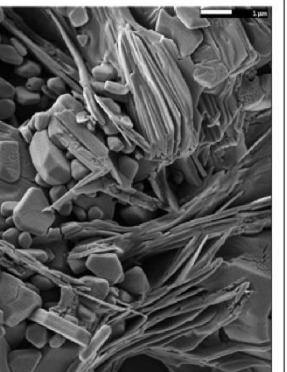
	Apatitic Cement		Brushitic Cement
	Single Component	Multiple Components	
Reactives	α -TCP	TTCP + DCPA/DCPD	β -TCP + MCPM/MCPA
Reaction	$3\alpha\text{-Ca}_3(\text{PO}_4)_2 + \text{H}_2\text{O} \rightarrow \text{Ca}_9(\text{HPO}_4)(\text{PO}_4)_5(\text{OH})$	$2\text{Ca}_4(\text{PO}_4)_2\text{O} + 2\text{CaHPO}_4 \rightarrow \text{Ca}_{10}(\text{PO}_4)_6(\text{OH})_2$	$\beta\text{-Ca}_3(\text{PO}_4)_2 + \text{Ca}(\text{H}_2\text{PO}_4)_2 \cdot \text{H}_2\text{O} + 7\text{H}_2\text{O} \rightarrow 4\text{CaHPO}_4 \cdot 2\text{H}_2\text{O}$
Type of Reaction	Hydrolysis	Acid-Base	Acid-Base
Setting mechanism and crystal morphology	 <p>Initial α-TCP particles</p> <p>Dissolution - Precipitation</p> <p>Final CDHA crystals</p>	 <p>Initial TTCP/DCP particles</p> <p>Dissolution - Precipitation</p> <p>Final HA crystals</p>	 <p>Initial β-TCP/MCP particles</p> <p>Dissolution - Precipitation</p> <p>Remaining β-TCP</p> <p>Final Brushite crystals</p>
SEM		<p>← APATITE</p> <p>BRUSHITE →</p>	

Figure 4:

Overview of the two common CPC products, apatitic and brushitic cement, giving details about reactives, corresponding setting mechanisms as well as crystal morphology and characterization reproduced from [51] with permission from Elsevier.

2.2.4 Calcium phosphate cements as drug delivery materials

Since CPCs can be prepared and precipitated *via* low-temperature setting reactions with an availability of intrinsic pores or porous channels, they are excellent candidates for the incorporation of active pharmaceutical ingredients (APIs). This implements not only drugs, also biological molecules or even cells that are consequently not exposed to high temperatures, which may lead to cell death, denaturation or loss of activity [51]. To further increase CPC's bone regeneration

capacity or allow a local treatment of diseases like infections or skeletal disorders, current research always tries to integrate different drug substances in cement matrixes. Within these approaches, several parameters are influencing the release of the drug that are listed in a review of Ginebra *et al.* [51] about CPCs as drug delivery systems. First of all, (i) the microstructure affects both, incorporation as well as release within the fine crystal network. With smaller porous structures, an increase in drug retardation will be observed. Secondly, keeping in mind the two main classes of cements based on calcium and phosphate, a higher dissolution and consequently resorbability of the mineral *in vivo* can also influence the liberation of the drug out of the matrix. This (ii) potential degradation is also directly connected to the liberation rate and time. From another point of view, API properties influence the mechanism of release, too. There are two possibilities of drug incorporation. On the one hand, the drug can be dissolved in the liquid phase that is used for cement preparation. Consequently, (iii) drug solubility is another limiting parameter for release kinetics. On the other hand, the API can be mixed in the raw powder for cement hardening and has to be dissolved during the setting process. For both variations, (iv) interactions between drug and matrix can hinder the diffusion of the molecules in the surrounding media. Possible habitation of the drug can be dissolved within the pores, absorbed or covalently bond on the crystal surfaces or crystallized in a solid state [62].

In the following section, bioceramics as drug delivery systems are highlighted with respect to variations of already used drugs for bone tissue applications.

Bisphosphonates

In the field of osteoporosis, bisphosphonates (BPs) are widely used as gold standard for the treatment of vertebral and non-vertebral osteoporotic fractures. Patients suffering from diseases like postmenopausal or glucocorticoid induced osteoporosis have an imbalance in osteoblast and osteoclast interaction. Concerning osteoblast activity, the process of bone formation is reduced resulting in decreased bone tissue formation [63]. Additionally, osteoclast activity remains constant resulting in a higher rate of bone turnover, which is associated with a decrease in bone mass and density. The importance of this hormonally controlled

functional unit of osteoblasts and osteoclasts leads to different indications of BPs: postmenopausal osteoporosis, Paget's disease of bone and hypercalcemia as a consequence of bone metastasis or malignant tumor induced bone destruction.

The chemical structure of BPs is derived from pyrophosphates, whereas the central oxygen atom of the phosphor-oxygen-phosphor-(P-O-P)-backbone is replaced with carbon. Due to this structural change, a metabolic stability is given and results in substances, which are resistant to enzymatic hydrolysis [64]. The variety of BPs can be found in different modifications of the side chains [65]. They are categorized in nitrogen (N)-containing and non-N-containing drugs. The presence of N has an influence on pharmacological effectiveness, biochemical and physiological properties as well as mechanism of action and triggered targets [66]. It is postulated, that the N-atom in the side chain in position three to five related to the geminal carbon atom of the phosphonate groups determines the mechanism of action of BPs [64]. The following scheme gives an overview of different BPs and their categorization in two groups (see **Figure 5**).

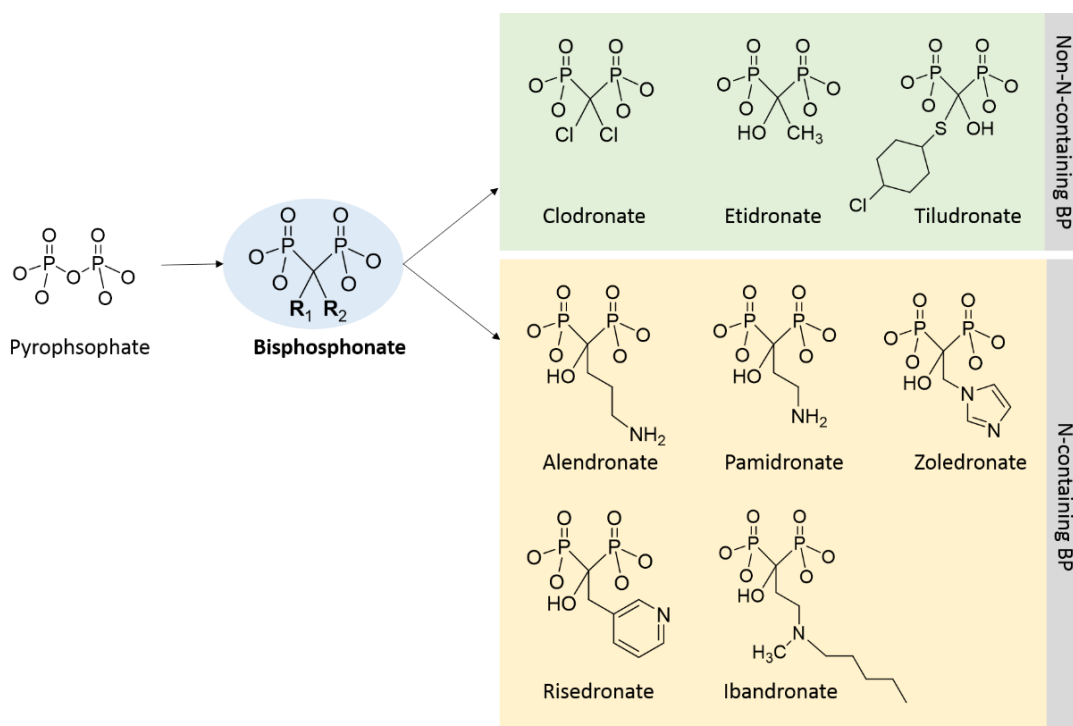


Figure 5:

Overview of the two bisphosphonate (BP) categories. There is a classification in nitrogen (N)-containing and non-N-containing drugs. Due to the presence of the N-atom, there is a variation in the mechanism of action, efficacy and consequently dosage.

BPs have a strong affinity to the bone mineral HA, which results in a certain “selective targeting”. Concerning the cellular level, BPs interact with osteoclasts. On the one hand, they inhibit the accumulation of calcium salts in body tissue. On the other hand, they prevent the breakdown of HA. Concerning the mechanism of action, there is a difference between N-containing BPs like alendronate, ibandronate or risedronate in comparison to N-free structures like clodronate or etidronate. The latter BPs form cytotoxic adenosine triphosphate (ATP) analogs, which promote osteoclast apoptosis. The principle mechanism of action for the N-containing substances is based on the inhibition of the farnesyl diphosphate (FPP) synthase. The blocking of this enzyme of the cholesterol pathway is linked to the suppression of isoprenylation and inhibition of bone resorption [64].

CPCs are used as drug carrier systems for BPs. They have the big advantage that the setting of the paste occurs at room temperature. This follows that there is no risk of thermal degradation for the API [63]. On the other hand, the given porosity of the cement system allows the incorporation of drugs in the network. The release

of the substance is controlled by diffusion processes through the cement matrix [67]. Fazil *et al.* reviewed novel drug delivery systems for BPs and had a closer look on CaPs as representatives for bioceramics. BPs like pamidronate and alendronate have an influence on the setting properties and *in vitro* bioactivity of CPCs. Moreover, both drugs showed an effect on the proliferation of osteoblasts. In a study of Panzavolta *et al.* [68], this system was also postulated to be used as local drug depot as alternative to the oral application. Though BPs have a relatively good safety profile with only few adverse events, the most common are gastrointestinal discomforts like diarrhea or esophageal erosions [69]. To overcome these possible effects, a local application could be a promising alternative. Furthermore, the combination of drug delivery and surgical performance improves the compliance of the patient and the acceptance regarding this treatment option. Therefore, Murphy *et al.* [70] established a multicomponent scaffold of collagen-HA with recombinant human bone morphogenetic protein (rhBMP-2) and the BP zoledronic acid. They could show positive effects with this scaffold material and the synergistic release of an anabolic and an anti-catabolic agent. Another interesting outcome of a study performed with the latter BP by Verron *et al.* [71] was the induction of new-bone-formation by using a combination of zoledronate with CDHA. The third-generation BP risedronate was presented in a study of Gong *et al.* [72] by incorporation of this API into a CaP silicate cement. Performing an *in vivo* study with osteoporotic rabbits, they investigated osteoporosis- and bone resorption-related biomarkers and noticed a promotion on osteoblast proliferation and differentiation.

Besides CPCs, also silica-based glasses and various formulations are in the focus as drug delivery systems for BPs. Using adsorption processes on the surface, Mosbahi *et al.* [73] studied the use of risedronate and bioactive glass (46S6), which formed an association due to strong interactions between the molecules. They verified the successful formation *via* nuclear magnetic resonance (NMR) as well as Fourier transform infrared (FTIR) and Raman spectroscopy. Another publication deals with the functionalization of mesoporous bioactive glass nanospheres with alendronate for the treatment of osteosarcoma as a malignant cancerous bone tumor. The group investigated the *in vitro* behavior using different

tumor cell lines (MG-63, RAW 264.7) and showed an approach for one possibility of local drug targeting [74].

Anti-inflammatory analgesics

If tissue is damaged, inflammatory mediators are released and distributed in the surrounding area. One important messenger in pain transmission is the group of prostaglandins (PGs). They bind to pain receptors at the nerve ends in the tissue and trigger a signal pathway to the brain that patients sense a pain transmission. It is well known that the effectiveness of nonsteroidal anti-inflammatory drugs (NSAIDs) is based on the inhibition of PG biosynthesis with the key enzyme cyclooxygenase (COX). It catalyzes the conversion from arachidonic acid, an unsaturated fatty acid, to the cyclic endoperoxides PG of the type PGH_2 with further transformation to different derivatives (PGI_2 , PGF_2 , PGE_2 and thromboxane (TX) type TXA_2). There is the distinction of two sub-types of this key enzyme, COX-1 and COX-2, which are proteins with about 60 % structural homology [75]. In general, COX-1 is formed in a constitutive manner whereas the isoform COX-2 is mainly expressed at inflammation sites which concludes that its blocking could reduce the formation of PGs as phlogistic messengers [76]. The mechanism of ibuprofen, a propionic acid derivative, depends on the binding to the enzyme as a competitive inhibitor [77]. This means that the drug, which interacts as antagonist to the substrate, has similar binding structures as the substrate itself (for example carboxylic group, defined interspace between certain atoms in case of arachidonic acid and ibuprofen; structures see **Figure 6**). These binding structures are important for the affinity to the active center. The ratio of COX-1 to COX-2 affinity is smaller than 1 for ibuprofen [78], which means that inhibition occurs in a higher rate for the COX-2 enzyme. A second option of inhibition of the COX-enzyme, next to the reversible competitive inhibition, is the irreversible inactivation. The inhibition process of the salicylic acid analogue aspirin relies on the irreversible acetylation of the amino acid serine (Ser) of the active site. Consequently, the production of PGs and TXA_2 is decreased. This results in reduction of fever or coagulation. The inhibition of platelet TX has a certain dose-dependency and needs a repeated low dose administration in order to have a cumulative effect [79].

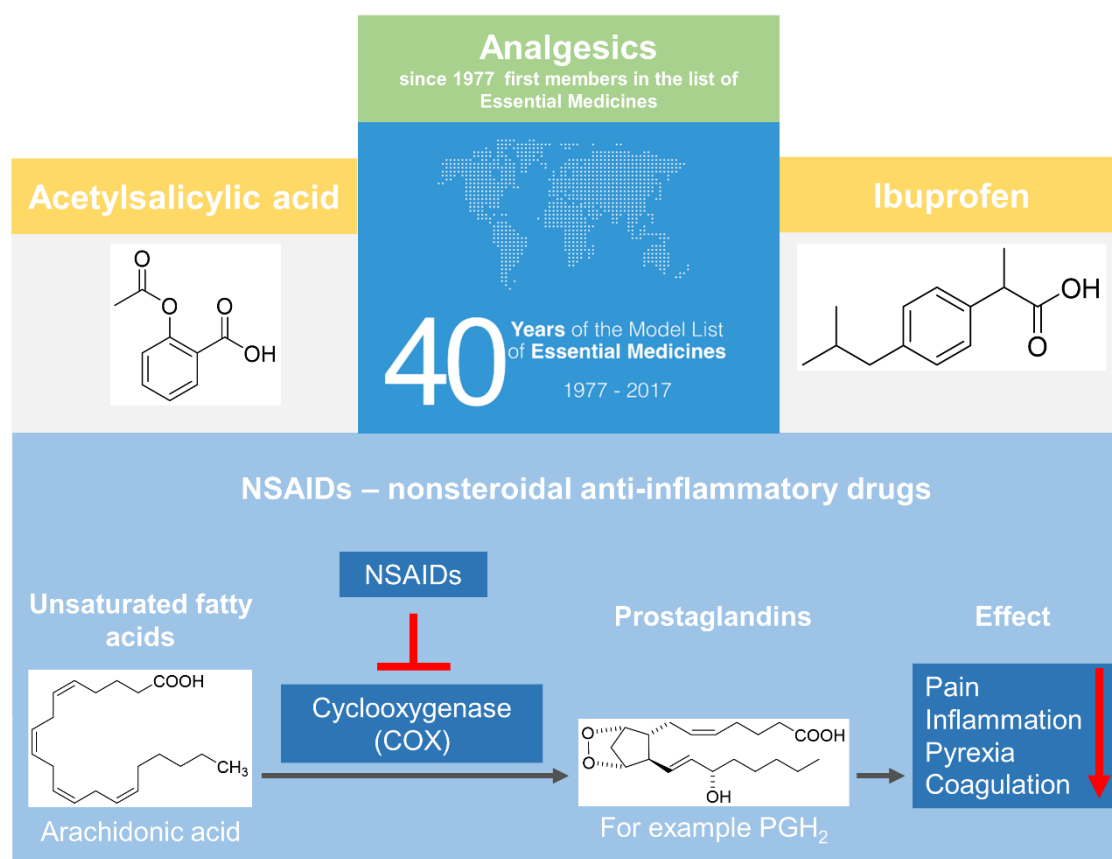


Figure 6:

Chemical structures of the discussed analgesics aspirin and ibuprofen as well as the target of nonsteroidal anti-inflammatory drugs (NSAIDs) and the pharmacological effect at a glance. The picture of the 40th anniversary of the Model List of Essential Medicines was taken from [80] and is distributed under the Creative Commons Attribution License which permits unrestricted use, distribution and reproduction in any medium.

Both, ibuprofen and aspirin, have a carboxyl group in their molecular structure which can interact *via* complexation with positively charged ions. This functional group should be kept clearly in mind when working with CaPs or other cation containing bioceramics in order to avoid or consider interactions. Ginebra *et al.* [81] noticed a decrease in the reaction rate of an apatitic α -TCP-based cement with a salicylic acid derivative due to complexation effects. Furthermore, the mechanical strength, both the compression (25 %) and bending (80 %), could be increased based on a decreased porosity and smaller crystal structures. The well-known dependency of drug release on porosity could be seen in a study with aspirin and HA-based cements as drug carrying system. The amount of drug released into the surrounding media increased with increasing porosity [82]. Another group focused on CaP granules as reservoir for ibuprofen-loading [83]. Two different types of

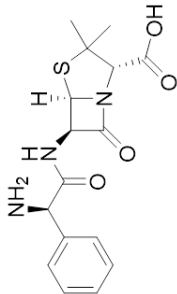
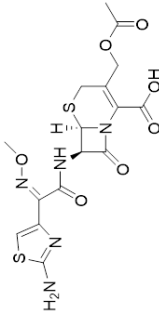
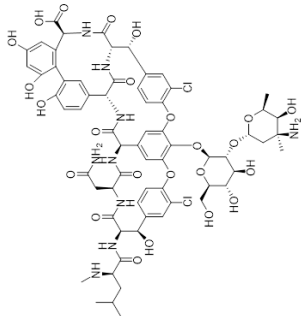
granules were produced and loaded with different amounts of ibuprofen (up to 46 %). With a drug-loading higher than 22 %, the pharmaceutical was not only deposited on the surface of the granules, but it was also filling agent of porous structures inside the samples. Additionally, the incorporation of ibuprofen increased the mechanical performance of the granules so that an application as bone defect fillers might be favored. In a recently published study [84], CaP cement, gypsum and a mixture of both were analyzed regarding their incorporation with ibuprofen (1 % and 2 %). There was a difference in drug-release-profiles depending on the composition of the inorganic phase. A delayed and incomplete release of ibuprofen was noticed for the formulations containing gypsum. Another interesting study concerning drug load of bioactive glasses with ibuprofen was performed by Ladrón de Guevara-Fernández *et al.* [85] and focused on the controlled release of this NSAID with poly(lactic acid) (PLA) as biodegradable compound to facilitate drug release and poly(methyl methacrylate) (PMMA) as polymeric variation to avoid a burst release. These polyphasic materials were prepared by free radical polymerization (FRP) within a mixture of glass, monomers and polymers as well as benzoyl peroxide as initiator. A fast release with an anti-inflammatory effect of ibuprofen was noticed in the first 8 hours and the formation of an apatite-like layer was observed. The addition of PLA led to an increase in the rate of both, the apatite-like layer generation and the release of ibuprofen.

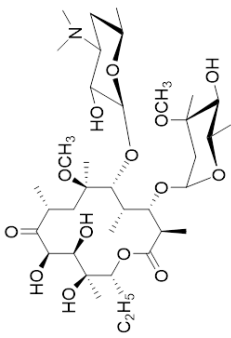
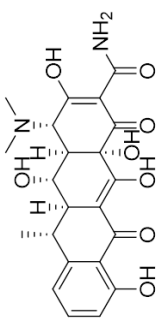
Antibiotics

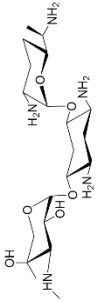
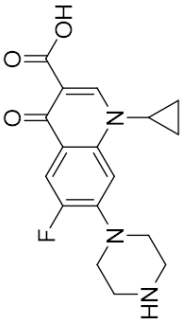
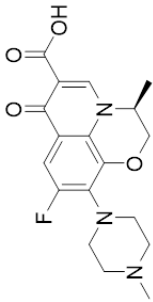
A combination of a bioceramic implant with antibiotics is intended for both, the treatment of infected bone areas (osteomyelitis) and the prophylaxis of post-operative infections. The complexity of bone infection treatment is given by the poor tissue penetration of antibiotic drugs and the treatment of osteomyelitis needs therapy variations, which are easy to handle without a high cost factor. Here, the most commonly applied material class are antibiotic loaded polymeric PMMA bone cements (for example with gentamicin [86] or vancomycin [87]), which have the main drawback of an insufficient and slow release due to the non-porous nature of the cement. Furthermore, this cement class is not degradable, in comparison to for example brushite cements, and consequently foreign substances will stay in the

body that have the potential to cause inflammatory reactions. Formulations based on CaPs were investigated as alternative materials due to their high porosity resulting in a higher amount of released drug combined with their osteoconductive properties. This avoids a second operation step to remove the implant [88]. In order to give an overview of the different antibiotics, which were used in combination with bioceramics, **Table 3** illustrates various classes with the corresponding mechanism of action, structural formula of a representative and pharmaceutical information [89], including also studies published in the last few years regarding this topic. An informative and highly recommended review was published in 2012 by Ginebra *et al.* [62], which deals with the combination of antibiotics and mineral bone cements.

Table 3: Overview of different antibiotic classes with a selection of relevant and actual studies.

Class of antibiotics	Mechanisms of action	Bacteria/disease	Structural formula of representatives	Selected studies incl. reference
Beta-lactam antibiotics	Inhibition of peptidoglycan or murein synthesis via binding to enzymes with transpeptidase-activity, so-called penicillin binding proteins	- Gram-positive coccus (for example <i>Streptococcus</i>) - Gram negative coccus (for example <i>Gonococci</i>) - Spirochete - Diphtheria bacteria	<p>Ampicillin</p>  <p>Cefotaxime</p> 	<p>CaPs:</p> <ul style="list-style-type: none"> - Injectable magnesium-doped brushite cement for controlled drug release application [90] <p>Mesoporous silica:</p> <ul style="list-style-type: none"> - Adsorption and release of ampicillin antibiotic from ordered mesoporous silica [91]
Glycopeptides	Inhibition of cell wall synthesis and influence → binding to precursor acyl-D-Alanine (Ala)-D-Ala → prevention of the transglycosylation [97]	Gram-positive bacteria: - <i>Staphylococcus</i> (incl. Methicillin-resistant <i>Staphylococcus aureus</i> (MRSA)) - <i>Streptococcus</i> - <i>Enterococcus</i> - <i>Corynebacterium</i> - <i>Clostridium difficile</i>	<p>Vancomycin</p> 	<p>CaPs:</p> <ul style="list-style-type: none"> - Effect of porosity on drug release kinetics from vancomycin microspheres/CPC composites [92] - Microbial biofilm formation on PMMA bone cement loaded with gentamicin and vancomycin [93] <p>Bioactive glasses:</p> <ul style="list-style-type: none"> - Antibacterial and anticancerous drug loading kinetics for mesoporous bioactive glasses [94] (see also tetracycline antibiotics) - Poly(3-hydroxybutyrate-co-3-hydroxyvalerate) (PHBV) microspheres/45S5 bioactive glass composite scaffolds [95]

Class of antibiotics	Mechanisms of action	Bacteria/disease	Structural formula of representatives	Selected studies incl. reference
Polyketides I: Macrolides	Antibacterial mechanism: inhibition of protein synthesis binding at the large subunit of the bacterial ribosomes [101]	<ul style="list-style-type: none"> - Gram-positive coccus (mainly <i>Streptococcus</i> and <i>Staphylococcus</i>) - Selected Gram-negative organisms like <i>Bordetella pertussis</i> but often bacterial resistances 	<p>Clarithromycin</p> 	<p>CaPs:</p> <ul style="list-style-type: none"> - β-TCP with clarithromycin loaded poly(lactic-co-glycolic acid) (PLGA) microspheres enhances bone formation in bone defects [98]
Polyketides II: Tetracyclines antibiotics	<ul style="list-style-type: none"> - Inhibition of protein synthesis - \rightarrow blocking of the 30S bacterial ribosomal subunit - \rightarrow inhibition of aminoacyl-transfer ribonucleic acid (RNA) attachment 	<ul style="list-style-type: none"> - <i>Chlamydia</i> - <i>Mycoplasma</i> - <i>Treponema pallidum</i> (syphilis) - <i>Acne vulgaris</i> 	<p>Doxycycline</p> 	<p>CaPs:</p> <ul style="list-style-type: none"> - Osteogenic activity of cyclodextrin-encapsulated doxycycline in a CaP/polycaprolactone (PCL) and PLGA composite [99] - Surface modification of β-TCP ceramics by atmospheric plasma surface engineering for regulated drug release of doxycycline [100]
				<p>Bioactive glasses:</p> <ul style="list-style-type: none"> - Antibacterial and anticancerous drug loading kinetics for mesoporous bioactive glasses [94] (see also glycopeptides)

Class of antibiotics	Mechanisms of action	Bacteria/disease	Structural formula of representatives	Selected studies incl. reference
Aminoglycosides	Inhibition of the protein synthesis by coupling at the 30S ribosomal subunit with consequent intervention in peptide elongation	<ul style="list-style-type: none"> - Gram-negative, aerobic bacteria - Synergistical action against Gram-positive bacteria - Infections of abdomen and urinary tract - Prophylaxis of endocarditis [105] 	<p>Gentamicin</p> 	<p>CaP:</p> <ul style="list-style-type: none"> - Controlled release of gentamicin from CaP/PLGA composite bone cement [88] <p>Bioactive glasses:</p> <ul style="list-style-type: none"> - Gentamicin release from glass-polymer-antibiotic composites [98] - Bioactive sol-gel glass implant for <i>in vivo</i> gentamicin release [102]
Quinolones	Targets: Gyrase and topoisomerase IV: inhibition of bacteria deoxyribonucleic acid (DNA) enzymes without following DNA supercoiling and DNA strand crack [106]	<ul style="list-style-type: none"> - <i>Chlamydia</i> - <i>Mycoplasma</i> - <i>Treponema pallidum</i> (syphilis) - <i>Acne vulgaris</i> 	<p>Ciprofloxacin</p>  <p>Levofloxacin</p> 	<p>CaP:</p> <ul style="list-style-type: none"> - Insights on the properties of levofloxacin-adsorbed Sr^{2+}- and Mg^{2+}-doped phosphate powders [103] <p>Bioactive glasses:</p> <ul style="list-style-type: none"> - Antioxidative activity and regenerating bone capacity of ciprofloxacin loaded porous poly(vinyl alcohol) (PVA)/bioactive glass hybrids [104]

Anticancer Drugs

Most APIs in the pipeline of research companies are focused on the field of anti-cancer therapeutics. Nowadays, there is the need to find a balance between the chance of curing, increase of survival and improvement of the patients' quality of life next to the cost management of health insurances and the management of present side effects. The following part of this chapter describes selected anti-cancer therapies with new approaches for the combination with bioceramics to treat bone cancer.

Methotrexate (MTX) is used as chemotherapeutic agent and disease-modifying drug also for the treatment of osteosarcoma. The chemical structure is similar to folic acid (vitamin B₉) and inhibits as antagonist the key enzyme dihydrofolate reductase. This enzyme catalyzes the hydration from dihydrofolic acid to tetrahydrofolic acid. As consequence, the production of tetrahydrofolic acid decreases, but this substance is used for the formation of purine nucleotides and thymidine and can interfere in the deoxyribonucleic acid (DNA) and ribonucleic acid (RNA) synthesis [107]. This results in an interruption of the cell cycles and a stop in the reproduction of tumor cells (see **Figure 7**). The pharmaceutical compound is used as gold standard for the treatment of rheumatoid arthritis, auto immune diseases like multiple sclerosis or Crohn's disease (low-dose-therapy) and as cytostatic drug for malignant tumors like osteosarcoma (high-dose-therapy). Interesting investigations combining alendronate with the anti-cancer substance were performed by Chu *et al.* [108] in combination with CaP nanoparticles. A linear PEG was functionalized with the BP alendronate to achieve a binding to HA for bone-targeted drug delivery. The nanoparticles were then loaded with MTX and showed an inhibition of cancer cells in a comparable manner as the free drug. Cisplatin (*cis*-diammine-dichloro-platinum (II)) is another very potent cancer therapeutic agent since 1973 for the treatment of several tumors as ovarian or lung cancer [109]. The mechanism of action is based on the formation of DNA adducts *via* interstrand or intrastrand cross-linking between platinum (Pt) and two guanine or adenine bases of the DNA (interaction with position N 7). Hence, a damage of proteins and signal molecules occurs with a following activation of apoptosis of fast proliferating cells [110].

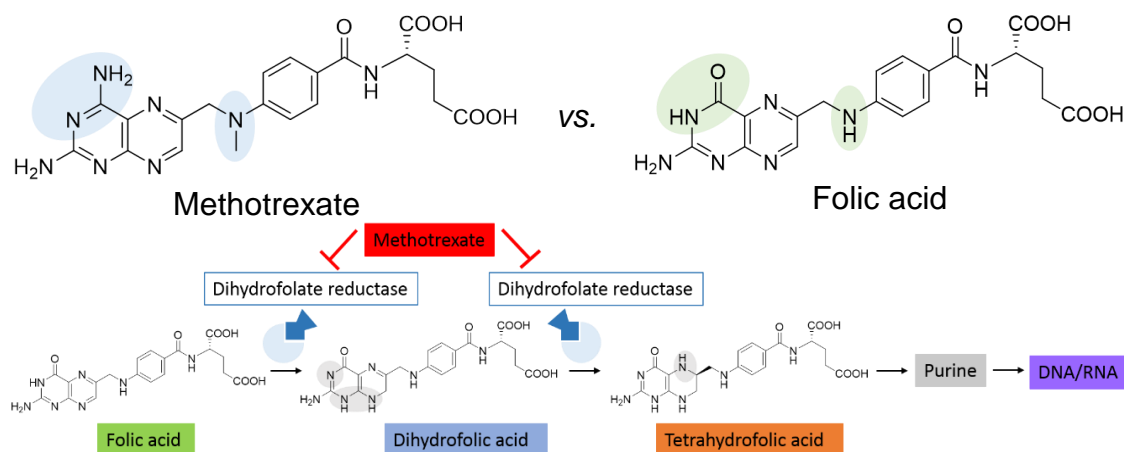


Figure 7:

Methotrexate (MTX) as antagonist of the dihydrofolate reductase inhibits the key enzyme of the folic acid pathway. Due to the structural similarity of MTX and folic acid, a competitive, reversible inhibition is used as mechanism of action.

The combination of cytostatic compounds with other drugs seems to have a synergistic effect on the therapy and to increase their toxic effectiveness *versus* tumor cells. Therefore, a co-delivery of cisplatin and doxorubicin from CaP beads/matrix scaffolds was tested as treatment option for osteosarcoma therapy. TCP/alginate beads were used as drug carrier and incorporated in a scaffold matrix of HA and silicon dioxide. Hees *et al.* [111] observed a burst release of cisplatin and a continuous release of the antibiotic drug. Doxorubicin was loaded either in the matrix or in the beads with 22 % release in 40 days for matrix incorporation and about 52 % for the same time frame when loaded in beads. The combination of both drugs led to an improved toxicity towards MG-63 osteosarcoma cells in comparison to single-loaded composites. Farbod *et al.* [112] published a study in 2016 dealing with the controlled drug release of chemotherapeutic platinum Pt-BP complexes from injectable CPCs. They produced Pt-BP-loaded HA-nanoparticles, loaded the solid phase of the cement and added poly(lactic-co-glycolic acid) (PLGA) microspheres in order to influence the degradation *versus* shorter time frames by the presence of this porogenous structure. The increase in degradation rate had no effect on the drug release. Furthermore, the antiproliferative activity of the Pt-BP-complexes was analyzed using human osteosarcoma cancer cells (MG-63) and human bone marrow-derived mesenchymal stroma cells with a certain dose-dependent positive outcome and a chemotherapeutic activity.

Others

Apart from the aforementioned low molecular weight drugs, bioceramics could also serve as delivery matrix for biological molecules based on proteins. An example are growth factors like bone formation inducing rhBMP-2s or angiogenesis inducing factors such as vascular endothelial growth factor (VEGF) [113]. The formation of new blood vessels is based on the release of the latter protein that triggers a cellular cascade of liberation, migration and proliferation and finally induces the formation of pre-vascular, tubular structures [114]. In a study of Schumacher *et al.* [115], HA and mesoporous bioactive glass granules were used as drug carrier matrix for two different proteins: the enzyme lysozyme and VEGF. The two proteins were loaded into the bioglass granules and the incorporation of the substances in the cement matrix did not influence the biological activity of both proteins. The same authors are furthermore focused on the VEGF release from other bioceramic systems like three-dimensional (3D)-plotted scaffolds made of CPC with encapsulated VEGF in chitosan-based microparticles [116] or a biphasic scaffold design *via* multichannel plotting combining CPC with VEGF-loaded alginate/alginate-gellan gum hydrogels [117]. Both studies had an investigation period of 7 days and could observe a burst release of VEGF in the first two hours. Regarding CPC and rhBMP-2, the group of Jansen had a closer look on the release profile of rhBMP-2 for different CaP formulations with porous structures [118, 119] or entrapped PLGA microparticles [120] and analyzed the influence on the osteoinductive effect *in vivo*. In a study published in 2012, van de Watering *et al.* [121] were able to use different loading methods for rhBMP-2 in combination with CPCs ((1) incorporation into the liquid phase of CPC, (2) adsorption on the surface on preset porous CPC or (3) on PLGA microparticles). They demonstrated similar release profiles for (1) and (3) over a time frame of 28 days. The surface-loaded specimens (2) showed a similar rhBMP-2-release aside from an initial burst release. The biological effect of the different loading methods remains still unclear.

2.3 Hydrogels

2.3.1 Definition and classification

Hydrogels can be defined as 3D networks based on hydrophilic precursors becoming water-insoluble after polymerization or cross-linking [122]. Depending on the composition, precursors can form homo- or copolymeric meshes. Moreover, these constructs are able to swell with water or biological fluid imbibition and reach weights that are 3-4 times higher than their initial mass. This swelling process is relatively complex and can be divided into several parts with respect to Gibbs and Iwona [123]. The first one consists of a hydrating process of polar and hydrophilic groups by water molecules that penetrate in the polymer network. This absorption leads to bonding of so called primary bound water. After this step, the hydrogel matrix swells and also more hydrophobic groups interact with water molecules resulting in secondary bound water [124]. Both, primary and secondary water together, are leading to the total amount of bound water. This parameter is depending on temperature as well as structure and nature of the polymer thus always creating specific interactions for a certain hydrogel system. Due to this swelling capacity, hydrogels behave very elastic with a consistency similar to soft, rubbery tissues and offer the application in different biomedical fields like contact lenses [125], materials for 3D printing [126] or in medical and pharmaceutical sectors as drug delivery devices [127]. Hydrogels are highly attractive and versatilely used in biomedical fields due to their similarity with extracellular matrix (ECM) offering excellent conditions for cells or resemblance to living organs. The aqueous environment has a certain protecting effect on incorporated substances like cells or embedded drugs that sometimes are needed for a controlled liberation at implantation side. This exchange of drugs or nutrients for cell metabolism increases the attractiveness of these networks. First reports on hydrogels trace back to the development of polyHEMA by the scientific group of DuPont's in 1936. It was described as brittle, glassy polymer without further interest of notification [128]. With the pioneering work of Wichterle and Lim [129] 24 years later who firstly described cross-linked hydrogels based on polyHEMA, a new era started with this milestone for today's hydrogel research. Main properties regarding hydrogel networks that are mostly used for their characterization are molecular weight of neighboring cross-linkers (M_c), mesh size (ξ) as well as kind of cross-linking

points [130]. The different parameters are illustrated in **Figure 8**. Molecular variations are also given by different structures of hydrogel precursors like linear or branched polymers as well as block- or graft-copolymers.

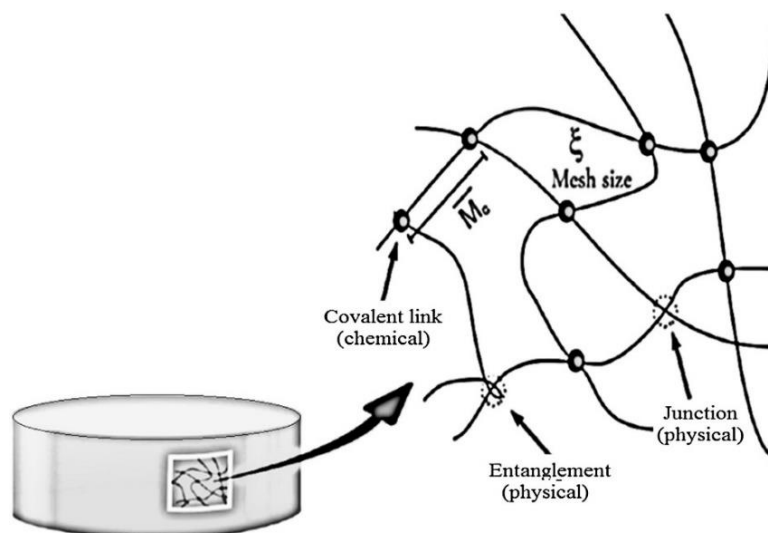


Figure 8:

Round shaped hydrogel specimen with a magnified detail of the typical mesh structure of a polymeric network and the different methods of cross-linking (physical *versus* chemical) reprinted of [128] with permission from Elsevier. M_c = molecular weight of neighboring cross-linkers.

A main hydrogel classification can be drawn according to the (i) type of cross-linking or (ii) the original source of precursor as well as monomer. This is correlated to the fact if the origin derives from natural, synthetic or hybrid molecules. Such hybrid structures include for example designed peptide-polymer hybrids including alginate as well as proline-rich peptide sequences as one component in a bioink formulation for 3D-printing [131, 132]. From the point of cross-linking, they can form physically stable entanglements and junctions or covalent links that are based on chemical interactions. Both distinctions are highlighted in the following two sections. Furthermore, hydrogels can be categorized according to (iii) degradability of being non- or biodegradable, (iv) preparation techniques meaning copolymeric or homopolymeric gels and interpenetrating networks, (v) ionic charges with neutral, anionic, cationic or ampholytic hydrogels as well as physical structures (amorphous or semi-crystalline) [18, 128].

2.3.1.1 Chemical *versus* physical cross-linking

A distinction between physical and chemical cross-linking can be drawn resulting in a main categorization of formed gels with different properties. Chemical or permanent hydrogels' reaction is based on a covalent cross-linking so that irreversible and permanent links are formed due to configurational changes. This mechanism runs by direct interaction of branched or linear polymers. Furthermore, cross-linking agents that are mostly bifunctional, small molecular weight molecules can be added to the monomer solution and induce network formation. One example are gelatin hydrogels cross-linked *via* glutaraldehyde and thus forming stable constructs, of course in dependency to the amount of cross-linker [133]. Due to inhomogeneous distributions of the cross-linker, high network density and water swollen regions, so called "clusters" can be formed [124]. In some cases, depending on parameters like temperature, precursor concentration and solvent availability, this may lead to phase separation with water filled pores or even syneresis effects. Swelling capacity of these hydrogels under physiological conditions is limited to the distance between polymer chains and their maximum elongation.

In contrast to this class, physical hydrogels are often called smart or conventional hydrogels and their process of gel formation is based on physical interactions that show a reversible behavior. This can be achieved by interactions like hydrophobic associations, chain aggregations or hydrogen bonding [128]. Furthermore, entanglements of high molecular polymer chains, ionic interactions, hydrogen bridges also induce physical cross-linking [134]. This process is reversible due to conformational changes and has the big advantage that no additives, for example cross-linkers, photo-initiators or radical catalysts, have to be added. Formed links are non-permanent and often result in a constant equilibrium of polymer partner interactions [135]. Due to relatively weak entanglements or van der Waals forces between polymer strands, a deswelling and destruction of the structure can easily be performed by temperature changes or simple dilution processes. Consequently, the concentration of the dissolved precursors has a high effect on mechanical and rheological properties of physically cross-linked hydrogels, which leads to a disjunction of entangled polymer chains and an increase in flowability [135].

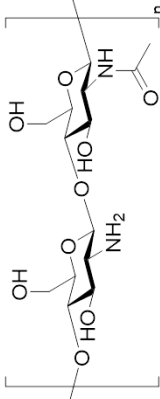
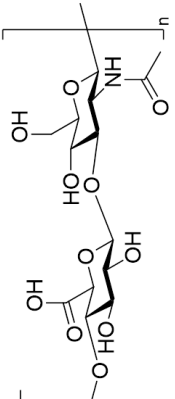
A combination of both, physically and chemically cross-linked hydrogels, results in double network systems that show high toughness and mechanical properties based on electrostatic interactions [128]. A rigid skeleton of cross-linked polyelectrolytes as first network is combined with a second network that consists of a poorly cross-linked neutral polymer as ductile and soft component [136, 137]. The first reported system was developed by Gong *et al.* [138] in a two-step sequential free-radical polymerization of poly(2-acrylamido-2-methylpropanesulfonic acid) (PAMPS) and poly(acrylic acid) (PAA) leading to a network formation.

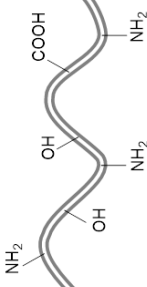
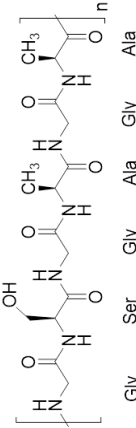
2.3.1.2 Natural *versus* synthetic hydrogels

With respect to the origin of hydrogel precursors, these 3D polymeric networks can be classified as natural and synthetic hydrogels. According to their structure and building units, they are divided in polysaccharides or proteins. Many of them are isolated from plants like cellulose derivatives or alginate as well as derived from animals like collagen or fibroin. **Table 4** gives an overview of natural hydrogels with selected prominent representatives based on polysaccharide and protein biopolymers, respectively.

Table 4:

Overview of polysaccharides as well as proteins forming natural hydrogels. Information is taken from [130, 135].

Natural hydrogels	Representative and structural formula	Type of polymers for bone applications	Cross-linking
Polysaccharide hydrogel	<p data-bbox="416 1240 448 1368">Chitosan</p>  <p>The diagram shows the repeating unit of chitosan, a polysaccharide composed of N-acetylglucosamine units. Each unit is a six-membered pyranose ring with a hydroxyl group at C2, a hydroxyl group at C3, a hydroxyl group at C4, and an N-acetyl group at C2. The units are linked by beta-1,4-glycosidic bonds. The structure is enclosed in brackets with a subscript 'n'.</p>	<p data-bbox="416 618 839 1055">Sintered chitosan microspheres, chitosan/fibroin/HA, β-TCP/chitosan, chitosan/alginate multilayer scaffold, chitosan/gelatin, titania/chitosan composite, photo-cross-linkable chitosan, chitosan/collagen, ceramic nanoparticles/chitosan, silk/chitosan</p>	<p data-bbox="416 338 663 539">Physically triggered by anions or chemically by reaction with cross-linker</p>
Polysaccharide hydrogel	<p data-bbox="927 1196 959 1413">Hyaluronic acid</p>  <p>The diagram shows the repeating unit of hyaluronic acid, a polysaccharide composed of D-glucuronic acid and N-acetylglucosamine units. The glucuronic acid unit is a six-membered pyranose ring with a hydroxyl group at C2, a hydroxyl group at C3, a hydroxyl group at C4, and a carboxylic acid group at C5. The N-acetylglucosamine unit is a six-membered pyranose ring with a hydroxyl group at C2, a hydroxyl group at C3, a hydroxyl group at C4, and an N-acetyl group at C2. The units are linked by beta-1,3-glycosidic bonds. The structure is enclosed in brackets with a subscript 'n'.</p>	<p data-bbox="895 618 1094 1055">Amine/aldehyde-containing hyaluronic acid, hyaluronic acid/PVA, matrix metalloproteinase-sensitive hyaluronic acid</p>	<p data-bbox="895 338 1094 539">Physically mediated or chemically for modified hyaluronic acid</p>

Natural hydrogels	Representative and structural formula	Type of polymers for bone applications	Cross-linking
Protein hydrogel	<p data-bbox="368 1160 400 1256">Gelatin</p> 	<p data-bbox="368 680 400 965">HA chitosan/gelatin, glutaraldehyde cross-linked gelatin, HA/gelatin, β-TCP/gelatin, gelatin/poly(ϵ-caprolactone) nanofibers, gelatin microcarriers/polyester, micro- and nano-HA/chitosan/gelatin, gelatin-based photopolymers</p>	<p data-bbox="368 226 616 495">Physically induced by temperature changes or chemically by reaction with cross-linker</p>
Protein hydrogel	<p data-bbox="879 1160 911 1256">Fibroin</p> 	<p data-bbox="879 591 1086 965">Silk fibroin/chitosan/PLLA, chitosan/fibroin-HA, nonmulberry silk gland fibroin, nonmulberry and mulberry silk gland fibroin</p>	<p data-bbox="879 226 1046 495">Physically triggered by temperature changes, ultraviolet (UV)-irradiation</p>

Collagen is the major protein of ECM and thus the most abundant protein in mammalian species [139]. It may be considered as an “anhydride” of the biopolymer gelatin [140] which is gained by partial hydrolytic conversion of collagen under acidic or basic conditions [140]. In contrast to collagen, it can be considered as purified protein and consequently shows less antigenicity [141]. Therefore, the interest for the use in biomedical fields increases. During production, yield molecules vary in molar mass due to uncontrolled fragmentation of collagen. Consequently, it is a mixture containing amino acids as smallest unit that are arranged to peptides or even oriented as proteins. The variety of molecular weight is very broad deviating in the range of 15,000-400,000 Da [140]. To check the quality of the used gelatin in this thesis, it was analyzed regarding molecular weight *via* gel permeation chromatography (GPC) eluting with an aqueous solution that was supplemented with $8.5 \text{ g}\cdot\text{L}^{-1}$ sodium nitrate (NaNO_3) and $0.2 \text{ g}\cdot\text{L}^{-1}$ sodium azide (NaN_3). Gelatin from porcine skin (Type A, Sigma Aldrich, Steinheim, Germany) was dissolved in the eluent ($C_{\text{sample}} = 0.564 \text{ mg}\cdot\text{mL}^{-1}$) and evaluated with Multi-Angle Light Scattering (MALS) Detection. Measured values were $M_w = 133,838 \text{ Da}$, $M_n = 245,395 \text{ Da}$ with a dispersity $\mathcal{D} = 1.833$ calculated as quotient of M_n and M_w . This factor naturally occurring variation has always to be considered when preparing gelatin solutions which are transparent and odorless with a sol-gel transition temperature of about $30 \text{ }^\circ\text{C}$ [130].

Another important criterion is its fast degradation due to swelling and rapid dissolution at body temperature and in aqueous environments [142]. By using cross-linking agents like diisocyanates, carbodiimides, glutaraldehyde [143], dextran dialdehyde or the more cytocompatible genipin [144], an irreversible formation of covalent bonds can be performed. Based on this reaction, mechanical properties can be modified as well as controlled. Furthermore, a functionalization of for example free amine groups with methacryloyl or acryloyl moieties [145] may serve as a platform for tissue engineering applications. The attractiveness of gelatin in biomedical fields was also growing due to low immunogenicity as well as cytotoxicity and capability for drug loading and encapsulation of biomolecules [146].

Besides the great interest of natural hydrogels, different synthetic gel forming materials are already used for scaffold fabrication. Prominent candidates and

derivatives are PEG [147] or poly(oxazolines) (POX) [148] as recognized hydrophilic PEG-alternative, PAA [149] as well as poly(vinyl alcohol) (PVA) [150]. One big advantage is their reproducibility by performing synthesis and thus controlling parameters like repeating units or molecular weight [151]. Over the last few years, the interest in PEG-based hydrogels increased enormously due to their versatile usability for example in drug delivery [152] or surface modification [153] in tissue engineering. PEG as basic module for such systems can either be linear or branched (see **Figure 9 A** and **B**) and its chain terminal hydroxy groups (-OH) can be modified or substituted as well as conjugated with drugs or protein structures. In correlation to molecular weight, PEGs can either be a viscous liquid ($M_w < 400$ Da) or have a solid state ($M_w > 400$ Da) [147].

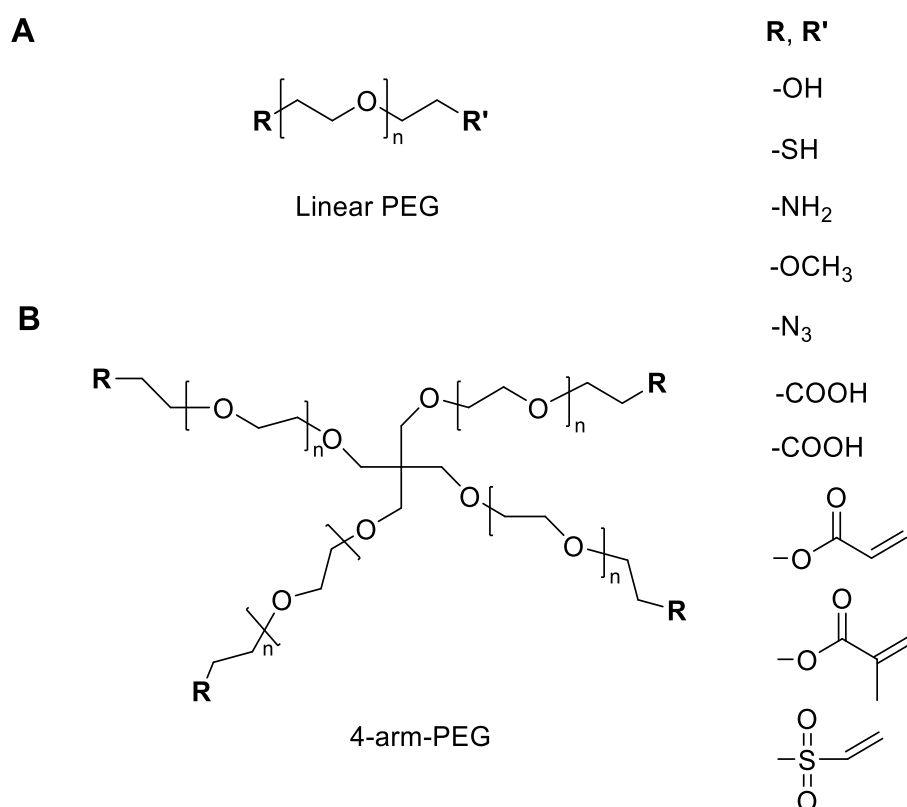


Figure 9: Linear (**A**) and branched (**B**; 4-arm) PEG molecules with different substitutes. In case of $R = R'$, linear PEG has a symmetric structure. The chemical structures are adapted from [154].

The outstanding advantages of PEG are its hydrophilicity, commercial availability and biocompatibility. It is soluble in water as well as many other organic solvents like methanol, ethanol or dichloromethane (DCM), always with respect to its molecular weight that can reach levels of about 20,000 Da. Additionally, the elimination process and excretion rate is also depending on the molecular weight as well as size and shape of the polymer [155]. The threshold for renal elimination for PEG macromers is 30,000 Da. Above this level, they are eliminated through the liver. The backbone itself has a non-degradable structure with a high ether-C-O-binding energy of $360 \text{ kJ}\cdot\text{mol}^{-1}$ [156] besides the possibility of enzymatic decomposition (for example peroxidases) or *via* microbial cleavage. By integration of hydrophobic PLA-units, degradation behavior can be controlled [157] as well as hydrogel characteristics like swelling or elasticity can be changed. The majority of PEG-hydrogels is prepared *via* photo-polymerization of PEG(-copolymeric) acrylates. This common technique depends on the reaction of monomers like diacrylated or dimethacrylated PEGs (PEG-DMA) [154] using radical reactions mechanisms by (i) photocleavage or (ii) hydrogen abstraction from a H-donor site [158]. In combination with nontransparent second matrixes like CPCs, the polymerization cannot be induced by visible or ultraviolet (UV) light.

2.3.2 Polymerization reactions and cross-linking of hydrogels

Hydrogels are formed according to their definition by polymerization reactions creating a water-insoluble cross-linked network [159]. The reaction has to be carried out in an aqueous solution by dissolving the mainly solid precursors. Among cross-linker or monomer concentration, initial degree of dilution, also hydrogel structure and thus the corresponding properties are related to the chemistry of polymerization [159]. Generally, a distinction between two processes can be drawn. On the one hand, low molecular weight monomers can react by forming high molecular weight polymeric structures. In some cases, cross-linking agents like for example bifunctional compounds have to be added in order to create 3D networks. Another option are cross-linking mechanisms of high molecular weight hydrogel precursors that result, on the other hand, in polymeric structures.

Furthermore, also a combination of monomeric polymerization in presence of cross-linking agents is feasible.

With focus on the genesis of polymers by reaction of monomers, there are various techniques, however a main classification of reaction types can be drawn with respect to their kinetic process. Firstly, (i) step growth reactions can be performed for all organic components with two functional groups that are able to form a chemical bond [160]. In this polymerization, molecular weight increases slowly by random growth starting from a dimer that reacts with another monomer to form a trimer. Hence, there is only one continuous reaction that is responsible for polymer formation [161]. The final distribution is relatively broad whereas a very high conversion is required for a high molecular polymeric weight. On the next level, a classification in polyaddition and polycondensation for technical relevant engineering plastics like polyesters, polycarbonates or polyamides as well as reactions of isocyanides and ring-opening polymerization is feasible. Secondly, (ii) chain growth polymerizations represent the second category of reaction type. The mechanism is divided in several parts: initiation, propagation and termination are the three different modules. In contrast to step growth reactions, the monomer concentration decreases constantly within the polymerization. A high molecular weight of the formed polymer is generated in a very fast manner. Radical reactions are used very often for polymerization and are initiated by the radical formation from initiator molecules (for example homolytical cleavage of peroxides) and the transfer of the radical on the first monomer (for example a C-C-double bond). With addition of another monomer unit, chain growth is processed *via* formation of a macroradical [160]. By combination of two radicals, a covalent bond is generated which prevents further monomer coupling. A special form of this final stop mechanism is disproportionation and thus the production of a polymer with a terminal unsaturated group and another one with a saturated end-functionality. Among chain growth reactions, also ionic polymerizations are triggered by an active compound that starts the process. In comparison to radicals, cations or anions react in an electronically neutral solution in presence of a counterion and are initiated by Lewis- or Bronsted bases [162]. The charge of the terminal end group (for example C-C-double bond) is depending on vicinal substituents. Thus, groups having a donor effect like -OR, -NR₂, -C₆H₅, or -CH₃ [160] will favor the formation of positively charged ions and react *via* electrophilic addition with another

monomer. Functionalities like -CN, -COOR or -CONR₂, however, preferentially undergo anionic polymerization. Without addition of a terminating compound, chains will grow constantly due to similar charged ends and stay active in form of a living polymerization.

Furthermore, covalent linkages between polymer strands for gelation can be formed by different reactions or interactions regarding chemical or physical cross-linking. According to a review of Lu *et al.* [163], methods for physical interactions are based on non-covalent bonding. Formed junctions are usually temporary, however stable and strong enough to create a water-insoluble network. In contradiction, chemically cross-linked hydrogels can be prepared by (i) radical polymerization, (ii) reaction of complementary groups, (iii) enzymes or (iv) energy irradiation. The most common reaction for gelation is radical polymerization of monomers or radical cross-linking of hydrogel precursors whereas a chemical reaction occurs by forming a network. In some cases, a combination of low molecular weight monomers in the presence of a cross-linking agent is an established route for hydrogel formation. As explained before, it can be divided in several steps. This route is chosen for acrylates, amides or vinyl lactams. The good control over molecular weight and functionality is claimed for radical polymerizations [164]. Functionalities like amines (-NH₂) can be used to form hydrogels by referring to reactions with aldehydes in case of Schiff base formation [165] or thiols (-SH) that are clicked to C-C double bonds *via* radical Michael addition or thiol-ene-click chemistry [166]. Some formations are triggered by chemical or biochemical responses like pH-values, glucose or enzymes. The latter one exhibits a high specificity under mild conditions for hydrogels used as matrix for tissue engineering or in biomedical fields.

2.3.3 Hydrogels as drug delivery systems

With respect to a temporal regulation of drug release out of hydrogel systems, the big goal is to control the liberation at a certain time or to extend the duration of release [167] especially for highly metabolized or eliminated compounds [168]. With traditional dosage forms like tablets or injections, an initial increase in drug concentration is observed after application until the maximum concentration is

reached. Afterwards, the level drops down until the next administration of the drug. With sustained drug release, maximum peaks should be enhanced by reaching a constant liberation of the active pharmaceutical compound over the time between a maximum desired and minimum effective level [169]. The two different releasing profiles are depicted in **Figure 10 A** and **B**.

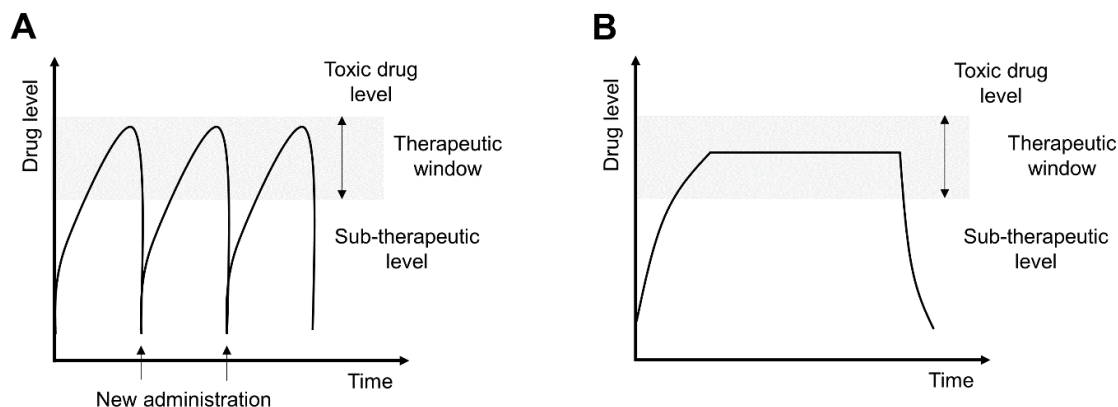


Figure 10:

Drug level curves of a traditional application form like tablets with several maxima after administration (**A**) as well as controlled release with a plateau phase in the therapeutic window over a longer period (**B**). Both graphs were adapted from [168-170].

Drug delivery in hydrogels is mainly based on the following three primary mechanism: (i) diffusion, (ii) swelling with afterwards diffusion processes for drug liberation and (iii) dissolution, degradation or erosion of the polymer matrix [169]. A distinction between the terms “degradation” and “erosion” refers to the mechanistical process behind the loss on polymeric mass. According to Uhrich *et al.* [168], degradation is based on a chemical bond cleavage whereas erosion can be described as decomposition of the material. With this change in chemical structure, APIs can be released *via* bulk erosion with the break of long polymer chains into smaller fragments thus a drug liberation is preferentially feasible. A second option are surface eroding systems where the hydrogel reservoir with the pharmaceutical compound is decreased in size and volume form the outside to the inner core by dissolution or degradation processes. Furthermore, referring to the definition of hydrogels, these 3D polymeric networks have the ability to imbibe > 20 % of its weight of water while staying stable. Such swelling-

controlled hydrogels are affected by changes in shape, mesh size of the polymeric network as well as increase in volume [171]. In a review of Qui *et al.* [172], numerous stimuli with respect to swelling followed by diffusion are explained that can also trigger drug release out of hydrogel matrixes. Here, they describe environment-sensitive hydrogels, for example pH-sensitive formulations where hydrogel precursors contain acidic (carboxylic groups -COOH) or basic (ammonium salts -NH₄⁺) groups that react on an environmental decrease or increase in proton (H⁺) concentration. Furthermore, temperature-sensitive structures are also well-established systems. A certain hydrophobicity is required that is given by hydrophobic alkyl groups like methyl (-CH₃), ethyl (-C₂H₅) or propyl (-C₃H₇). However, hydrophobicity should be handled with care for not losing dissolution capacity in water. In most cases, polymers increase their water solubility with increasing temperature. If polymers have a lower critical solution temperature (LCST), an inverse swelling behavior occurs that stimulates hydrogel formation. Other possibilities are glucose-sensitive systems for self-regulated insulin delivery and electric or light-sensitive hydrogels. Most of these structural changes are reversible and can be retracted or repeated by changing the environmental conditions to the initial state [169].

The most prominent and best characterized candidates for biodegradable systems is the class of poly(esters) with PEG-based copolymers, either PLA or PGA alone or in combination as PLGA and PCL [168]. The focus on PEG-based systems with the high variation in shape and molecular weight range increased due to the excellent protein resistance *in vivo* without toxicity [173]. Further applications of PEG-PLA copolymers that connect hydrophilic (PEG) with hydrophobic (PLA) properties were investigated by Han *et al.* [174] who used acrylate functionalities to generate cross-linked hydrogels.

2.4 Established dual setting systems and their comparison

Dual setting systems were firstly reported in 1999 by Dos Santos *et al.* [175] who described this new kind of mechanism. It is based on a simultaneous run of cement setting and the gelation process. The parallel run of both reactions favors interlocked cement crystals in a hydrogel. It is one approach that is used to tune mechanical performance of CPCs by shifting them from rather brittle characterization towards elasticity and ductility. The *in situ* formation of such hybrid materials, based on an inorganic network with an incorporated hydrogel, results in reduced interfaces between both matrixes with less fracture sites. Due to the soft gel phase, crystal growth and entanglement of the cement crystals is still possible and a homogenous distribution within the composite is guaranteed. However, crystal growth rate, crystal size as well as shape and form can be affected by the second phase.

The principle of preparation is illustrated in **Figure 11** where an aqueous low molecular weight monomer solution (orange) is mixed with a solid phase (grey), for example (i) α -TCP with favored formation of HA or (ii) a multi-phase powder of β -TCP and MCPA with conversion to brushite cement. After homogenous mixing, polymerization as well as setting reaction take place by generation of the dual setting system. However, also polymeric structures can be used for the gelation within the composite biomaterial by cross-linking and formation of networks or a combination of both procedures.

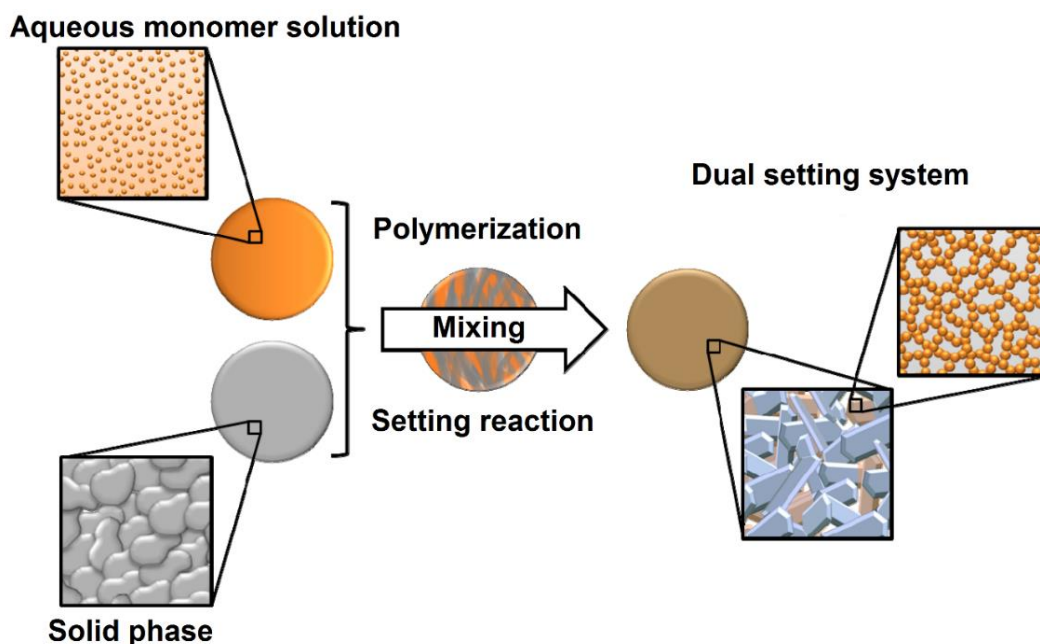


Figure 11:

Scheme illustrating the principle of a dual setting system based on an aqueous monomer solution that polymerizes in parallel to the cement setting reaction of a solid phase.

The inscription of the image was adapted whereas the scheme is reproduced from [176] as open access article distributed under the Creative Commons Attribution License which permits unrestricted use, distribution and reproduction in any medium.

In a review of Neumann *et al.* [177], several possible combinations of polymers and CPCs are listed in general, not only focusing on dual setting systems. The variation in inorganic CaP phase reaches from HA, fluorapatite or carbonated apatite to β -TCP as well as other CPCs. An even greater range of availability is given for the different kinds of biocompatible polymers, which can be incorporated *via* mechanical mixing or coprecipitation. Polyesters (PLA, poly (glycolic acid) (PGA), PCL), collagen or gelatin, respectively, alginate, chitosan and PMMA are reported in literature [177]. Shifting the focus now on the dual mechanism, less studies were already performed and published. Established systems including the developed formulations of this thesis are listed in **Table 5**, which gives an overview of different dual setting approaches based on CPCs, their hydrogel phases and various gelation mechanisms. As inorganic phase, both, apatite as well as brushite cements were investigated as matrix for this kind of reinforcement strategy. First reports date back to 1999, where Dos Santos *et al.* [175] firstly described the idea of the nowadays defined dual setting systems. Monofunctional acrylamide (AA) with an amount of 5-20 % was combined with the bifunctional *N,N'*-methylene

bisacrylamide (MBAM) (0.5-2 %) and radically polymerized using ammonium persulfate (APS) and *N,N'*-tetramethylethylenediamine (TEMED) as initiator system. With this co-existing of cross-linked poly(acrylamide) (PA) hydrogel in the cement bulk material, a remarkable increase in compressive strength was observed. X-ray diffraction (XRD) analysis proved the successful conversion from α -TCP to HA, however with a slightly slower transformation. One step further, the same working group published the first dual setting CPC modified with ammonium polyacrylate in 2003 [178]. Over the time, other research groups also focused on the development of dual setting systems trying different organic or inorganic phases. A multiplicity in combinations of CPCs (apatite or either brushite cement) with hydrogel matrixes can be found in literature ranging from polyHEMA networks [179] over six-armed isocyanate terminated polymers [180] to natural biopolymers like silk fibroin [181].

With respect to the new approaches in this thesis (see **Chapter 4** and **Chapter 5**), synthetic PEG-hydrogels as well as natural gelatin in combination with CPCs are briefly highlighted. Gelatin as natural biopolymer is often combined with CPCs in order to facilitate bone cell adhesion and migration [182]. Besides an improvement in mechanical properties, these hybrid materials also accelerate the hardening process of the inorganic matrix [183]. Furthermore, gelatin can be used as porogen in HA-matrixes to trigger the formation of porous scaffolds [184]. However, there is no report on a dual setting mechanism in combination with brushite cement. PEG was added to CPCs in order to create malleable, formable “pastes” that can be used for example as bone waxes with hemostatic and osteoconductive properties [185]. During cement setting, PEG gets dissolved by interpenetrating water that is needed for the dissolution-precipitation reaction.

Regarding pharmaceutical application, Habraken *et al.* [186] also reported on composites used for drug delivery. Both, the incorporation of ceramic particles in polymeric carriers with extension in osteogenic proteins as well as CPC scaffolds with polymeric addition that, depending on the structure, also facilitate higher degradation rates. With respect to drug loading, initial bursts are reduced, and sustained effects are generated by this organic phase.

Apart from organic monomers, also combinations of two inorganic materials resulted in the concept of a dual setting system shown by Geffers *et al.* [187] who modified a brushite forming cement paste with a second inorganic silica-based

precursor generated by hydrolysis and condensation of tetraethyl orthosilicate (TEOS). With a decrease in pH while cement setting, a simultaneously initiated condensation led to an incorporated composite with infiltrated CPC macropores by a microporous silica gel.

Further strategies to improve mechanical properties and to overcome brittleness are fiber reinforced constructs as well as nanocomposite formulations. The first one is a toughening strategy for brittle CPCs to enhance fracture resistance by incorporation of different kind of fibers. In a review of Krüger *et al.* [188], a recapitulation of the state of the art of fiber-reinforced research was drawn in the year 2012. They compiled an overview of mechanical properties like increased strength or ductility and thus energy absorption, biological evaluation (both *in vitro* and *in vivo*) as well as some existing clinical data. An example for higher flexible behavior was investigated in a study based on C-fibers in an HA matrix where the fiber surface was chemically modified to adjust the interface of both components. By that, an increase in bending strength from 9.2 ± 1.7 MPa up to 38.4 ± 1.7 MPa [189] was obtained. The second strategy, nanocomposites, can be described as multiphase solid materials by nanostructures that are embedded in a ceramic or polymer matrix within a nanometer scale (≥ 100 nm) to avoid crack spreading. By that, also flexibility can be increased in a very high range. *In situ* forming silica matrixes that were prepared by sol-gel processing are for example combined with non-reactive CaP particles that modify physical properties [190].

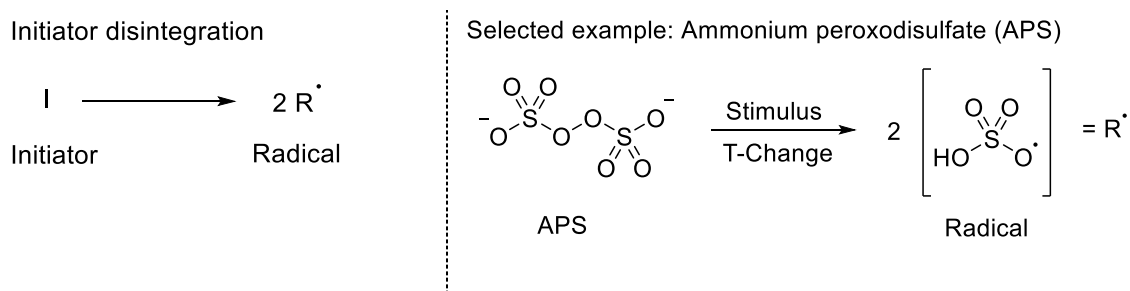
Table 5:

Overview of different dual setting systems based on apatite and brushite forming cements in combination with different hydrogel systems.

CPC-phase	Hydrogel-phase	Gelation mechanism	Ref.
Hydroxyapatite	AA and ammonium PA	Radical polymerization (APS/TEMED)	[178]
Hydroxyapatite	2-Hydroxyethyl methacrylate (HEMA) or an advancement with PEG-PLLA-DMA cross-linker	Radical polymerization (APS/TEMED)	[179] and Chapter 3 (see also [191])
Hydroxyapatite	Glycidyl methacrylated dextran (Dex-MA)	Radical polymerization (APS/TEMED)	[192]
Hydroxyapatite	Six-armed star-shaped molecule functionalized with isocyanate groups as reactive termini (Star-P(EO- <i>stat</i> -PO))	Reaction with nucleophiles (for example water) with conversion from isocyanates to carbonyl diamides	[180]
Brushite	Silk fibroin	Physical cross-linking due to a conformation change induced by acidic pH-values	[181]
Brushite	PEG-DMA either in high or low molecular weight and PEG-PLLA-DMA as hydrogel precursors	Radical polymerization (ascorbic acid/hydrogen peroxide)	Chapter 4 (see also [193])
Brushite	Gelatin	Chemical cross-linking <i>via</i> genipin due to reaction with primary amines in biopolymer backbone	Chapter 5

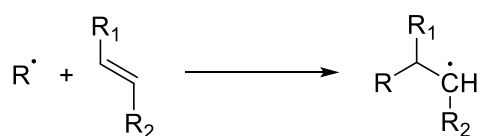
2.4.1 Variation in cross-linking reaction mechanisms

One prominent mechanism used for the formation of hydrogels simultaneously to the cement setting is polymerization of monomeric compounds based on radical reactions. APS as thermally induced initiator in combination with the catalyst TEMED was chosen for the breakthrough of the first dual setting systems by Dos Santos *et al.* [175, 178] and further developments of Wang [192] or Christel *et al.* [179]. Within the cement matrix, FRP takes place in an aqueous medium whereas the initiator was mixed in the solid phase and TEMED was added to the liquid phase. In a previous step, reactive, radical species have to be generated *via* homolytical disintegration, which can be thermally or photo chemically induced (for example by Irgacure[®] 2959). With respect to biological testing, the effective dose should be as much as needed, but as less than possible. Furthermore, also redox reactions can be the source of radicals when they are produced during intermediate stages. In an (i) initial stage, these radicals then react with monomers and form the start for the following chain growth. Newly generated radicals increase the chain by addition of further radicals in the so called (ii) propagation. Polymerization stops by combining two radicals either in a combination step, a disproportionation forming (un-) saturated molecules or a parallel sequence of both. This kinetical distinction between these two (iii) termination reactions is for example temperature-dependent: with increase in temperature, disproportionation is favored [160]. The interaction of all these processes is very complex and even more tricky running in an inorganic matrix. An overview of the general FRP process with APS as selected initiator example is depicted in **Scheme 1**.

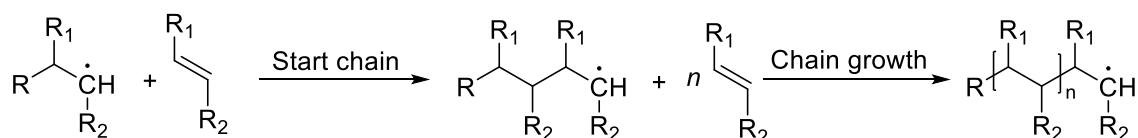


Chapter 2

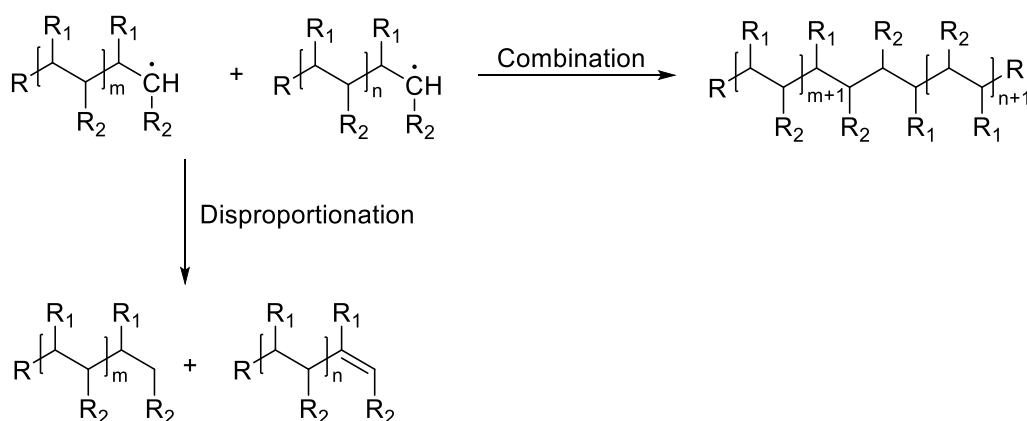
1. Initiation



2. Propagation



3. Termination

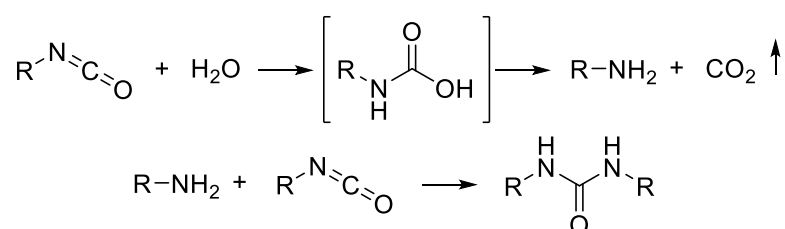


Scheme 1:

Different steps of a free radical polymerization (FRP). A previous disintegration of the initiator (for example thermally induced by APS) starts the reaction with following (i) initiation, (ii) propagation as well as (iii) termination with a combination of two radicals resulting in (un-) saturated molecules [160].

A second reaction mechanism in a dual setting system composed of HA and six-armed star molecules functionalized with isocyanate groups as reactive termini (NCO-sP(EO-*stat*-PO)) is based on a nucleophilic reaction of the electrophilic isocyanate functionality with water molecules (H₂O) provided by the aqueous 2.5 wt% diammonium hydrogen phosphate ((NH₄)₂HPO₄) solution as liquid phase of the setting reaction. In this case, cross-linking of polymeric structures occurs *via* hydrolysis to amines upon carbon dioxide release as driving force for reaction equilibrium on product site with an in-between intermediate state forming a carbamic acid derivate (see **Scheme 2**). In another reaction of an

isocyanate with the previously formed amide, the nucleophilic attack results in a stable carbonyl diamide structure. Rest R is the polymer backbone with a molecular weight of 12 kDa and a composition of statistically copolymerized propylene oxide (PO; 20 %) and ethylene oxide (EO; 80 %) [194].



Scheme 2:

Reaction of isocyanates with the nucleophile water upon a carbamic acid-based intermediate step with formation of amines upon release of carbon dioxide. With attack of another isocyanate, the final urea-derivate is formed. In this case, gelation occurs *via* cross-linking of polymeric structures.

Besides chemically cross-linked hydrogels in dual setting systems, also physical interactions that induce gelation play an important role in already established formulations (see **Table 5**). A prominent example for this approach is silk fibroin [181], which is a water-soluble protein upon its α -helical and random coil conformation. Gelation occurs *via* sol-gel transition that is triggered by a conformational change on a molecular level. By shifting α -helical and random coil conformation to the more stable β -sheet form, cross-linking and stabilization of the gel is performed [195]. Different parameters like pH-value, ionic interactions, concentration or temperature directly influence the gelation. Decreasing the pH to acidic conditions by matching the silk fibroin solution with brushite forming cement, firstly weak interchain hydrogen bonds and hydrophobic interactions are generated with a second formation of stable β -sheet protein structures. Hydrogel systems based on gelatin follow a similar conformational change. Hereby, α -chains of the biopolymer arrange in helical structures upon hydrophobic elements (especially the amino acids phenylalanine (Phe), proline (Pro) and hydroxyproline (Hyp). Furthermore, a stabilization occurs due to local development of inter- or intrastrand hydrogen bridges [141]. Additionally, water molecules are incorporated and

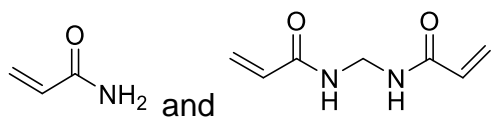
interact with hydrophilic hydroxy groups of amino acids with an additive gel stabilization effect.

2.4.2 Variation in organic and inorganic phase

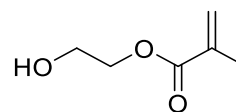
The diversity in different kind of hydrogels is not restricted in general, however a limitation exists in matching both phases in the hybrid material and creating a phase compatibility. With silk fibroin as representative for a natural biopolymer, cross-linking was performed by decrease in pH with an irreversible conformation change on macromolecular protein level [181]. Furthermore, glycidyl methacrylated dextran (Dex-MA) as modified biopolysaccharide was mixed with CPC raw powder and afterwards with the initiator APS as well as accelerator TEMED [192]. Besides the third candidate gelatin that was investigated in this thesis (see **Chapter 5**), the other dual setting systems used synthetic monomers for polymerization. Acrylamides (AA, MBAM, PA) were used in the first studies of Dos Santos *et al.* [175, 178], where a composite material with improved compressive (55 MPa that corresponded to an enhancement of 149 %) and tensile strength (21.2 MPa that corresponded to an augmentation of 69 %) was created. Bifunctional cross-linking agents in acrylic hydrogels are commonly used for superabsorbent materials [196]. However, the idea creating a polymer-cement-composition was new and at the same time inspiring for other researchers. By maintaining the radical initiator system of APS and TEMED, a new approach was developed based on polyHEMA and HA. In this study [179], the hydrogel network was generated by FRP of HEMA-monomer units with the cross-linking agent ethylene glycol dimethacrylate. Furthermore, due to purification procedures, the purchasable quality often contains these bifunctional molecules and enables gelation [197]. The advancement of this approach with the dimethacrylated PEG-poly(lactic acid) hydrogel precursors PEG-PLLA-DMA (see **Chapter 3**) was laying the foundations for further developments focused on a degradable dual setting system [193].

Scheme 3 depicts an overview of the chosen hydrogel precursors for gelation as interpenetrating network in an inorganic cement matrix.

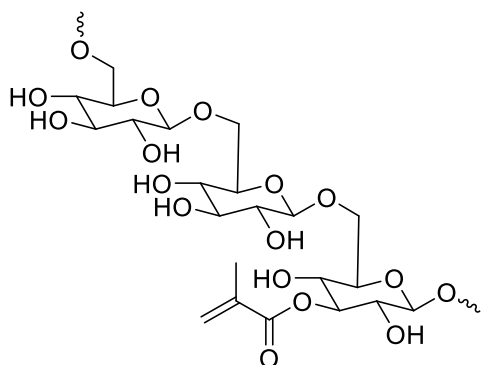
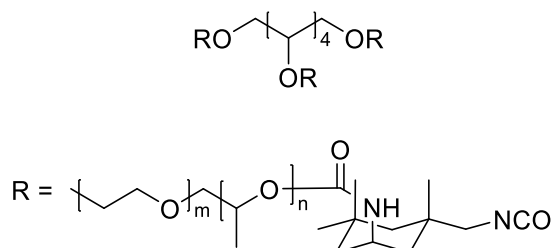
AA and MBAM



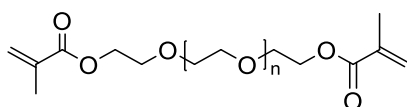
HEMA



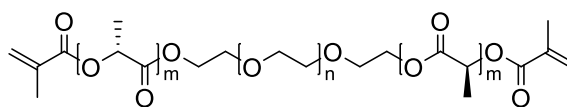
Dex-MA

Six-armed star-shaped macromer with
statistical copolymer backbone(NCO-sP(EO-*stat*-PO))

PEG-DMA



PEG-PLLA-DMA

**Scheme 3:**

Overview of monomers used in established dual setting systems polymerizing to incorporated hydrogels in an inorganic matrix.

Differences in strength for dual set composites are strongly depending on the fact if the inorganic phase is composed of apatite or brushite forming cements. In general, even HA without polymeric addition facilitates higher compressive strength levels up to 900 MPa in comparison to DCPD with only 60 MPa [23]. This is, of course, controlled by the PLR, the particle size and shape of the raw powder, porosity as well as density and degree of entanglement of the crystal network. However, both CPC classes are attractive for the formulation development of dual setting systems correlating to the desired properties and potential applications.

Chapter 3

Tough and elastic α -tricalcium phosphate cement composites with degradable PEG-based cross-linker

Chapter 3 was published as original research article (Michaela Rödel, Jörg Teßmar, Jürgen Groll, Uwe Gbureck, Tough and elastic α -tricalcium phosphate cement composites with degradable PEG-based crosslinker in *Materials*, 2019, pp. 53), reproduced from [191] as open access article distributed under the Creative Commons Attribution License which permits unrestricted use, distribution and reproduction in any medium.

The article is based on work of the author of this thesis Michaela Rödel, who performed all experiments, data evaluation and composition of the manuscript.

3.1 Abstract

Dual setting cements composed of an *in situ* forming hydrogel and a reactive mineral phase combine high compressive strength of the cement with sufficient ductility and bending strength of the polymeric network. Previous studies were focused on the modification with non-degradable hydrogels based on polyHEMA. Here, we describe the synthesis of suitable triblock degradable PEG-PLLA cross-linker to improve the resorption capacity of such composites. A study with four different formulations was established. As reference, pure HA cements and composites with 40 wt% HEMA in the liquid cement phase were produced. Furthermore, HEMA was modified with 10 wt% of PEG-PLLA cross-linker or a test series containing only 25 % cross-linker was chosen for composites with a fully degradable polymeric phase. Hence, we developed suitable systems with increased elasticity and 5-6 times higher toughness values in comparison to pure inorganic cement matrix. Furthermore, conversion rate from α -TCP to HA was still about 90 % for all composite formulations whereas crystal size decreased. Based on this material development and advancement for a dual setting system, we managed to overcome the drawback of brittleness for pure CPCs.

3.2 Introduction

Bone is often described as natural miracle due to its impressive mechanical properties. On the one hand, it has a very high load-capacity of ~ 90-190 MPa [8] for cortical bone, while at the same time it provides elastic and ductile properties with a high fracture resistance. This high stability is based on its structural composition as natural bone is a composite mainly consisting of apatite, collagen and water [1, 198]. This leads to the idea to mimic bone structure in synthetic materials by combining an inorganic phase based on CPCs with an organic polymeric matrix.

CPCs are widely used as substitutes for non-load bearing defects. They are promising materials for replacement of damaged bone and formed from a solid raw powder and a liquid phase [199]. According to the chosen pH-values during setting reaction as well as different solubility product constants K_{sp} , one can distinguish between brushite ($\text{pH} \leq \sim 4.2$) and apatite ($\text{pH} \geq \sim 4.2$) forming cements. The latter one is clinically a very well established system due to its outstanding properties like bioactivity, osteoconductivity [200] and stoichiometric similarity to mineral components present in bone and teeth [48]. Furthermore, Bohner [23] describes an “excellent” biocompatibility of apatite CPCs despite their slow biodegradability. The drawback of such cements is their inherent brittleness and low tensile and bending strength, which can be overcome by either fiber reinforcement or by creating dual-setting cement systems [176]. The latter is characterized by a simultaneous cement setting reaction and polymerization of organic additives, which consequently form a homogenous and incorporated network. Previously described dual setting cement systems are mainly based on HA forming cements modified with organic matrices such as PA [178], glycidyl methacrylated dextran [192] or six armed star molecules functionalized with isocyanate groups as reactive termini (NCO-sP(EO-*stat*-PO) [180]. Furthermore, Christel *et al.* [179] reported on a dual setting system with HEMA as water soluble, polymerizable monomer in the liquid solution. The gelation was performed *via* radical polymerization using APS and TEMED as radical system. With incorporation of a polyHEMA network, mechanical properties could be improved without influencing workability and processability of this cement system. However, polymerization of

this monofunctional monomer only results in non-cross-linked polymeric chains, which form a dense entangled and non-degradable network.

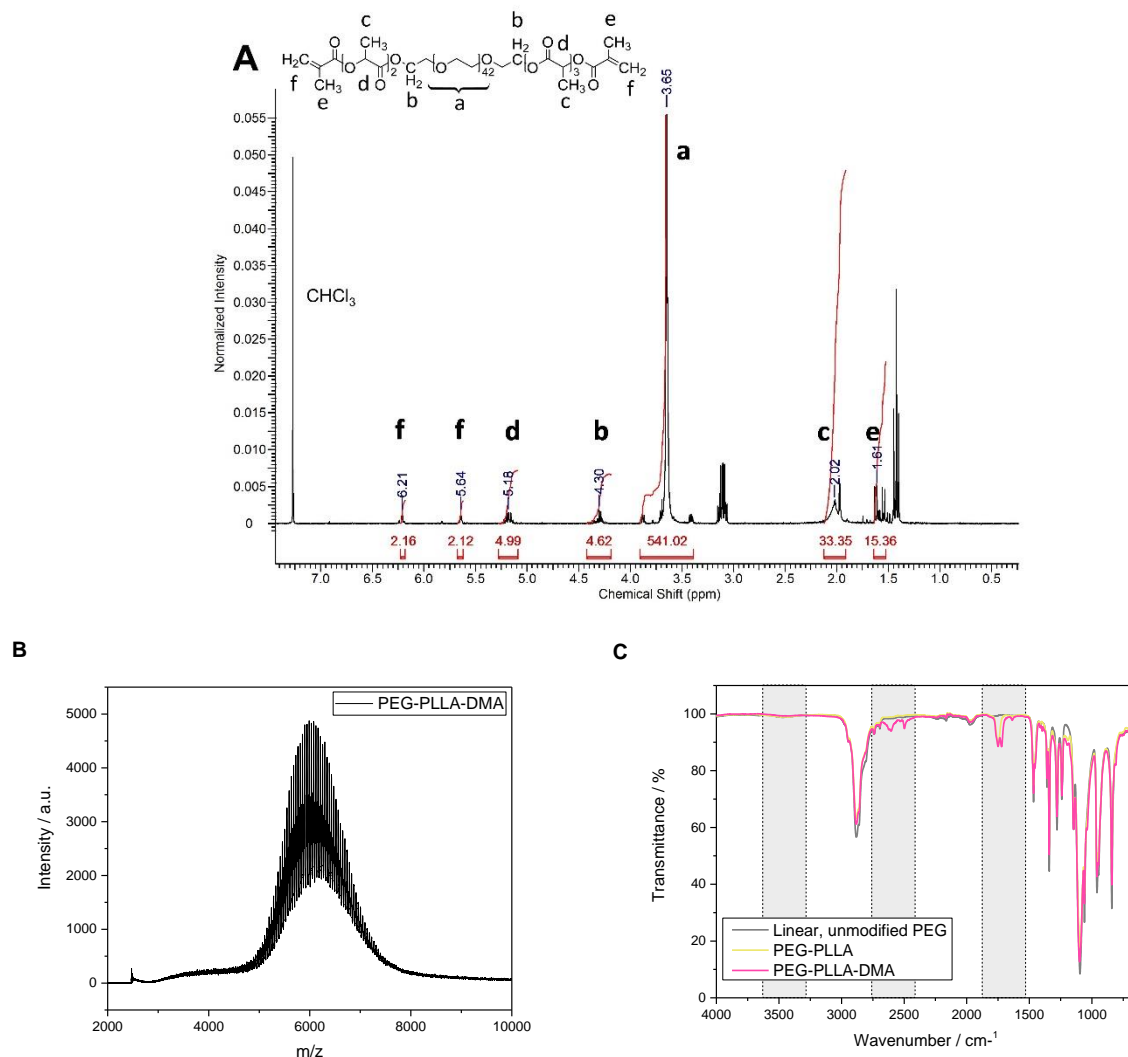
Here, we further modified this cement system by the addition of a degradable PEG-PLLA cross-linker, which is thought to further ameliorate the mechanical properties of the system and increase bending strength and ductility [193]. Focusing on HA, which has a high similarity to the mineral component of bone tissue, the following study was performed using α -TCP with a 2.5 wt%- Na_2HPO_4 -solution as accelerator for the setting process. Both, PEG-PLLA hydrogels and cement composites were thoroughly characterized regarding their mechanical properties and the influence of the modification on the cement setting reaction was investigated.

3.3 Results

3.3.1 Cross-linker and hydrogel characterization

3.3.1.1 Cross-linker characterization

Briefly, the successful synthesis of the linear triblock cross-linker based on PEG and PLA-units was verified by ^1H NMR spectroscopy (solvent CDCl_3 : $\delta = 1.61$ (s, methyl group methacrylic acid), $\delta = 2.02$ (s, methyl group lactic acid), $\delta = 3.65$ (s, H of PEG backbone), $\delta = 4.30$ (m, H next to ester bonds of PEG backbone), $\delta = 5.18$ (m, H in lactic acid), $\delta = 5.64$ and $\delta = 6.21$ (s, methylene groups). Calculated number of protons corresponds well to theoretical values (see **Figure 12 A**). Further *N,N*-dimethylformamide (DMF)-GPC analysis in the current study confirmed a monomodal distribution and narrow dispersity of $\mathcal{D} = 1.08$ ($M_n = 6,789 \text{ g}\cdot\text{mol}^{-1}$, $M_w = 7,330 \text{ g}\cdot\text{mol}^{-1}$ in comparison to the expected value of $6,498 \text{ g}\cdot\text{mol}^{-1}$; chromatogram not depicted). Also, matrix-assisted laser desorption-ionization time-of-flight mass spectrometry (MALDI-ToF) measurements showed a mean molar mass of $6,077 \text{ Da}$ and clearly detectable PEG-units with $m/z = 44$ (see **Figure 12 B**). Moreover, FTIR measurements revealed additional absorption bands for the first and second ester bond ($\nu = 2,300 \text{ cm}^{-1}$ and $\nu = 1,725 \text{ cm}^{-1}$). Unmodified, linear PEG with free hydroxy groups at both sides showed a strong signal of the PEG-backbone with its CH-valence vibration ($\nu = 2,875 \text{ cm}^{-1}$) and a slight alcohol OH-stretch at $\nu = 3,455 \text{ cm}^{-1}$. With esterification of the end functionalities, another signal appears in the wavenumber range of the corresponding carboxylic ester stretch at $\nu \approx 1,725 \text{ cm}^{-1}$. In the second step of the synthesis, terminal PLA-units are transformed with methacrylic acid units and the incorporation of double bonds. The equivalent alkenyl C-C-double bond stretch appears at $\nu \approx 2,300 \text{ cm}^{-1}$ (see **Figure 12 C**).

**Figure 12:**

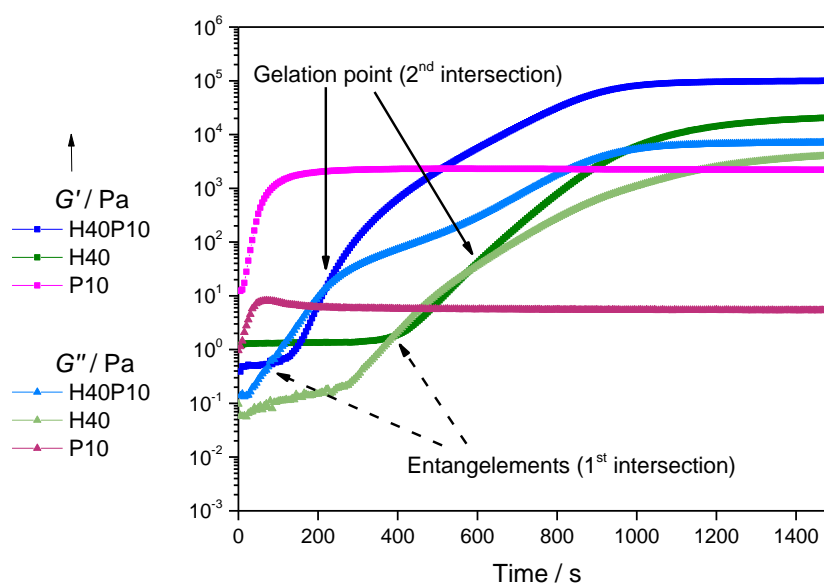
Characterization of cross-linker synthesis. PEG-PLLA-DMA hydrogel precursor was produced *via* two-step mechanism with ring-opening polymerization and afterwards functionalization with methacrylic groups on both terminal hydroxyl groups. Both, ¹H NMR (**A**) and FTIR spectra (**C**) confirmed the successful synthesis of triblock monomers. DMF-GPC measurements (no elugram shown) as well as MALDI-ToF analysis (**B**) revealed a polymer in the theoretically expected range of 6,498 Da.

3.3.1.2 Hydrogel characterization

In order to characterize the gelation process, which occurs simultaneously to the cement setting reaction in the dual compound system, the gel point was determined *via* oscillating rheology. Therefore, time sweeps of the three different polymeric systems containing 40 wt% HEMA, 10 wt% PEG-PLLA-based hydrogel precursor (P10) or a combination of both (H40P10) were investigated (see **Figure 13 A**). Two cross-over points for the formulations with HEMA could be observed.

The first was detected after 385 s (= 6 min 25 s) with a second intersection after 585 s (= 9 min 45 s). Due to the effect of short chain entanglements or aggregation of the monomers, there is a domination of the elastic properties at the beginning of the measurement. After destruction of the formed pre-structures in solution, the loss modulus G'' dominates and the starting properties for an initial gelation are regained. The second intersection of storage modulus G' and loss modulus G'' is determined as gel point of the polymeric systems. For the hydrogel composed of HEMA and cross-linker (H40P10), the first intersection is reached earlier after 70 s (= 1 min 10 s) due to an increase in reaction kinetics with fast gelation of the cross-linker. With respect to this higher reactivity of the synthesized cross-linker, it was not possible to measure the intersection of both moduli for the hydrogel formation of the batch based on 10 wt% PEG-PLLA-DMA (P10) in the given time frame of less than one minute caused by initializing and starting processes of the rheometer.

A



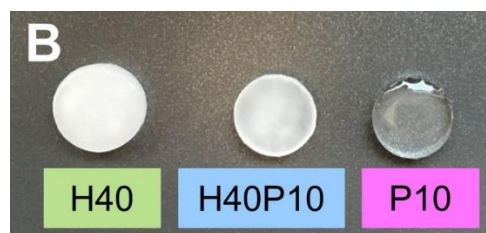


Figure 13:

Gelation point measurements of the different pure hydrogel systems composed of 40 wt% HEMA (H40), 10 wt% PEG-PLA-based hydrogel precursor (P10) or a combination of both (H40P10) at 16 °C over 30 min (A). Image B depicts the structure of the different hydrogel samples with a very turbid and milky look of the HEMA sample to the clear and transparent PEG-PLLA-hydrogel.

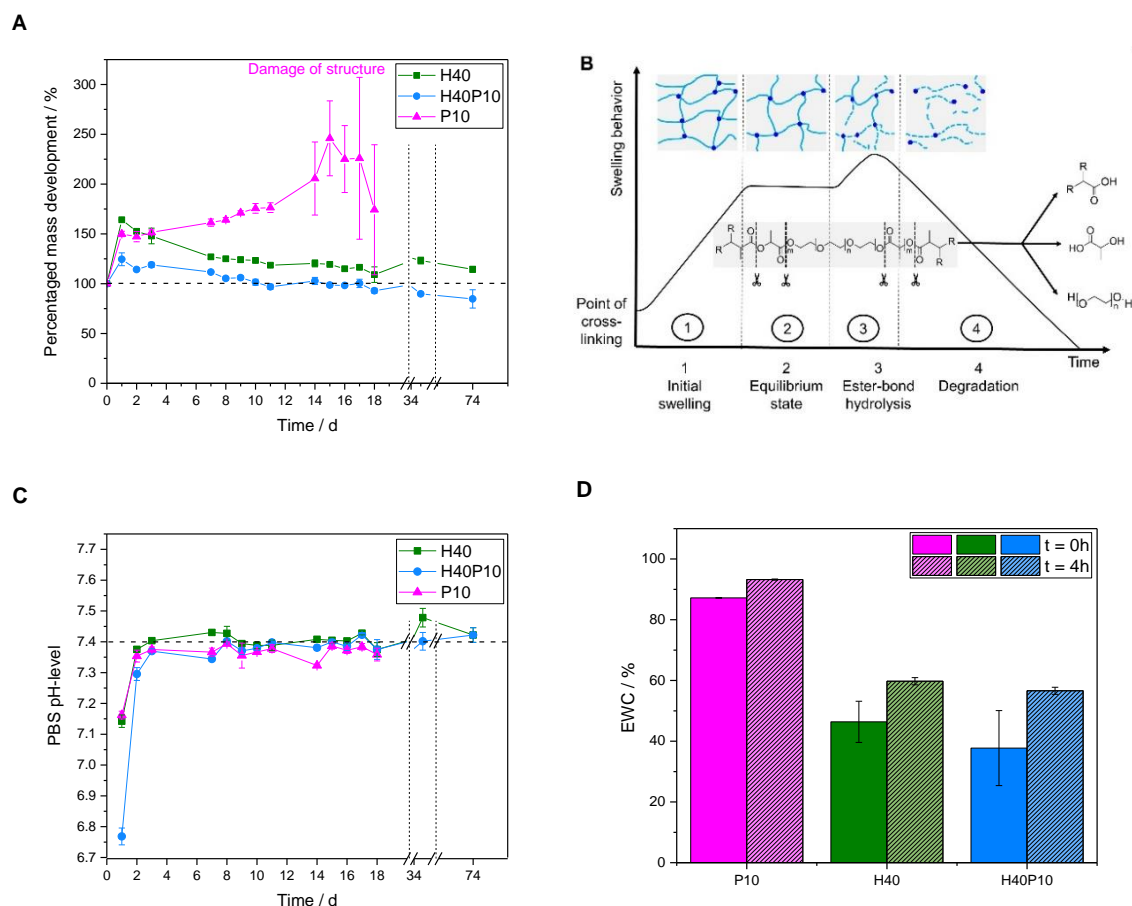
With addition of the cross-linker, the elastic behavior of the system could be improved in the way that the elastic modulus G' , which refers to the stored deformation energy in the system, reached a level of about 10^5 Pa. The elasticity corresponds also to the water content in the different gel systems. The pure PEG-PLLA-gel system behaved like a typical hydrogel system with a wide polymer network, exhibiting the highest equilibrium water content (EWC; see **Figure 14 D**) and a duplication of the swelling ratio Q_v from 7.81 ± 0.05 for $t = 0$ h to 14.82 ± 0.40 after 4 h. Both batches containing HEMA (H40 and H40P10) were dominated by the presence of a high number of short chain molecules and a denser hydrogel network. Consequently, produced samples were not transparent and showed lower Q_v -levels (H40: $t = 0$ h = 1.90 ± 0.26 , $t = 4$ h = 2.49 ± 0.07 ; H40P10: $t = 0$ h = 1.66 ± 0.29 , $t = 4$ h = 2.31 ± 0.06). Gels of the different batches are depicted in **Figure 13 B**.

3.3.1.3 Degradation behavior of hydrogels

Regarding the degradation behavior of the different samples in phosphate buffered saline (PBS), the samples containing polyHEMA in a relatively high amount of 40 wt% (H40) showed an initial mass increase with a slight decrease to constant values over 10 weeks. Furthermore, no swelling was observed and the constructs were still round shaped and without any cracks or missing parts. This effect of a polyHEMA-based polymeric network was also investigated for gels combined with high molecular weight cross-linker. By incorporation of a degradable hydrogel precursor in a weight amount of 10 wt% (H40P10), the short chain-polymeric system was still dominating. After one day, mass increased about 25 % but turned

into a stable hydrogel formation over the time with an almost constant mass for approximately 10 weeks observation (see **Figure 14 A**).

Additionally, hydrogels of pure PEG-PLA-based cross-linker (P10) were analyzed. At the beginning, an increase in mass of about 50 % was observed. Hydrogels behaved like expected for ester-containing substances (see **Figure 14 B**): after point of cross-linking, a certain equilibrium state for the water-up-take of the hydrogel network was reached. This period lasted for about 12 days, until ester bond hydrolysis started. Samples became instable, fragmented and were broken after 18 days (see **Figure 14 A**; damage of the structure). Due to the breakdown of the structure indicated by the decrease in mass and high standard deviations due to the loss of fragments, a mass determination was not feasible any more. This was only observed for P10, whereas for HEMA-containing formulations the short and low molecular weight polymers are the dominating factor. In addition to mass change development, pH-values of PBS storage solution were measured. First pH-levels of all batches (day 1) started in acidic regions of 6.75 for H40P10 and 7.15 for H40P10 as well as P10. After three days, reached values were in the physiological range about a pH of 7.4 (see **Figure 14 C**). To characterize also uptake of water, EWC of the different hydrogels was determined in the range of immediately after production ($t = 0$ h) and after 4 h. Hydrogels based on synthesized cross-linker showed a very high EWC of about 80-90 % after 4 h. In contrast to that, gels based on polyHEMA (H40 and H40P10) reached lower EWC-values of about 40 % for the first time point and increased up to 50 % after 4 h (see **Figure 14 D**).

**Figure 14:**

Overview of the gel characterization for the specimens with 40 wt% HEMA (H40), a combination of HEMA and cross-linker (H40P10) and the pure PEG-PLA triblock hydrogel with 10 wt% polymer (P10). The different batches were analyzed regarding mass development in PBS buffer at pH 7.4 (**A**), pH-level of the storage medium (**C**) as well as EWC (**D**). Additionally, a schematic curve of the degradation study corresponds to obtained data (**B**).

3.3.1.4 Determination of methacrylate units in gelation as well as degree of modification

Free methacrylic acid added to the eluent was used as standard for calibration within the range of $0.05\text{-}280\ \mu\text{g}\cdot\text{mL}^{-1}$. A linear correlation with a regression coefficient R^2 of 0.9997 and a linear equation of $y = 49,645x + 63,906$ was obtained for calibration (see **Figure 15 A**). Furthermore, retention time (R_t) of the analyzed compound was 4.3 min within a run duration of 10 min. **Figure 15 B** gives an overview of a chromatogram at $\lambda = 210\ \text{nm}$ showing the pure hydrogel precursor as control, the hydrolyzed hydrogel itself as well as a methacrylic acid standard with a concentration of $0.5\ \text{mg}\cdot\text{mL}^{-1}$. High performance liquid chromatography (HPLC)-measurements verified a very high degree of cross-

linking efficiency by reaching $92.95 \% \pm 1.45$ of acid units for PEG-PLLA-DMA-hydrogels (see **Figure 15 C**).

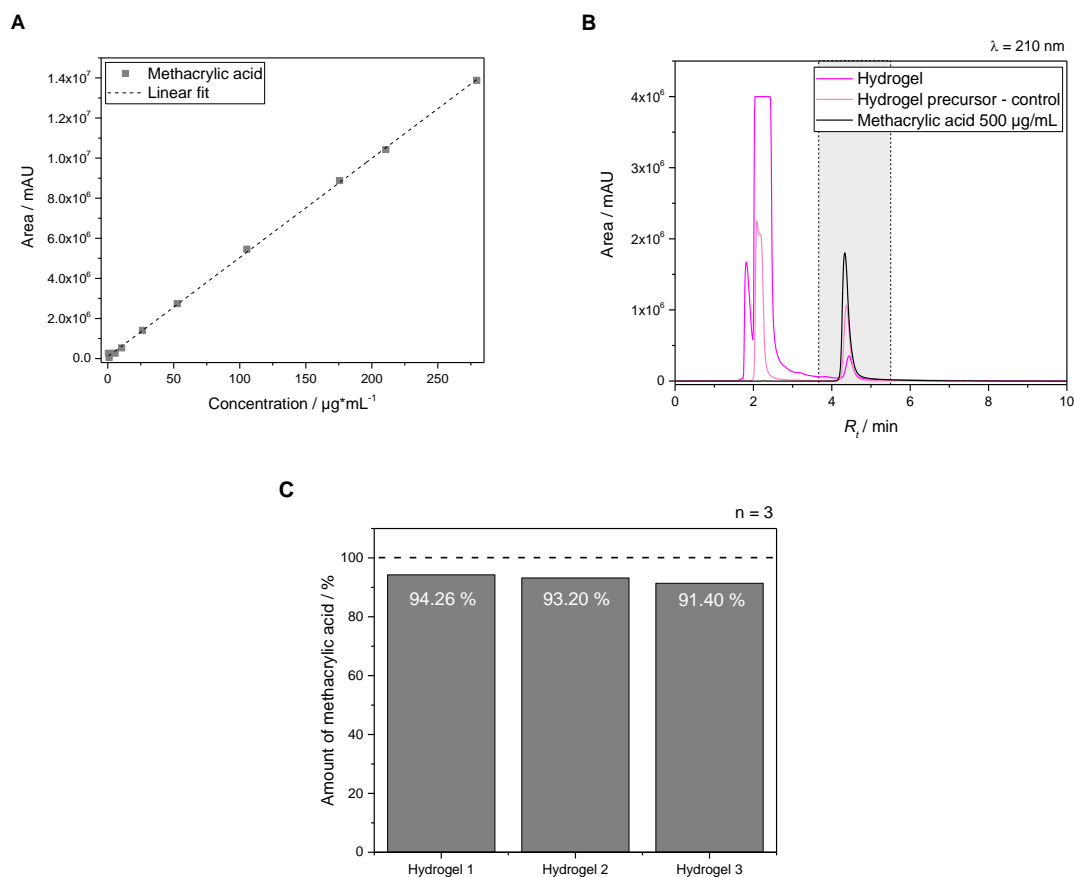


Figure 15:

Determination of methacrylic acid units for degree of modification as well as incorporation of functions for gelation. HPLC was used as method for quantification. Calibration curve of methacrylic acid standards (**A**) as well as a chromatogram (**B**) showing hydrogel, control and standard profile are depicted. Furthermore, the total amount per PEG-PLA-based hydrogel was in the range of 92.95 ± 1.45 (**C**).

3.3.2 Inorganic reference and composite characterization

3.3.2.1 Determination of initial setting time

Initial setting times of pure HA and all composite formulations were analyzed *via* Gillmore needle test with a customized device (set up see **Figure 16 A**). Significant differences in setting times were observed with about 180 s (= 3 min) for the reaction of α -TCP to HA without any additives in the liquid or solid phase, respectively. Simultaneous gelation reactions that run in parallel to cement setting

decreased the initial setting time to less than 120 s (= 2 min) for a polyHEMA-based composite material (H40). Batches with 25 wt% polymeric hydrogel precursor showed even faster setting reactions less than 60 s (= 1 min). This polymer was the dominating factor for the as well very quick conversion and concurrent hydrogel formation for batch H40P10 with 40 wt% HEMA and 10 wt% cross-linker (see **Figure 16 B**).

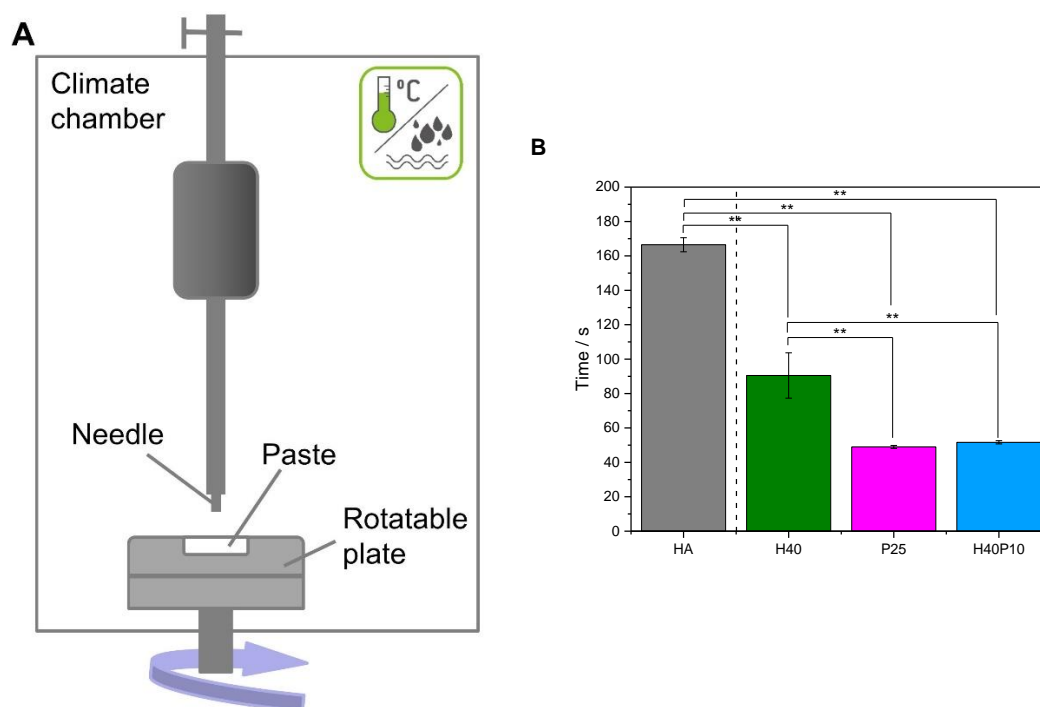


Figure 16:

Performance of Gillmore needle test for determination of initial setting times. Part **A** depicts the set-up of the used equipment with an overview of results (**B**) measured for the pure inorganic reference HA in comparison to the composite formulations with 40 wt% HEMA (H40), HEMA in the same concentration combined with 10 wt% degradable cross-linker (H40P10) as well as a hydrogel produced out of 25 wt% polymer (P25).

3.3.2.2 Analysis of parameters of biological and material technological relevance

The additional polymer phases incorporated in inorganic matrix also influenced initial pH-development. Pure HA showed a setting reaction under alkaline conditions with a basic pH-maximum of 9.4 after 2 h. A drop down of the pH-level after 24 h resulted in a still decreasing plateau phase under the physiological pH-level (see dotted line in **Figure 17 A**). By addition of polyHEMA and/or PEG-PLA-based cross-linker, respectively, maximum pH-values decreased to a pH of 8 with

a relatively constant and slow shift to 7.4. No swelling or increase in mass was observed over 8 d of storage (see **Figure 17 B**). Moreover, all PBS media showed acidic conditions after 2 d in the range of 6.7-6.9. Over two weeks, pH-values increased up to 7.0-7.2 and approximated a pH-level of 7.4 (see **Figure 17 C**).

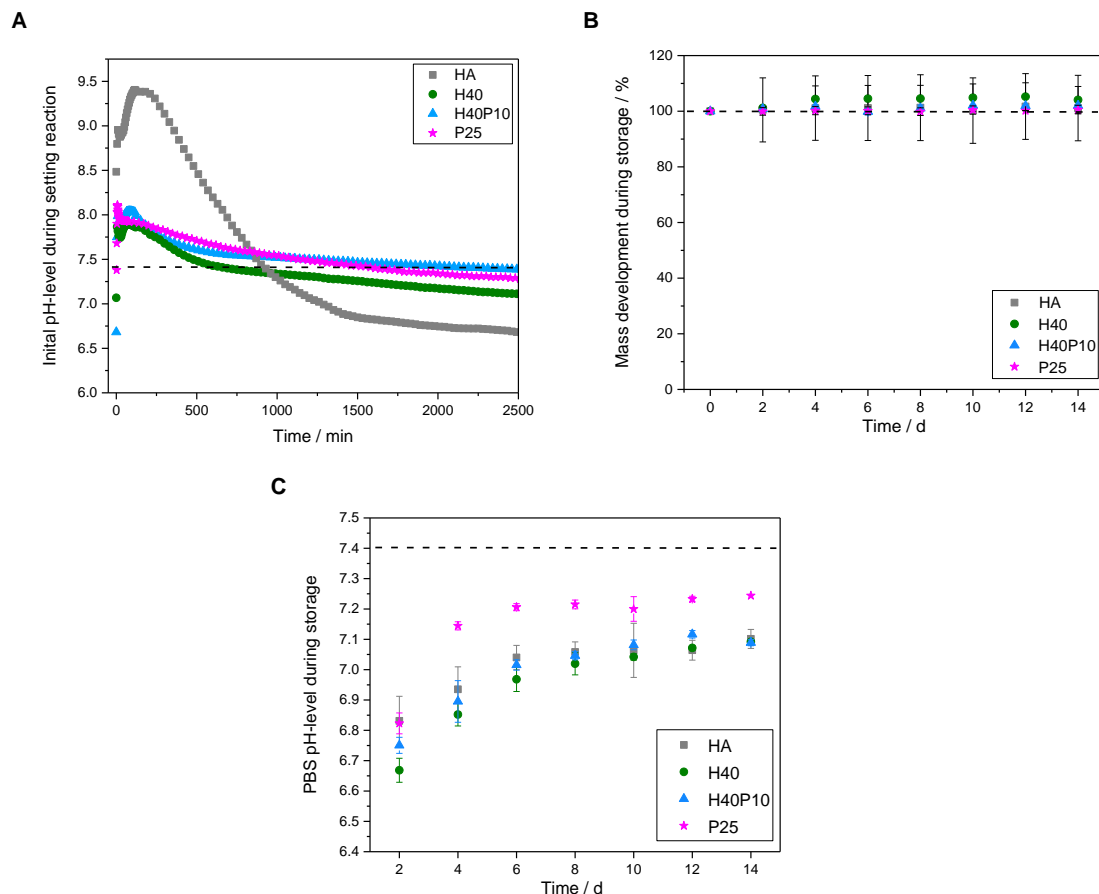


Figure 17:

Analysis of different parameters for characterization of composite formulations. Regarding material technological relevance, initial pH-level during setting was measured (**A**). Furthermore, mass development during storing was observed (**B**). With respect to biological relevance, pH-levels of PBS storage solutions were determined (**C**).

3.3.2.3 XRD measurements and Rietveld refinement

Particles or a second phase in a CPC matrix always influence conversion rate as well as crystal growth. Their characterization was performed for HA as pure inorganic reference as well as composite materials. Without polymeric addition, XRD diffractograms showed a decrease in α -TPC signal intensity and

corresponding increase for the prominent HA diffraction pattern at 26°. This disappearance revealed an almost complete conversion after 14 days of storage under physiological conditions (100 % relative humidity, 37 °C). Therefore, both reference pattern of the reactant (α -TCP) and the product (HA) were added (see **Figure 18 A**). In general, a hydrogel incorporation based on polyHEMA and/or cross-linker resulted in a slower conversion and setting reaction from α -TCP to HA (see **Figure 18 B-D**). Moreover, with added polymeric phase, diffraction patterns were slightly shifted from crystalline to a more amorphous character for the composite materials.

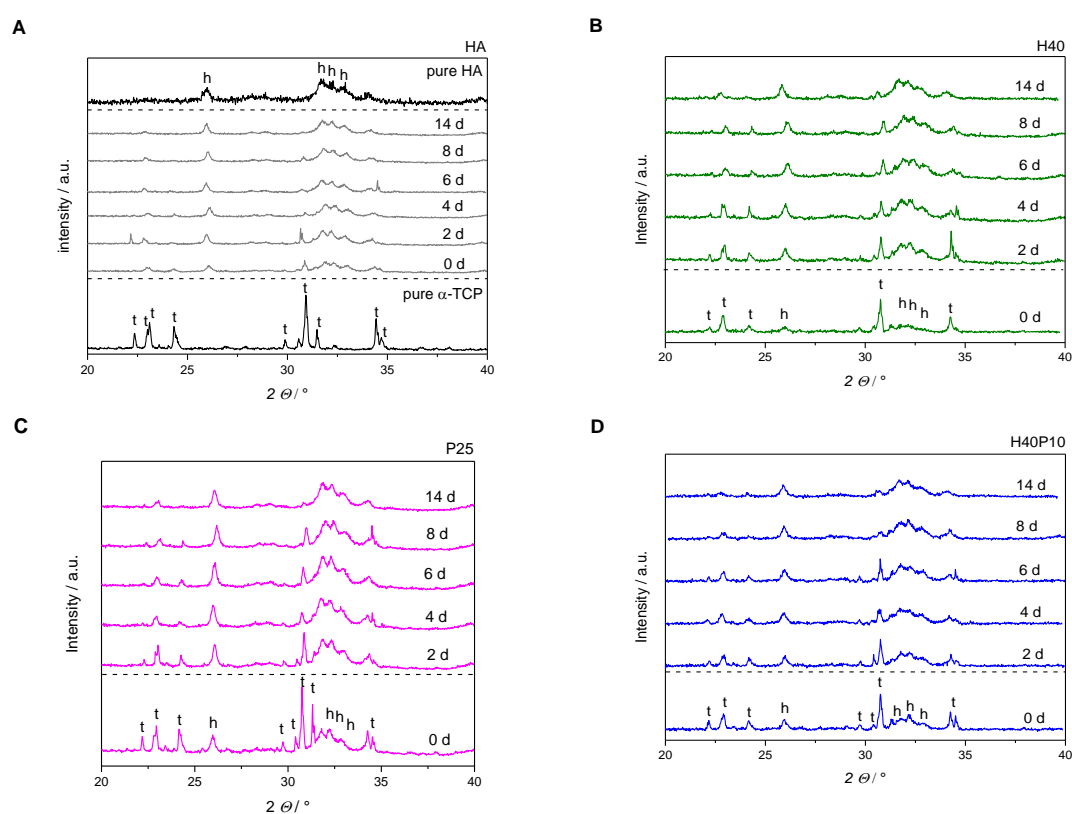
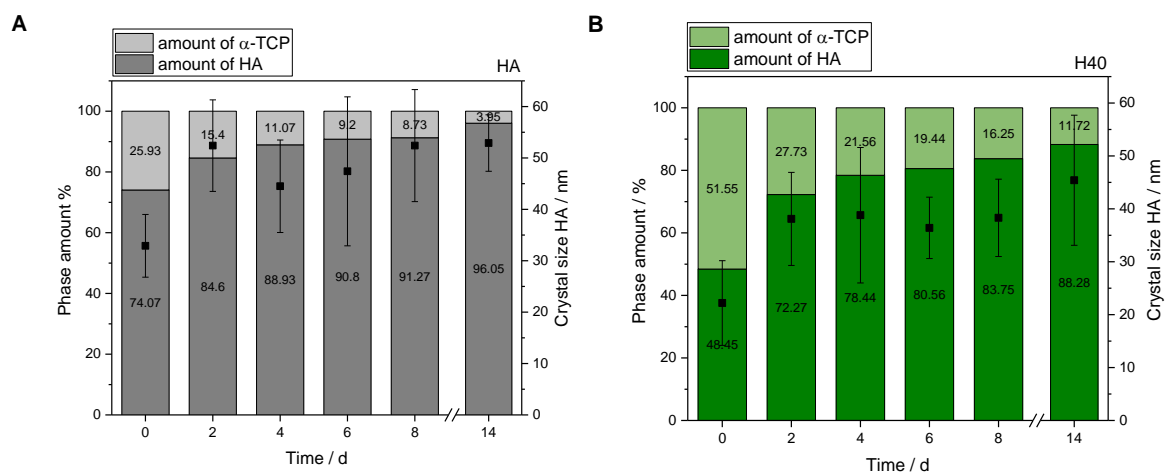
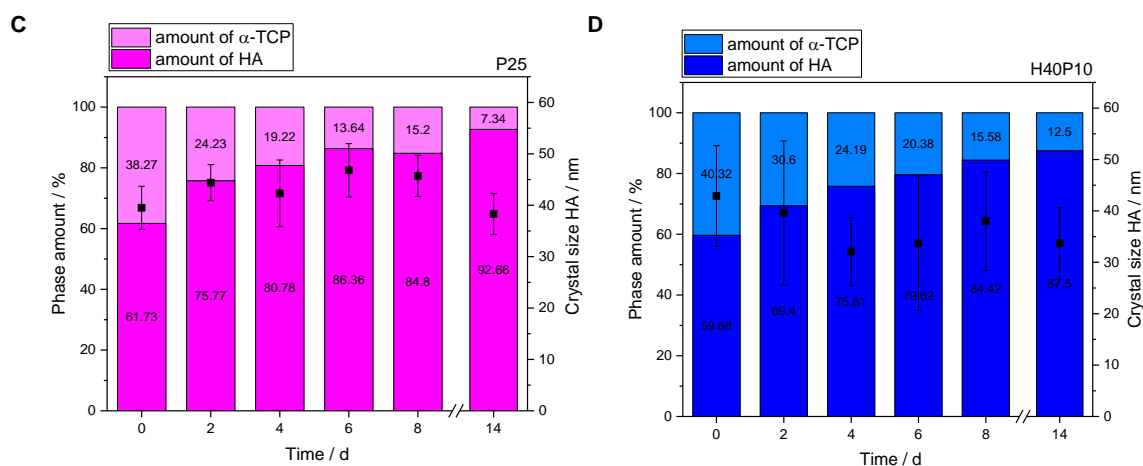


Figure 18:

XRD diffractograms of pure HA in comparison to composite batches. All formulations converted to HA over 14 days. With higher polymer amount, amorphous phases increased. Furthermore, a higher polymeric content also increased the time frame for HA formation (h = diffraction pattern HA, t = diffraction pattern α -TCP). **A:** Inorganic reference HA in comparison to the reference diffraction pattern of pure α -TCP and HA, respectively. **B:** HA with polymeric addition of 40 wt% HEMA (H40) in liquid phase. **C:** HA with polymeric addition of 25 wt% synthesized hydrogel precursor (P25) in liquid phase. **D:** HA with a combination of 40 wt% HEMA and 10 wt% cross-linker (H40P10) in liquid phase.

As mentioned above, with addition of a second hydrogel phase, transformation to HA was not as fast and complete as for the pure reference, where a hardening rate of nearly 96 % was reached after 14 days (see **Figure 19 A**). The combination of HEMA with 10 wt% cross-linker (H40P10) had the biggest influence on the transformation, given that after storage in PBS buffer, the conversion rate was about 10 % lower. Not only conversion rate decreased, also HA crystal size was reduced by about 20 nm (see **Figure 19 D**). Samples containing only polyHEMA as hydrogel system (H40), especially at the starting point, showed a distribution of half raw material and final setting product (see **Figure 19 B**). However, this imbalance with respect to the desired CPC formation recovered quickly after two days and led to 88 % HA amount at the end with 12 % residual α -TCP, respectively. Regarding batch P25 with gelled PEG-PLLA-based hydrogel, size of HA crystals was about 38 nm and thus smaller in comparison to pure inorganic matrix. This polymeric system had less influence on the conversion and resulted in almost 92 % of the desired mineral structure (see **Figure 19 C**).



**Figure 19:**

Overview of Rietveld refinement with analysis of HA crystal size. **A:** Inorganic reference HA. **B:** HA with polymeric addition of 40 wt% HEMA (H40) in liquid phase. **C:** HA with polymeric addition of 25 wt% synthesized hydrogel precursor (P25) in liquid phase. **D:** HA with a combination of 40 wt% HEMA and 10 wt% cross-linker (H40P10) in liquid phase.

3.3.2.4 Microscopical surface characterization

Results of Rietveld refinement regarding HA crystal size were also confirmed by scanning electron microscopy (SEM) images. At different time points, samples were analyzed with respect to organic structures, their appearance as well as distribution in main parts of the cracking surfaces. HA references verified the typical plate-like and rosette-oriented growth of crystals (see **Figure 20 A**). The same form and shape, but smaller needles, were observed for the composite materials H40, P25 and H40P10. Polymeric films in the samples that were dried during the transfer in the microscope were covering inorganic structures. With higher magnifications, the influence of the hydrogel phase on HA crystal structure was clearly visible: needles were smaller and not as defined with clear demarcations at crystal borders (see **Figure 20 B-D**).

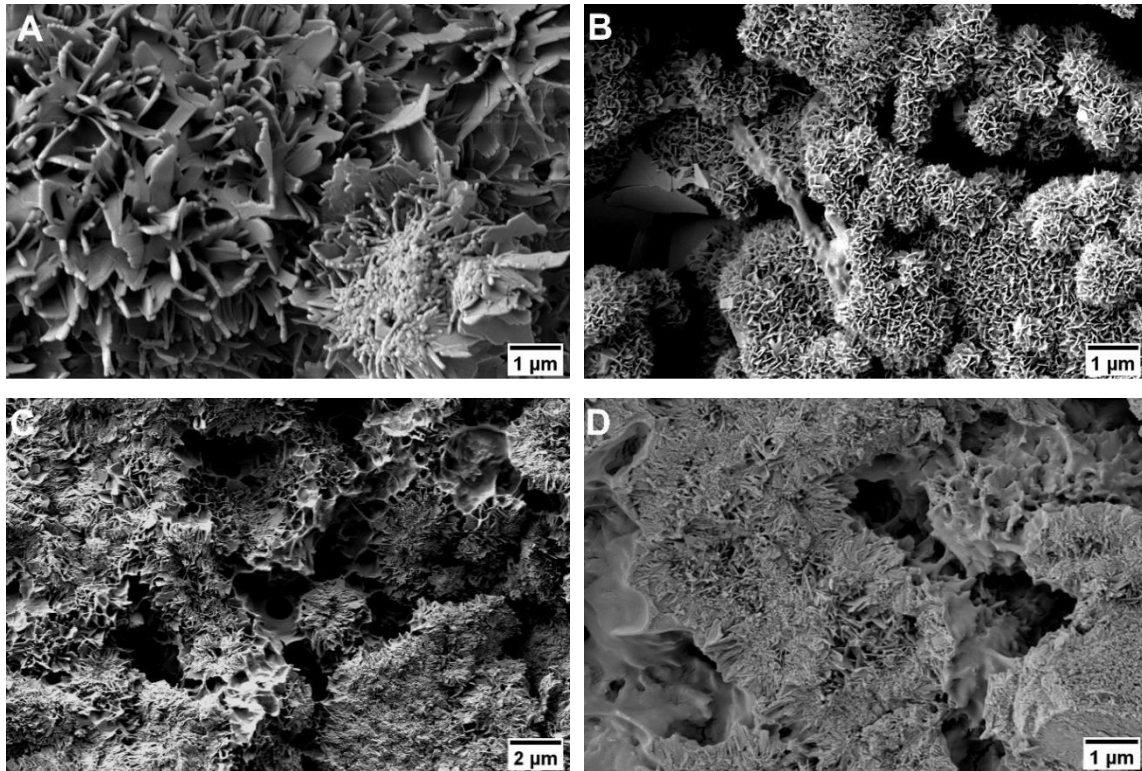


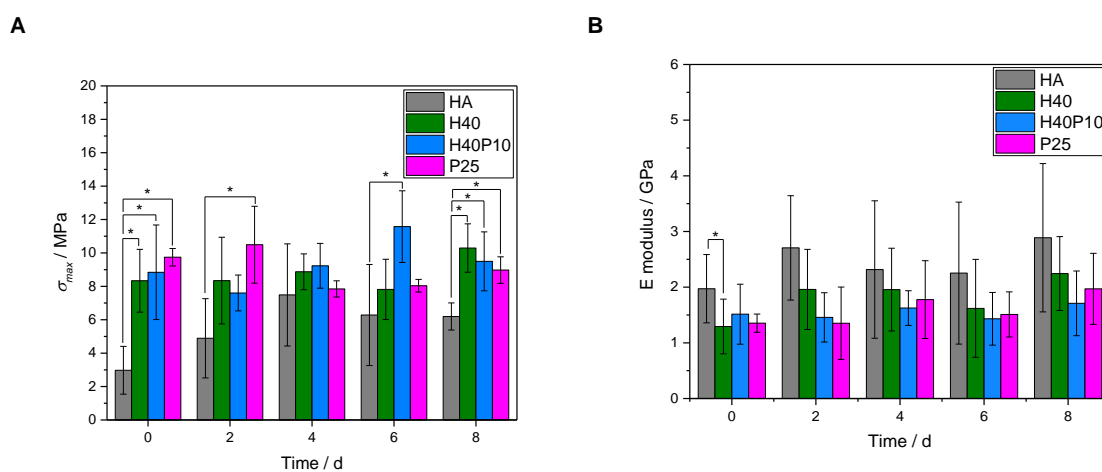
Figure 20:

SEM images with different magnifications and details of the samples for surface characterization of HA and the different composite formulations H40, P25 and H40P10 after 8 d of storage. **A:** Pure inorganic cement matrix showing typical HA needle-like structures (HA). **B:** Batch with 40 wt% HEMA-addition depicting both, a successful setting and HA-formation as well as gelation (H40). **C:** Smooth areas covering HA-needles and platelet structures indicating hydrogel formation for the batch containing 25 wt% hydrogel precursor PEG-PLLA-DMA (P25). **D:** Combination of HEMA (40 wt%) and cross-linker (H40P10) resulted in a successful conversion to HA with an incorporated hydrogel mix of polyHEMA and cross-linked PEG-PLLA-based polymers.

3.3.2.5 Bending strength

An increase in bending strength as well as ductility and flexibility was achieved by addition of the polymeric phase. 4-point bending strength could be significantly increased from about 6 MPa for the pure reference without polymeric additions to about 9 MPa for the samples with organic hydrogel phase (see **Figure 21 A**). For different polymers, the highest value of about 10 MPa was observed for the combination of 40 wt% HEMA with 10 wt% cross-linker (H40P10). Although pure hydrogel phases based on polyHEMA seemed to have higher viscous and elastic behavior (G'' respectively G' with highest value, see **Figure 13 A**), a 4-point bending strength in the same range of batch H40 could be measured for the pure cross-linker, *i.e.* the hydrogel system based on degradable methacrylate modified

triblock PEG-PLLA-DMA-precursors. Over the time frame of 8 days, all dual-setting systems showed a relatively stable value of 4-point bending strength in comparison to the reference where the strength increased related to the time-dependent hardening process of the cement. HA references had higher E-modulus values between 2-3 GPa in comparison to the dual set formulations. Lowest E-moduli and thus highest elasticity and lowest slope were determined for samples containing 25 wt% cross-linker (P25). This observation refers to the determined density of hydrogels and EWC showing highest elastic behavior (see **Figure 21 B**). Highest energy absorption capacity and toughness was given by the combination of both, short and long chain polymers that formed an incorporated, homogenous hydrogel network (H40P10, see **Figure 21 C**). Calculated elasticity was significantly advanced by the different hydrogel phases whereas a combination of 40 wt% HEMA and 10 wt% PEG-PLA-based hydrogel precursor showed the overall highest effect (see **Figure 21 D**).



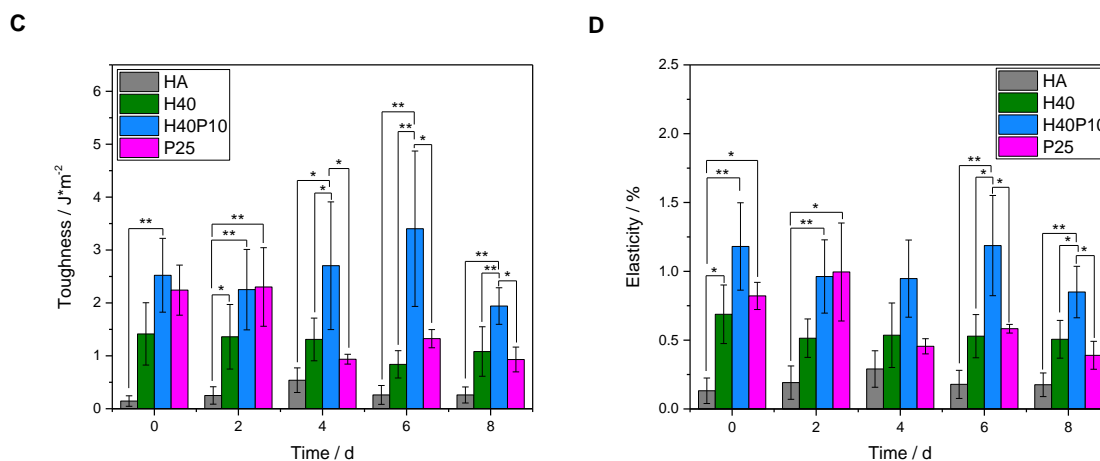


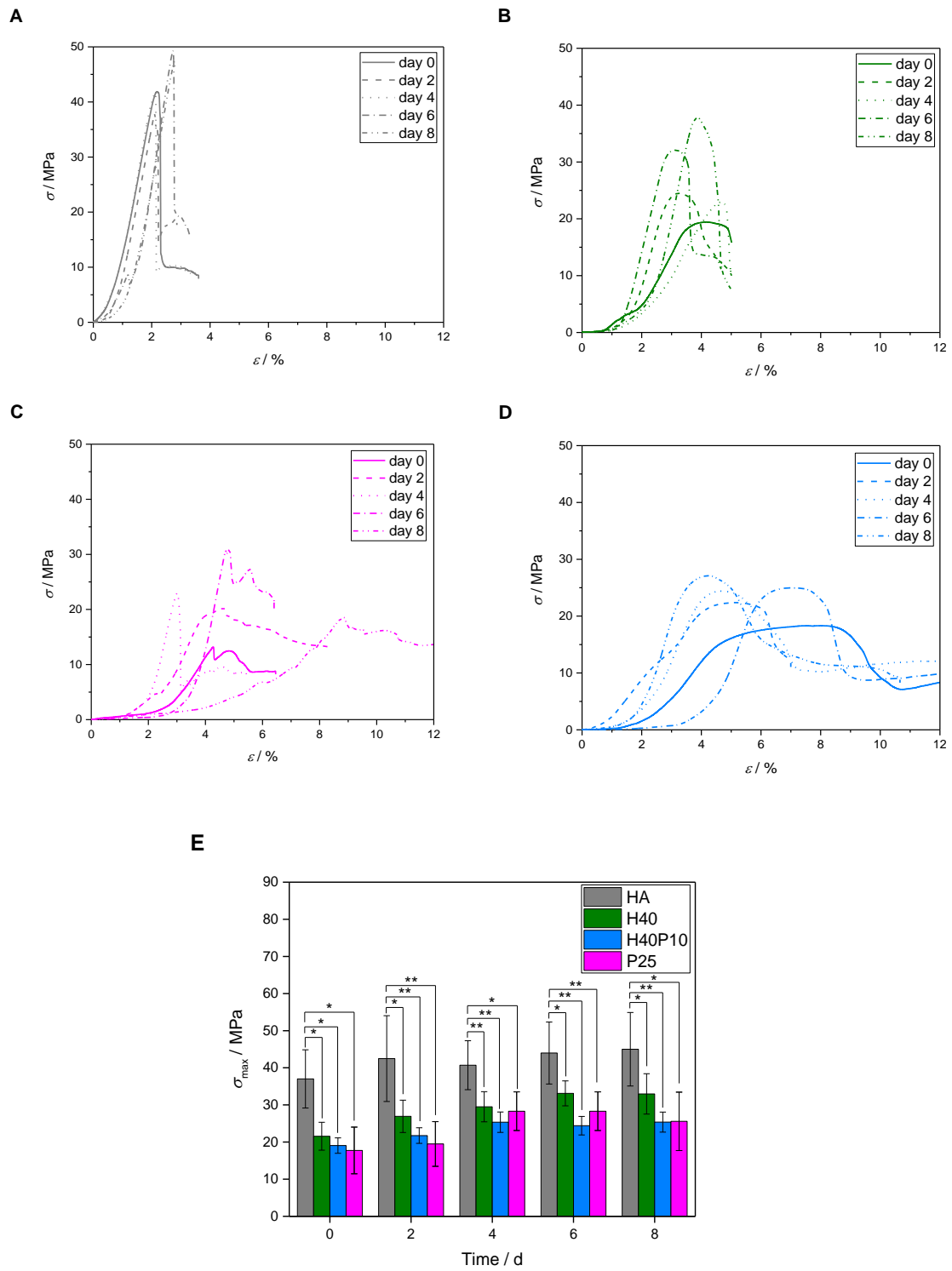
Figure 21:

Overview of different parameters calculated out of 4-point bending test. First, maximum bending strength of all batches over a period of 8 days was determined (A). Furthermore, a calculation of relevant measures for evaluating influence of polymeric additions was performed for E-modulus (B), toughness (C) as well as elasticity (D) of the system.

3.3.2.6 Compressive strength

Stress-strain curves of the inorganic reference without any polymeric content (HA) revealed the typical brittle behavior with a high stress of 40-50 MPa until immediate break and a corresponding strain maximum of about 2 % (see **Figure 22 A**). Incorporation of a polyHEMA network in HA-matrix (H40) led to a doubling of strain-values up to 4%. During 8 days, the final conversion to HA and thus a higher entanglement of HA-needles resulted in higher stress-levels that were almost in the same range (~ 30-40 MPa) and thus comparable to pure HA, but more elastic (see **Figure 22 B**). Hydrogels based on high molecular weight PEG-PLA precursor with the softer gel phase led to even more ductile properties but at the same time lower maximum stress levels (see **Figure 22 C**). By combining both, stiffer polyHEMA and softer PEG-PLLA-based hydrogels, an increase in elasticity with high energy-up-take and a deformation up to 10 % was achieved. With 40 wt% HEMA and 10 wt% cross-linker (H40P10), maximum stress points were converted to broad peaks or plateau phases (see **Figure 22 D**). While having higher maximum compressive strength values for pure HA, all composite formulations showed still stable levels of about 50-75 % compared to pure inorganic matrix. Over time, an increase was noted due to further entanglements of the HA crystal network within the hydrogel matrix (see **Figure 22 E**). Additionally, a certain cohesiveness could be observed for composite samples

after testing as the specimens did not disintegrate along the crack after mechanical testing (see **Figure 22 F**).



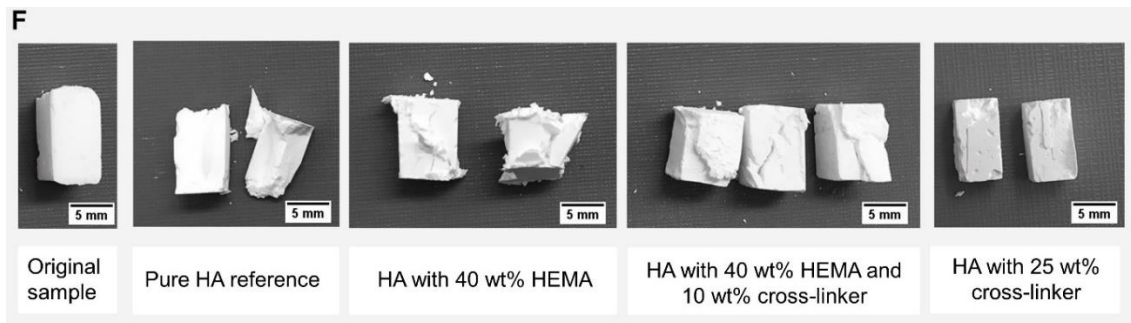


Figure 22:

Stress-strain curves of inorganic reference in comparison to composite materials as well as overview of maximum stress-values over 8 d. **A:** Inorganic reference (HA) with typical brittle behavior – high initial stress with low strain-levels. **B:** Formulation containing 40 wt% HEMA in liquid phase (H40) showing an increase in ductility with high stress-values comparable to pure HA cement. **C:** Samples based on 25 wt% cross-linker (P25) with increase in ductility. **D:** Most ductile system composed of HEMA (40 wt%) and hydrogel precursor (10 wt%) with plateau phases instead of maximum stress peaks and deformations up to 10 %. **E:** Maximum stress of all batches during time frame of 8 d. Image **F** depicts specimens before and after compressive strength testing at day 0.

3.4 Discussion

The polymerization of HEMA as a monofunctional methacrylate monomer results in the formation of long polymer chains, which form a hydrogel by the physical entanglement of the chains without further chemical cross-linking. The effect of HEMA modification on the mechanical properties of an apatite calcium phosphate cement was demonstrated in a previous study [179]. Here, we hypothesized that a further chemical cross-linking of HEMA by a bifunctional methacrylate precursor will further enhance the elasticity of the cement composites and will also enable hydraulic cleavage of the network by ester hydrolysis of the lactide moieties within the chemical structure.

By combining or replacing polyHEMA with a PEG-PLLA-based hydrogel precursor, setting time was decreased significantly in comparison to pure HA. Both batches, H40P10 and P25, that were produced with the synthesized cross-linker, resulted in an even faster setting that only took half of the time than the formulation with 40 wt% HEMA (H40) alone. This result correlates well with the determined gelation points of the pure hydrogel systems. Due to higher molecular weight of the precursor as well as the included bifunctionality, the compound reacts and cross-links even faster *via* radical polymerization, even if the amount of single short chain HEMA monomers might be higher. For the bifunctional precursor, the extend of effective cross-links is increased and network formation is accelerated. Moreover, this logically also implements the HPLC study where an integration of over 90 % of methacrylic acid units of hydrolyzed hydrogels was detected to be involved in gel structure. Consequently, the reaction of the high molecular weight precursor can be concluded as fast with a high reaction rate. This high degree of conversion in the polymerization was also investigated by Clapper *et al.* [201] who used an UV induced gelation of dimethacrylated triblock monomers of PEG and PLA. All these facts successfully demonstrated that the second gel forming reaction could run in parallel to the setting reaction without any restrictions. Also the adhesiveness of the samples after compressive strength testing indicated a certain cohesiveness by incorporated hydrogel networks and inter-locked HA crystals. Nevertheless, the fast organic reaction did not inhibit or change the conversion of the inorganic part completely. We could observe an influence on conversion rate and crystal size, but

this did not affect mechanical stability or lead to a disintegration of the cement samples. XRD diffractograms showed a continuous decrease in α -TCP pattern over the time with a successful setting reaction to HA. The detected increase in amorphousness with higher polymeric content as well as reduced transformation were also observed by Hurle *et al.* [202] who assumed a lower HA formation by a reduced availability of water. This results in less dissolution of α -TCP raw powder and consequently production of precipitated setting product.

Regarding mechanical properties, we could clearly increase toughness and elasticity by addition of the synthesized PEG-PLLA-based cross-linker as a third component in the system. A switch from brittle to ductile behavior was achieved and also bending strength increased in contrast to pure HA. Stress-strain curves of compressive strength testing also showed a high deformation for the batch H40P10. This also correlates with the homogenous testing sample that stuck together after compression. We could create a certain plateau that means a change in direction of the x-axis (strain) without altering the detected response or force on the y-axis (alternatively: stress). Thus, a high energy could be retained in the constructs. This was also seen for 4-point bending testing and high toughness levels that were obtained for this formulation, which were comparable to the mechanical performance of pure HEMA cement composites from a study by Christel *et al.* [179] as well as acrylamide modified cements from the pioneering work of Dos Santos *et al.* [178]. With addition of the degradable cross-linker, strength values were found to be in the range of samples containing 50 wt% HEMA but with the advantage of a degradable component. This is in contrast to a study using the cross-linker in combination with more degradable brushite cement, where strength values decreased extremely compared to the addition of about 50 wt% PEG-hydrogel phase [193]. The high flexibility and deformation of such brushite composites resulted in values of less than 1 MPa for tensile strength, which can be correlated to the different shape, size and entanglement of cement crystals compared to apatite forming counterparts. The same trend was observed for brushite cement and silica gel hybrid materials [187] which were prepared *via* simultaneous hardening and gelation mechanism and also showed lower strength levels in comparison to the here established formulations. It is hence obvious that the nanosized character of the precipitated HA crystals from the current study is

responsible for the higher strength of cement-hydrogel composites. This is likely caused by a better entanglement of smaller crystals within the polymeric network since for both cement types no chemical interactions between cement crystals and hydrogel are expected.

An advantage of the high molecular weight PEG-PLLA-DMA cross-linker is the possibility of composite degradation in an aqueous environment. With additional ester linkages in the molecule, a hydrolytic degradation is enabled compared to the practically non-degradable HEMA matrix. At the same time, the ceramic's resorption can occur due to an acidic environment with osteoclasts attaching at the surface and forming lacunas with an afterwards subsequent phagocytosis and degradation of crystals by macrophages [203]. With this new approach, the resorption rate is increased over the time by an appropriate concentration of PEG-PLLA-DMA in the formulation as seen for the mass change of the pure hydrogels. Cleavage of ester bonds occurs homogeneously [204] within several weeks by bulk erosion [157] and can accelerate the overall degradation behavior of the composite.

3.5 Conclusion and outlook

Overall, we advanced a dual setting system based on HA and polyHEMA formed *via* radical polymerization by incorporation of an additional degradable cross-linker. Ductile as well as elastic properties could be increased by only 10 wt% addition to a system based on HA and polyHEMA (here: 40 wt% HEMA; H40P10). Pastes were still moldable though a relatively high polymeric content was embedded in the liquid phase. Moreover, hydrogel formation did not affect setting reaction and both reactions were able to process. Further investigations are needed to optimize the final concentrations of both organic compounds. In conclusion, we could successfully create a promising tool for biomedical applications by incorporation of a degradable hydrogel precursor to improve the mechanical properties of a dual setting cement system.

Chapter 4

Degradable dual setting systems based on PEG-hydrogels and brushite cement as composite material for biomedical applications

Chapter 4 was published as original research article (Michaela Rödel, Jörg Teßmar, Jürgen Groll, Uwe Gbureck, Highly flexible and degradable dual setting systems based on PEG-hydrogels and brushite cement, *Acta Biomaterialia*, 79, 2018, pp. 182-201), reproduced from [193] retaining the rights by Elsevier to include it in this thesis.

The article is based on work of the author of this thesis Michaela Rödel, who performed all experiments, data evaluation and composition of the manuscript.

4.1 Abstract

With respect to the composition of natural bone, we established a degradable dual setting system of different PEG-based hydrogels combined with a brushite cement. The idea was to reinforce the inorganic CaP mineral phase with an organic, polymeric phase to alter the cement's properties towards ductility and elasticity. Extremely flexible samples were produced *via* this dual setting approach with a fully reversible elasticity of the samples containing high molecular weight PEG-based hydrogel precursors. Using the decalcifying agent ethylenediaminetetraacetic acid (EDTA), the whole inorganic phase was dissolved due to Ca^{2+} complexation and dimensionally stable hydrogels were obtained, indicating a homogenous polymeric phase within the composites. This was also confirmed by SEM analysis, where no discontinuities or agglomerations of the phase were observed. Additional XRD measurements proved a significant influence of the coherent polymeric matrix on the conversion from β -TCP/MCPA to brushite with a decrease in signal intensity. The results confirmed a parallelly running process of setting reaction and gelation without an inhibition of the conversion to brushite and the formation of interpenetrating networks of hydrogel and cement. The strengths of this newly developed dual setting system are based on the material degradability as well as flexibility, which can be a promising tool for bone regeneration applications in non-load bearing craniomaxillofacial defects.

4.2 Introduction

Natural bone is a composite material mainly composed of an inorganic hydroxyapatite phase (~ 70 wt%) and an organic collagen phase (~ 20 wt%), which results in combined tough as well as elastic material properties [4, 205, 206]. There are different approaches for the replacement of lost bone [207], where the autograft transplantation is still the gold standard in terms of defect regeneration [208, 209]. Another option are allografts provided by a suitable donor that can be used in order to repair the bone defect [210]. Since both methods implement some risks like donor site morbidity or pathogen transfer, synthetic materials as alternative approaches for clinical bone replacement materials like ceramics or cements based on CaP are usually applied in the field of non-load bearing defects. These material replacements can be either prepared *via* thermal treatment (high-temperature calcium phosphates) or by precipitation from aqueous solutions (low-temperature calcium phosphates). The latter preparation route is the preferred method for *in situ* forming CPCs, in which a solid phase composed of mixtures of different phosphates like primary (H_2PO_4^-) or secondary (HPO_4^{2-}) phosphates [23] is reacted with an appropriate cement liquid to form either HA or brushite as setting products. Based on a dissolution-precipitation reaction, the particles of the solid raw powder are dissolved in the liquid and form an entangled network of precipitating crystals during setting [43].

One typical disadvantage of these bone cements is their brittleness, whereas several strategies exist to overcome this limitation and to improve the mechanical properties. Besides fiber reinforced constructs [176, 188, 211-213] or nanocomposites [214, 215], dual setting systems with an additional stabilizing network can be used to increase the overall strength as well as elasticity and flexibility of this biomaterial class. These systems can be described as a combination of an organic (hydrogel) and inorganic cement phase in form of two interpenetrating networks, which are formed during setting and cross-linking reaction.

Different compositions of dual setting systems are already reported in literature, for example Christel *et al.* [179] established a system based on low molecular weight HEMA in combination with α -TCP and reported an improved work of fracture and

reduced brittle fracture behavior for the cement-polymer composite with the additional polyHEMA phase. The applied gelation mechanism was based on a thermally induced cross-linking using APS as radical initiator and TEMED as polymerization accelerator. In another study, the same radical system was used for the polymerization of AA in combination with α -TCP. An increase in mechanical strength up to 149 % (55 MPa) in comparison to pure bone cement reference was also observed here. This effect was related to an overall decrease in porosity for the coexisting PA and inorganic phases [178]. Composites with compressive strength values of about 100 MPa were obtained by Wang *et al.* [192], who developed a dual setting cement based on an *in situ* cross-linking polymerization of Dex-MA and the hydrating CPC. Furthermore, Schamel *et al.* [180] described the mineralization of a hydrogel matrix composed of a six armed star molecule functionalized with isocyanate groups (NCO-sP(EO-*stat*-PO)) and HA with a strength improvement 30 times higher in comparison to a merely particle filled hydrogel.

Despite of excellent mechanical achievements, all described cement-hydrogel systems were using low soluble apatite cements in combination with non- or only poorly degradable hydrogel matrices, such that the composites are thought to be permanently stable under *in vivo* conditions without the possibility of a bone remodeling of the filled defect. In contrast to the commonly applied HA, brushite sets at acidic conditions (preferential pH-value $< \sim 4.2$) and is already resorbed under physiological conditions at a pH-level of 7.4 [59, 216]. Due to its good biocompatibility, osteoconductivity and biodegradability, brushite is already clinically used as bone replacement material [43, 217, 218]. There is also reported on two former studies focusing on brushite as inorganic reference and organic components. Both deal with the addition of PEG-based substances to the cement system [219, 220]. The simplest method is mixing of low molecular, liquid PEG to the aqueous setting solution. This was performed by Roy *et al.* [219] who introduced 2.0 and 5.0 wt% PEG to the liquid phase. They observed a slight increase in compressive strength after PEG incorporation with overall values between 6 and 10 MPa over 7 days. Further, a study of Engstrand *et al.* [220] depicted the influence of microparticles as polymeric material on a premixed acidic CPC. The microparticles consisted of PLGA plasticized with PEG 400 Da. The

incorporation of 1.25 wt% resulted in a compressive strength of about 15 MPa which means an increase about 20 % compared to the particle free reference.

Both studies do not implement a dual setting mechanism and a phase incorporation of inorganic and organic system. Here, challenging issues would be to find a suitable hydrogel system that reacts also in a short time frame similar to brushite cement [221] and that is degradable after setting. An appropriate mechanism was found to be radical polymerization of dimethacrylated PEG-based hydrogels [222], whereby the chain growth polymerization is a fast and random cross-linking reaction [223]. These hydrogel precursors were combined with brushite cement to create a dual setting system that sets in parallel to the cement setting and cross-linking of the hydrogel phase. Linear PEG with a molar mass $< 20,000$ Da is known to be non-toxic. It is water-soluble, biocompatible and well-established for biomedical applications and internal consumption [224-226]. Slightly degradable PEG-DMA with either low (PEG-DMA_{lmw}) or high (PEG-DMA_{hmv}) molecular weight were used as hydrogel precursors in comparison to a degradable gelation system obtained by incorporation of hydrophobic PLA-units with several ester functions (PEG-PLLA-DMA). The latter is known to show a faster degradation by hydrolysis of the ester-bonds *in vivo* [227]. The amount of hydrogel was varied in the range of 10 to 50 wt% referred to the used cement liquid. These variations are influencing both, the network density or mesh size of the hydrogel, whereas the hydrophobic PLA-spacer is thought to further affect the swelling behavior of the material. Here, we analyzed the material properties of pure hydrogels as organic reference, brushite cement as inorganic reference and cement composites in terms of their mechanical performance, phase composition and morphology.

4.3 Results

4.3.1 Polymer characterization

The successful synthesis of the linear triblock cross-linkers was verified by ^1H NMR spectroscopy and DMF-GPC measurements using conventional calibration.

4.3.1.1 PEG-DMA_{lmw} (analysis of commercial substance)

^1H NMR (solvent CDCl_3): $\delta = 1.95$ (s, $-\text{CH}_3$), $\delta = 3.65$ (m, PEG-backbone- H), $\delta = 3.75$ (m, ether-neighboring PEG-backbone- H), $\delta = 4.30$ (m, ester-neighboring PEG-backbone- H), $\delta = 5.57$ and $\delta = 6.13$ (s, $(=\text{CH}_2)$). The measured amount of protons fit very well to the theoretical values. The molecular weight of the polymer was below the lower separating limit of the used column and accordingly not quantified.

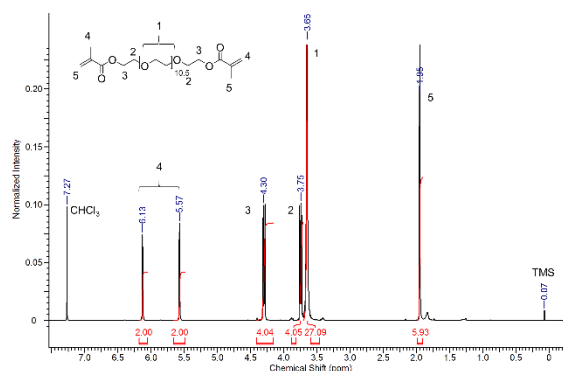
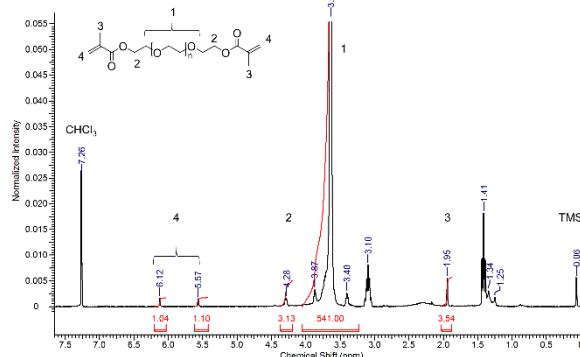
4.3.1.2 PEG-DMA_{hmw}

^1H NMR (solvent CDCl_3): $\delta = 1.95$ (m, $-\text{CH}_3$), $\delta = 3.64$ (s, PEG-backbone- H), $\delta = 4.28$ (m, ether-neighboring PEG-backbone- H), $\delta = 5.57$ and $\delta = 6.12$ (s, $(=\text{CH}_2)$). The obtained amount of protons demonstrated the successful methacrylation with an average functionalization of one hydroxyl group. DMF-GPC analysis showed a monomodal distribution and a narrow dispersity of $\text{Đ} = 1.07$ ($M_n = 6,504$ Da, $M_w = 6,965$ Da in comparison to the expected value of $6138 \text{ g}\cdot\text{mol}^{-1}$).

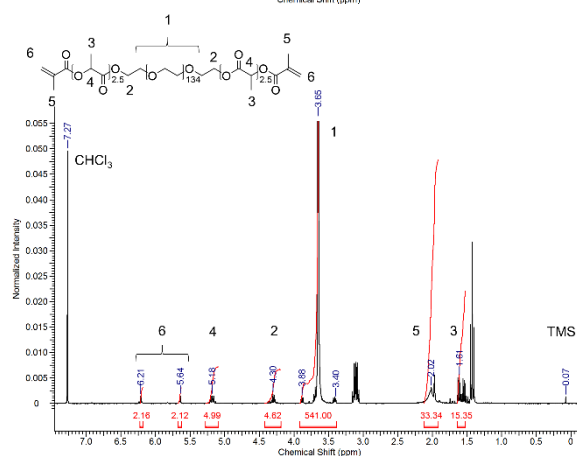
4.3.1.3 PEG-PLLA-DMA_{hmw}

^1H NMR (solvent CDCl_3): $\delta = 1.61$ (m, $-\text{CH}_3$), $\delta = 2.02$ ($-\text{CH}_3$ lactic acid unit), $\delta = 3.65$ (PEG backbone- H), $\delta = 5.18$ (H in lactic acid), $\delta = 5.64$ and $\delta = 6.21$ (s, methylene groups). The detected amount of protons fit very well to the theoretical values. DMF-GPC analysis again showed a monomodal distribution and a narrow dispersity of $\text{Đ} = 1.08$ ($M_n = 6,789 \text{ g}\cdot\text{mol}^{-1}$, $M_w = 7,330 \text{ g}\cdot\text{mol}^{-1}$ in comparison to the expected value of $6,498 \text{ g}\cdot\text{mol}^{-1}$).

An overview of the results for the synthesized hydrogel precursors is shown in **Figure 23**.

PEG-DMA_{lmw}¹H NMRDMF-GPC
Not evaluablePEG-DMA_{hwm} $M_n = 6,504 \text{ g} \cdot \text{mol}^{-1}$
 $\bar{D} = 1.07$

PEG-PLLA-DMA

 $M_n = 6,789 \text{ g} \cdot \text{mol}^{-1}$
 $\bar{D} = 1.08$ **Figure 23:**

The cross-linker PEG-PLLA-DMA was synthesized *via* a two-step mechanism with ring-opening polymerization and afterwards functionalization with methacrylic acid on both terminal hydroxyl groups. Both, the ¹H NMR and the FTIR spectra confirmed the successful synthesis of the PEG-based hydrogel precursors. Moreover, the esterification of the high molecular weight PEG was performed for one hydroxyl groups with methacrylic units. In order to complete the data, the commercial low molecular weight-based PEG-DMA was analyzed accordingly.

4.3.2 Analysis of dual set composites

4.3.2.1 Analysis of preparation procedures

Measurements of the initial pH-level during setting reaction of the composites showed acidic values for all four formulations. Brushite forming cement as inorganic reference had a starting pH of about 2.5 with a following decrease after 15 min to about pH 2 and increased up to a pH of 4.2 after one hour. The dual setting systems had the same starting level with a pH of 2.5. The batch containing PEG-DMA_{lmw} showed also a similar minimum with a pH of 2. This level was already reached after 5 min. A quarter-hour later, the pH increased up to about 2.5 with a plateau phase until the end of the measurement. Formulation PEG-DMA_{hmw} as well as PEG-PLLA-DMA decreased their pH continuously from 2.5 to about pH 2 over 60 min (see **Figure 24 A**). The setting reaction conditions (pH < 2) influenced the pH-values of the PBS storage solution (see **Figure 24 B**). A similar trend regarding the initial setting temperature was observed for the brushite reference and PEG-DMA_{lmw}-composites. The temperature of the pure inorganic formulation increased after 15 min up to 45 °C whereas the composite with low molecular weight PEG-DMA reached 42 °C after 10 min. After 30 min, a decrease up to 25 °C was measured. For the high molecular weight PEG-formulations (PEG-DMA_{hmw} and PEG-PLLA-DMA), a temperature peak was completely prohibited. The organic phase had a significant buffering effect on the initial setting temperature which started at 25 °C and increased up to 28 °C after 40 min with a following small reduction to again 25 °C (see **Figure 24 A**). Furthermore, the polymer containing samples showed varying behavior after storage in PBS. This is depicted in **Figure 24 C**. The original dimensions of the samples were given by the silicon mold (6*6*12 mm³). The size increased for the formulations containing PEG with a molecular weight of 6,000 Da. Due to swelling processes of the hydrogel phase, batch PEG-DMA_{hmw} grew 17 % in width (length side a = 7.04 ± 0.09 mm, length side b = 7.13 ± 0.24 mm at day 8) whereas PEG-PLLA-DMA increased in size up to 25 % (length side a = 7.49 ± 0.19 mm, length side b = 7.55 ± 0.19 mm at day 8). The pure brushite cement formulation, batch PEG-DMA_{lmw} as well as the height of the high molecular weight containing specimens showed no notable dimensional changes of the samples. An overview of the size changes (lengths side a and b) is

depicted in **Figure 24 D**, which shows the development of one length over the time for all 4 formulations.

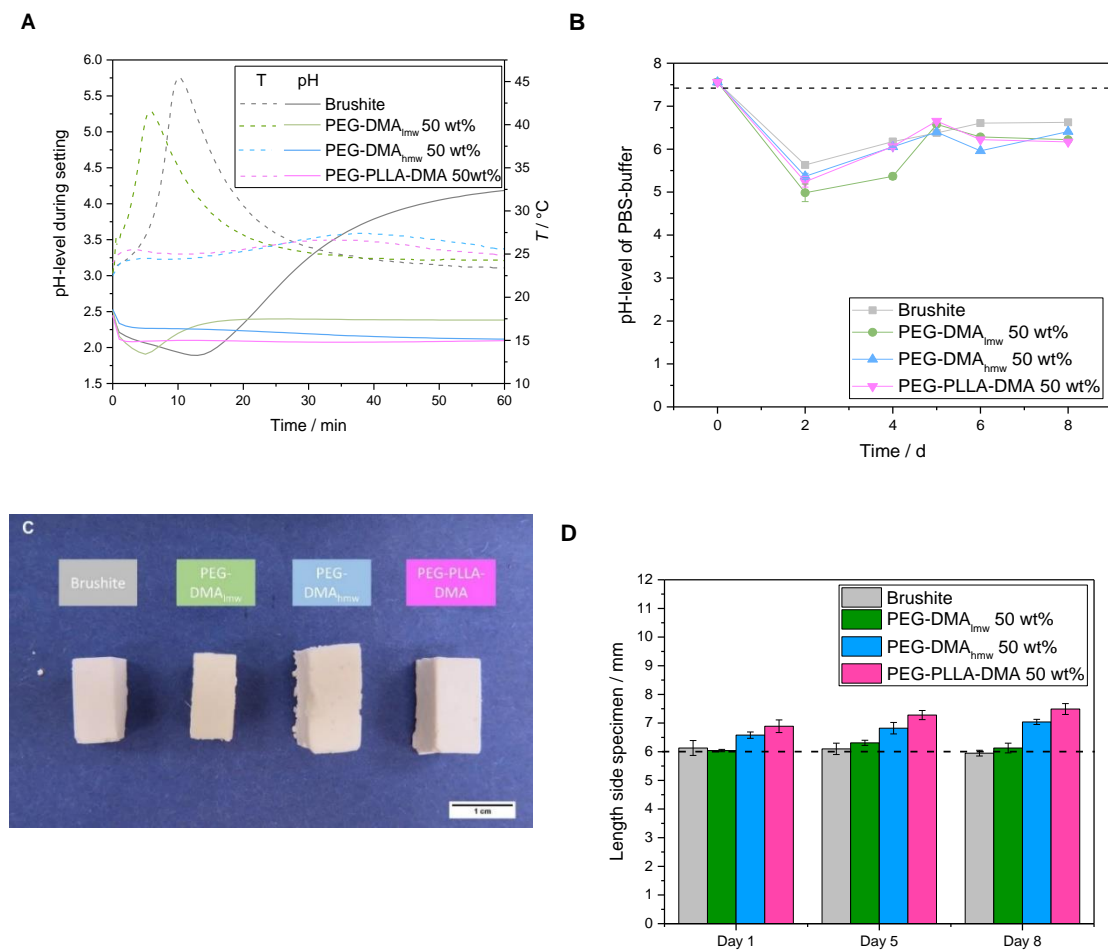


Figure 24:

Results of the pH-development during setting reaction (**A**) as well as the pH-measurements of the PBS solutions (**B**) over a period of 8 days. Additionally, the initial setting temperatures of the brushite reference and the composite batches were measured (**A**). For the composites with polymeric addition of PEG-DMA_{hwmw} and PEG-PLLA-DMA (all depicted samples with 50 wt% hydrogel precursor referred to the liquid phase), an increase in size due to swelling of the hydrogel phase after storage in PBS could be observed (**C**). An overview of the determined values for the different time points is depicted in part **D**.

4.3.2.2 Phase coherence and composition analysis

The pure brushite reference was completely dissolved after 4 days and there was no remaining specimen in the solution due to complexation of Ca^{2+} ions in the brushite forming cement (see **Figure 25**, first row of image **A**, **B** and **C**). The composite materials showed more stable samples, which was even extended with

increasing hydrogel phase content up to 20 days. The whole inorganic phase was dissolved by then and the remaining hydrogels were still dimensionally stable. This was proven for both PEG-DMA batches, the low as well as the high molecular weight one. The initial slight orange color resulted from oxidation processes of the used radical initiator ascorbic acid, but vanished after 4 days. Due to the longer polymer chains, the hydrogels were more transparent for formulations containing the high molecular weight PEG. With a molecular weight of only 600 Da, the chain lengths were much shorter and the resulting mesh size was significantly decreased, which in combination with the cement setting resulted in much crumblier hydrogel specimens. Over time, samples exhibited different chemical degradation or mechanical erosion patterns in the neutral aqueous EDTA solution, which were further investigated using gravimetric analysis.



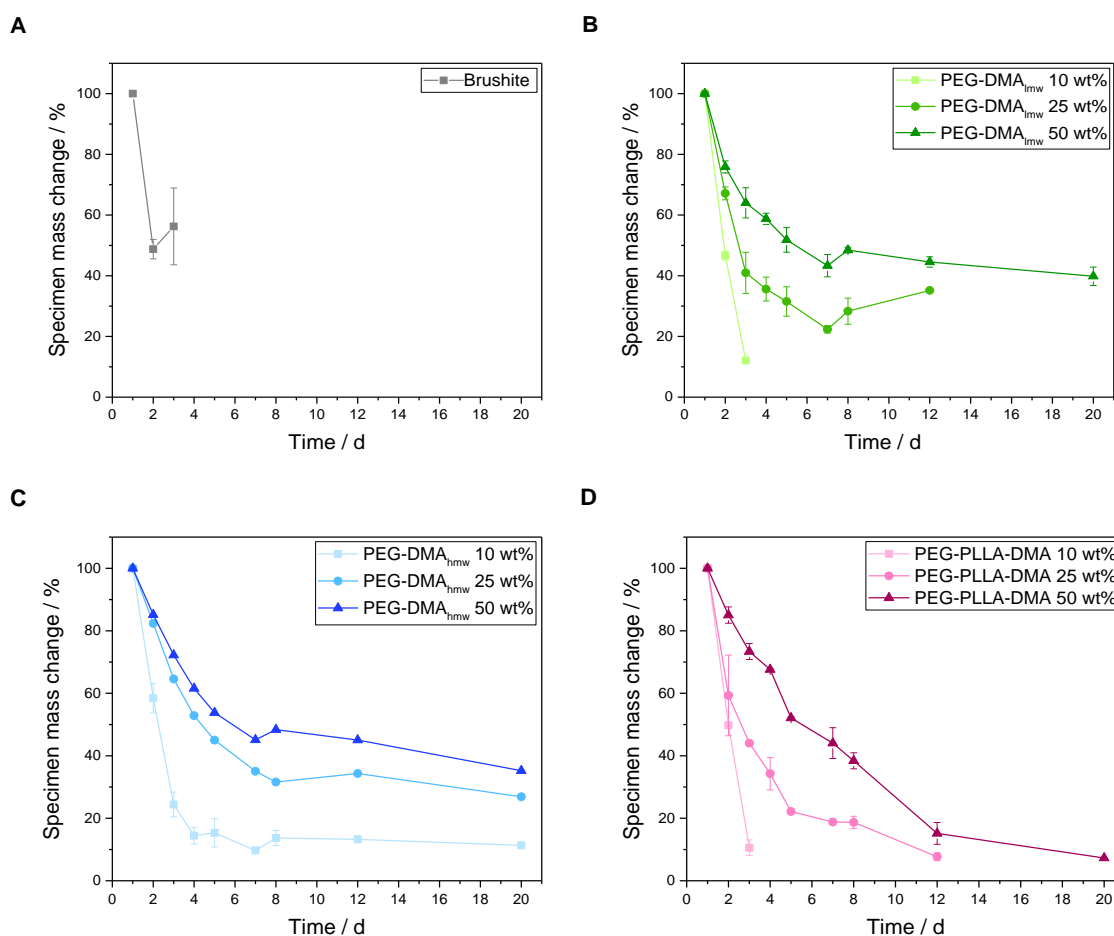
Figure 25:

Optical control of the samples immersed in EDTA-solution at day 1, 2, 4, 8, 12 and 20. The first line of each image shows the pure inorganic brushite specimen. Furthermore, the three different amounts of hydrogel phase (10 wt%, 25 wt% and 50 wt%) are depicted for the three different batches (**A** = PEG-DMA_{low}, **B** = PEG-DMA_{high} and **C** = PEG-PLLA-DMA; grey scale bar $\hat{=}$ 5 mm).

A decrease in mass could be observed for all formulations and all different polymer concentrations (**Figure 26 A-D**). One has to keep in mind that both, the loss of mineral and polymer, can lead to a loss of weight.

All composite formulations exhibited a fast release of the mineral phase, followed by a slower mass loss depending on the polymer concentration and coherence of the hydrogel network. Due to incorporated ester-bonds in PEG-PLLA-DMA, the hydrogel mass for this formulation decreased efficiently for all polymer contents, which can be attributed to a faster degradation of this polymer. For the less degradable formulations with 50 wt% hydrogel phase (PEG-DMA_{lmw} and PEG-DMA_{hmw}), a continuous weight was obtained over three weeks.

A closer look on the samples at day 2 clearly showed the dissolution of brushite phase from the outside to the inside of the specimen with a remaining hard inorganic core. This inorganic residual is marked with black lines in **Figure 26 E** for the batches containing PEG-DMA_{hmw} and PEG-PLLA-DMA. The samples with PEG-DMA_{lmw} were not transparent and a closer composition could not be seen due to the friable distribution of the gel in the composite.



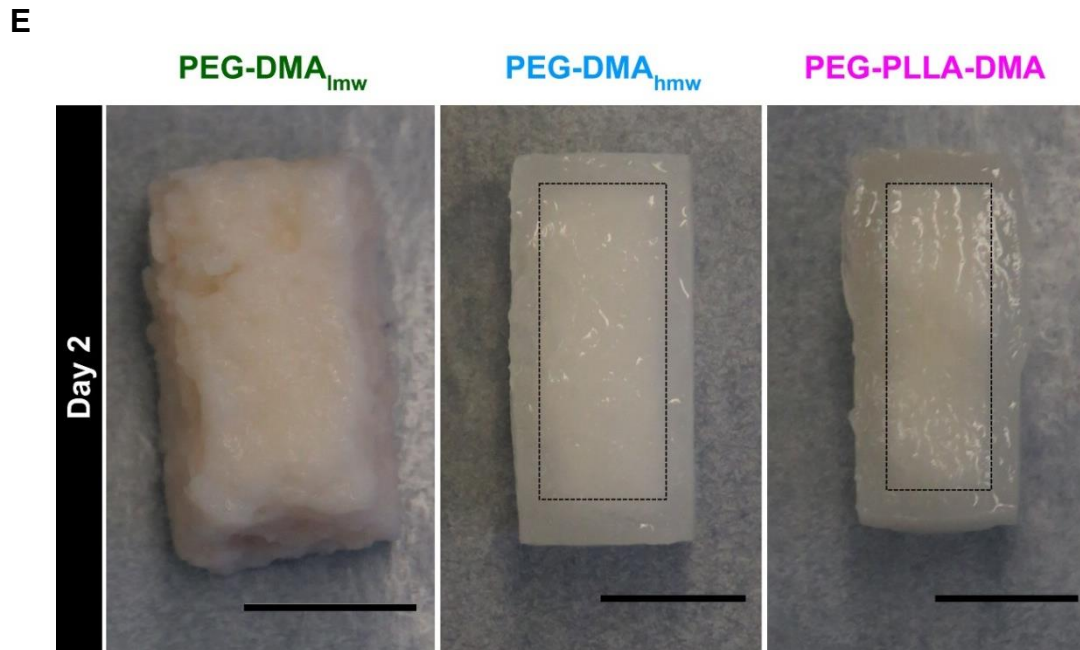


Figure 26:

Mass change of the samples was measured for the pure brushite reference as well as all composite formulations over the time (**A** = Brushite, **B** = PEG-DMA_{lmw}, **C** = PEG-DMA_{hmw}, **D** = PEG-PLLA-DMA). A detailed picture of the samples after two days of storage in EDTA solution (**E**) shows the process of demineralization from the outside to the inside with a remaining inorganic core (see black lines for the batches containing PEG-DMA_{hmw} and PEG-PLLA-DMA; black scale bar \cong 5 mm).

Furthermore, the phase distribution of the different composites was also analyzed using SEM (see **Figure 27**). The cracked surface of samples with a very high content of polymeric phase (50 wt%) showed bigger crystal structures of brushite forming cement in comparison to the pure inorganic batch. Thus, the hydrogel phase in the cement system had a significant influence on brushite crystal growth. Additionally, due to the necessary drying for electron microscopy, some dry hydrogel structures covered the inorganic network (for example for PEG-PLLA-DMA; highest magnification). Apart from that, no polymer agglomerations could be observed and the surface had an overall homogenous appearance.

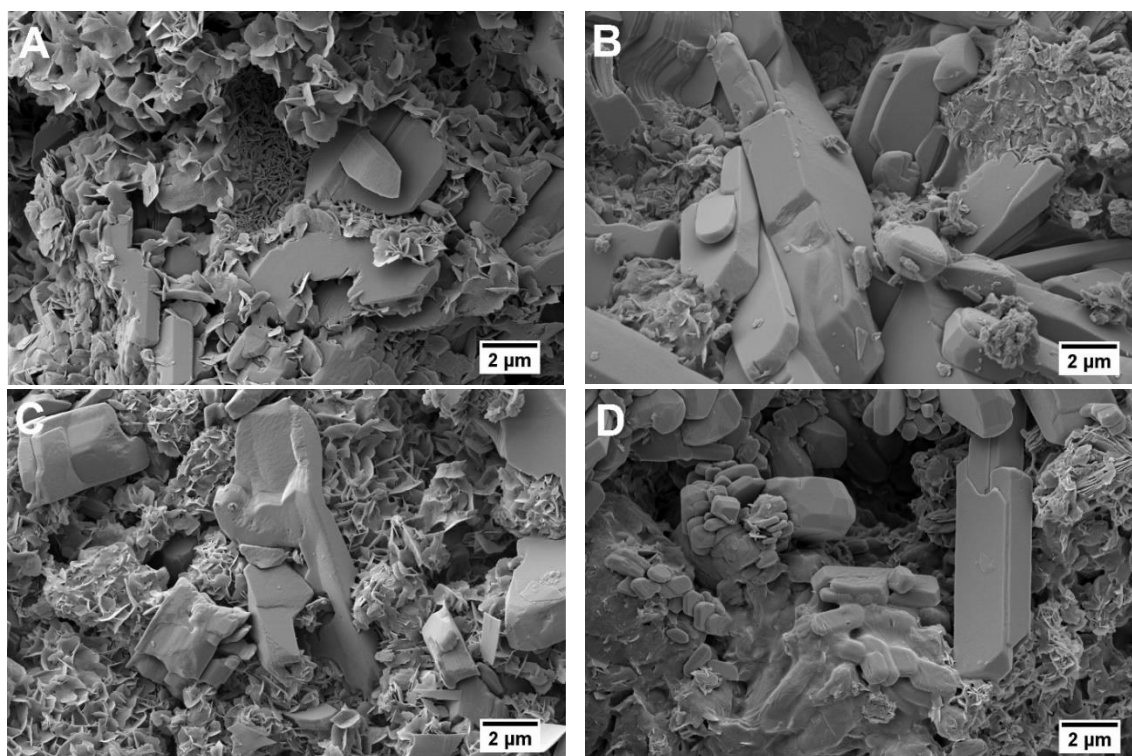


Figure 27:

Cracked surfaces of samples without (brushite, **A**) as well as formulations with organic phase (**B-D**) after 8 days of storage in PBS. **A:** SEM image of the inorganic reference with the typical plate-like structure of brushite cement. **B:** SEM image of a sample containing PEG-DMA_{lmw} (50 wt% referred to the liquid phase). **C:** SEM image of a sample containing PEG-DMA_{hmw} (50 wt% referred to the liquid phase). **D:** SEM image of a sample containing PEG-PLLA-DMA (50 wt% referred to the liquid phase).

The visual appearance of the phase composition was completed by XRD analysis to prove the composition of the mineral phases (see **Figure 28**). After the first day, the formation of brushite was observed, both for the pure reference without polymer addition as well as for the composite materials. Prominent reflections at 11.8° and 21.1° indicated the presence of brushite phase. The ratio and intensity of the different diffraction patterns were generally reduced for all hydrogel containing samples. This decrease indicated amorphous fractions or smaller CPC crystals, which were also detectable next to extremely big crystals in the SEM images. In all cases, the crystal water-free form monetite (CaHPO_4) was also measured in the set sample. Within 8 days of storage, no further changes in phase composition were detected. At day 5, an amorphous halo was measured in the range of $10\text{--}15^\circ$. This was observed for composite materials containing PEG-DMA with low or high molecular weight, respectively.

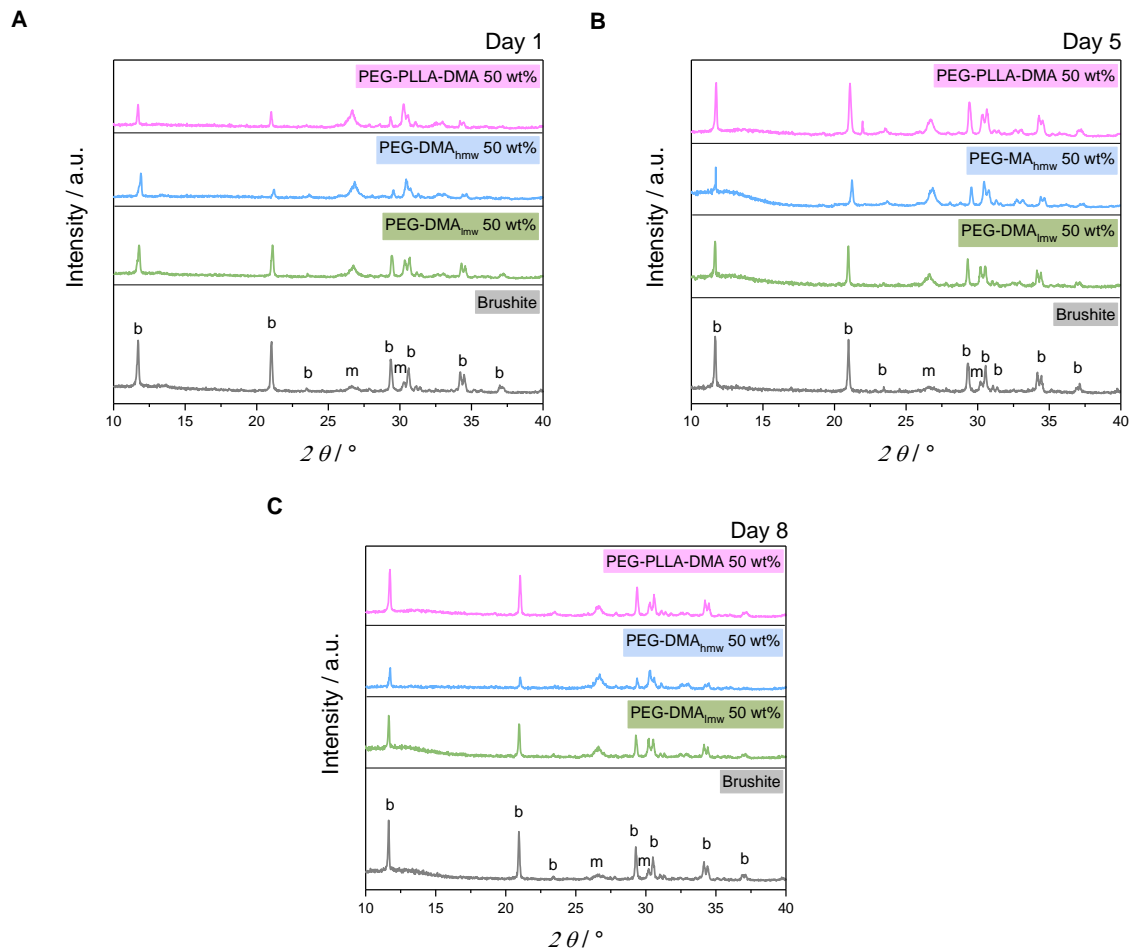


Figure 28:

XRD pattern of the brushite reference as well as the three different composite batches with 50 wt% polymeric content referred to the liquid phase. Samples were analyzed regarding their phase composition at three different time points (day 1 (**A**), day 5 (**B**) and day 8 (**C**)) in a range of 10 to 40 ° (b = diffraction pattern brushite, m = diffraction pattern monetite).

Furthermore, swelling of the hydrogels was analyzed for high molecular weight PEG-based composites. This observation can play an important role for example due to self-fixation of the implant in the defect. With respect to degradation, changes in network structure should therefore be considered and are notable investigations. Pure brushite and PEG-DMA_{lmw} batches had almost constant mass values whereas the other formulations, PEG-DMA_{hmw} and PEG-PLLA-DMA, showed the typical swelling behavior caused by the hydrogel. They increased in mass of ~ 90 % and doubled their weight over 11 days (see **Figure 29**). Consequently, the hydrogel phase most likely dominated the mass development.

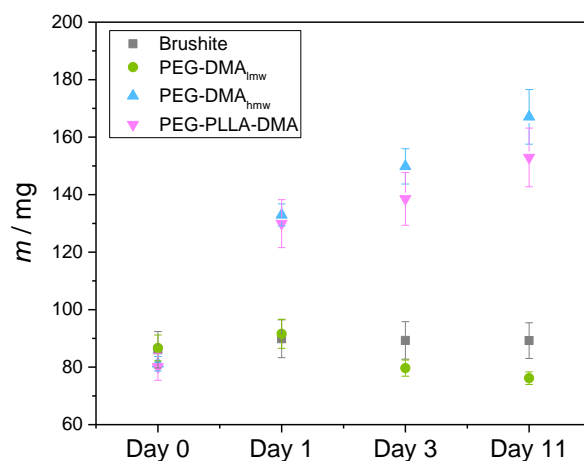


Figure 29:

Mass development of stored composites over a period of 11 days. An increase due to swelling of the hydrogel was detected for the batches PEG-DMA_{hwmw} and PEG-PLLA-DMA. Masses of the formulations with PEG-DMA_{lmw} and without polymeric content (brushite) were relatively stable.

A chemical identification of both phases in the composites was also verified by FTIR measurements. **Figure 30** shows the spectra of dual set samples with highest hydrogel concentration in comparison to pure brushite cement. Relevant peaks for the inorganic phase are listed in a publication of Hofmann *et al.* [228]. The four sharp, defined PO/P-O(H) stretching vibrations in the range of 1,150-870 cm^{-1} as well as the OH-stretching vibrations between 3,600-3,000 cm^{-1} and one around 1,650 cm^{-1} (H_2O bend) are detected for the cement containing samples. The grey parts in the spectra correspond to the signals detected for the organic phases. A dominant CH-stretching at about 3,000 cm^{-1} was measured for the dual set composites. Additionally, the stretching of the carbonyl group ($\text{C}=\text{O}$) was also visible in the spectra. Wavenumbers in the range of 1,450-1,360 cm^{-1} indicated the presence of the PEG-backbone (CH-bending).

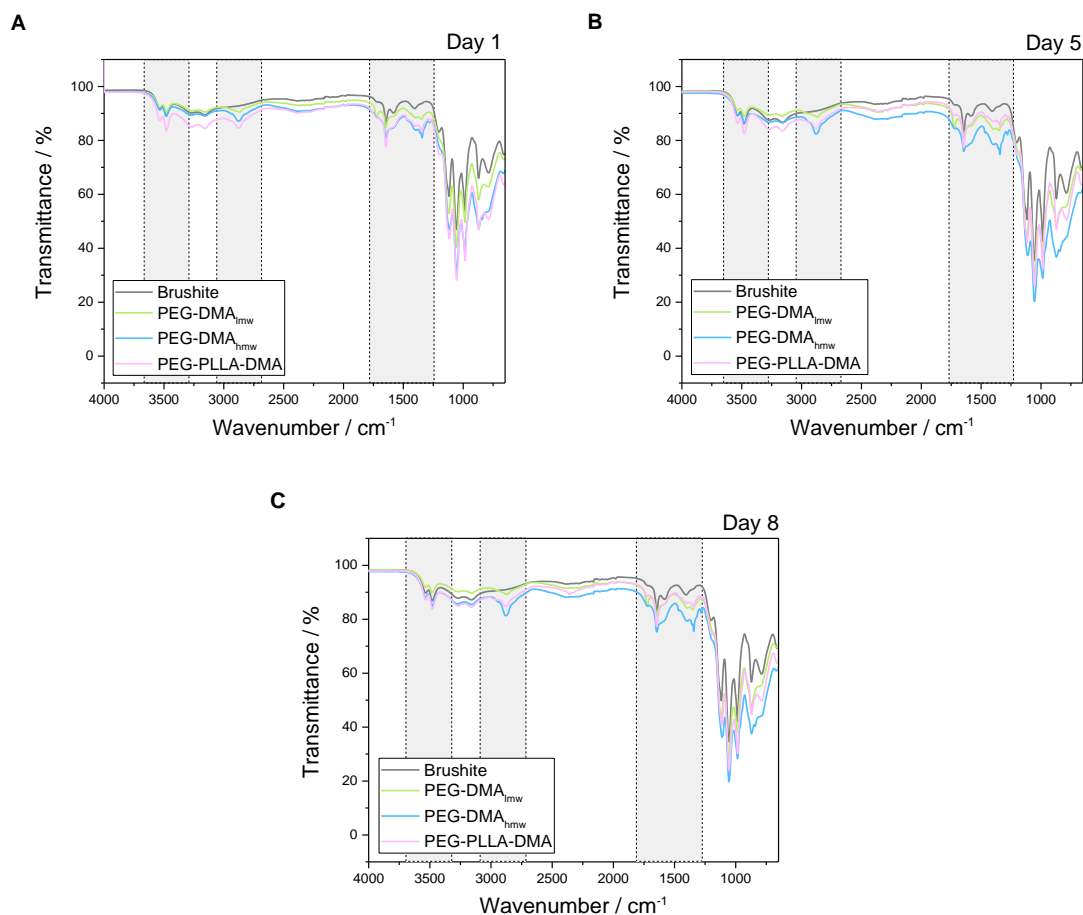


Figure 30:

FTIR spectra of composites with PEG-DMA_{lmw}, PEG-DMA_{hmw} as well as PEG-PLLA-DMA (all formulations with 50 wt% hydrogel precursor) for the identification of both phases, organic and inorganic, respectively (day 1 (A), 5 (B) and 8 (C)). The grey areas indicate the relevant regions for the chemical identification of the hydrogel phase in the composites.

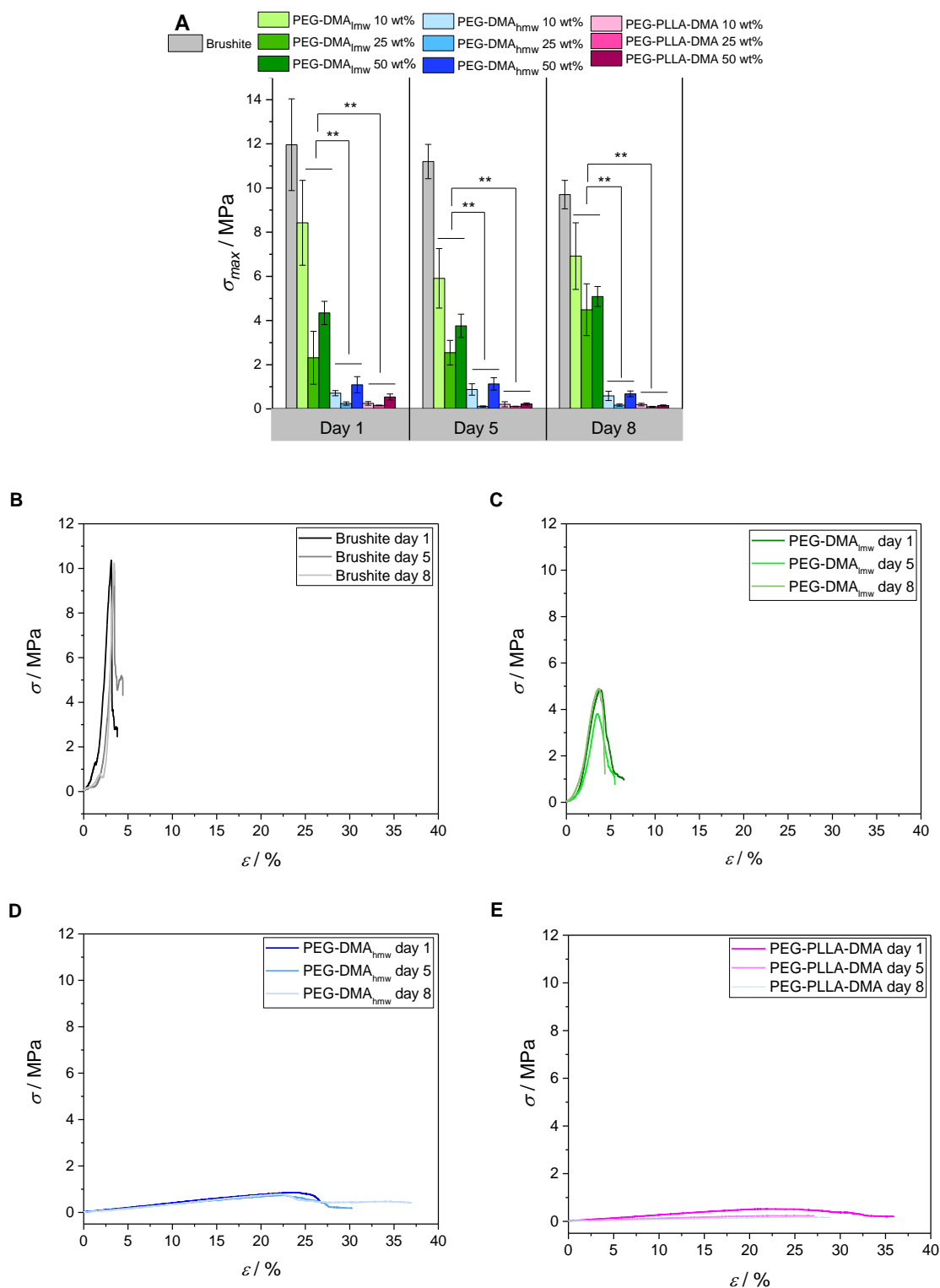
4.3.2.3 Compressive strength

Samples were tested under wet-conditions at three different time points after storage in PBS (day 1, day 5 and day 8). The maximum compressive strength σ_{max} was smaller for all composite materials containing an organic hydrogel phase. Accordingly, these values varied between 0.02 MPa and 12 MPa based on the composition. Due to different chain lengths of the PEG-backbone (~ 600 Da versus ~ 6,000 Da) as well as three different concentrations (10 wt%, 25 wt% and 50 wt% hydrogel precursors referred to the liquid phase), the results were in this broad range. For pure brushite cement, values of about 12 MPa for day 1 and day 5 were reached and decreased its compressive strength to 10 MPa after 8 days (see Figure 31 A).

Having a closer look for example at the results of day 1 for the batch with high molecular weight polymer (PEG-DMA_{hmw}), compressive strength was 0.71 MPa for the formulation with only 10 wt% hydrogel precursor. An increase to 25 wt% resulted in a significant reduction (approx. 70 %) of σ_{max} to 0.24 MPa. Doubling of the hydrogel precursor to 50 wt% again led to compressive strength values which were about 50 % higher (1.09 MPa) referred to the sample with the lowest polymeric content. This pattern of mechanical strength with different content of organic phase was observed for all composite formulations.

With respect to time course of mechanical strength, samples with 10 wt% low molecular weight polymer (PEG-DMA_{lmw}) showed strength levels between 8.5 MPa for day 1 and 5.9 MPa for day 5. At day 8, compressive strength again increased slightly to about 7 MPa. Here, especially these formulations reached similar values to pure inorganic brushite samples. A closer look on the stress-strain curves in comparison to high molecular weight PEG-DMA revealed a more ductile behavior with an increase in maximum stress up to 5 % for PEG-DMA_{hmw} (see **Figure 31 B** and **C**).

Both batches with high molecular weight PEG (PEG-DMA_{hmw} and PEG-PLLA-DMA) showed the trend of a decreasing compressive strength from day 1 to day 8 for each concentration. One exception were the composites with PEG-DMA_{hmw} in a concentration of 25 wt%. Here, the value increased from 0.11 MPa at day 5 to 0.17 MPa at day 8. The variation with PLA-units led to relatively low compressive strength values of 0.13 MPa for 10 wt% polymeric phase, 0.10 MPa for 25 wt% hydrogel phase and 0.15 MPa for the samples with 50 wt% organic content. Though the amount of hydrophobic PLA-spacer only increased the polymer molecular weight and accordingly the chain length slightly (approx. 6%), the strength values decreased extremely compared to non-degradable PEG-DMA_{hmw}. Here, for example, 0.59 MPa could be reached for the samples with 10 wt% hydrogel after 8 days of storage. A remarkable elastic and ductile behavior was observed for all these batches. Strain-levels of 25 to 35 % were reached and extremely deformable and also re-shapeable specimens were produced which returned into their original shape after removal of the force (see **Figure 31 D** and **E**).

**Figure 31:**

Compressive strength testing of the different cement-hydrogel formulations. **A:** Overview of the maximum compressive strength values for the three different time points, the three different hydrogel precursors with different composition in molecular weight and their variation in content. **B-E:** Stress-strain curves of the batches brushite (**B**), PEG-DMA_{lmw} 50 wt% (**C**), PEG-DMA_{hnmw} 50 wt% (**D**) and PEG-PLLA-DMA 50 wt% (**E**). The higher the molecular weight of the hydrogel precursor, the more ductile the behavior of the samples. Formulations with 50 wt% PEG-DMA_{hnmw} as well as PEG-PLLA-DMA also returned into their original shape after removal of the applied force and first cracks in the specimen.

To compare the results of the composites with pure hydrogel samples of the three different polymeric batches (PEG-DMA_{lmw}, PEG-DMA_{hmw}, PEG-PLLA-DMA), small round specimens were produced with the highest content of hydrogel precursor (50 wt%). Calculated Young's moduli of the pure organic phases as well as dual set systems were compared (see **Figure 32**). PEG-DMA_{lmw}-composites showed values of about 3,000 kPa whereas PEG-DMA_{hmw}-samples only reached levels of about 300 kPa. The Young's modulus further decreased about 50 % for specimens made of PEG-PLLA-DMA. The values of the pure hydrogel could only be measured for PEG-DMA_{hmw} and PEG-PLLA-DMA and were determined as 28 kPa and 23 kPa, respectively.

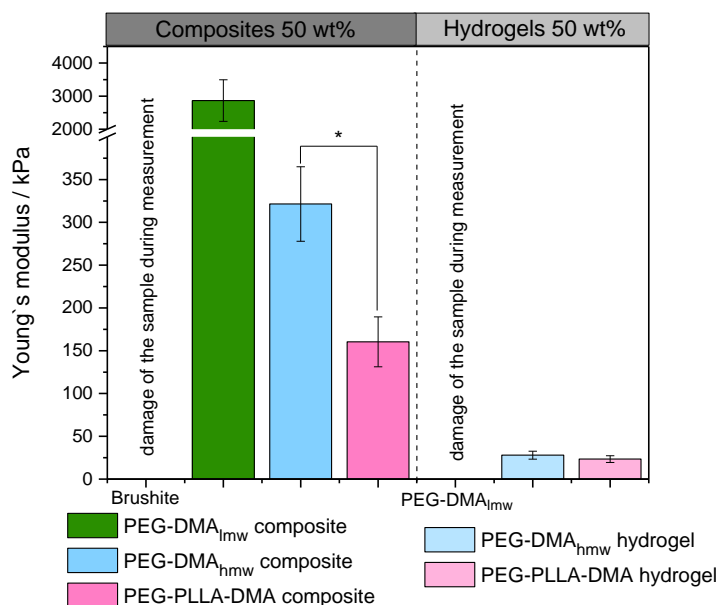


Figure 32:

Young's moduli of composites *versus* hydrogels, both containing 50 wt% of hydrogel precursor for each of the different formulations.

For the composites, additional dynamic compressive strength testing was performed. PEG-DMA_{lmw}-samples were destroyed during the measurement since they were too hard and lacking the elastic properties necessary for the cyclic deformation. Stress-strain curves already illustrated the destruction starting from the first testing cycle in a continuous decrease of true stress level. Consequently, single measurement cycles shifted and were not congruent any more. The initial maximum value of the true stress was about 6,000 kPa (see **Figure 33 A**).

For high molecular weight PEG-containing formulations, a similar elastic hysteresis was observed indicating a slow relaxation after removal of the load. Stress-strain curves were narrowly distributed over 10 cycles with an excellent reversible behavior. After the first slope, the hydrogel samples showed congruent curves for a deformation of 0.5 mm with a maximum stress of 35 kPa for the PEG-DMA_{hmw}-hydrogel and 27 kPa for the PEG-PLLA-DMA-hydrogel (see **Figure 33 B and C**).

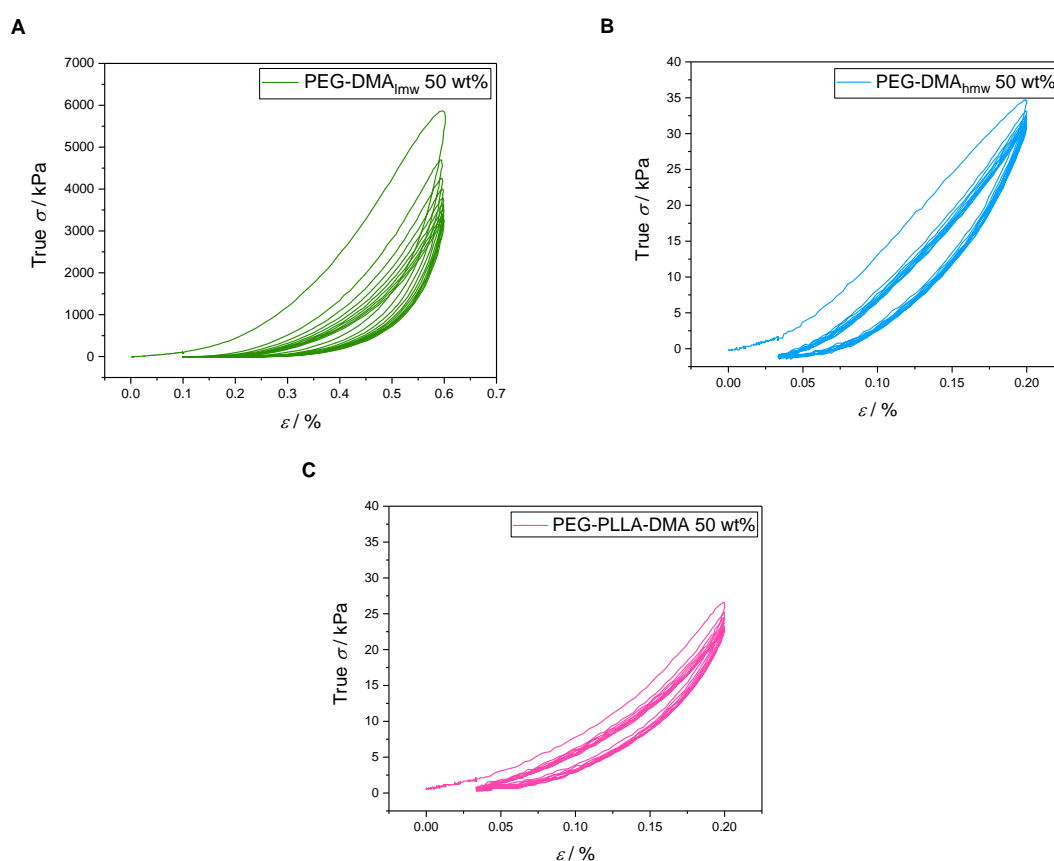


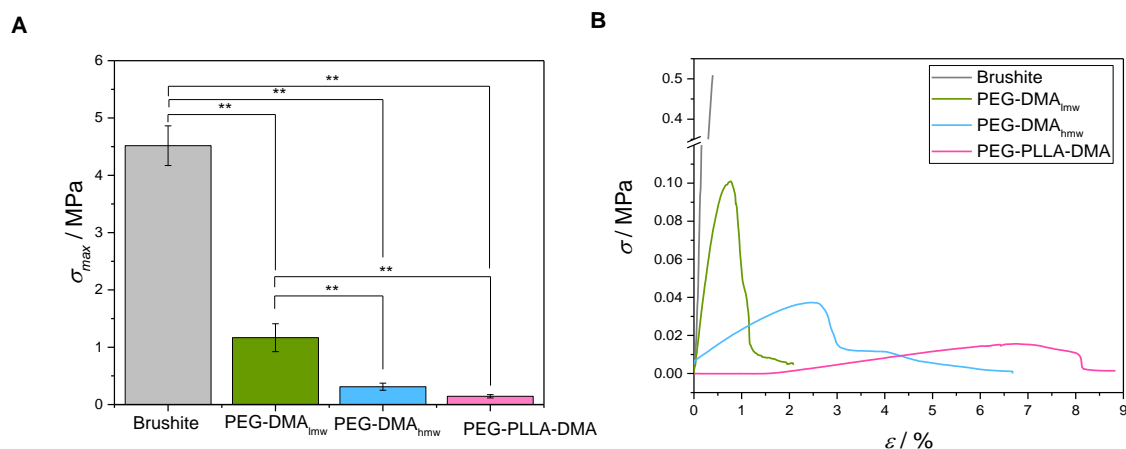
Figure 33: Overview of stress-strain curves of the dynamic testing for the batches PEG-DMA_{lmw} (A), PEG-DMA_{hmw} (B) and PEG-PLLA-DMA (C) with 50 wt% hydrogel precursor referred to the liquid phase.

4.3.2.4 Bending strength and toughness

Regarding 3-point bending test, composite materials behaved flexible and showed the same trend as seen for compression test. The pure brushite reference behaved stiff, failed after a few seconds and reached a maximum flexural strength of about 4.5 MPa. However, the composite materials were more bendable. Formulation

PEG-DMA_{lmw} reached strengths values of about 1.2 MPa that were four times higher compared to the high molecular weight PEG-batch (PEG-DMA_{hwm}). With incorporation of PLA-units, the bending strength further decreased to about 0.2 MPa (see **Figure 34 A**). Indeed, this formulation showed the highest reflection within a range of about 8 % (see **Figure 34 B**). These results corresponded with the size indications for compressive strength testing. Overall, higher molecular weight PEG-backbones resulted in an elongated deformation and an increased ductility of the composite materials.

Additionally, toughness as dimension of absorbed energy and plastic deformation without fracture was determined. All three batches containing PEG-DMA_{lmw}, PEG-DMA_{hwm} and PEG-PLLA-DMA were compared with toughness values of the pure brushite reference which were about 19 J*(m⁻²) (see **Figure 34 C**). The highest toughness levels were reached for samples containing 50 wt% PEG-DMA_{hwm} with 67.4 J*(m⁻²). This formulation was also used to demonstrate the extreme flexibility by hammering a nail in the round shaped specimen without a crack whereas the pure brushite sample failed the nailing test by breaking in two parts (see **Figure 34 D**). With increasing degradability for the formulation with PEG-PLLA-DMA, toughness was reduced to about 18 J*(m⁻²). This value was comparable to the pure brushite cement. However, elasticity increased extremely. Samples containing PEG-DMA_{lmw} were in the range of 25 J*(m⁻²).



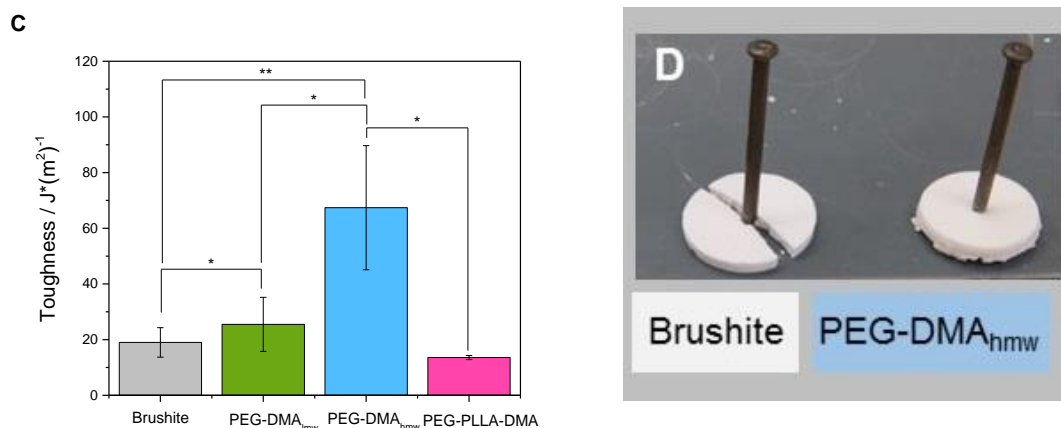


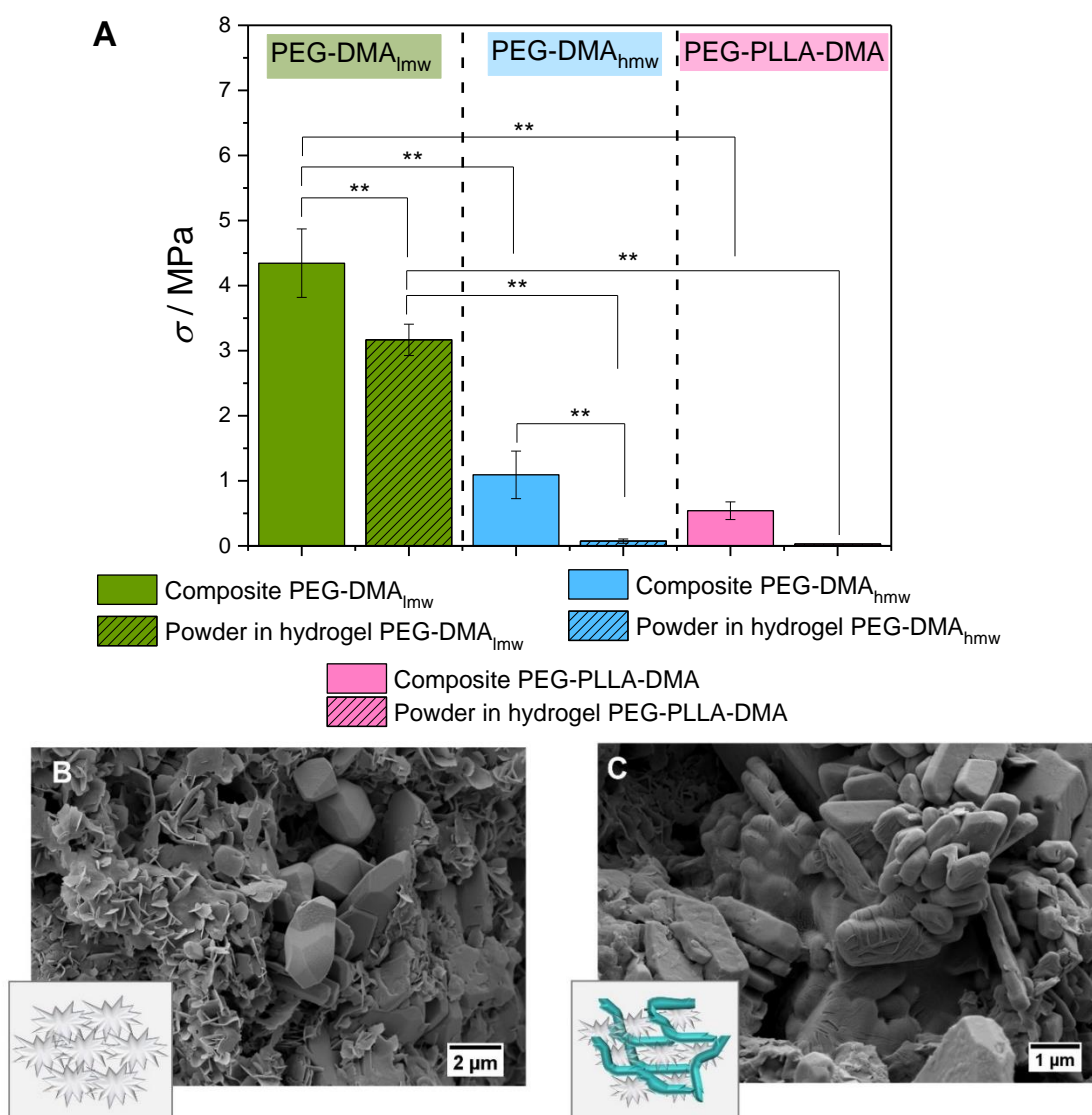
Figure 34:

3-Point bending test of the inorganic reference in comparison to the dual set composites. **A:** Maximum bending strength of tested samples. With organic phase, values decreased from 4.5 MPa to about 1.2 MPa for PEG-DMA_{lmw}, 0.3 MPa for PEG-DMA_{hmw} and 0.2 MPa for PEG-PLLA-DMA. **B:** Stress-strain curves of different formulations. Samples containing PEG-PLLA-DMA showed a very ductile behavior with a maximum deformation of 8 %. **C:** Toughness evaluation of bending strength testing for all composite formulations. Formulations containing PEG-DMA (low as well as high molecular weight) with an amount of 50 wt% hydrogel precursor (referred to the liquid phase) increased in toughness compared to pure inorganic reference. **D:** This image shows once more the brittleness of brushite without any hydrogel addition and the elasticity of a sample containing PEG-DMA_{hmw} (50 wt%). For this disk, nail incorporation was feasible without a crack or fissure.

4.3.2.5 Particle filled hydrogels *versus* composite materials

Mechanical testing of ground cement powder filled hydrogels in comparison to the *in situ* formed composites (all formulations with 50 wt% polymeric content referred to the liquid phase) showed significant differences in compressive strength for the formulations with low and high molecular weight PEG-DMA (see **Figure 35 A**). The samples of PEG-DMA_{lmw} composites reached levels of 4.34 MPa in comparison to the particle filled hydrogel, which only reached 70 % of the composite's value. This decrease in compressive strength was even higher for the formulations PEG-DMA_{hmw} and PEG-PLLA-DMA. The dual setting mechanism led to samples with a compressive strength of 1.09 MPa and 0.54 MPa, respectively. For the pure hydrogel with pulverized brushite, only 6-7 % of the composite's values were observed. The comparison of the dual set materials with the powder filled hydrogel was almost significant ($p < 0.054$). This resulted in the reduction of free and available methacrylic functions due to the highest chain length and molar mass.

A characterization of the crack surface *via* SEM illustrated the typical plate-like structure of brushite crystals for the pure inorganic reference (see **Figure 35 B**). Composite materials with 50 wt% PEG-PLLA-DMA showed bigger crystal structures due to a preferential inhibition of the growth of small crystals caused by the organic polymer phase (see **Figure 35 C**). Pulverized brushite powder in the PEG-PLLA-DMA hydrogel (50 wt%) on the other hand exhibited a particle filled hydrogel matrix without any network structures of mineral crystals (see **Figure 35 D**).



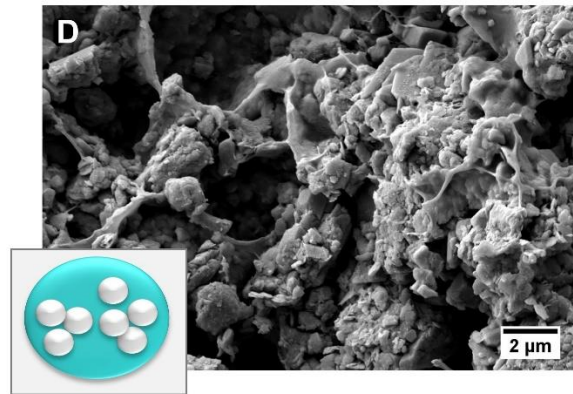


Figure 35:

Comparison of powder filled hydrogels for verification of an incorporated network and a dual process of hydrogel formation and cement setting reaction. **A:** Compressive strength overview of pulverized brushite in the different hydrogel systems and the corresponding composite formulations (hydrogel precursor concentration for all formulations 50 wt%). **B:** SEM image of pure brushite reference. **C:** SEM image of dual set composite material with brushite cement and 50 wt% PEG-PLLA-DMA. **D:** SEM image of powder filled hydrogel with 50 wt% PEG-PLLA-DMA as hydrogel phase and pestled brushite.

4.4 Discussion

About 20 years ago, Dos Santos *et al.* [175] reported the first time of the new class of dual setting systems to overcome issues like brittleness for improving mechanical performance or to avoid burst release of drugs like antibiotics for creating a controlled drug release. In this study, we advanced the idea of a simultaneously started process of cement setting and synthetic hydrogel formation in direction of a fully degradable system. Therefore, brushite cement was chosen as inorganic matrix due to its faster degradation *in vivo* compared to HA [229]. The mechanism of its setting is based on the reaction of an acidic phosphate source like MCPM in combination with an alkaline calcium source, for example β -TCP. Three principle steps are passed through until the final product brushite is formed [43]. First, the raw powder mixture has to be dissolved in the liquid phase with formation of a super-saturated gel. Within this matrix, crystal growth or nucleation is initiated and a solid network of interlocked crystals is generated *via* entanglements. The question arises, how a second phase (in this study different PEG-based hydrogel) affects cement setting. Furthermore, what is the influencing effect of the setting mechanism on the radical reaction of the gelation?

Via EDTA-coherence study, a homogenous phase distribution was verified. There were no local hydrogel agglomerations which indicated the successful radical polymerization through the whole specimen. Moreover, XRD measurements were used to control the conversion of the inorganic phase from an equimolar β -TCP/MCPA-mixture to brushite cement. FTIR analysis further confirmed that both reactions (cement setting and gelation) occurred during sample hardening. Regarding dual set materials, an initial pH-decrease during setting was detected for the pure brushite formulation and the batch PEG-DMA_{lmw}. For the specimens containing PEG-DMA_{hwmw} and PEG-PLLA-DMA, the pH-level was almost constant within a pH-interval of 2-2.5. All composites with an organic phase retained these acidic pH-levels after 60 min, which can be attributed to the ascorbic acid necessary for the cross-linking reaction. Nevertheless, hydrogels especially with high molecular weight PEGs remained in a swollen state. This means that during setting and gelation there were enough water molecules available for both reactions: layering between the CaP sheets of brushite crystals on the one

hand [230] as well as hydrogel formation and maintaining of the hydrated state on the other hand. Furthermore, the observed swelling of the hydrogel phase upon incubation in fluids could be used for further fixation of the composite at the implantation side. For initial setting temperature, an additional positive effect could be observed for the batches with high molecular weight PEGs. These samples showed in comparison to the brushite reference and the PEG-DMA_{lmw} formulation no temperature increase (up to 45 °C for brushite). Temperatures stayed stable in the range of 22-28 °C and proved the buffering effect of the hydrogel phase. This is thought to be advantageous for clinical applications to avoid damage of surrounding tissues since thermal necrosis in bone is already induced at temperatures higher than 50 °C for more than one minute [231]. In comparison to that, PMMA cements for example can reach temperatures up to 120 °C during setting depending on the size of the sample [232]. Similar beneficial effects were observed in a study of Zhao *et al.* [233], where they used a system based on brushite (with β -TCP and MCPA as raw material) in combination with poly(propylene glycol-co-lactide) dimethacrylates (PPGL-DMA; 90 wt%), HEMA and camphorquinone as initiator even without the addition of water. Instead, they used blue light exposure to start the polymerization and thereby solid composite disks were produced. The reduced heat release was explained by the high molecular weight polymers and a consequently low methacrylate concentration. This eventually can also be transferred to the results with high molecular weight PEGs. Moreover, no thermal damage was even observed within an *in vivo*-study with embedded β -TCP granules in a DCPD matrix, where no dead cells in the adjacent tissue next to the implant side were detected [59].

Hydrogel properties distinguished the materials from our study from previous works of Abou Neel *et al.* [234] who used brushite cement filled PPGL-DMA polymers as bone adhesives whereas the absence of a PEG-unit within the polymer prevents the formation of a gel phase within the composite. In contrast, the dual setting mechanism in the current study was developed based on a brushite forming cement setting and a parallel hydrogel formation. The incorporation of different PEG-DMA-based hydrogel phases (molecular weight range of approx. 600-6,000 Da and a variation with PLA-units) allowed an extreme plastification of the composite material.

Regarding mechanical performance, compressive strength levels of brushite samples without polymer addition are comparable to values found in literature where similar PLRs and 0.5 M citric acid solution were used [235]. Pure brushite cement reached a maximum compressive strength value of about 12 MPa. A decrease in strength was observed during a storage time of 8 days which can be explained due to a starting degradation of the cement [236]. With addition of PEG-based hydrogels, the properties of all composites were shifted to a more elastic behavior. For the formulation with PEG-DMA_{lmw}, values indicate a tight network of the hydrogel with rather smaller mesh sizes and eventually highly defective network structures. Therefore, achieved deformation was less for this composite material. With high molecular weight PEG-based polymers, samples were much more ductile and behaved flexible with a very high strain (up to 30 % for PEG-DMA_{hmw} and PEG-PLLA-DMA). In this case, mesh sizes of the hydrogel seemed to be much wider and allowed a fully elastic deformation. With increasing polymer content, an improved stability also arose from the coherent hydrogel networks within the composite specimens. However, HA-based dual setting cements provided much higher strengths compared to brushite based materials of the current study. Thus, the combination of 50 % HEMA with α -TCP resulted in an increase of cement bending strength by ~ 50 % [179]. We speculate that brushite dual setting systems have much lower strength in comparison to apatite cement due to shape and size of the precipitated cement crystals. While the form of nanosized HA crystals is often spicular and needle-like, crystals can grow more easily, entangle in the hydrogel network and hence provide a high mechanical performance. In contrast, size of brushite crystals is in the μm -range and due to the plate-like character a less effective entanglement is achieved during setting. Consequently, mechanical enhancement by a second phase in brushite cements is not as strong as for relevant cements containing HA.

Results of 3-point bending test showed the same trend regarding stress values as seen for compression testing. With the highest amount of PEG-DMA_{hmw} in the composite material (50 wt% referred to the liquid phase), the toughness increased up to 67 J*(m⁻²). This is three times higher compared to pure brushite cement without a second organic phase. A review of Krüger *et al.* [188] gives an overview of fiber reinforced CPCs with a list of several toughness values reported in

literature. Both modifications, the fiber reinforcement as well as the dual setting system approach, should lead to enhanced toughness. The highest values reached for high molecular weight PEG-containing formulations were comparable to pure HA matrixes with levels of about $50 \text{ J} \cdot (\text{m}^{-2})$ [237]. This correlates to the above described fact of different crystal structure, form, arrangement and architecture for brushite *versus* apatite cement. Reported values are mainly based on fiber reinforced constructs. However, similar levels regarding bending strength were found for another composite formulation that was measured under wet conditions, too. In this study, also brushite cement was combined with a hydrogel phase based on silk fibroin. The addition of the polymeric compound resulted in bending strength values less than 1 MPa [181].

Young's moduli of pure hydrogels without mineralization were similar to values found in literature [238]. However, the observed strengthening effect with increasing hydrogel precursor concentration was also comparable with the results investigated in the EDTA-study. Here, coherence and degradability were important for the retention of the hydrogel. PEG-DMA_{lmw} samples had a friable look after storage in neutral EDTA-solution which represented a network with short chain lengths and small meshes. Regarding strength, this was attended by much stiffer material properties. In contrast, the two formulations with PEG-DMA_{hmw} and PEG-PLLA-DMA were well cross-linked and dimensionally more stable as hydrogel blocks (see **Figure 25**). A mixture of erosion and degradation could be seen for all three composites based on the instability of the ester bonds and network homogeneity. Especially for PEG-PLLA-DMA hydrogels it is obvious that with time ester bonds break down and remaining hydrogels lose their initial shape. An increase in mechanical strength was especially observed when comparing higher molecular weights and 25 wt% *versus* 50 wt% polymeric content. Increased stability of the polymeric network was based on the free radical chain growth polymerization. In case of diacrylated PEGs, this cross-linking mechanism leads to irregular randomly cross-linked networks [239]. Previously, different radical initiator systems were tested in combination with PEG-hydrogel precursors as well as the brushite forming system. It was challenging to identify ascorbic acid as suitable candidate, which is stable under acidic conditions in combination with H_2O_2 as catalyst for the radical polymerization. These conditions were provided by the liquid

phase (0.5 M citric acid solution was used in order to have a setting retardant) as well as the setting condition itself ($\text{pH} \leq \sim 4.2$). In a study of Luo *et al.* [240], the brushite setting process was analyzed in the first minutes of the reaction. They noticed a rapid nucleation and a brushite crystal growth within 18 seconds. The fast hardening was also observed in this study during processing of the material. Also, XRD patterns showed reproducible phase compositions from day 1 to day 8. After day 5, an amorphous halo at about 12° was observed for the composite materials containing PEG-DMA. This signal is related to the presence of this polymer and was observed independently of the molecular weight for the formulations PEG-DMA_{lmw} and PEG-DMA_{hmw}, respectively. Killion *et al.* [241] described this effect and noticed an amorphous reflection for this kind of hydrogels containing β -TCP which resulted in regions with a low crystallinity. However, in our study a strong domination of the inorganic phase and an overlap with brushite reflections was given in the region between 10 - 15° . In comparison to the study of Killion *et al.* [241], we had no pure hydrogel with incorporated β -TCP-particles, but a dual set system. Furthermore, the added organic phase had no influence on the nature of the setting reaction to the final product, but significantly affected the size of the brushite crystals which could be observed in different SEM images (see **Figure 27**). With appearance of PEG, the same effect which was also noticed by Engstrand *et al.* [220] led to a conversion to mainly brushite cement. Due to hygroscopic properties of PEG, water is highly attracted in the samples and increased the rate of brushite formation in competition to monetite. This indicated a homogenous phase distribution of the hydrogel within the cement matrix, too. On the one hand, plate like structures were bigger in comparison to brushite crystals of the inorganic reference. On the other hand, smaller fractions were detected for the composites and generated a second crystal formation. The latter phenomenon was also seen in previous studies dealing with dual setting systems [181]. EDTA-demineralization study as well as SEM images showed a homogenous interpenetrating network of both, the cement and hydrogel phase. The uniform distribution of the two components demonstrated once more the successfully running process of setting and gelation within the dual setting system with intersecting time frames of both reactions.

Regarding cytocompatibility of the composite, subsequent studies showed *in vitro* tests using brushite cement, also in combination with a second phase like collagen or silk [187, 217] as well as PEG [219]. Though the addition of PEG, human fetal osteoblast (hFOB) cell proliferation decreased, whereas the activity of alkaline phosphatase as well as the cell differentiation increased. Unfortunately, no further details regarding molecular weight (liquid, for example about 500-600 Da) or chemical provider of the used PEG were noted in this study.

One critical point of view in the current study might be the use of the radical initiator ascorbic acid and the catalyst H_2O_2 for the gelation reaction *via* radical polymerization. However, in a study of Wistlich *et al.* [242], cytocompatibility tests were performed in presence of another system for radical polymerization: D,L-camphorquinone was used as initiator in combination with TEMED (0.1 %). An elution test showed a good cytocompatibility though the presence of TEMED. In our study, ascorbic acid and H_2O_2 were used in order to induce the radical reaction. First, ascorbic acid is well known as radical initiator and essential vitamin as well as the pH-value of the setting to brushite already had to be rather acidic. Second, H_2O_2 was found to have also a certain antibacterial effect in orthopedic applications [243] and is used for disinfection in a concentration of 3 % [244]. In this study, a concentration of 1.5 % was used for hydrogel formation which could additionally be a big advantage and prevent infections next to implantation side.

For a clear prediction of the constructs' degradation, *in vivo* studies of the optimal composition with animal testing are required. However, there are several reports in literature dealing with the degradation of both, brushite as well as PEG-based hydrogels, that an expectation of biodegradation can be hypothesized. Regarding degradation of PEG-hydrogels, the structure presumes a susceptible oxidation of the ether backbone as well as hydrolytically labile terminal ester functions. Browning *et al.* [204] investigated the degradation of hydrogels (10 wt%) based on diacrylated PEG monomers (10 kDa) *via* subcutaneous implantation in rats. They demonstrated that hydrolysis of the ester end groups of stable gels over a time of 12 weeks is the primary mechanism of *in vivo* resorption. With an additionally methyl functionality for dimethacrylated PEGs that are used in this study, the reaction kinetic decreased due to an increase in hydrophobicity. Incorporation of

lactic acid-spacers at both ends of the linear PEG-chain (PEG-PLLA-DMA) resulted in another ester bond for the reaction with water molecules. It was shown in a similarly composed hydrogel system, that lactide ester linkages are cleaved homogeneously in the gel. Metters *et al.* [157] reported on an *in vitro* degradation behavior with complete bulk-erosion which led to water soluble remaining substances (PEG and lactic acid) of a previously insoluble gel. Consequently, an advanced cleavage of cross-links within the hydrogel influenced the network density and different properties like elasticity, mesh size or degree of swelling [245, 246].

Focusing on *in vivo* degradation of the inorganic phase of the composites, brushite is resorbed in a higher extent than apatite cement. There are mainly two mechanisms that lead to degradation of brushite cement: on the one hand dissolution processes, on the other hand cellular activities whereas the latter one is the dominating parameter [43, 247]. Furthermore, also disintegration can lead to weight loss of brushite as another disintegration approach [248]. In a study of Bohner *et al.* [249], implanted DCPD in sheep showed selective dissolution in the first 2 weeks of implantation due to the low pH-value in the early state of embedding. After 6-8 weeks, a transformation into still resorbable apatite crystals occurred.

Overall, stability and resorption behavior of both phases *in vivo* will be a very complex and challenging process. As seen for other polymeric additives like hyaluronic acid which decreases the resorption rate *in vivo* [250], the second component in the inorganic brushite cement will affect biological properties.

4.5 Conclusion and outlook

This study was performed to develop and characterize a newly established dual setting system based on brushite cement and dimethacrylated PEG-hydrogels with different mesh sizes due to different polymer chain lengths. Small molecular weight, liquid PEG-DMA_{lmw} showed much stiffer properties of the composite material in comparison to the formulations produced with high molecular weight PEG-DMA-variations. These composites on the other hand exhibited a slight swelling after storage in PBS, which consequently indicated bigger hydrogel network structures for these polymers and might improve the fixation of the replacement material at implantation site.

Both preparation processes, the cement setting reaction and (hydro-) gelation, run parallelly as well as compatible to each other and resulted in an incorporated network of inorganic and organic phase. This was confirmed after demineralization of the samples using the complexation agent EDTA. The hydrogel phase did not have an influence on the conversion from β -TCP in combination with MCPA (equimolar ratio) to brushite, which was verified using XRD analysis. Only the nature of the brushite crystal size was affected by the organic additive. Regarding mechanical properties, the produced samples strongly increased in elasticity in comparison to pure brushite cement. For the formulations containing PEG-DMA_{hmw} and PEG-PLLA-DMA, strain-levels up to 25 % were reached and a complete return into the original shape after compressive strength testing was observed.

These constructs are a promising tool for bone regeneration in non-load bearing defects where a certain elasticity should be given for example due to an incorporation of materials into not easily accessible regions. This elastic effect can improve surgical handling when it is necessary for flexural implants, for example in craniomaxillofacial surgery. Starting from the two extremes with polymers of 600 Da and 6,000 Da, the ideal formulation with the optimized molecular weight and hydrogel mesh size still has to be found to adjust the mechanical properties for a certain application. Furthermore, the role of degradability with a higher amount of PLA-units or other instable linkages, like acetals or specifically degradable peptides, can be investigated to further improve these composite systems.

Chapter 5

Dual setting system based on brushite cement and genipin cross-linked gelatin with increased ductility and sustained drug release

Chapter 5 is written in form of an original research article which is submitted to the journal *Materials Science and Engineering: C* by submission time of this thesis. The article is based on work of the author of this thesis Michaela Rödel, who performed all experiments, data evaluation and composition of the manuscript.

5.1 Abstract

A novel dual setting system based on gelatin and brushite cement was developed. Cement setting occurred at acidic conditions in parallel with a physical as well as chemical cross-linking of gelatin by genipin, that started simultaneously to dissolution-precipitation reaction of the mineral matrix. By the successful combination of an inorganic and organic phase, an increase in elastic properties with a certain cohesiveness due to gelatin hydrogel with a concentration of 10.0 w/v% was achieved. For a PLR of 2.5 g*mL⁻¹, a shift of initial maximum stress value during compression testing was observed up to 5 % deformation, whereas pure brushite cements only reached 2 %. This increase in flexibility involved a change of maximum stress values from about 10 MPa without polymeric phase to 6 MPa with 2.5 w/v% gelatin addition, 5.5 MPa with 5.0 w/v% gelatin and 3 MPa with 10.0 w/v% incorporated gelatin. The obtained composites of the different formulations were characterized regarding phase composition, porosity as well as drug loading capacity with two different antibiotic compounds, namely rifampicin or vancomycin. For the latter, a sustained and prolonged release was realized with a high linearity in drug release profile according to Higuchi-model and a release exponent of 0.5 for the formulation with a PLR of 2.5 g*mL⁻¹ and an incorporation of 10 w/v% gelatin.

5.2 Introduction

Among important phases in biomedical field like CDHA or OCP [251], the water-containing form brushite [252] as well as the water-free form monetite [253] are two of the stable systems that are used as bone replacement materials in the category of CPCs [23]. Both are formed in a hydraulic setting reaction *via* dissolution-precipitation reaction: a fraction of the raw powder is dissolved in the liquid phase and forms a super-saturated gel; subsequently, crystal growth starts in this matrix by setting to an interlocked and entangled cement network providing the final mechanical stability. Brushite cements are prepared by homogenous mixing of an acidic and basic CaP component. Mostly, MCPA and β -TCP are used in an equimolar ratio. Depending on the amount of water, either brushite or monetite is formed whereas with lower availability of water molecules and higher ionic strength of the cement liquid, monetite formation is generally preferred [60]. The Ca/P ratio of the final product is 1.00, which explains the need for an additional acidic phosphate source, like MCPA or H_3PO_4 . In contrast to HA, brushite cements need an acidic environment for their setting reaction ($pH \leq \sim 4.2$). As consequence, the formed cements exhibit a certain pH-sensitivity which ultimately results in a pH-dependent degradation under physiological conditions ($pH = \sim 7.4$) that is driven by pure dissolution processes or even active cell mediated resorption [247]. Overall, the solubility product constant K_{sp} of DCPD is $2.57 \cdot 10^{-7}$ and thus many times higher than the value of HA ($K_{sp} < 10^{-116}$) [23], which explains the significantly higher solubility that can be used to create degradable systems for implantation mainly in non-load bearing defects.

This limitation is due to the fact, that both mineral bone cements show a quite brittle behavior which can result in defects and consequently implant failures. A well-known reinforcement strategy for such cements to overcome this drawback is the *in situ* formation of hybrid materials that are composed of polymeric network(s) and inorganic matrix(es). These so called dual setting systems provide the big advantage of a homogenous distribution of both phases with interlocking cement crystals and a continuous hydrogel network and thus resulting in mechanical properties with increased elasticity and flexibility. The first report of a dual setting system was published by Dos Santos *et al.* [178] who created a hybrid model by

in situ polymerization of AA and ammonium PA with added α -TCP. Further polymer-cement systems on dual setting approaches were based on a combination of HEMA and HA [179, 191] or PEG hydrogels and brushite cements [193]. All studies used a radical polymerization for gelation with a radical initiator mixed in the solid phase as well as a catalyst dissolved in the liquid phase. Other two modifications were developed by Schamel *et al.* [181] with one system leading to a physically cross-linked silk fibroin network induced by a pH-shift to acidic pH-values in a brushite matrix. A second method was established using a nucleophilic reaction of isocyanates and the *in situ* generated amines from six armed star-shaped molecules (NCO-sP(EO-*stat*-PO) to carbonyl diamides during setting reaction of the inorganic phase to HA [180].

A commonly used biopolymer in pharmaceutical, photographic or food industry is gelatin, which is produced by denaturation of collagen *via* hydrolysis under acidic (type A; isoelectric point at pH 7-9) or basic conditions (type B; isoelectric point at pH 4.7-5.0). In comparison to collagen, denatured gelatin as purified protein has less antigenicity, which also makes it more suitable for medical applications [141]. In order to induce biopolymer gelation parallel to setting, gelatin of type A was chosen in this study due to its gelling ability at pH of 3.2, which is in the pH-range of the chosen cement setting [254]. Another important criterion is its fast degradation due to swelling and rapid dissolution at body temperature and in aqueous environments [142]. To overcome the reversible gelling behavior, gelatin has to be chemically cross-linked by different bifunctional agents like diisocyanates, carbodiimides or glutaraldehyde [143]. The latter is the most prominent candidate, which results in constructs with the highest mechanical stability. Nevertheless, all the above mentioned cross-linkers are also known to influence cell growth and have adverse effects on cells *in vivo* and *in vitro* [255]. As alternative, biocompatible component, genipin as natural cross-linker with less cytotoxicity [144] was used in this study to assure an irreversible cross-linking of the hydrogel phase and prevent its fast dissolution.

Different formulations of other CPCs and gelatin without simultaneous starting of gelation and setting are already established and reported in literature. Cements were modified with gelatin for example in an approach of Bigi *et al.* [256] in order to

obtain biomimetic bone cement. A suspension of gelatin solution and α -TCP was produced in petri dishes, dried, crushed and sieved. This powder was mixed with 5 wt% of DCPD. Produced composite materials exhibited a faster transformation to CDHA with smaller crystal sizes in comparison to pure inorganic phase with improved mechanical properties [257, 258]. Another strategy is reinforcement of gelatin foams by HA and afterwards cross-linking with a carbodiimide derivate [259]. By this means, HA particulates contributed to stiffness and rougher surfaces, but still elastic properties are provided by the gelatin gel. Consequently, to the best of our knowledge, there is no report in literature regarding brushite and cross-linked gelatin combinations that are formed *via* dual setting mechanisms. Here, we focused on a strategy for the simultaneous gelatin cross-linking by genipin simultaneously to cement setting reaction of brushite.

In this study, we developed a novel approach for a dual setting system which was characterized regarding its phase composition, mechanical performance (in comparison to pure organic and inorganic matrix), conversion rate and influence of the hydrogel phase on the setting reaction. With this broad analysis of the established formulations as well as the ability of sustained drug release of vancomycin, these composites based on brushite cement and genipin cross-linked gelatin are a promising tool for the use in biomedical applications, for example for the treatment of osteomyelitis.

5.3 Results

5.3.1 Characterization of gelatin-brushite composite formulations in comparison to brushite cement as inorganic reference and pure gelatin hydrogel as organic reference

5.3.1.1 Analysis of preparation procedures

The development of a dual setting system containing gelatin as hydrogel phase in an inorganic brushite cement matrix was successfully performed. An irreversible cross-linking of gelatin was induced by reaction with genipin which was mixed in the solid phase of the β -TCP/MCPA raw powder. Specimens without genipin were not dimensionally stable and disintegrated into their individual components due to swelling of the gelatin hydrogel. In a study based on pH-dependency and collagen reaction with genipin, significant differences in swelling capability, resistance against enzymatic hydrolysis as well as cross-linking degree were reported [260]. Due to the color change by creating a chromophore system with genipin and the macromolecular biopolymer, a homogenous gelation with incorporation of the hydrogel in the inorganic matrix was confirmed (see **Figure 41 E**). The blue pigments of cross-linked genipin, however, were characterized to be highly stable to heat (up to 90 °C), pH (pH-range of 5-9) and light (exposure up to 20,000 lux) [261].

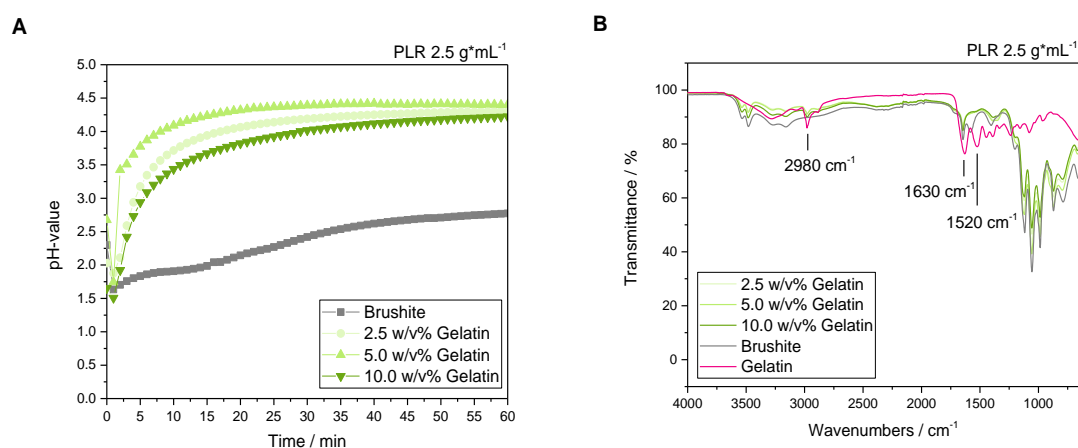
To test setting conditions of both, pure brushite cement as well as composite materials, pH-values during setting and gelation were observed. The inorganic reference showed pH-levels in the range of 1.5-2.75. Similar pH-developments for the different PLRs were measured with congruent curves over 60 min. In contrast to these results, composites with gelatin exhibited a certain buffering effect on the pH due to the second phase as seen in another degradable dual setting system based on brushite cement and PEG-hydrogels [193]. This can be explained by more constant pH-levels during physical gelatin gelation itself at more basic conditions (pH = 5.5) for all three concentrations. Additionally, pure genipin solution with 1 wt% had a pH-value of 4.4. For one hour, a constant pH-level increased the overall values for the composites independent of the used gelatin concentration. A certain plateau was reached after 20 min for almost all different PLRs (this means gelatin contents in the system) and biopolymer concentrations.

However, a higher amount of solid to liquid phase resulted in an increase in pH-variations between the different formulations. Furthermore, with higher gelatin concentration ($2.5 < 5.0 < 10.0$ w/v%), an increased shift to neutral pH was observed (see **Figure 36 A**). The highest amount of gelation (10.0 w/v%) had most influence on the pH-change for the different PLRs.

Chemical changes in gelatin phase and thus also the cross-linking reactions were verified *via* FTIR spectra. Pure brushite cements, composites as well as gelatin raw powder were measured. Spectra of gelatin showed typical characteristic peptide signals of amide I and amide II [262]. They refer to C=O-stretching vibrations ($1,700-600$ cm^{-1}) of the amide group for amide I coupled with NH-bending and CN-stretching ($1,580-1,480$ cm^{-1}) for amide II. The latter one is reduced in all composite spectra. This indicates a change in secondary structure and thus might correlate to physical cross-linking of the gelatin phase. Furthermore, the presence of gelatin is additionally assigned by the vibration at $2,980$ cm^{-1} , which was only noticed in the gelatin raw powder as well as composite formulations. Spectra of pure brushite with the different PLRs were the dominating fraction for the corresponding composites especially in finger-print area and wavenumber regions higher than 3000 cm^{-1} . The cement related peaks were sharp, defined PO/P-O(H) stretching vibrations in the range of $1,150-870$ cm^{-1} and OH-stretching vibrations between $3,600-3,000$ cm^{-1} . Additionally, a water bend at around $1,650$ cm^{-1} was detected [228]. All spectra do not show any differences in peak distribution or intensity due to a higher amount of inorganic phase, thus a dependency on PLR was not given (see **Figure 36 B**).

XRD was used for phase analysis and influence determination on the conversion to brushite cement in the dual set composites. Inorganic references mainly set to brushite cement (b) with small residues of remaining β -TCP (w). Besides that, some monetite (m) as water-free form of DCPD was also detected. Gelatin phases in different concentrations had an influence on the overall conversion of the raw-powder-mixture β -TCP and MCPA to brushite. Dual set samples showed different ratios of DCPD to DCPA resulting in pattern with higher intensity for monetite. XRD analysis also identified a higher content of reactant-component β -TCP (see **Figure 36 C**).

Furthermore, data obtained by XRD measurements were used for Rietveld refinement. Composition of brushite, monetite and remaining β -TCP as well as brushite crystal size were analyzed. Inorganic references had a brushite conversion $\geq 90\%$ and crystal sizes of 97 nm (PLR = 1.5 g*mL⁻¹), 94 nm (PLR = 2.0 g*mL⁻¹) and 82 nm (PLR = 2.5 g*mL⁻¹). This decrease in size was observed comparing the different dual set samples with the same gelatin concentration, for example PLR of 1.5 g*mL⁻¹. With a gelatin concentration of 2.5 w/v%, the measured crystal size was 127.2 nm. Doubling the amount of gelatin up to 5.0 w/v%, crystals were in the range of 122.5 nm. The highest gelatin concentration of 10.0 w/v% showed crystal sizes of 104.9 nm. Regarding the effect of gelatin for a certain PLR, the second phase influenced the nucleation and mineral growth in that way, that formed brushite crystal structures overall were not that small. Depending on PLRs, different trends for the phase composition were observed. Samples with a PLR of 1.5 g*mL⁻¹ had the highest content of monetite. Furthermore, an increase in gelatin concentration up to 10.0 w/v% favored the formation of brushite. Overall, the conversion to brushite was in the range of $\geq 70\%$ for all different dual set composites. With additional gelation and cross-linking of the gelatin phase, a complementary requirement for water molecules relocates the setting to monetite as the water-free form in comparison to the pure brushite reaction (see **Figure 36 D**).



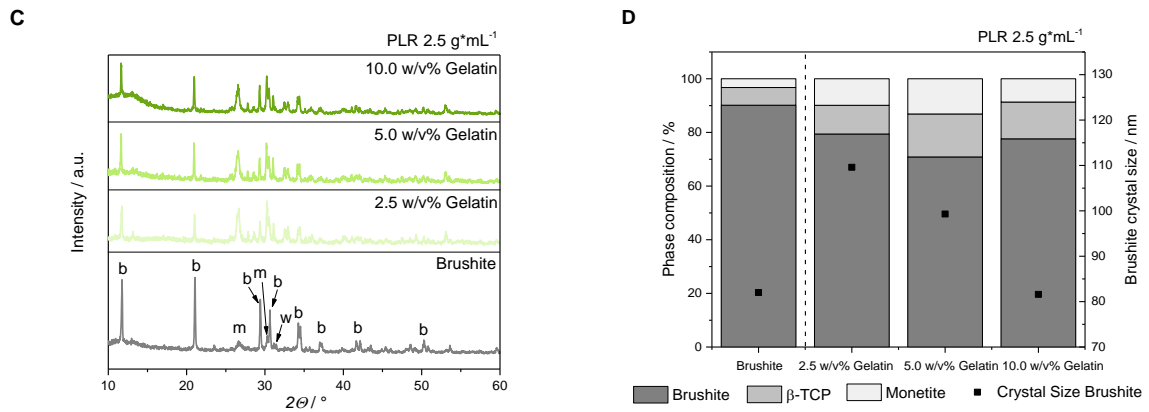


Figure 36:

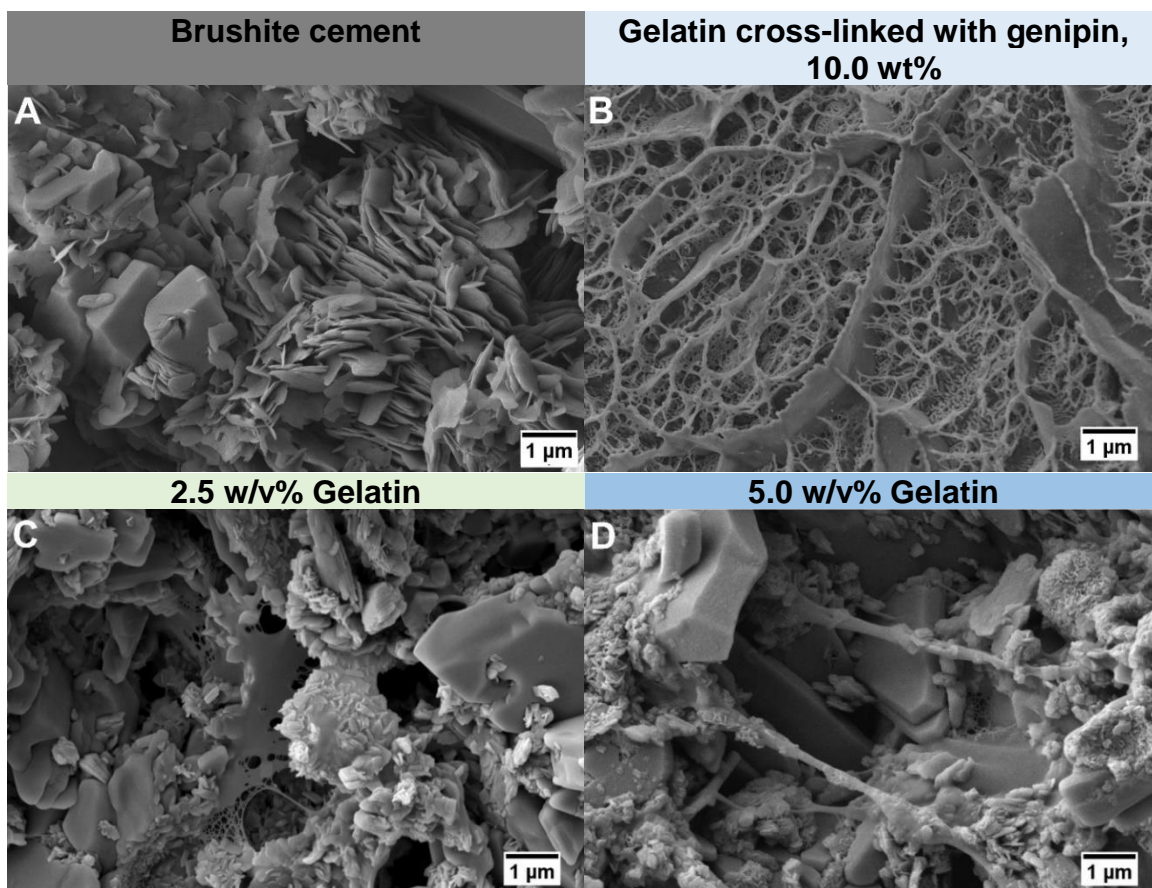
Overview of all different parameters concerning setting reaction for the batches with a PLR of 2.5 g·mL⁻¹. Both, PLR of 1.5 g·mL⁻¹ and 2.0 g·mL⁻¹ show a similar trend. **A:** Evaluation of pH-development during setting reaction resulted in a range of 1.5-2.75 for pure brushite reference with addition of genipin (1 wt%). By incorporation of gelatin, pH-values increased up to 4.5 with no real difference between the varying gelatin concentrations and further tested PLRs. **B:** FTIR spectra of pure brushite reference, raw gelatin powder as well as composite formulations were measured in the range of 4,000-650 cm⁻¹. A correlation of signals either to organic or inorganic phase could be drawn. **C:** XRD diffractograms of brushite reference and composite formulations after storage in PBS for one day. A change in brushite to monetite ratio was observed for dual set samples in comparison to pure brushite cement. Furthermore, amorphous parts were observed for the composites, especially with a PLR of 2.5 g·mL⁻¹ in the range of 10-18 ° (b = diffraction pattern brushite, m = diffraction pattern monetite, w = diffraction pattern whitlockite/β-TCP). **D:** Rietveld refinement for analysis of phase composition and determination of the average brushite crystal sizes.

5.3.1.2 (Cryo-) SEM images of pure cement and hydrogel references in comparison to composites with distinction between inorganic and organic phase

The pure inorganic reference was characterized regarding mineral forms and surface appearance. The typical plate- and needle-like structure of brushite cement is shown in **Figure 37 A**. For the pure organic reference, cryo-SEM mappings of chemically cross-linked gelatin were performed in order to estimate hydrogel distribution and structure incorporated in the brushite cement crystal matrix. Analysis of pure gelatin led to a different network structure for a physically (see **Figure 38**) or a chemically cross-linked hydrogel, respectively (see **Figure 37 B**). At higher magnifications, a clear differentiation between a super-ordinated thin wall system with an embedded porous network structure could be detected for the covalently cross-linked form. Small pores were homogeneously oriented with fine connections to bigger walls. A narrow pore radii distribution was in the range

of ~ 200-270 nm. With increasing temperature up to 37 °C, a shrinkage effect was noticed macroscopically and also SEM-analysis revealed an inner gel structure with even more branches and a much smaller porous network. After storage at higher temperatures, consequently the pore dimensions decreased to ~ 40 nm for the smaller topological parts and ~ 100 nm for the bigger compartments.

Gelatin hydrogels were clearly visible in SEM images taken for all different composites varying in PLR and biopolymer concentration. On local spots, dried organic films were on top of needle- and plate-like structures and covering the cement matrix. Overall, pictures presented a homogenous distribution of both, organic and inorganic phase. A classification of all components in the dual setting system was feasible: (i) monetite and (ii) brushite crystals can be assigned in SEM images as well as cross-linked gelatin (see **Figure 37 C and D**).



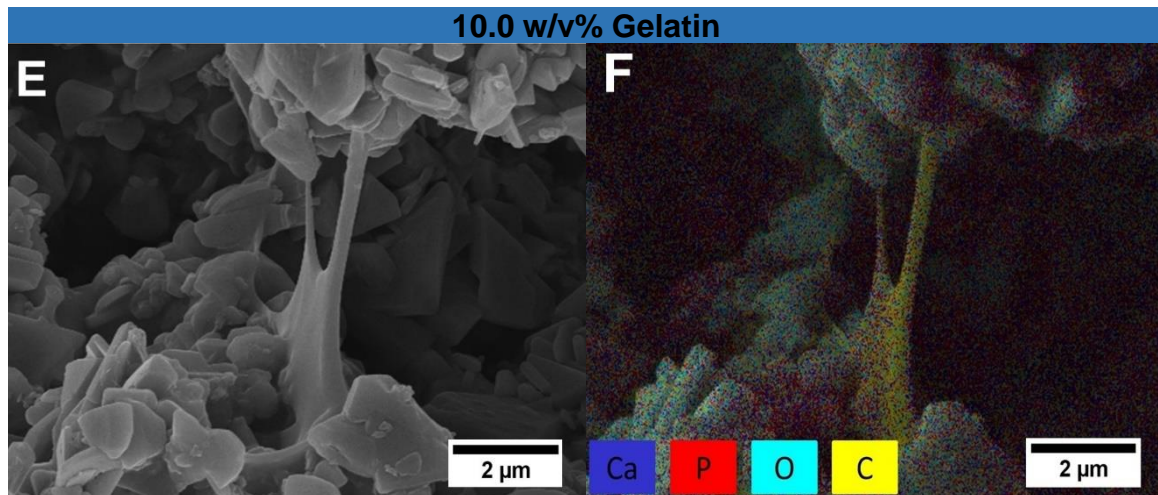


Figure 37:

SEM images of composite formulations containing genipin cross-linked gelatin and brushite cement (**C** and **D**) in comparison to pure brushite (**A**) as well as pure hydrogel (cryo SEM; **B**). Samples were analyzed after preparation and storage in PBS for one day. A clear determination of the different parts can be drawn: homogenous distribution of monetite and brushite crystals within a hydrogel matrix. Furthermore, EDX analysis of the formulation with the highest gelatin content of 10 w/v% (**E** and **F**) was analyzed with organic parts (yellow) and inorganic structures (dark blue and red).

For differentiation of organic and inorganic phases, energy-dispersive X-ray spectroscopy (EDX) was additionally performed. CPC parts consisted mainly of the two detectable elements calcium (Ca) and phosphor (P). They are colored in dark blue (Ca) and red (P). The slingshot looking like hydrogel construct was composed of carbon due to the amino acids in the protein structure and has a yellowish color in the elemental EDX overlay (see **Figure 37 E** and **F**). Consequently, this proved the look of dried hydrogel residuals in the composite materials with a very smooth surface between the crystals of the cement matrix.

In comparison to the fine and dense network structure for samples cross-linked by genipin, a gelation based on physical effects resulted in a completely different inner gel shape. **Figure 38 A** depicts the overall structure of gelatin that formed a hydrogel due to temperature decrease. Pores were bigger than for genipin-treated samples. Their determination in size showed values in the range of $2.165 \pm 0.035 \mu\text{m}$ for big network structures as well as $1.03 \pm 0.041 \mu\text{m}$ for smaller pores sizes. A collage with different magnifications illustrates the homogenous and regular pore distribution with small spider's web look-alike constructs that were detected in bigger pores (**Figure 38 B**).

Both cryo-SEM mappings of either physically or chemically cross-linked gelatin were performed in order to estimate hydrogel distribution and structure incorporated in the brushite cement crystal matrix.

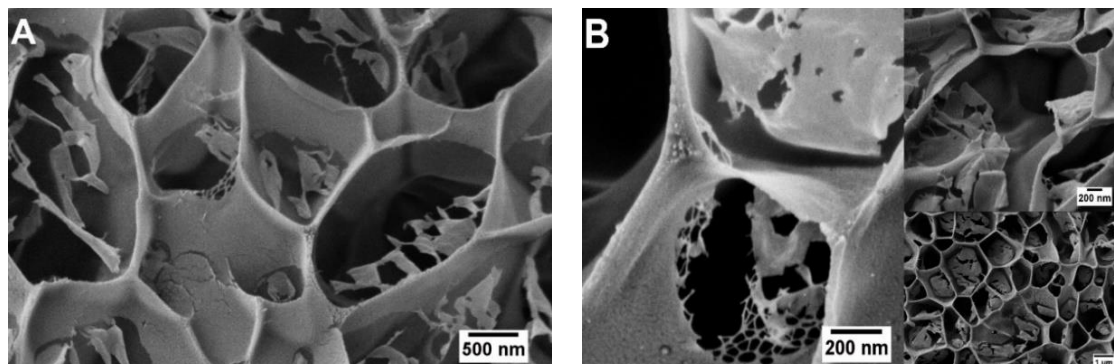


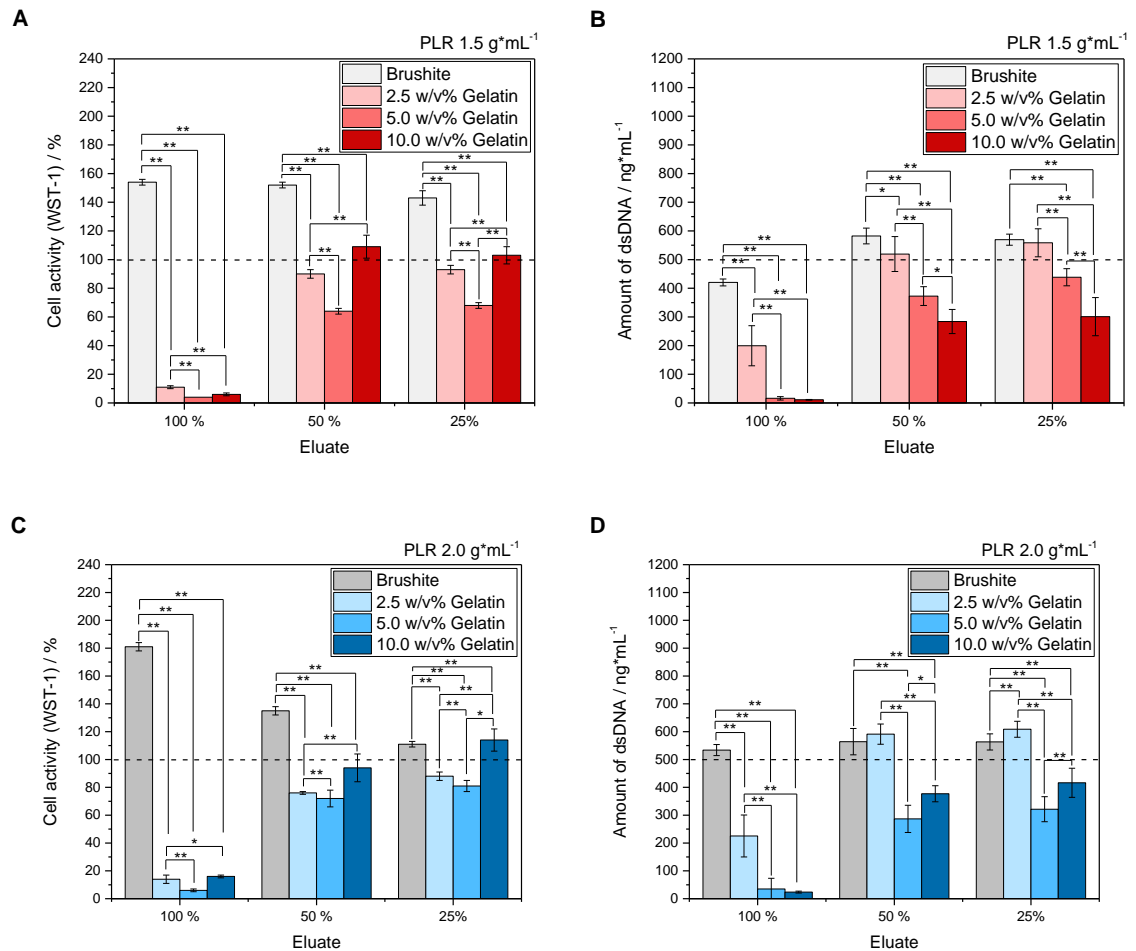
Figure 38:

Cryo-SEM images of physically cross-linked gelatin (10.0 w/v%). **A:** Gelation induced by temperature decrease resulted in bigger pores of the hydrogel network structure in comparison to cross-linked samples with genipin (see **Figure 37**). **B:** Structure diversity of gelatin with a concentration of 10.0 w/v%. The collage depicts different perspectives and magnifications of the gelatin sample.

5.3.2 Cytocompatibility testing

Cell test were performed according to an eluate testing with human osteoblastic cell line (MG-63) and three different dilutions of samples' eluate. For all brushite formulations, an increase in cell number and activity (~ 20-80 % rise) was observed with respect to the internal reference polystyrene (PS) (see **Figure 39 A-F**). Higher PLRs of pure cement resulted in an increase in cytocompatibility with increasing dilution up to 25 % and a very strong cell growth. Accordingly, cells did not have enough space and attaching area in the well that they were detaching from the bottom, rolling and forming aggregates. Composites containing 2.5 w/v% gelatin showed a certain cytotoxic effect for the pure eluate with activity less than 20-30 %. We were wondering which compound could cause this result. Concentration of genipin was 1 wt% referred to the solid phase and as seen for the pure brushite reference not harmful to the cells. Gelatin itself showed also good biocompatibility in porous scaffolds over a period of 21 days [263]. Logically, a higher eluate dilution led to higher survival rate for MG-63 cells. A further decrease in cell number and activity was observed for higher gelatin concentrations up to 10.0 w/v%. Regeneration of these parameters was observed after dilution (50 %

and 25 %). With higher amounts of solid phase (PLR of $2.5 \text{ g} \cdot \text{mL}^{-1}$), cytotoxic effects decreased and the pure eluate of the composite formulation containing 2.5 w/v% gelatin with the latter PLR resulted in a cell number of almost 70 % of the internal reference on PS ($502 \pm 99 \text{ ng} \cdot \text{mL}^{-1}$).



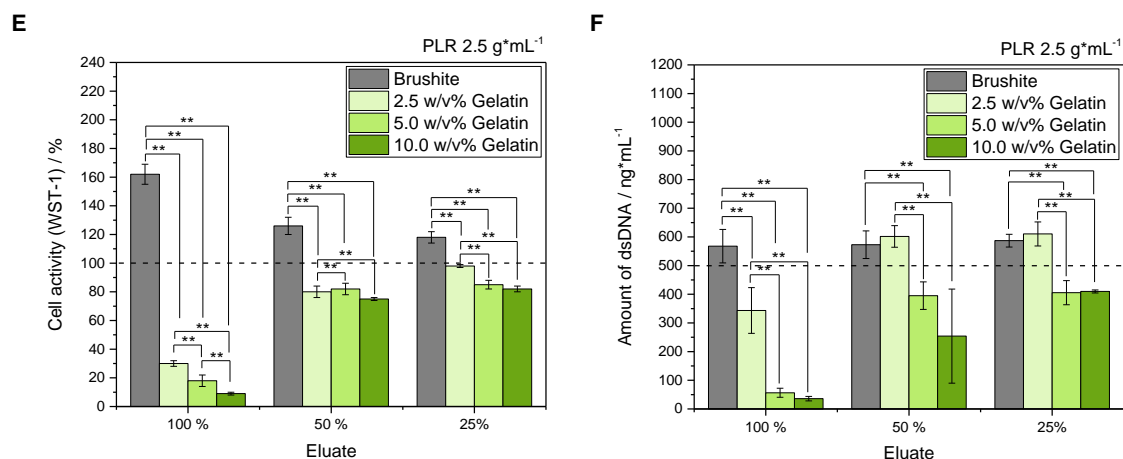


Figure 39:

Cytocompatibility testing of pure brushite cement in comparison to composite materials. Depicted data shows cell activity (**A**, **C**, **E**) as well as quantified amount of double stranded DNA (dsDNA; **B**, **D**, **F**). Dotted lines refer to control on PS which was set to 100 % for cell activity and $502 \pm 99 \text{ ng} \cdot \text{mL}^{-1}$ as determined total amount of dsDNA.

Additionally, fluorescence images were taken of samples with a PLR of $2.5 \text{ g} \cdot \text{mL}^{-1}$. The pure brushite reference showed a dense and coherent cell area with living cells that attached to each other and the well bottom. Furthermore, a relatively small amount of death cells was detected (**Figure 40 A**). Though total values of cell activity and number decreased for formulations containing 2.5 w/v% gelatin, cells were still alive and showed a survivable shape (see **Figure 40 B**). Unfortunately, an increase in gelatin concentration led to a cell number reduction (see **Figure 40 C** and **D**).

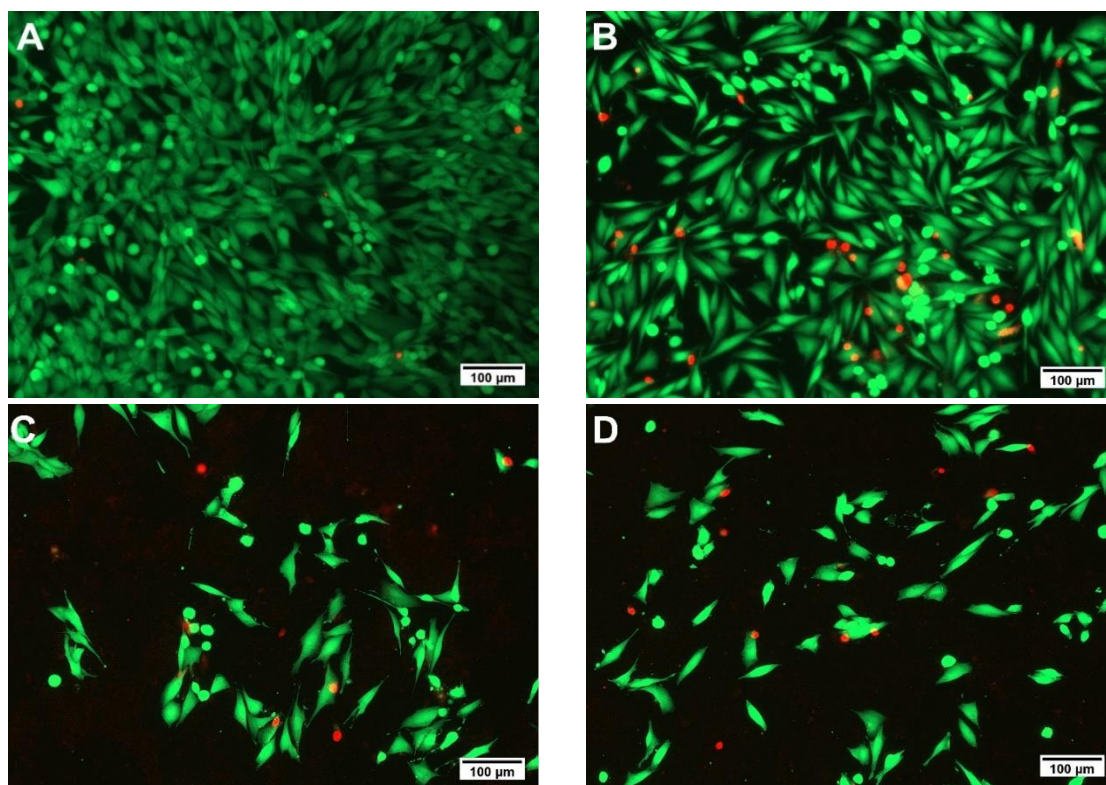


Figure 40:

Live/dead staining of batches with a PLR of $2.5 \text{ g} \cdot \text{mL}^{-1}$. For all formulations, pictures were taken of pure eluates without dilution (100 %). **A:** Pure brushite reference. **B:** Composite with 2.5 w/v% gelatin. **C:** Composite with 5.0 w/v% gelatin. **D:** Composite with 10.0 w/v% gelatin.

5.3.3 Mechanical advantages of gelatin-brushite composites compared to pure brushite cement

With addition of gelatin to the inorganic brushite cement matrix, an increase in ductility with a decrease in maximum stress levels occurred. This was observed over a period of 8 days (see **Figure 41 A-C**). For pure brushite cements, with higher amount of solid phase and therefore material for crystal nucleation, matrixes were more stable and resulted in compressive strength values for day 1 of about 2.6 MPa for a PLR of $1.5 \text{ g} \cdot \text{mL}^{-1}$, 6.7 MPa for a PLR of $2.0 \text{ g} \cdot \text{mL}^{-1}$ and 10 MPa for a PLR of $2.5 \text{ g} \cdot \text{mL}^{-1}$. After incubation in PBS, these values decreased about 30-40 % to about 1.5 MPa for a PLR of $1.5 \text{ g} \cdot \text{mL}^{-1}$, 3.5 MPa for a PLR of $2.0 \text{ g} \cdot \text{mL}^{-1}$ and 8 MPa for a PLR of $2.5 \text{ g} \cdot \text{mL}^{-1}$. Furthermore, composites were analyzed with different gelatin concentrations (2.5 w/v%, 5.0 w/v% and 10.0 w/v% referred to the liquid phase) as well as varying PLRs. With respect to gelatin-brushite composite materials, a higher content of biopolymer increased the maximum compressive

stress values. Additionally, with a PLR of $1.5 \text{ g}\cdot\text{mL}^{-1}$, measured values were constant for all composite formulations independent of the added amount of gelatin. An effect was logically given by the different PLRs. With increasing amount of solid phase, compressive strength also increased. Samples with a PLR of $2.5 \text{ g}\cdot\text{mL}^{-1}$ and $10.0 \text{ w/v}\%$ gelatin concentration had maximum stress levels comparable to pure brushite with a PLR of $1.5 \text{ g}\cdot\text{mL}^{-1}$. However, over the time, values of composite materials did not decrease in the same range as noticed for the pure brushite reference (see **Figure 41 B** and **C**). After 5 days of storage, composites with a PLR of $2.5 \text{ g}\cdot\text{mL}^{-1}$ led to stress values of about 4 MPa with $2.5 \text{ w/v}\%$ and $5.0 \text{ w/v}\%$ gelatin with a decrease to 2 MPa for samples containing $10.0 \text{ w/v}\%$ biopolymer. There was no reduction in stress over the time up to 8 days. Furthermore, genipin cross-linked gelatin-brushite constructs were also form stable and did not swell or shrink upon incubation in PBS.

In order to estimate the effect of gelatin concentration on the composites' mechanical properties, pure hydrogels as reference were additionally tested regarding compressive strength. With higher gelatin concentration, maximum stress values increased. Measured compressive strength values of gels that were stored at $37 \text{ }^\circ\text{C}$ resulted in a narrower range of 1.9-4.9 MPa. Due to variations in gelatin content, it is obvious that moduli increased with higher biopolymer content. Comparing analysis of samples with $10.0 \text{ w/v}\%$ gelatin, Young's moduli were $0.18 \pm 0.04 \text{ kPa}$. Specimens with $5.0 \text{ w/v}\%$ that were tested reached levels of $0.09 \pm 0.02 \text{ kPa}$ at $37 \text{ }^\circ\text{C}$. As an exception, formulations containing $2.5 \text{ w/v}\%$ gelatin resulted in moduli of $0.05 \pm 0.01 \text{ kPa}$. Logically, the strengthening dependency on gelatin concentration was observed for both, pure gels as well as composites.

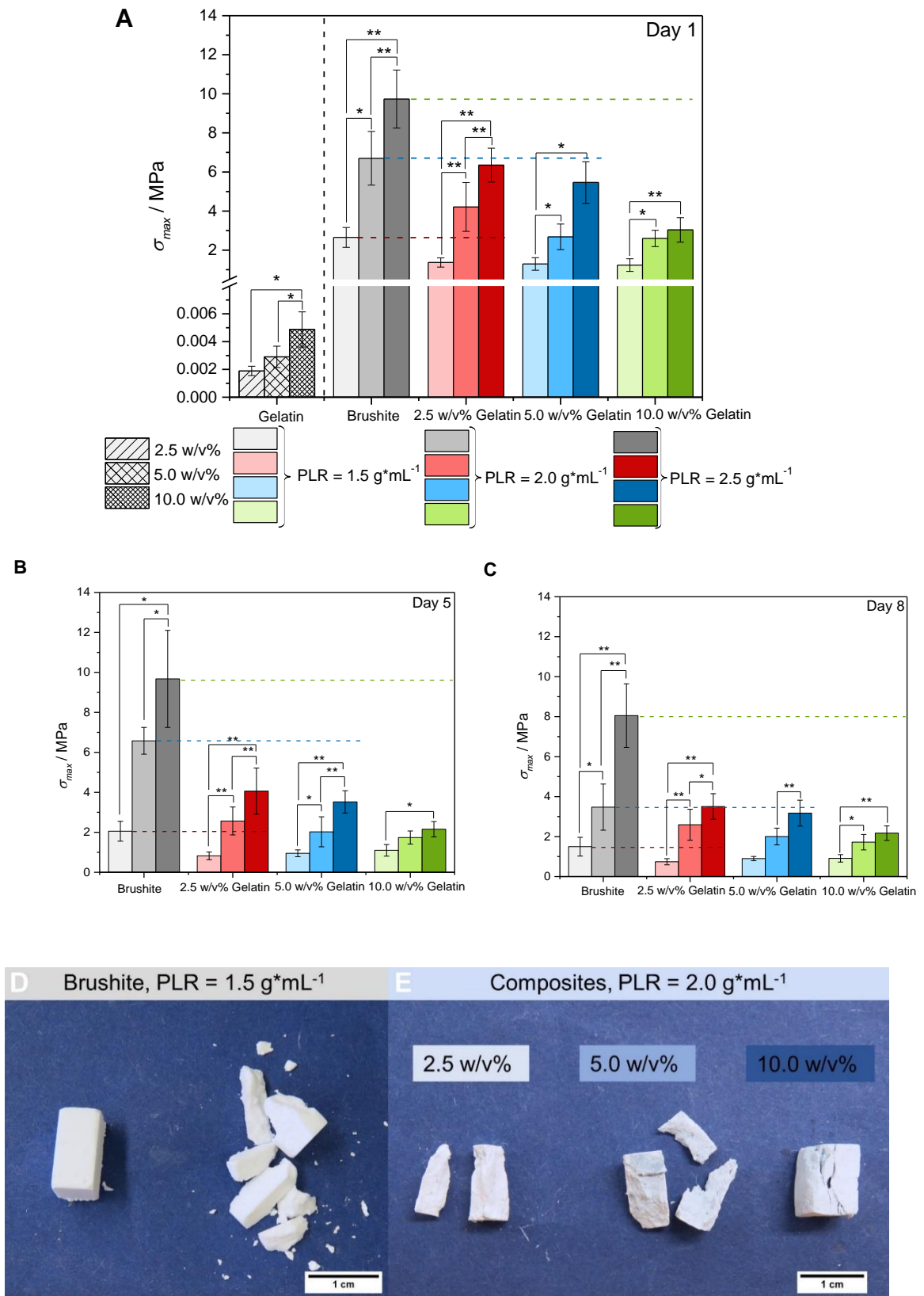
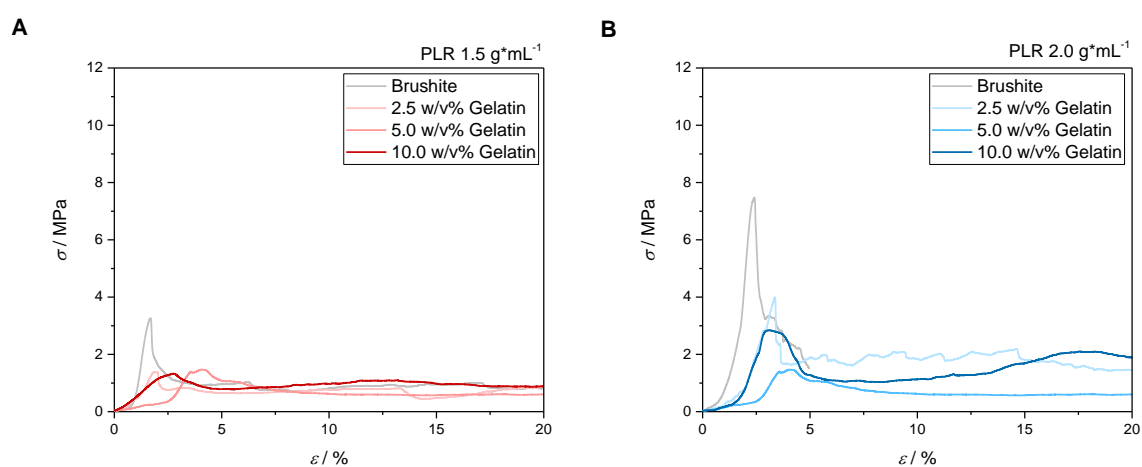


Figure 41: Time-dependent maximum stress of pure brushite reference *versus* composite materials (A-C) with corresponding specimens before as well as after compressive strength testing (D and E).

An interesting effect was observed for composites containing 10.0 w/v% gelatin. They behaved more ductile with a certain cohesiveness. After testing, samples stuck together although cracks and fissures were visible. This is exemplarily represented in **Figure 41 E**. This image also illustrates the homogenous bluish coloring of the samples, which proves again a homogenous distribution of hydrogel phase in the composite materials. Moreover, samples with gelatin showed bigger fragments after compressive strength testing in comparison to pure brushite cement (see **Figure 41 D and E**). All stress-strain curves for composite formulations maintained constant levels in stress after maximum compression was reached (see **Figure 42 A-C**). Regarding ductility, deformation increased especially for higher PLRs of $2.0 \text{ g}\cdot\text{mL}^{-1}$ and $2.5 \text{ g}\cdot\text{mL}^{-1}$. With 10.0 w/v% gelatin amount, the curves' initial slope decreased and associated linear regions increased. To complete the comparison, curve process (see **Figure 42 D**) and determined Young's moduli confirmed the same trend.



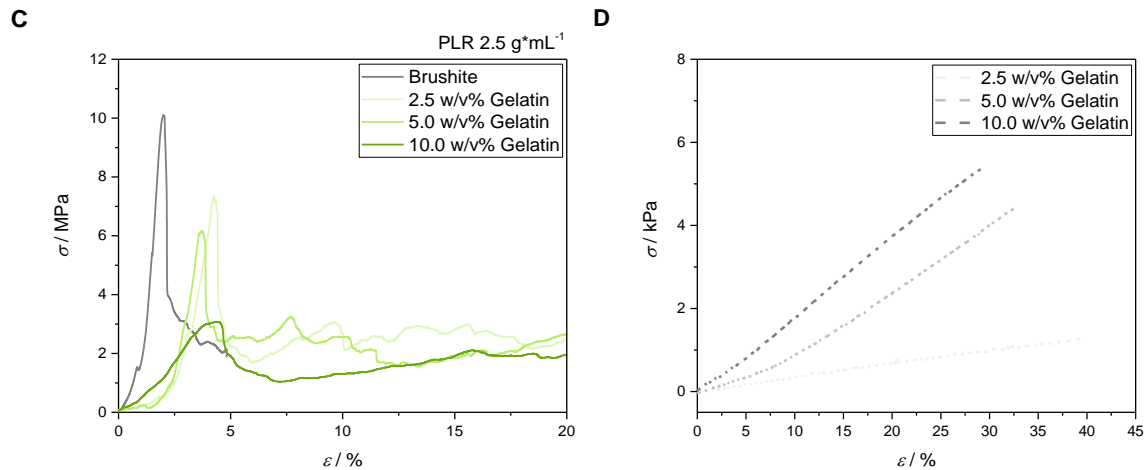


Figure 42:

Stress-strain curves of tested composite materials as well as brushite reference. With increasing PLR, values of maximum compressive strength increased (PLR = 1.5 g*mL⁻¹ (A), PLR = 2.0 g*mL⁻¹ (B), PLR = 2.5 g*mL⁻¹ (C)). Furthermore, a higher gelatin concentration resulted in decreasing maximum stress values. Results of compressive strength testing of pure gelatin samples cross-linked by genipin is depicted in image D regarding their stress-strain behavior.

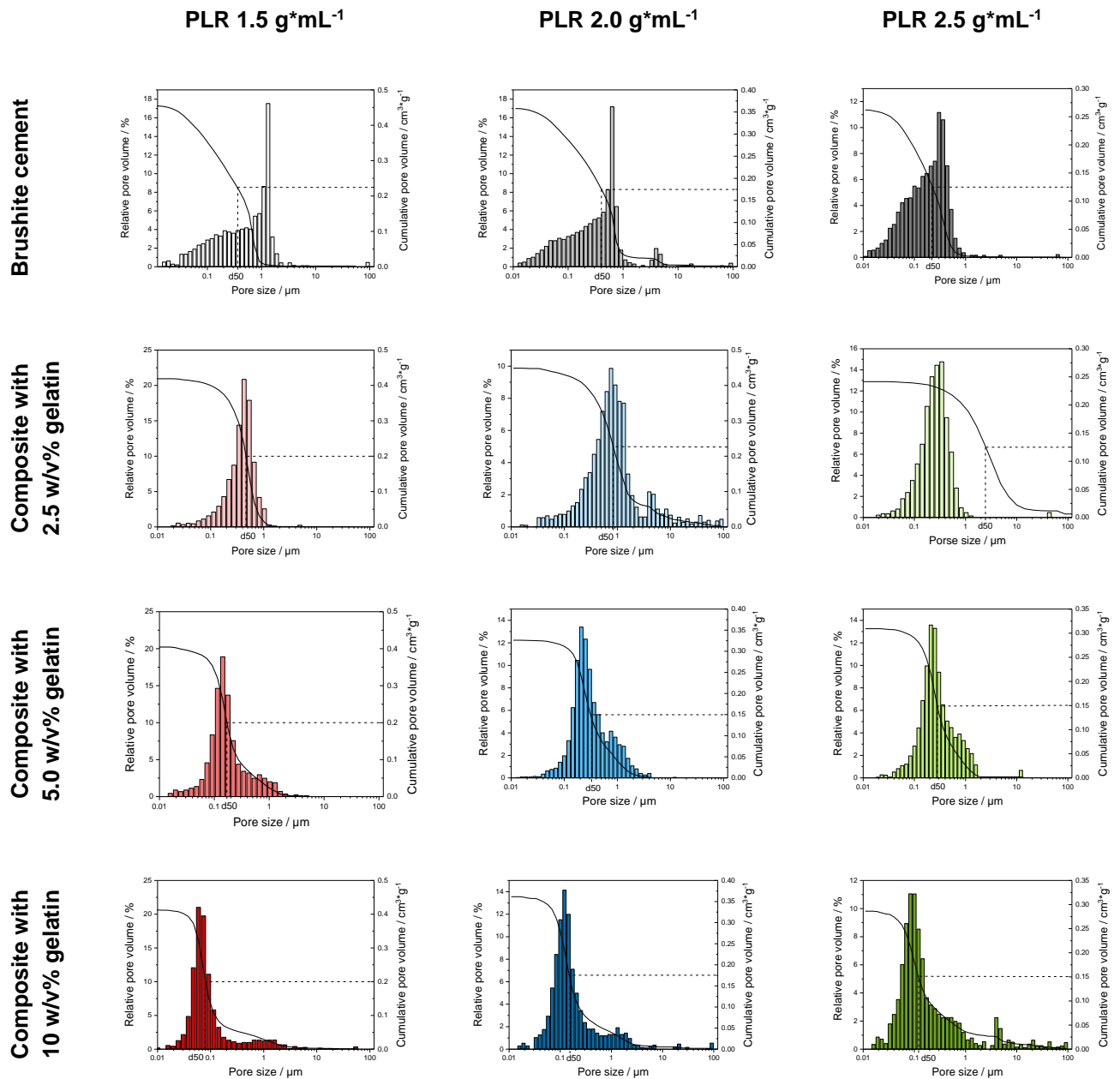
5.3.4 Porosity measurements and drug release of antibiotics

5.3.4.1 Porosity

Using mercury porosimetry, the largest entrance to a pore [264], often named as “pore size”, was determined for all formulations. Pure brushite references with a PLR of 1.5 g*mL⁻¹ showed d50-values of 0.53 μm and consequently about 52 % of the whole pore volume were in the range of ≥ 0.50 μm. In this section, pore entrance of about 0.5 μm was taken as fixed value for the percental comparison of overall amount in the constructs.

With increasing PLR, the determined “d50-pore sizes” decreased in average to 0.36 μm and 0.21 μm, respectively, for PLR 2.0 g*mL⁻¹ and PLR 2.5 g*mL⁻¹. Gelatin incorporation in all formulations with a PLR of 1.5 g*mL⁻¹ led also to a reduction in mean average values for determined pore entrances from 0.43 μm for a gelatin concentration of 2.5 w/v% over 0.18 μm for 5.0 w/v% biopolymer up to 0.07 μm with the highest gelatin content of 10.0 w/v%. The same trend was observed for percental ranges of the overall pore volumes regarding pores ≥ 0.50 μm. Reached values were 34 % of 0.50 μm pores or bigger for a PLR

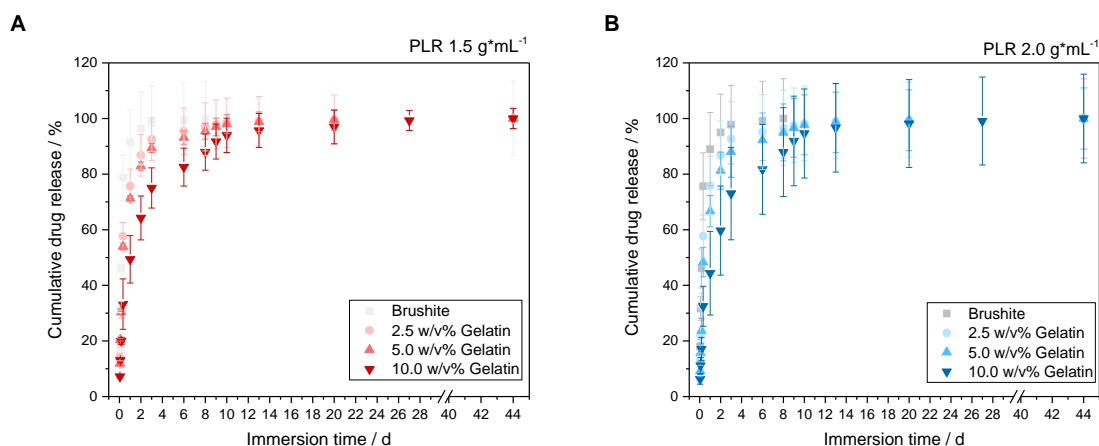
of $1.5 \text{ g}\cdot\text{mL}^{-1}$, 14 % for a PLR of $2.0 \text{ g}\cdot\text{mL}^{-1}$ and 11 % for a PLR of $2.5 \text{ g}\cdot\text{mL}^{-1}$. Comparing porosity data with respect to the different gelatin concentrations, a higher amount of hydrogel phase resulted in smaller pore sizes and higher domination of smaller pores for the whole construct. Porosity measurements were performed with dry samples and thus also a collapsing gelatin networks might minimize pore entrance size. However, this argument can be refuted by rational reflection having a higher powder fraction at a PLR of $2.5 \text{ g}\cdot\text{mL}^{-1}$ with more nucleation clusters and growing crystals. On these grounds, space is more limited, and pores cannot grow in the same extent as observed for lower PLRs.

**Figure 43:**

Porosity histograms of all different formulations showing relative pore volume (%) and cumulative pore volume (cm³*g⁻¹). The higher the amount of solid phase related to the liquid solution, the smaller the indicated pore entrance in the constructs.

5.3.5 Release of vancomycin and rifampicin

Antibiotic drugs (either vancomycin or rifampicin) were dissolved in the different liquid phases and mixed with the raw powder in order to encapsulate them in the pure brushite cement or the composite materials, respectively. For vancomycin, inorganic reference samples released the whole amount of API within 8 days. In contrast, gelatin containing samples had a more sustained release due to the hydrogel phase with an overall release of 28 days. With higher gelatin concentrations, the retarding effect of the hydrogel phase on vancomycin drug release increased. This was observed for all PLRs with highest retardation for $2.5 \text{ g} \cdot \text{mL}^{-1}$ (see **Figure 44 A-C**). The general release dose of all formulations was in the range of 700-800 μg . Vancomycin drug release was correlated to the pore entrance size distributions: small porous structures in the construct as seen for PLR of $2.5 \text{ g} \cdot \text{mL}^{-1}$ exhibited the highest drug release effect. Furthermore, a release out of these structures took longer due to a delayed diffusion out of the pores. Additionally, there was a certain retaining effect of the gelatin phase. Assuming Higuchi-model as release model, a linear plot of cumulative drug release *versus* time (first 10 days until a release of about 60 % was reached) for formulations with a PLR $2.5 \text{ g} \cdot \text{mL}^{-1}$ resulted in a high linearity with increasing gelatin concentrations (see **Figure 44 D**). The release exponent as slope of the curve determined according to power law approximated the value of $n = 0.5$ with increasing amount of gelatin. With this coefficient, the Higuchi-model was confirmed.



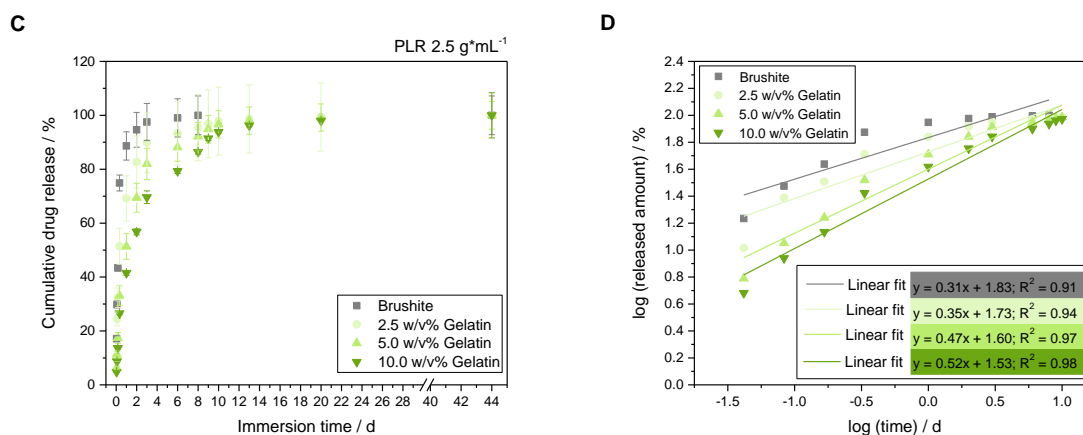
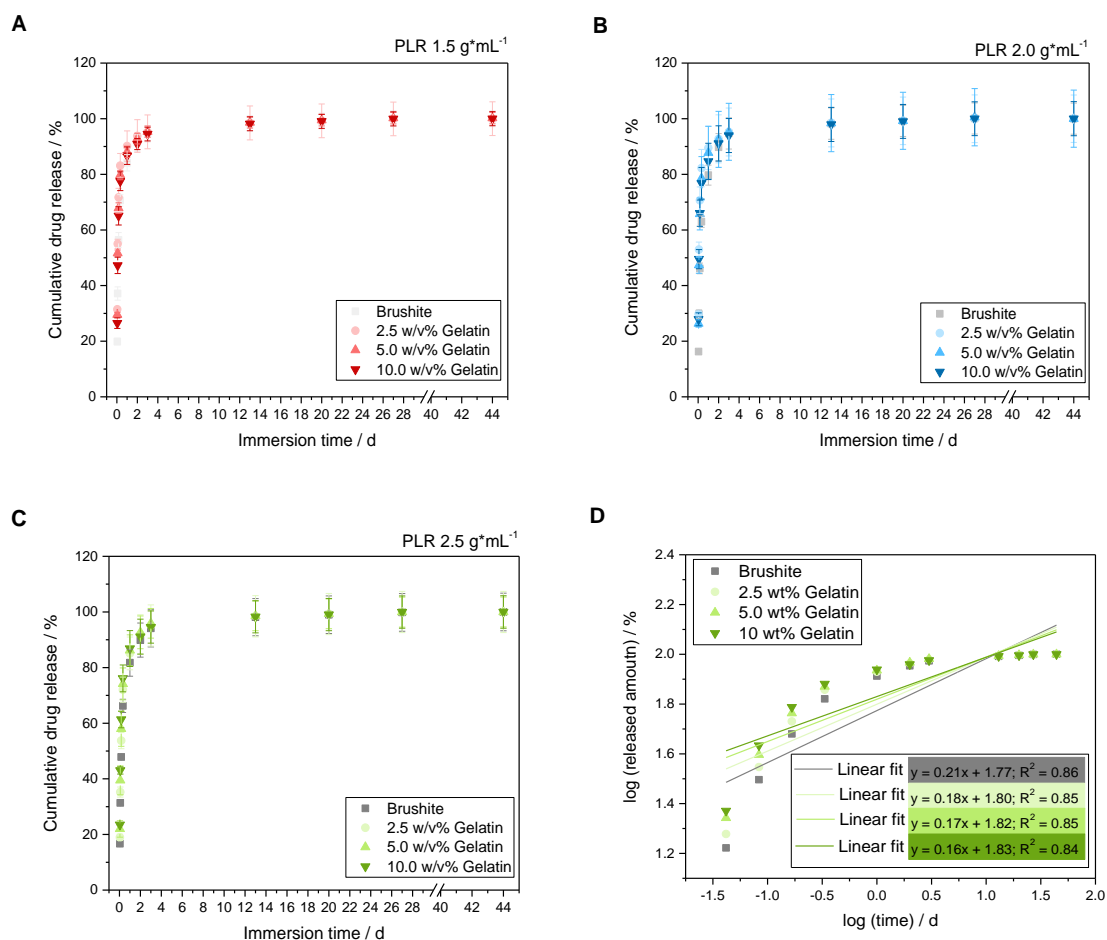


Figure 44:

Cumulative drug release of vancomycin from brushite cement as well as composites. With increasing gelatin concentration (2.5 < 5.0 < 10.0 w/v%), a sustained release of the antibiotic drug was obtained. This effect occurred for all three PLRs (**A-C**). For a linear correlation ($x = 0.1$ -10 d) according to Higuchi-model, a logarithmic plotting of cumulative percentage of released compound *versus* log time was performed for the selected PLR of 2.5 g*mL⁻¹ (**D**). Additionally, corresponding linear equations as well as regressions were determined for the different batches. With increasing gelatin concentration, the retardation effect for drug release increased and thus slope and grade of linearity *alias* regression. The determined Higuchi-coefficients approximated $n = 0.5$ with increasing gelatin content up to 10.0 w/v%.

Samples containing rifampicin did not demonstrate a sustained, but a burst release with a total drug liberation after 4 days. In this case, gelatin phase had no sustaining effect and the antibiotic diffused through the cement and hydrogel matrix more easily. Both, pure brushite reference as well as dual set composites, resulted in the same profile (see **Figure 45 A-C**). With respect to mass depending encapsulation, the overall released amount of rifampicin was about 1500 μ g for all formulations, irrespective of PLR and gelatin concentration of the dual set systems. The determination of release exponent as slope by linear fittings revealed that all formulations resulted in the same value of $n = 0.2$, similar linear equations and consequently regressions with very poor correlation (see **Figure 45 D**). This confirmed the fact, that there was no retaining effect of rifampicin by incorporation of naturally cross-linked gelatin hydrogels.

**Figure 45:**

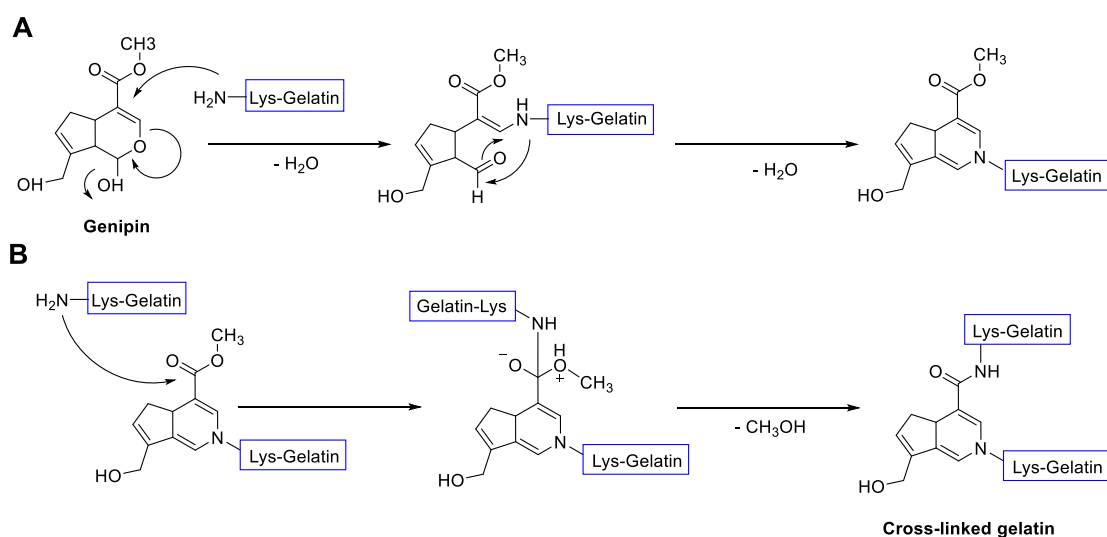
Cumulative drug release of rifampicin over a period of 44 days. Released amounts of antibiotic were similar for all formulations. An initial burst release was observed with an almost complete release of the drug after three days. Profiles are depicted for the different PLRs (A-C). A linearity was obtained by logarithmic plotting of percental cumulative drug release over the time with a release exponent of about $n = 0.2$ (D). For further information, corresponding linear equations and regressions were added which confirmed the observed trend of batch equality.

5.4 Discussion

By combining a genipin cross-linked gelatin network with an inorganic brushite matrix, mechanical properties, sustained drug release capacity as well as phase composition were strongly affected. This is the first time, that a dual set system of a biopolymer and degradable CPC was established and thoroughly characterized. Nevertheless, there are several systems in literature dealing with a combination of CPCs and gelatin networks. Bigi *et al.* [183] reported on combining α -TCP and gelatin and studied the effects on setting properties by biopolymer addition up to 20 %. They observed a linear increase in mechanical strength as function of gelatin content. Moreover, this was also caused by a reduction in porosity and changes in the cement microstructure induced by gelatin incorporation. Another investigated topic are gelatin microspheres that were prepared (i) in oil emulsion to increase their sphericity, their size and dispersion and that were subsequently mixed to the forming cement to improve adhesion [265] or (ii) added in order to create macropores due to *in situ* degradation of the biopolymer [266]. The simplest method of creating such porous structures for brushite cement was investigated using non-cross-linked gelatin as latent porogen in a β -TCP/MCPA-mixture which was dissolved after immersion within 1-4 weeks at 37 °C in PBS [267]. With coexisting of gelatin next to the cement phase, compressive strength was reduced about 30 % with higher gelatin content up to 15 % due to the formed macropores with sizes of 100-200 μm .

However, there is no report in literature of a dual system based on brushite cement that sets simultaneously to gelatin hydrogel formation which is based on both, physical as well as chemical cross-linking *via* genipin. Its secondary mechanism of organic phase's cross-linking is based on the reaction of amino functions with genipin [268]. The applied chemical reaction of gelatin and genipin is depicted in **Scheme 4**. Instead of the amino acid lysine (Lys), other reaction partners with free amino acid groups can also be hydroxylysine (Hyl) or arginine (Arg) residues. In a first step, an intermediate is formed by a nucleophilic attack of one amine at the double bond in the cyclohexane ring of the genipin molecule. Secondly, another amine reacts by nucleophilic substitution at the methyl ester of the formed intermediate. Finally, there is a rearrangement to a stable amide structure with the

release of methanol and a blue colored pigments is obtained [269]. Regarding gelatin, several amino acids carry the required functionalities for cross-linking with genipin, however, they are present in different extents depending on the denaturation process and source. The here chosen gelatin of type A (porcine skin) contains for example three reactive amino acids: 4.1 % Lys, 1.0 % Hyl and 8.3 % Arg [140].



Scheme 4:

Cross-linking reaction of genipin with free amino functions of gelatin (exemplary amino acid: lysine (Lys)). Alternatively, other amino acids that are part of the amino acid composition of gelatin with amine groups are hydroxylysine (Hyl) and arginine (Arg). This scheme was adapted from Rose *et al.* [270]. **A:** First reaction of genipin with a nucleophilic attack of the amine function which results in a stable intermediate structure. **B:** Second step represents a nucleophilic substitution by another free amine at the carbonyl function of the ester group with subsequent amide formation while methanol (CH_3OH) is released.

In parallel, cement setting takes place by dissolution of the raw powder mixture in the liquid phase with afterwards nucleation and entanglement of growing cement crystals [43]. By incorporation of gelatin, we observed a decrease in setting time due to the preliminary gelation with a pH-shift as well as interactions with present ions (Ca^{2+} or PO_4^{3-}). This was noticed while mixing of the paste and production of specimens. Furthermore, crystal growth during the precipitation reaction was affected by gelatin gelation, consequently entangled brushite networks with smaller crystals in comparison to the inorganic reference were formed. This was evaluated

via Rietveld refinement as well as microscopic analysis. In a similar study of Cama *et al.* [271], SEM images of monetite and brushite cements before and after immersion in media were compared. They also noted typical thick platelet shapes for brushite as well as monetite whereas the latter one showed thinner plates with a higher homogeneity in size. Both, SEM and XRD analysis as well as Rietveld refinement confirmed the growth of either DCPD or DCPA. This general observation is not surprising having in mind the simultaneous gelation of gelatin towards physically cross-linked hydrogels, which certainly inhibited the cement reaction. Furthermore, with respect to the fact that hydrogels can be described as “highly water swellable polymer networks” [122], there is an increased need for water captured by the hydrogel formation that DCPA conversion is favored with increasing PLR and consequently less amounts of free liquid phase. Parts of the gel structures were homogeneously distributed in the constructs and continuously incorporated in the inorganic matrix. Additionally, investigated pure hydrogel cryo-SEM images demonstrated a dense polymer network after cross-linking with genipin. Physical gelation was performed as reference to compare results with already published studies [272]. Big porous structures as well as small branched details were also seen in frozen 6 % gelatin scaffolds and confirmed once more the comparability and reproducibility of our cryo-SEM images. A detailed description of the correlation between cryogenic parameters and physico-chemical properties of gelatin cryogels are described in a publication of Vlierberge *et al.* [273]. According to this study, we also argue that the concentration of gelatin directly controls pore size and total porosity due to a higher extent of gel nucleation and thus higher amount of biopolymer chains [18].

CPCs as drug releasing matrixes are generally considered to be diffusion-controlled devices [49] due to the fact of being non-degradable systems. However, the here used brushite cement is a metastable formulation and to a certain extent resorbable *in vitro/in vivo* due to dissolution processes and therefore the achieved releasing mechanisms are depending on additional study parameters and consequently even more complex. By incorporation of the antibiotic compounds in the liquid phase, solubility issues of the drug parallelly to the dissolution of the raw powder as well as encapsulations during precipitation and crystal nucleation can be circumvented. A combination of both, porous CPC matrix and gelatin hydrogel

phase can be used to slow down the liberation of low molecular weight compounds, which can be a promising tool for sustained drug release. A possible drug candidate, vancomycin, is indicated for the treatment of infections caused by gram-positive bacteria [274]. It belongs to the antibiotic class of glycopeptides whose mechanism of action is based on the inhibition of peptidoglycan synthesis [275] by steric blocking of the enzymes responsible for the transglycosylation and thus interfering in bacterial cell wall synthesis [276]. It was a front-line antibiotic and one of the only active compounds to treat Methicillin-resistant *Staphylococcus aureus* (MRSA). The second candidate, rifampicin, is a reserve antibiotic against mycobacteria (gram-positive and gram-negative) to treat infections in rare cases of bacterial resistance. In combination with other drugs like isoniazid, it is for example used as therapeutic agent against tuberculosis. The mechanism of action is based on the inhibition of the DNA-dependent RNA-polymerase [277]. As proof of principle, both candidates were incorporated in the liquid phase and drug release profiles were investigated over 44 days to evaluate prolonged release given by the gelatin hydrogel phase. In CPC formulations, drug delivery is mainly interesting to treat local infections at the implantation site. Additionally to antibiotics, also anti-inflammatory drugs like ibuprofen [83], cancer therapeutics like cisplatin [111] or growth factors like rhBMP-2 [120] could be added to the formulations to treat symptoms or diseases accompanying the defect.

The used drugs in this study, vancomycin as well as rifampicin, both have functionalities like hydroxyl or carbonyl groups that might interfere in a small amount with for example Ca^{2+} ions of the solid phase and though influencing the formation of the cement matrix. Introducing a second phase in the system, a diffusion barrier is created, interactions between active pharmaceutical compound and hydrogel can occur and further slowdown release kinetics. Obtained release profiles of drugs can be explained by critical factors influencing the diffusion of drugs with sustained release from hydrophilic matrices. A review of Maderuelo *et al.* [278] deals with parameters concerning the drug itself, the used polymer or formulation criteria. With focus on the different properties of vancomycin and rifampicin, the two different releasing profiles tend to follow logical trends. Since the molecular weight of vancomycin ($M_w = 1,449.265 \text{ g}\cdot\text{mol}^{-1}$) is nearly double of the molecular weight of rifampicin ($M_w = 822.953 \text{ g}\cdot\text{mol}^{-1}$), a diffusion of

the glycopeptide antibiotic through cement and hydrogel matrix is slowed down and can be determined in a certain way as inhibited transfer. This effect was already described for two much smaller drug molecules, indomethacin ($M_w = 397.78 \text{ g}\cdot\text{mol}^{-1}$) and caffeine ($M_w = 194.2 \text{ g}\cdot\text{mol}^{-1}$) [279]. Their diffusivity was identified in 4 % xanthan gum gels. It is obvious, that mobility correlates with molecular size and weight and accordingly affects the apparent diffusion rate. Thus, we have to take this additional parameter into account. A second factor is the drug solubility which also strongly influences drug release. In safety data sheets of different companies, water solubility of vancomycin is about $50 \text{ g}\cdot\text{L}^{-1}$ at $20 \text{ }^\circ\text{C}$. For rifampicin, reached values are in the range of $2.5 \text{ g}\cdot\text{L}^{-1}$ at $25 \text{ }^\circ\text{C}$ and thus more than twenty times lower compared to the glycopeptide antibiotic. This relatively low solubility can be correlated with a lower dissolution rate which is depending on the penetration rate of water and a certain erosion of the system.

Regarding release kinetics, all drugs require a constant and drug-independent release to guarantee the effective concentration over a certain time. This steady state of drug concentration can be easily achieved by a drug delivery system following zero order release kinetics, which means a linear relation between drug release and dissolution time. One of the first mathematical models to calculate and estimate drug release was established in 1961 by Higuchi [280]. In this model, release is depending on the penetration of the drug through a stable matrix by diffusion. The rate limiting step is consequently the diffusion out of pores, channels or second matrixes and can be altered by changing porosity as well as the diffusion constant of the drug [281]. This model is expressed by **Equation 5**, where m_t is the amount of drug released in a certain time frame, t referred to the surface area A of the specimen, D is the diffusion coefficient of the compound, c_0 is the initial concentration, c_s is the drug solubility in the surrounding media, τ is tortuosity and ε is porosity [282].

$$\frac{m_t}{A} = \sqrt{\frac{D\varepsilon}{\tau} (2c_0 - \varepsilon c_s) c_s * \sqrt{t}}$$

Equation 5

Due to a domination of the inorganic brushite matrix, we expected a drug release in the specimens mainly controlled by Higuchi-model with a homogeneously incorporated drug during setting and crystal growth as well as gelation [280]. However, the main process that controls drug release in CPCs is still the later diffusion through the cement matrix [51]. Another important influencing parameter is the material's porosity. This indirectly correlates to diffusion coefficients of the matrix as well as tortuosity τ in which the latter one can be defined as quotient of the real diffusion path Δl divided by particle per unit length Δx (see **Equation 6**) [19].

$$\tau = \frac{\Delta l}{\Delta x} \quad \text{Equation 6}$$

Related to porosity measurements, smaller pores with higher drug release were observed for samples with a PLR of 2.5 g*mL⁻¹. With consideration to these porous CPC matrixes, micro- or nano-porous systems were formed and the effective diffusion coefficient D_{eff} can be described as ratio between diffusion coefficient D' and porosity ε to tortuosity τ of the cement (see **Equation 7**). With decreasing pore size with even higher gelatin contents, the drug diffusion was hindered through the hydrogel network and cement matrix and thus the release for vancomycin was sustained.

$$D_{eff} = \frac{D' * \varepsilon}{\tau} \quad \text{Equation 7}$$

Based on power law (Korsmeyer-Peppas) [282], we determined the release exponent as slope of double logarithmized liberation profiles based on **Equation 8**. Hereby, m_t is defined as absolute cumulative amount of released drug at time point t , m_∞ is the initial and maximum released drug amount, k is a constant including structural modifications and geometrical parameters of the system and n is the release exponent.

$$\frac{m_t}{m_\infty} = k * t^n$$

Equation 8

With $n = 0.5$, we confirmed the assumption of Higuchi-kinetics ($t^{0.5}$) whereas only 60 % of the total drug release should be taken in account. To condense all parameters to the main expected mathematical model, the one of Higuchi was taken into account. A study performed by Hofmann *et al.* [283] showed a release of 80 % vancomycin in 24 h for pure brushite cement with a PLR of $2.5 \text{ g} \cdot \text{mL}^{-1}$ by addition of 2 wt% drug to the solid phase. Comparable to our maximum released amounts, they also observed an effect of the cement matrix with lower porosity, *i.e.* high PLR, that demonstrated a sustained release. With decreasing PLR, the porosity of the cement increased, and larger pores were formed due to augmented separation between aggregates resulting from larger distances between the original particles [51, 200, 284]. Comparable to Zhou *et al.* [285], our constructs could achieve drug levels over an extended duration of 44 days. Release out of genipin cross-linked gelatin matrix of vancomycin showed also a sustained drug release. Furthermore it should be noted, that gelatin is an appropriate candidate as carrier matrix for drug delivery in tissue engineering [286]. Above all, there are also other drugs that are combined with CPCs like gentamicin [287] or rhBMP-2 in combination with gelatin [288].

Moreover, a third probable advantage of the created dual set system besides the mechanical and sustained drug release properties was hypothesized as raise in biocompatibility with improved cell activity and growth by incorporation of gelatin hydrogel which was compared *via* cytocompatibility testing with pure brushite cement. It is known that cell number as well as cell activity increase due to the presence of “RGD-sequences” in gelatin chains [289, 290]. This prominent motif consists of the amino acids Arg, glycine (Gly) and aspartate (Asp) and is known to improve cell adhesion and consequently survival. Results of indirect cell testing showed an increase in cell growth for all brushite cements without dilution of the eluates in comparison to PS. Concentration of gelatin directly influenced cell number as well as activity. Surprisingly, an increase in gelatin concentration resulted in a decrease in cell proliferation. This is in contrast to outcomes by

Bigi *et al.* [257] who investigated gelatin enriched CPCs based on α -TCP regarding MG-63 culturing on sample surface for 21 days. With incorporation of the biopolymer, the production of alkaline phosphatase activity, collagen and transforming growth factor β 1 were stimulated. This indicated an increased osteoblast proliferation, activation as well as metabolism due to a higher differentiation rate by creating a composite material [257]. We assume a dissolution of ions in a concentration leading to apoptosis of cells as observed in another dual setting system based on brushite and silica [187]. Furthermore, challenges regarding cell testing of CPCs are not that rare. Decreased cell growth can be explained by acidic pH-values and acidic setting and gelation conditions. With respect to Rietveld refinement, a higher extent of β -TCP remains in the inorganic matrix with corresponding higher gelatin content. Consequently, more unreacted MCPM can be dissolved and an increased amount of phosphate ions (PO_4^{3-}) can influence the cytocompatibility of the systems. Nevertheless, our composite formulations are biocompatible with higher dilutions. Also body fluids are in a permanent equilibrium state with a constant flow and hence removal of substances. So further investigations are needed to estimate biological properties and *in vitro* as well as even *in vivo* behavior though there are several examples in literature showing the opposite effect, which means an increase in cell number and activity.

5.5 Conclusion and outlook

A novel approach for a dual setting system based on brushite cement and gelatin cross-linked *via* genipin was successfully established. Though influencing the cement setting reaction by simultaneous gelation which was observed for brushite crystal size as well as phase composition, stable formulations with strength values in the region of cancellous bone (5-10 MPa) for formulations with a PLR of $2.5 \text{ g}\cdot\text{mL}^{-1}$ and gelatin with a concentration of 2.5-10.0 w/v% as liquid phase were obtained. For osteomyelitis treatment, these composite materials are a promising tool due to the sustained release of the glycopeptide antibiotic vancomycin. Higuchi-release model was confirmed by determination of the release exponent *via* power law resulting in $n = \sim 0.5$ and consequently a release proportional to $t^{0.5}$. A retarding effect was observed over a period of 44 days. All things considered, higher PLRs ($2.5 \text{ g}\cdot\text{mL}^{-1}$) and gelatin content (10.0 w/v%) showed a most effective drug incorporation capacity with sustained vancomycin delivery.

With respect to tested parameters like mechanical properties and controlled drug release of vancomycin, dual set materials of genipin cross-linked gelatin and *in situ* forming brushite cement have the potential to be used in biomedical applications for example for the treatment of osteomyelitis.

Chapter 6

Integral discussion and future directions

The development of different dual setting systems aiming to overcome brittleness of pure CPCs was successfully established and thoroughly characterized for three formulations based on apatite or brushite cement as well as synthetic PEG-hydrogels or gelatin, respectively. **Figure 46** depicts the different approaches established in this thesis. First, a one-component system based on α -TCP was modified using a polyHEMA network in combination with a more degradable, high molecular weight PEG-PLLA-hydrogel precursor. Significant increase in bending strength as well as elasticity was observed for the modified composites. One step forward with focus on degradability, an exchange from apatite to brushite cements was performed. Larger molecular weight of the polymeric precursors and therefore a less dense polymeric network as well as *per se* mechanically weaker DCPD constructs resulted in extremely flexible composite materials. The third system was obtained using an organic hydrogel phase by incorporating the natural polymer gelatin, which was chemically cross-linked in a reaction with genipin.

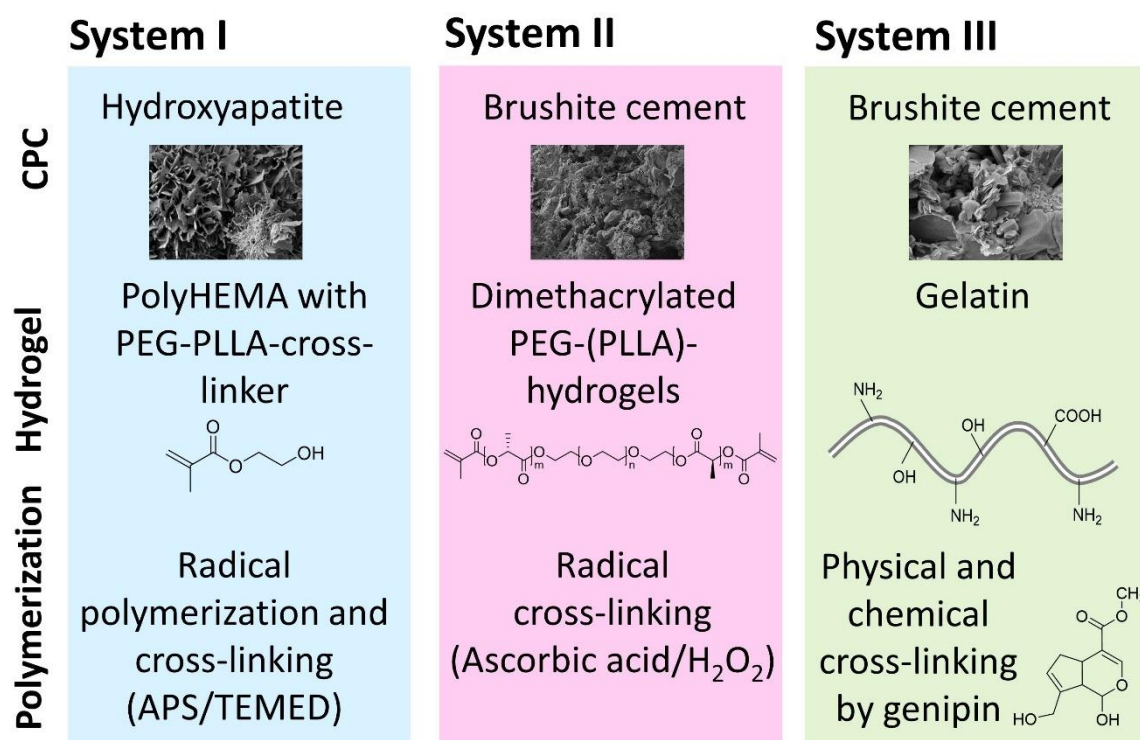


Figure 46:

Overview of the three established systems in this thesis. First, an advancement with a degradable PEG-PLLA-cross-linker of an already published dual setting system based on HA and polyHEMA was performed and resulted in improved mechanical properties (system I). The second approach was enhanced in ductility and elasticity by changing the hydrogel phase to PEG-based networks by incorporation in the *in vivo* resorbable brushite cement matrix (system II). Finally, the hydrogel phase was replaced by a natural biopolymer and chemically cross-linked *via* genipin (system III).

There are several reports that confirm the strength and effectiveness of polymeric additives to CPCs and consequently increase the attractiveness of composite materials for research groups. Polymers, appropriate monomers of hydrogels or precursor structures can either be incorporated in the liquid or the solid phase of a cement and then allow to improve setting time, macroporosity, cohesion or washout resistance, injectability, drug eluting properties, biological response, long-term degradation and of course mechanical properties of the resulting composites [291]. By that, intrinsic limitations of the pure inorganic phase are circumvented and many material immanent disadvantages can be ameliorated. For example, one benefit is the broader applicability of such composites also for load bearing defects due to the enhancement in ductility with a much higher deformation before failure, which is much more comparable to natural bone. Furthermore, an increase in compressive strength can be attributed to the polymer phase incorporated between the cement crystals, forming a more cohesive construct and increasing the absorbed energy and plastic deformation of the biomaterial [292]. Now, with an *in situ* formation of the interpenetrating hybrid system, mechanical brittleness of pure CPCs can be overcome and an interdigitated network results in even more prominent elastic properties. The development of such dual setting systems with simultaneously occurring processes of cement hardening and gelation is a one-step further concept that is investigated and still continuously refined in literature. So the question arises, which essential parameters are required for preparing such heterogenic monoliths consisting of inorganic and organic components. The setting time of the complex system is controlled by the polymerization/cross-linking as well as hydration conditions [32]. This directly influences the crystal size of the cement phase during the dissolution-precipitation reaction. The smaller their size, the better the entanglement of the growing crystals, which consequently results in higher mechanical strengths and an improved fracture behavior. Continuously, the surface/interface properties of the two phases, their interlocking as well as available water amount for both reactions, the gelation and the occurring setting, should be carefully evaluated for the development of an improved dual setting system. An improved interface design is not only important within the composite itself but also with respect to the interaction of the hybrid material with surrounding tissue. So it should be taken into account during the whole biomaterial development [293].

Integrally considered, when comparing the three systems developed and displayed within this thesis, the most determining component for the composite's mechanical stability still is the used inorganic phase, which exhibits higher compressive as well as bending strengths for apatite in comparison to brushite cements. In the soft hydrogel, nucleation and crystal growth is still feasible to a certain extent by generating an incorporated interlocking network of inorganic crystals in a simultaneously initiated dual network system. The interlocking of crystals provides the necessary mechanical stability whereas the 3D polymeric network contributes to a much less extent to the compressive strength of the composite. However, its main function is the modulation of the material's elasticity with a shift towards a more ductile behavior. Another important fact for all three formulations is the observed reduction in crystal size with increasing amount of polymeric components, especially in comparison to the corresponding polymer free references of apatite or brushite cement. Thus, a higher degree of entanglement is generated by the larger and more fissured surfaces of the cement crystals, which again raise the inner strength of each hybrid system though increasing flexibility with incorporated, bridging polymeric structures. However, there is also an upper limit of polymer amount that can be added or formed in the liquid phase. Viscosity limits as well as an inhomogeneous mixing of the solid raw powder and the setting solution do not favor the formation of an interpenetrated specimen anymore.

A future perspective for further improved dual setting systems would be the change of processing techniques for the preparation of CPC-based composite scaffolds. There are several methods that can be used instead of the classical *in situ* mixing of organic and inorganic phase. In a review of Ginebra *et al.* [200], several examples are given that now can be transferred to these hybrid materials by considering some points. First of all, approaches based on (i) rapid prototyping can be promising candidates. This means 3D printable systems that are produced by using a 3D powder printer or 3D plotter in combination with an appropriate liquid phase and potential additives that are required for hydrogel formation. Pioneering this field by printing brushite cement [294, 295], especially the third system based on gelatin hydrogels (see **Chapter 5**) could be used for 3D plotting. Pastes should not agglomerate or react during processing, which can be controlled by adjusting the pH-value in the syringe to neutral conditions. Moreover, they should be

rheologically stable without sedimentation of the raw powder phase and exhibit an appropriate initial viscosity. The obtained scaffold has to be dimensionally stable by incorporating the cross-linker genipin either in the powder phase or subsequently immersing the final construct in a genipin solution. As second option, 3D powder printing with a very thin fluid gelatin solution in a low concentration could be used. Though the reaction of β -TCP and MCPA in combination with the liquid phase is slower in comparison to a system composed of H_3PO_4 and β -TCP, gelatin solution could support the scaffold structure by providing the necessary shape fidelity. Shifting to powder filled gelatin solutions that form nucleation crystals for the cement setting, cell encapsulation within the hydrogel phase additionally increases the attractiveness of the composites for tissue bioengineering. Among natural hydrogels like alginate, collagen or hyaluronic acid [296], the polymeric structures could protect cells like osteoblasts and enable also the functionalization and inclusion of for example growth factors like rhBMP-2 [297].

Furthermore, (ii) cryo-structuring as already shown for silk fibroin solutions in combination with CaPs (in this study: MCPA) [298] can be another method for advanced dual setting systems by introducing a controlled macroporosity by an anisotropic temperature gradient within the sample. However, the challenge will be to find a suitable solvent for gelatin due to the fact that gelation of aqueous gelatin solutions already occurs by an applied temperature decrease and its thermos-reversibility. Even if it is not controlled, further preliminary tests of an aqueous pure gelatin solution resulted in the formation of a spongy like network in a water-based system instead of defined and anisotropically oriented pores. By changing the solvent for example to dimethyl sulfoxide, even with an uncontrolled freezing process vertically oriented channels were generated (see **Figure 47**).

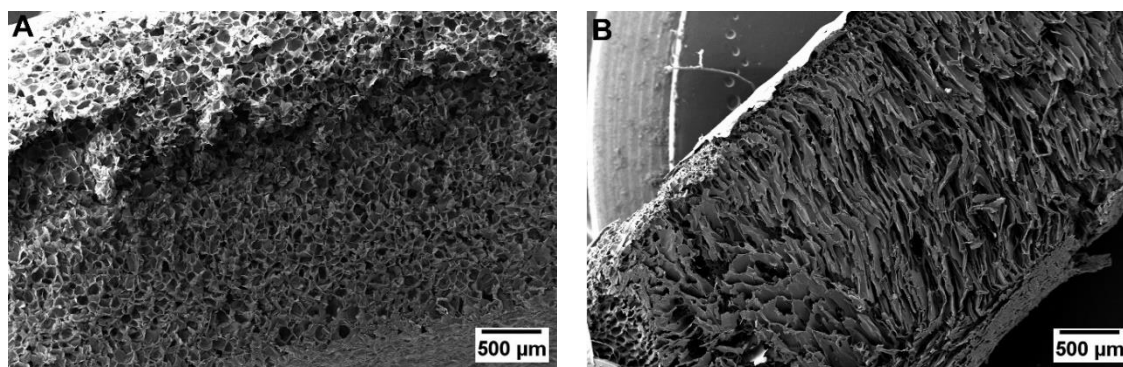
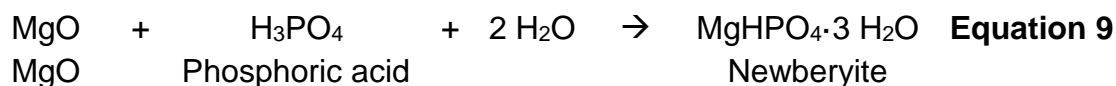


Figure 47:

Frozen gelatin scaffolds at $-20\text{ }^{\circ}\text{C}$ without controlled temperature for an aqueous gelatin solution (2.5 wt%) generating a spongy polymeric network by hydrogel formation due to a temperature decrease (**A**) and a structured construct with even vertically oriented pores of gelatin solution based on dimethyl sulfoxide (**B**).

In order to obtain composite materials, β -TCP can be mixed to the polymer solution and afterwards incorporated in H_3PO_4 triggering the conversion to brushite cement as shown in a proof of principle study with silk fibroin solution [298].

Another promising perspective can be (iii) the transfer of these systems to magnesium phosphate cements (MPCs). These alternative bone replacement materials with different composition similar to CPCs strongly depend on pH-conditions or ion supplementation during setting reaction. In an acid-base reaction comparable to brushite cement, magnesium oxide (MgO) reacts with an acidic component like H_3PO_4 . This favors the formation of newberyite ($\text{MgHPO}_4 \cdot 3\text{H}_2\text{O}$) which can reach compressive strength levels of about 30 MPa [299] (see **Equation 9**). Another important MPC is struvite ($\text{MgNH}_4\text{PO}_4 \cdot 6\text{H}_2\text{O}$) with an achievable stability up to 60 MPa after compression [300].



Focusing not only on the material side, especially cell-molecular interactions should be taken into account as the whole bone repair is a very complex process which needs a lot more time for the optimization of replacement materials. There are many new approaches developing CPC-based treatments with different kind

of additives. These can be additional organic hydrogel phases as described in this thesis or polymer meshes, fibers or nanoparticles [296]. Researchers are still questioning for the “ideal” biomaterial that first should be optimized and tested *in vitro* with further translational studies to achieve a transfer *in vivo* and in clinical trials to validate the optimized treatment approach.

Chapter 7

Summary / Zusammenfassung

Summary

Synthetic bone replacement materials have their application in non-load bearing defects with the function of (re-) construction or substitution of bone. This tissue itself represents a biological composite material based on mineralized collagen fibrils and combines the mechanical strength of the mineral with the ductility of the organic matrix. By mimicking these outstanding properties with polymer-cement-composites, an imitation of bone is feasible. A promising approach for such replacement materials are dual setting systems, which are generated by a dissolution-precipitation reaction with cement setting in parallel to polymerization and gelation of the organic phase forming a coherent hydrogel network. Hereby, the high brittleness of the pure inorganic network was shifted to a more ductile and elastic behavior.

The aim of this thesis was focused on the development of different dual setting systems to modify pure calcium phosphate cements' (CPCs') mechanical performance by incorporation of a hydrogel matrix. Besides limitations regarding poor mechanical properties of pure inorganic phases, biodegradation also played a major role in hybrid material creation. Three different formulations were established, which represent possible candidates that could be used in the biomedical field.

An already published dual setting system based on hydroxyapatite (HA) and cross-linked 2-hydroxyethyl methacrylate (HEMA) *via* radical polymerization was advanced by homogenous incorporation of a degradable cross-linker composed of poly(ethylene glycol) (PEG) as well as poly(lactic acid) (PLA) with reactive terminal methacrylate functionalities (PEG-PLLA-DMA). By integration of this high molecular weight structure in the HEMA-hydrogel network, a significant increase in energy absorption (toughness) under 4-point bending testing was observed. An addition of only 10 wt% hydrogel precursor (referred to the liquid phase) resulted in a duplication of stress over a period of 8 days. Additionally, the calculated elasticity was positively affected and up to six times higher compared to pure HA. With a constantly applied force during compressive strength testing, a deformation and thus strain levels of about 10 % were reached immediately after preparation (day 0). Furthermore, the incorporation of a second phase influenced the

composition towards decreased HA crystal sizes with a conversion of about 90 % for the desired mineral.

For higher degradability, the system was modified in a second approach regarding organic as well as inorganic phase. The latter component was changed by brushite forming cement that is resorbable *in vivo* due to solubility processes. This CPC was combined with a hydrogel based on PEG-PLLA-DMA and other dimethacrylated PEGs with different molecular weights and concentrations. Hereby, new reaction conditions were created including a shift to acidic conditions (pH < 4.2). On this ground, the challenge was to find a new radical initiator system. Suitable candidates were ascorbic acid and hydrogen peroxide that started the polymerization and successful gelation in this environment. These highly flexible dual set composites showed a very high ductility with an overall low strength compared to HA-based models. After removal of the applied force during compressive strength testing, a complete shape recovery was observed for the samples containing the highest polymeric amount (50 wt%) of PEG-PLLA-DMA. A study comparing powder filled hydrogels with identical volume ratios with the composite materials revealed significant differences in compression testing for the dual set materials in comparison to hydrogels with embedded powder particles. This underlines the importance of interfacial integration during the double setting. Regarding phase distribution in the constructs, a homogeneously incorporated hydrogel network was demonstrated in a decalcifying study with ethylenediaminetetraacetic acid (EDTA). Intact, coherent hydrogels remained after dissolution of the inorganic phase *via* calcium ion complexation. This disabled a possible agglomeration due to a very fast and rapid reaction mechanism by formation of both phases.

In a third approach, the synthetic hydrogel matrix of the previously described system was replaced by the natural biopolymer gelatin. Simultaneously to brushite formation, physical as well as chemical cross-linking by the compound genipin was performed in the dual setting materials. Based on this cross-linking agent, covalent bonds were formed by creation of blue colored pigments that already macroscopically indicated a homogenous phase distribution within the composite. Besides, thermally stable specimens were produced that did not disintegrate under

physiological conditions ($T = 37\text{ }^{\circ}\text{C}$) due to the dissolution and swelling of the organic phase. Thanks to the incorporation of gelatin, elasticity increased significantly, in which concentrations up to 10.0 w/v% resulted in a certain cohesion of samples after compressive strength testing. They did not dissociate in little pieces but remained intact cuboid specimens though having cracks or fissures. Furthermore, the drug release of two active pharmaceutical ingredients (vancomycin and rifampicin) was investigated over a time frame of 5 weeks. The release exponent was determined according to Korsmeyer-Peppas with $n = 0.5$ which corresponds to the drug liberation model of Higuchi. A sustained release was observed for the antibiotic vancomycin encapsulated in composites with a gelatin concentration of 10.0 w/v% and a powder-to-liquid ratio (PLR) of $2.5\text{ g}\cdot\text{mL}^{-1}$.

With respect to these developments of different dual setting systems, three novel approaches were successfully established by polymerization of monomers and cross-linking of precursors forming an incorporated, homogenous hydrogel matrix in a calcium phosphate network. All studies showed an essential transfer of mechanical performance in direction of flexibility and bendability. The various simultaneously running setting reactions of HA and brushite cement as well as hydrogel formations resulted in composite materials that are promising candidates for non-load bearing defects with application as bone replacement materials.

Zusammenfassung

Synthetische Knochenersatzmaterialien finden ihre Anwendung im Bereich nicht-lasttragender Defekte zum Wiederaufbau und Ersatz von defekter oder verlorener Knochensubstanz. Diese stellt aufgrund ihres Aufbaus aus mineralisierten Kollagen-Fibrillen selbst ein biologisches Komposit-Material dar, welches die mechanische Festigkeit des Minerals mit der Duktilität der organischen Matrix kombiniert. Eine Nachahmung dieser herausragenden Eigenschaften des Knochens wird im Sinne eines Ersatzmaterials durch geeignete Polymer-Zement-Komposite ermöglicht. Ein vielversprechender Ansatz für solche Komposite sind hierbei dual härtende Systeme, bei denen die Lösungs-Fällungs-Reaktion der Zementbildung parallel zur Polymerisation oder Gelierung der organischen Phase zu einem kohärenten Hydrogelnetzwerk abläuft. Die hohe Sprödigkeit und Bruchanfälligkeit rein anorganischer Netzwerke sollte dabei durch die Integration elastischer Polymerkomponenten hin zu mehr Flexibilität und Elastizität modifiziert werden.

In der vorliegenden Arbeit wurden verschiedene dual härtende Hybrid-Materialien entwickelt, um etablierte Calciumphosphatzemente durch Einbringen von zusätzlicher Hydrogel-Matrizes bezüglich ihrer mechanischen Eigenschaften zu modifizieren. Besonderer Fokus wurde hierbei - neben den erwähnten Bruch-Eigenschaften - auch auf die Bioabbaubarkeit der Zemente und Polymernetzwerke gelegt. Es wurden drei verschiedene Formulierungen etabliert, die als mögliche Kandidaten für eine biomedizinische Anwendung genutzt werden könnten.

In ein bereits bestehendes dual härtendes System aus Hydroxylapatit (HA) und radikalisch vernetztem 2-Hydroxyethylmethacrylat (HEMA), wurde ein abbaubarer Cross-linker aus Polyethylenglykol (PEG) und Polymilchsäure (PLA)-Einheiten homogen inkorporiert, der mittels einer Reaktion der terminalen Methacrylatfunktionen (PEG-PLLA-DMA) zur Ausbildung der Vernetzungen führte und mittels PLLA hydrolytisch labile Esterbindungen ins System integrierte. Durch Einbringen dieser hochmolekularen Polymere in das engmaschige HEMA-Hydrogelnetzwerk kam es zu einer signifikanten Erhöhung der Energieaufnahme des Konstruktes unter 4-Punkt-Biegebelastung im Vergleich zum bereits etablierten System. Durch Zusatz von 10 Gew% hochmolekularem Hydrogel

Präkursor (bezogen auf die flüssige Phase) konnte über einen Zeitraum von acht Tagen ein zweifach höherer Bruchwiderstand erhalten werden, verbunden mit einer bis zu sechsfach höheren Elastizität gegenüber reinem HA Zement. Bei einer konstant applizierten Kraft im Druckversuch erreichte die Verformung bereits unmittelbar nach der Herstellung (Tag 0) eine Dehnung von bis zu 10 %. Zudem wurde die Phasenzusammensetzung durch die eingebrachte Hydrogelphase insofern beeinflusst, dass kleinere HA Kristallgrößen bei einer Umsetzungsrate bis zu 90 % erhalten wurden.

Zur Steigerung der Bioabbaubarkeit wurde das System in einem zweiten Ansatz durch einen Austausch der anorganischen Komponente mit einem *in vivo* leichter resorbierbaren Brushit Zement weiter modifiziert. Dabei wurden darüber hinaus auch dimethacrylierte PEGs verschiedener Molekulargewichte in unterschiedlichen Konzentrationen mit dem Zementpulver kombiniert. Die Reaktionsbedingungen im sauren Milieu ($\text{pH} < 4,2$) erforderten den Austausch des radikalischen Initiator-Systems, wobei sich eine Kombination aus Ascorbinsäure und Wasserstoffperoxid als geeignet erwies. Die so erhaltenen dual härtenden Komposite zeigten eine sehr hohe Duktilität und Flexibilität bei insgesamt niedriger Festigkeit im Vergleich zu HA-basierenden Systemen. So fand im Druckversuch eine vollständige Relaxation zu den Ausgangsabmessungen des Prüfkörpers bei einem hohen Polymeranteil an PEG-PLLA-DMA (50 Gew%) statt.

Dieser Effekt wurde im Gegensatz zu den dual härtenden Systemen nicht für Partikel-gefüllte Hydrogele beobachtet, die signifikant niedrigere Spannung im Druckversuch zeigten.

Die homogene Verteilung der inkorporierten Polymerphase wurde mittels Decalcifizierung durch Ethylendiamintetraessigsäure (EDTA) bewiesen. Hierbei wurden durchgängige Hydrogele nach Herauslösen der anorganischen Phase durch Komplexierung von Calcium-Ionen erhalten, was die vermutete Ausbildung von möglichen Polymer-Agglomeraten durch einen zu raschen Reaktionsablauf bei der Bildung beider Phasen wirkungsvoll entkräftete.

Abschließend wurde die auf synthetischen Polymeren basierende Hydrogel-Matrix durch das natürliche Biopolymer Gelatine ersetzt. Neben der Brushit-bildenden Zement-Reaktion wurde das Polymernetzwerk sowohl durch eine physikalische

Gelierung als auch eine chemische Vernetzung mit Genipin stabilisiert. Dabei kam es zur Ausbildung kovalenter Bindungen unter Bildung blauer Farbpigmente, was bereits makroskopisch auf eine äußerst homogene Phasenverteilung aufgrund der einsetzenden Farbreaktion hindeutete. Außerdem wurden so thermisch stabile Prüfkörper erzeugt, die auch unter physiologischen Bedingungen ($T = 37\text{ °C}$) in Medium nicht thermo-reversibel desintegrierten. Durch die zusätzliche organische Phase wurden die Eigenschaften des Zementes hinsichtlich Elastizität erhöht, wobei bei einer Gelatine-Konzentration von 10,0 Gew% eine erneute Kohäsion der Prüfkörper nach mechanischer Druckbelastung beobachtet werden konnte. Diese zerfielen nicht in einzelne Teile, sondern wurden trotz Auftreten von Rissen als weitestgehend intakte Quader zusammengehalten. Weiterhin wurde die Wirkstoff-Freisetzung zweier antibiotisch aktiver Substanzen (Vancomycin und Rifampicin) über einen Zeitraum von fünf Wochen untersucht. Mittels Bestimmung des Freisetzungsexponenten nach Korsmeyer-Peppas konnte eine verzögerte Wirkstoffliberation für das Antibiotikum Vancomycin gemäß Wurzel-t-Kinetik (Higuchi-Modell) mit $n = 0,5$ für ein Pulverflüssigkeitsverhältnis von $2,5\text{ g}\cdot\text{mL}^{-1}$ bei einer Gelatinekonzentration von 10,0 Gew% erhalten werden.

Im Hinblick auf die Entwicklung verschiedener Formulierungen als dual härtende Systeme wurden in der vorliegenden Arbeit drei Varianten etabliert, die durch Polymerisation von Monomeren beziehungsweise Vernetzung von Hydrogel-Präkursoren zu einer inkorporierten, homogenen Hydrogel-Matrix im Calciumphosphatnetzwerk führten. Bei allen Ansätzen wurde ein wesentlicher Transfer der mechanischen Eigenschaften in Richtung Flexibilität und Biegsamkeit erzielt. Alle simultan ablaufenden Abbinde-Reaktionen sowie Hydrogel-Bildungen führten zu Kompositen, die als mineralisch-organische Zementverbindungen in nicht-lasttragenden Bereichen Anwendung als Knochenersatzmaterialien finden könnten.

Chapter 8

Experimental section

This chapter contains an overview of materials and methods used in **Chapter 3**, **Chapter 4** and **Chapter 5**.

Different sections are reproduced from [191] and [193] retaining the rights by Elsevier for the latter one. Furthermore, [191] can be distributed as open access article under the Creative Commons Attribution License which permits unrestricted use, distribution and reproduction in any medium.

8.1 Synthesis and characterization of polymers

8.1.1 Synthesis of PEG-based polymers

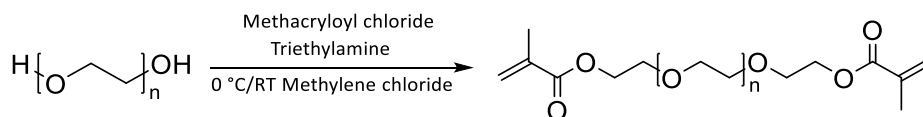
PEG precursors were functionalized with methacrylic acid groups as well as hydrophobic PLA-units (PEG-PLLA-DMA) to enable a faster degradation by hydrolysis of ester-bonds *in vivo* [227]. As references, only slightly degradable PEG-DMA with either low (PEG-DMA_{lmw}) or high (PEG-DMA_{hmw}) molecular weight were used and added in different mass percentages (10–50 wt%) to the cement liquid.

8.1.1.1 Dimethacrylated PEG based on low molecular weight backbone

Dimethacrylated PEG with low molecular weight ($M_n = \sim 550$ Da; Sigma Aldrich, Steinheim, Germany) was used as received for the preparation of the composites.

8.1.1.2 Dimethacrylated PEG based on high molecular weight backbone

This polymer preparation method was adapted from a methacrylation step reported in a procedure of Sawhney [301]. 30 g PEG (Sigma Aldrich, Steinheim, Germany) with a molecular weight of 6,000 Da were dried under vacuum for several hours before use. A second drying step was performed *via* azeotropic distillation with toluene (VWR, Ismaning, Germany) using a dean-stark receiver. 20 mL toluene were distilled off to remove residual water. Toluene was evaporated with subsequent dissolving of the purified educt in 300 mL dry methylene chloride (VWR, Ismaning, Germany). The reaction was performed while flushing with inert gas at 0 °C with ice cooling. Triethylamine (Sigma Aldrich, Steinheim, Germany) and methacryloyl chloride (Sigma Aldrich, Steinheim, Germany) were added to the reaction mixture in a four-time excess and stirred for 12 h at 0 °C and 36 h at room temperature. The solution was filtered and twice precipitated in cold diethyl ether (VWR, Ismaning, Germany). Finally, the product was dried under vacuum for several hours. The reaction is depicted in **Scheme 5**.

**Scheme 5:**

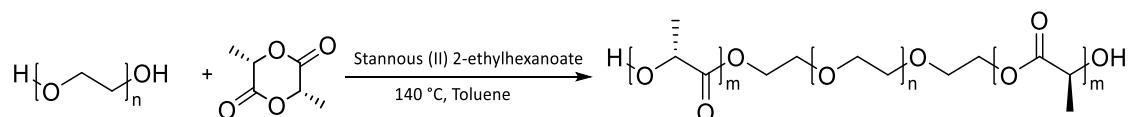
Reaction scheme of PEG-functionalization with methacryloyl chloride in methylene chloride (PEG-DMA_{hmw}). RT = room temperature.

8.1.1.3 Dimethacrylated PEG based on high molecular weight backbone with PLA-spacer units

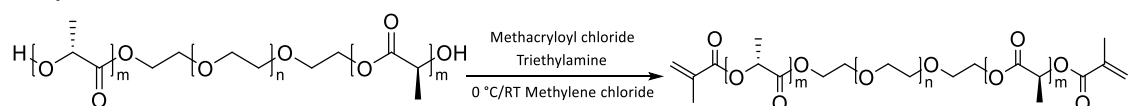
The linear triblock cross-linker composed of PEG and PLA was synthesized *via* standard ring opening polymerization in a molar ratio of 1:5, also adapted from Sawhney [301]. 30 g PEG (Sigma Aldrich, Steinheim, Germany) with a molecular weight of 6,000 Da were dried under vacuum for several hours before use and distilled as described in **8.1.1.2**. 5 g (3*S*)-*cis*-3,6-Dimethyl-1,4-dioxane-2,5-dione (L-lactide, 98%; Sigma Aldrich, Steinheim, Germany) were recrystallized from ethyl acetate (VWR, Ismaning, Germany) at 80 °C prior to use and afterwards 3.6 g were dissolved in toluene (VWR, Ismaning, Germany) and dried as described above. Both solutions, the PEG- and L-lactide-toluene-solution, were combined in a three-neck round bottom flask and the catalyst for the ring-opening polymerization (12 μ L stannous (II) 2-ethylhexanoate (Sigma Aldrich, Steinheim, Germany)) was added. The reaction mixture was stirred at 140 °C under reflux and oxygen free conditions for 6 h and then cooled down to room temperature. Toluene (VWR, Ismaning, Germany) was evaporated twice with subsequent dissolution of the remaining viscous liquid in methylene chloride (VWR, Ismaning, Germany), which was subsequently dried over calcium chloride (CaCl₂; Merck, Darmstadt, Germany) and filtered before use. In order to gain the product, the methylene chloride solution was added dropwise to cold diethyl ether (VWR, Ismaning, Germany) using a separating funnel and the precipitate was dried under vacuum for several hours. In a second step, the obtained PEG-PLLA block copolymer with free terminal hydroxyl groups was dissolved in 200 mL methylene chloride (Sigma Aldrich, Steinheim, Germany) and cooled down to 0 °C in an ice bath under oxygen-free conditions. Triethylamine (Sigma Aldrich, Steinheim, Germany) and methacryloyl chloride (Sigma Aldrich, Steinheim, Germany) were added to the reaction mixture in a four-time excess and stirred for 12 h at 0 °C and 36 h at room

temperature. The obtained solution was filtered and finally the product was precipitated twice in ice-cold diethyl ether (VWR, Ismaning, Germany). The obtained precipitate was dried under vacuum for several hours. The two-step reaction is depicted in **Scheme 6**.

Step I:



Step II:



Scheme 6:

Reaction scheme of the two-step synthesis. In the first step, the copolymer was generated *via* ring-opening polymerization using a stannous based catalyst. In the following reaction, terminal hydroxyl groups were functionalized with methacrylic acid groups (PEG-PLLA-DMA). RT = room temperature.

8.1.2 ¹H Nuclear magnetic resonance spectroscopy

10-20 mg of the polymer were dissolved in deuterated chloroform (CDCl₃; Euriso-top, Saint-Aubin Cedex, France) and ¹H NMR spectra were recorded on a Bruker Fourier 300 device (Bruker, Billerica, MA, USA) at 300 MHz with non-deuterated solvent signals as internal reference.

8.1.3 Gel permeation chromatography

GPC elugrams were recorded with a system from PSS, Agilent Technologies 1260 Infinity (Agilent Technologies Deutschland GmbH, Waldbronn, Germany; pump and refractive index detector) using DMF (Carl-Roth, Karlsruhe, Germany) as solvent with 1 g*L⁻¹ lithium bromide (LiBr; Sigma Aldrich, Steinheim, Germany) and a flow rate of 1.0 mL*min⁻¹. Column system was composed of one precolumn (PSS GRAM; PSS Polymer Standards Service GmbH, Mainz, Germany) and two

columns with a length of 300 mm, a width of 8 mm and a particle size of 10 μm (PSS GRAM; PSS Polymer Standards Service GmbH, Mainz, Germany) for a molecular weight analysis from 100-1,000,000 Da. For calibration, PEG standards (Malvern Panalytical, Herrenberg, Germany) were used.

8.1.4 Matrix-assisted laser desorption and ionization/Time-of-flight mass spectrometer

The linear copolymer was characterized regarding molar mass by MALDI-ToF MS. All MALDI mass spectra were acquired on a time of flight mass spectrometer (Bruker Daltonics autoflex II, Bruker Daltonik GmbH, Leipzig, Germany), equipped with a SCOUT™ MTP MALDI Ion Source. The following procedure was adapted from Marie *et al.* [302]. Standards were prepared by mixing a solution of 10 % cesium triiodide (CsI_3 ; Sigma Aldrich, Steinheim, Germany) in acetonitrile (ACN; Sigma Aldrich, Steinheim, Germany) with equimolar volumes (1 μL) of a 2.5 % solution of *trans*-2-[3-(4-*tert*-Butylphenyl)-2-methyl-2-propenylidene]malononitrile (DCTB; Sigma Aldrich, Steinheim, Germany) in ACN. Subsequent, the mixture was spotted ($V = 1 \mu\text{L}$) on the aluminum MALDI target (Bruker Daltonics MTP 384 massive target T; Part No.: 26755). Samples were then prepared by mixing the polymer solution (10 $\text{mg}\cdot\text{mL}^{-1}$ in chloroform; CHCl_3) with the matrix solution (50 $\text{mg}\cdot\text{mL}^{-1}$ DCTB in CHCl_3). A volume of 1 μL was spotted on the MALDI target. 100 shots at 20 Hz of a 337 nm nitrogen laser (LTB MNL205 BA352A61) were applied and spectra were accumulated.

8.1.5 Fourier transform infrared spectroscopy

FTIR spectra were recorded by a Nicolet™ iS™10 Spectrometer (Thermo Fisher Scientific, Waltham/Massachusetts, USA) within a wave number range of 4,000-650 cm^{-1} *via* attenuated total reflection mode. Therefore, scan number was selected with 16 scans per measurement and a resolution of 4.

8.2 Preparation and characterization of hydrogels

8.2.1 Pure hydrogel production and characterization of HEMA hydrogels, PEG-PLLA-DMA hydrogels and their combination

8.2.1.1 Determination of gelation point *via* rheological analysis

The gel point of each systems was monitored by oscillatory time sweeps with the rheometer MCR301 (Anton Paar GmbH, Graz, Austria). A plate-plate-geometry with a diameter of 25 mm was used for the measurements at a selected temperature of 16 °C. Time sweeps were carried out with a constant amplitude γ of 1 % and a constant frequency f of 1 Hz. Storage (G') and loss modulus (G'') were measured during a time frame of 30 min. The solutions for hydrogel formation were prepared according to **Table 6**. Therefore, a volume of 1 mL for each solution was used for rheological characterization. Abbreviations for the different batches are as follows: 40 wt% HEMA (H40), 10 wt% PEG-PLLA-DMA (P10) as well as a combination of both (H40P10). According to the very fast gelation kinetic of pure hydrogels composed of the PEG-PLLA-based cross-linker, the concentration was reduced to 10 wt%. However, a clear trend and prediction for higher concentrations like 25 wt% can be drawn.

Table 6:

Composition of the different liquid phases for composite formulations. H40 refers to 40 wt% HEMA-monomer in the solution, whereas P10 corresponds to 10 wt% cross-linker addition. The combination of 40 wt% HEMA and 10 wt% cross-linker is abbreviated with H40P10.

Substances <i>Abbreviations</i>	Percentage by weight / wt%		
	H40	P10	H40P10
HEMA	40	–	40
Cross-linker	–	10	10
2.5 % Na ₂ HPO ₄ -solution	59.25	89.25	49.25
APS		0.5	
TEMED		0.25	

8.2.1.2 Degradation and swelling behavior

For investigations concerning swelling behavior of the different hydrogel batches, solutions were prepared analogously to the composition overview in **Table 6**. Specimens were gelled in round silicone molds with a diameter of 10 mm and a height of 3 mm and put in a drying chamber with 37 °C for 5 min. In order to characterize the hydrogel systems, these small disks were weighed over a period of approximately 10 weeks and put into glass vials. Afterwards, they were placed in 5 mL of PBS and stored on a shaking gadget at 37 °C in an oven. The EWC as weight percentage was calculated using **Equation 10**. W_s and W_d are the weights of swollen and dry specimens, respectively.

$$EWC = \frac{W_s - W_d}{W_s} * 100\% \quad \text{Equation 10}$$

Furthermore, the volumetric swelling ratio Q_v as another expression for swelling degree was determined by the quotient of swollen polymer (W_s) and dry polymer (W_d) according to **Equation 11**. Both parameters were determined for two different time points: immediately after production as well as after 4 h.

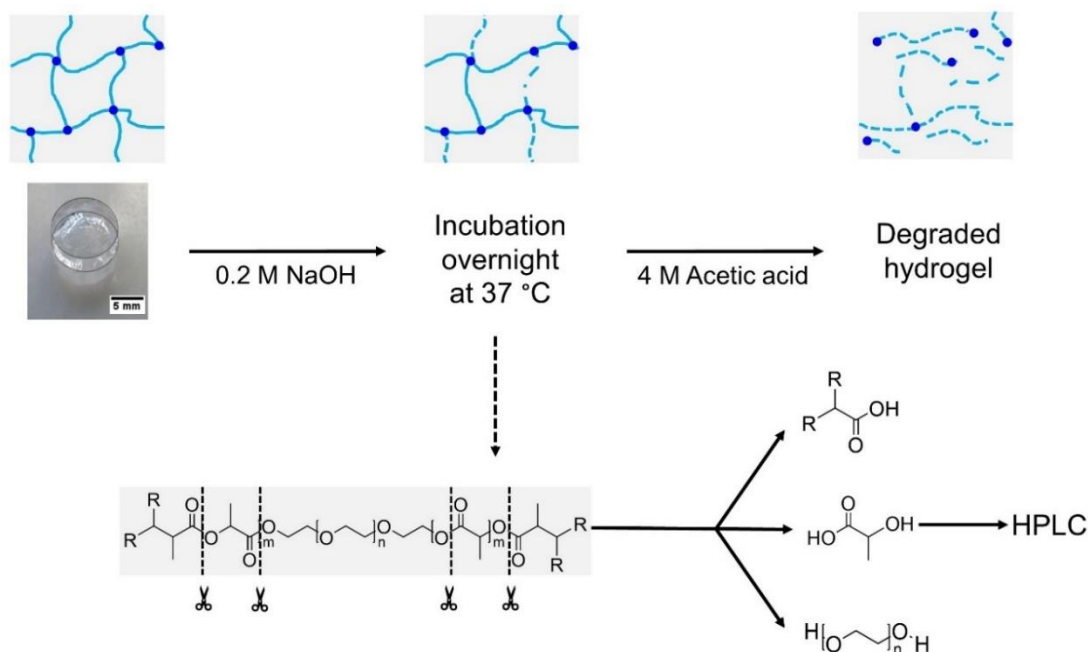
$$Q_v = \frac{W_s}{W_d} \quad \text{Equation 11}$$

8.2.1.3 Degree of cross-linking for synthesized hydrogel precursor via determination of methacrylic acid

Degree of cross-linking as well as methacrylation for PEG-PLLA-DMA-based hydrogels were both investigated using a method adapted from Abbadessa *et al.* [303]. Round specimens were produced according to the procedure described in **8.2.1.1** (composition in **Table 6**). Ester bonds of the polymeric network were basically hydrolyzed by addition of 0.2 M NaOH-solution (4 mL; produced out of NaOH, Merck, Darmstadt, Germany). Therefore, samples were incubated at 37 °C overnight. For protonation of released methacrylic acid,

3 mL of 4 M acetic acid (produced out of acetic acid, glacial, Alfa Aesar, Kandel, Germany) were pipetted to the gels. This process is illustrated in **Scheme 7**.

After degradation verified by transparent solutions, methacrylic acid was detected *via* HPLC (Shimadzu (LC-20AT) with autosampler (SIL-20AC); Shimadzu Deutschland GmbH, Duisburg, Germany) equipped with a C18 column (Luna 5 μm C18(2) 100 \AA , LC Column 150*4.6 mm; Phenomenex LTD, Aschaffenburg, Deutschland) and a photodiode array detector (SPD-M20A) with a chosen wave length λ of 210 nm. Eluent composed of water/ACN (Sigma Aldrich, Steinheim, Germany) in a ratio of 85:15 with a pH of 2 (adjusted with perchloric acid, Merck, Darmstadt, Germany) with a set flow of $1 \text{ mL} \cdot \text{min}^{-1}$. Calibration was performed using solutions of methacrylic acid (Sigma Aldrich, Steinheim, Germany) in the same eluent within a concentration range of $0.55\text{-}279.47 \mu\text{g} \cdot \text{mL}^{-1}$. For standards as well as samples, injection volume was set to $10 \mu\text{L}$.



Scheme 7:

Schematic overview of determined degree of methacrylation as well as amount of cross-linked free methacrylic acid. Different procedure steps starting from basic hydrolysis with incubation overnight to protonation of methacrylic acid until a complete degradation of the hydrogel is obtained. This compound was analyzed *via* HPLC according to a procedure of Abbadessa *et al.* [303].

Calculation of cross-linked methacrylic acid functionalities as measure for integrity in network formation was performed according to **Equation 12**.

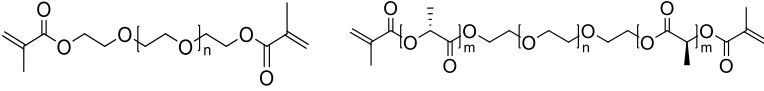
$$\% \text{ of cross-linked methacrylic acid} = 100 \% - \frac{\% \text{ of methacrylic acid in gels}}{\text{total of methacrylic acid in control}} \quad \text{Equation 12}$$

8.2.2 Preparation of pure PEG-based hydrogels as organic reference

As reference, pure hydrogel samples without inorganic phase were produced. The composition of hydrogels with 50 wt% amount of precursor is listed in **Table 7**.

Table 7:

Composition of the liquid solution for the pure hydrogel specimens with a concentration of 50 wt% polymer.

Liquid phase	
Polymers (hydrogel precursors)	PEG-DMA _{lmw} PEG-DMA _{nmw} PEG-PLLA-DMA
	
	50 wt%
H ₂ O ₂ -solution (30 wt%)	0.5 wt%
Ascorbic acid	0.5 wt%
0.5 M Citric acid solution	49 wt%

The hydrogel precursors were dissolved in 0.5 M citric acid solution (produced out of citric acid monohydrate, Sigma Aldrich, Steinheim, Germany) until a clear liquid was obtained. Then, ascorbic acid (Sigma Aldrich, Steinheim, Germany) was added. After the addition of H₂O₂ solution (Merck, Darmstadt, Germany), the vial was put on a vortexer (Vortex-Genie 2, Scientific Industries SI, New York, USA) for a few seconds and the solution was rapidly pipetted (V = 50 μL) in appropriate

cylindric silicon molds. Produced specimens were round with a height of 2 mm and a diameter of 6 mm. For swelling, the samples were stored in PBS on a shaker at 37 °C for one day. The day after, mechanical tests were performed using a mechanical testing device by Bose (see **8.5.2**).

8.2.3 Production of organic reference – gelatin hydrogels

Gelatin from porcine skin (Type A, Sigma Aldrich, Steinheim, Germany) was dissolved in demineralized water at 50 °C (oil bath) overnight while stirring at 200 rpm, whereas three different concentrations were produced (2.5 w/v%, 5.0 w/v% and 10.0 w/v%). 450 µL of each solution were pipetted in cubic silicon molds (6*6*12 mm³) and stored horizontally in a freezer at -20 °C. Afterwards, the samples were removed from the molds and incubated in an aqueous genipin-solution (1 w/v%; Challenge Bioproducts, Yun-Lin Hsien, Taiwan) in the fridge at 5 °C for 3 days. Afterwards, they were transferred to PBS and stored at 37 °C in a water bath.

8.2.4 Mechanical characterization of pure hydrogels

8.2.4.1 Compressive strength testing of PEG-based hydrogels

To compare the results of the inorganic reference and dual set composites with their corresponding pure hydrogels, additional measurements were performed using the dynamic mechanical analysis device Bose ElectroForce 5500 (Bose, Friedrichsdorf, Germany) and a 200 N load cell because smaller values of compressive strength were reached for the hydrogel controls.

Therefore, samples were prepared as described in **8.2.2** and **8.4.2.3**, and filled into round shaped silicon molds (diameter of 6 mm, height of 2 mm). They were initially placed onto the lower plate of the device and then compressed until a pre-load of 0.05 N was reached. Afterwards, the measured force was reset. For (i) static compressive strength testing, composite materials with 50 wt% hydrogel precursor were additionally analyzed. The chosen crosshead speed for the measurement was 0.01 mm*s⁻¹ and the maximum compression was set to 0.6 mm. From these

measurements, the Young's modulus was determined through the slope of the curve between 0.0 and 0.1 % strain. To demonstrate the elasticity, samples with 50 wt% polymeric content were subjected to (ii) dynamic mechanical measurements. Here, the measuring process was as follows: run of a ramp to a level of 0.1 mm with a rate of $0.01 \text{ mm} \cdot \text{s}^{-1}$ followed by a dwell at 0.1 mm for 10 s with at least a sine wave deformation from 0.1 mm to 0.6 mm with a frequency of 0.1 Hz and a speed of $0.1 \text{ mm} \cdot \text{s}^{-1}$. The samples were measured at day 1 after storage in PBS. The parameters for the stress-strain curve were calculated according to **Table 8**.

Table 8:

Calculated parameters of static and dynamic compressive strength testing using the dynamic mechanical analysis device with corresponding equations. Both, the composite materials as well as the pure hydrogel specimen were characterized.

Parameter	Equation	Explanation	
Strain ε	$\varepsilon = \frac{\Delta h}{h} * 100 \%$	ε = strain / % h = sample height / mm Δh = way of sample deformation / mm	Equation 13
Stress σ	$\sigma = \frac{F}{A}$ $= \frac{F * (h - \varepsilon)}{\pi * r^2 * h}$	σ = stress / MPa F = force / N A = area of the testing sample / mm^2 r = radius / mm h = sample height / mm ε = strain	Equation 14

8.2.4.2 Compressive strength testing of gelatin hydrogels

Gelatin hydrogels were mechanically analyzed using the device Bose ElectroForce 5500 (Bose, Friedrichsdorf, Germany) and a 250 g load cell ($\pm 2.45 \text{ N}$). The samples were pre-compressed until a force of $\sim 6 \text{ mN}$ was reached. For the measurement, the chosen crosshead speed was $0.01 \text{ mm} \cdot \text{s}^{-1}$ with a maximum defined compression of 3 mm. Young's moduli were calculated as slope of stress-strain curves between 10-20 % deformation.

8.3 Physicochemical characterization of inorganic references and dual set composites

8.3.1 α -/ β -Tricalcium phosphate preparation

α -TCP was synthesized by sintering a mixture of monetite (2.15 mol; J.T.Baker, Fisher Scientific GmbH, Schwerte, Germany) and calcium carbonate (CaCO_3 , 1 mol; Merck, Darmstadt, Germany) at 1400 °C for 5 h followed by quenching to room temperature and grinding in a ball mill (Retsch, Haan, Germany) for 4 h.

β -TCP as raw powder component of cement synthesis was produced *via* sintering process of dicalcium phosphate (Mallinckrodt-Baker, Renningen, Germany) and calcium carbonate (Merck, Darmstadt, Germany). Both educts were added in a molar ratio of 2:1, heated up to 1050 °C for 5 h with subsequent quenching reaction to room temperature. After crushing the sintered cakes and passing the obtained powder through a 355 μm mesh size-sieve, a milling step with 200 rpm for 60 min using a planetary ball mill (Retsch, Haan, Germany) was performed.

8.3.2 Measurement of pH-value and temperature during initial setting reaction

In order to characterize the influence of the polymeric phase on the cement reaction, initial setting temperature (Thermometer VOLCRAFT K202, Hirschau, Germany) as well as pH-development of the composite materials were measured for 60 min using the pH-meter inoLab pH Level 2 (Xylem Analytics Germany Sales GmbH & Co. KG, WTW, Weilheim, Germany). Therefore, liquid and solid phase were mixed as described and the pH-electrode was placed in the hardening paste. Data was recorded every minute over a time period of an hour.

8.3.3 Initial setting time determination *via* Gillmore needle test

Initial setting time was determined *via* Gillmore needle test in a chamber with a relative humidity of 95-100 % and a temperature of 37 °C. Samples were prepared with a capacity of 0.8 g and a PLR of 3 $\text{g}\cdot\text{mL}^{-1}$. Time measurement was started

after addition of the reaction solution to the powder phase. In case of no mark of the plunger could be seen on the set cement, time was stopped.

8.3.4 X-ray diffraction and Rietveld refinement

XRD patterns of dried and ground samples were measured using the D5005 diffractometer of Siemens (Munich, Germany) with monochromatic Cu $K\alpha$ radiation. Data were collected from $2\theta = 10-40^\circ$ or $2\theta = 20-40^\circ$, respectively, with a step size of 0.02° and a normalized count time of $1.5 \text{ s}\cdot\text{step}^{-1}$. Furthermore, phase composition was verified by means of Joint Committee on Powder Diffraction Standards (JCPDS) reference patterns of The International Centre for Diffraction Data (ICDD) for **Chapter 3** (HA (PDF Ref. 09-0432), α -TCP orthorhombic (PDF Ref. 09-0348) and α -TCP monoclinic (PDF Ref. 09-0359)) as well as **Chapter 4** and **Chapter 5** (brushite (PDF Ref. 09-0077), monetite (PDF Ref. 09-0080) and β -TCP (whitlockite, PDF Ref. 09-0169).

Rietveld refinement was accomplished with the software TOPAS 2 (Bruker AXS, Karlsruhe, Deutschland). The calculation of the phase composition was performed with respect to ICDD data base and the respective reference numbers of HA (090432) and α -TCP (290359) as well as β -TCP (090169), monetite (090080) and brushite (090077). Furthermore, also the crystal size of either apatite or brushite cement was determined.

8.3.5 (Cryo-) Scanning electron microscopy

SEM images were recorded with a scanning electron microscope (Crossbeam CB 340, Zeiss, Oberkochen, Germany) and an acceleration voltage of up to 5.0 kV. Samples were prepared by sticking small pieces of the mechanically tested samples with self-adhesive stripes on SEM plates or using conducting carbon cement (Leit-C) of Gloecke (Plano, Wetzlar, Germany) as special adhesive material for specimen fixation. For a better electrical conductivity, the surface of the samples was sputtered with a 4 nm thick platinum (Pt) layer using the High Vacuum Coater Leica EM ACE 600 (Emitech, Molfetta, Italy).

To study the structure of pure gelatin hydrogels in a concentration of 10.0 w/v%, samples were investigated using cryo-SEM. Therefore, gelatin solution was pipetted on the aluminium sample holder ($V = 10 \mu\text{L}$; BALTIC präparation, Niesgau, Germany), cross-linked in genipin-solution (1 wt%) and incubated in liquid nitrogen for freezing. Afterwards, the whole construct was transferred *via* cooled shuttle to the sputter coater ($-140 \text{ }^\circ\text{C}$). There, the three processes (i) freeze fracturing, (ii) freeze etching ($-85 \text{ }^\circ\text{C}$ for 10 min) as well as (iii) sputter coating with a platinum layer of 4 nm were performed. Following these preparation steps, the samples were analyzed in the cooled SEM device ($-140 \text{ }^\circ\text{C}$) with regard to network structures of the chemically cross-linked hydrogels *via* genipin. In comparison, physically cross-linked samples were also investigated by pipetting the liquid solution on the specimen holder and transferring the sample after cooling in the SEM-device.

8.3.6 Energy-dispersive X-ray spectroscopy

Elemental composition of different regions (organic gelatin *versus* inorganic brushite phase) was evaluated using EDX with EDX INCA Energy 350 AzTec Advanced system and a X-MaxN 50 silicon drift detector (Oxford Instruments, Abingdon, United Kingdom). The chosen photon energy for the X-ray spectrum of the sputtered sample (see 8.3.5) was up to 10 keV.

8.3.7 Fourier Transform Infrared spectroscopy

FTIR spectroscopy is explained in section 8.1.5.

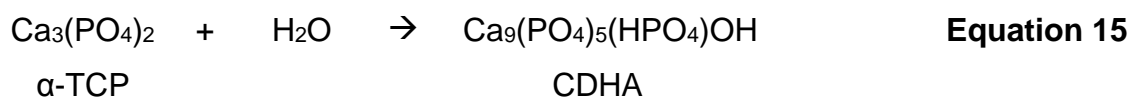
8.3.8 Mercury porosimetry

Porosity characteristics were measured by mercury (Hg) porosimetry (PASCAL 140/440, Porotec GmbH, Hofheim, Germany). Used parameters for calculation were a contact angle of 141.3 ° and a surface tension of $480 \text{ mN}\cdot\text{mm}^{-1}$ of mercury.

8.4 Preparation procedures of pure inorganic references and dual set composites

8.4.1 Dual setting system based on apatite cement

As inorganic reference, pure HA was produced by mixing the solid phase with a solution without any polymeric additives, catalysts or initiators. Therefore, samples with a PLR of $3 \text{ g} \cdot \text{mL}^{-1}$ were produced by mixing 2.5 % disodium phosphate solution (Merck, Darmstadt, Germany) with α -TCP raw powder (see 8.3.1). The obtained setting reaction sets to a matrix of CDHA within several days. This process is shown in **Equation 15**.

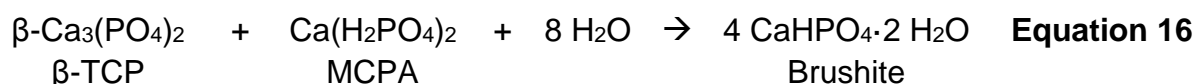


For dual setting composites, the radical starter APS (0.5 wt%; Sigma Aldrich, Steinheim, Germany) was homogeneously mixed with α -TCP raw powder (99.5 wt%) using an electric coffee grinder (Clatronic, Kempen, Germany) for 60 seconds. Base of the liquid phase was a 2.5 % Na_2HPO_4 -solution (Merck, Darmstadt, Germany) with addition of the radical catalyst TEMED (2.5 wt%; Sigma Aldrich, Steinheim, Germany). Three different formulations were tested: (i) the first batch contained 40 wt% HEMA (H40; Sigma Aldrich, Steinheim, Germany) added to the liquid phase. A (ii) second formulation combined the short-chain monomer HEMA (40 wt%) with the synthesized polymeric cross-linker PEG-PLLA-DMA (10 wt%; H40P10). The third mixture (iii) was based on the pure synthesized PEG-hydrogel precursor (25 wt%; P25). The selected PLR was $3 \text{ g} \cdot \text{ml}^{-1}$ for all three formulations. Cement setting to HA as well as radical polymerization was initiated by homogenous mixing of cement powder and liquid on a glass slab.

8.4.2 Dual setting system based on PEG-hydrogels and brushite cement

8.4.2.1 Pure brushite cement as inorganic reference

DCPD related brushite cements were produced by mixing β -TCP powder (10 g; see **8.3.1**) in an equimolar ratio with MCPA (7.55 g; Chemische Fabrik Budenheim, Budenheim, Germany) in an electric coffee grinder (Clatronic, Kempen, Germany) for 60 seconds. The solid phase was used for the pure cement reference directly after mixing without any additional compounds followed by mixing these powders with a 0.5 M citric acid solution (produced out of citric acid monohydrate, Sigma Aldrich, Steinheim, Germany) at a PLR of 2.5 g*mL⁻¹. The reaction is depicted in **Equation 16**.



8.4.2.2 Hydrogels filled with pulverized brushite

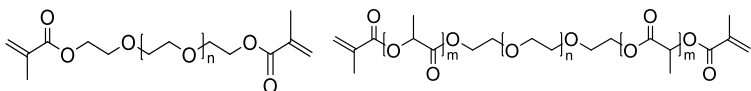
To produce a hardened cement, equimolar amounts of β -TCP (see **8.3.1**) and MCPA (Chemische Fabrik Budenheim, Budenheim, Germany) were weighed in a coffee mill (Clatronic, Kempen, Germany) and mixed for one minute. Pure brushite samples were produced with a PLR of 2.5 g*mL⁻¹ using 0.5 M citric acid solution (produced out of citric acid monohydrate, Sigma Aldrich, Steinheim, Germany) and placed in a water bath at 37 °C for 4 h of setting time. The specimens were then filled in a mortar, grinded with a pistil and sieved with the DIN-ISO 3310/1 analysis sieve mesh size $\leq 355 \mu\text{m}$ (Retsch, Haan, Germany (Ser-No. 5672512)). Afterwards, powder filled hydrogels with a concentration of 50 wt% hydrogel precursors for each polymer type were produced with a PLR of 2.5 g*mL⁻¹ as shown in **8.4.2.1** whereas the raw powder mixture of β -TCP and MCPA was replaced by grinded and sieved brushite powder. Samples were produced using identical silicon molds as for the composites and stored in the water bath at 37 °C for 4 h. After demolding, specimens were placed in PBS and stored in a water bath for one day before testing mechanical properties.

8.4.2.3 Dual set composites

For dual setting composites, the radical starter ascorbic acid (5 wt%; Sigma Aldrich, Steinheim, Germany) was added to the equimolar raw powder mixture of β -TCP (see 8.3.1) and MCPA (Chemische Fabrik Budenheim, Budenheim, Germany) using an electric coffee grinder (Clatronic, Kempen, Germany) for 30 seconds. The 0.5 M citric acid solution was the basis for the liquid phase of the composites and the following substances were added respectively dissolved. Using a mass percentage hydrogel precursor amount of 10 wt%, 25 wt% and 50 wt% with respect to the liquid phase, the three different polymeric phases were investigated using PEG-DMA_{lmw}, PEG-DMA_{hmw} as well as PEG-PLLA-DMA. Furthermore, the catalyst of the radical polymerization reaction, H₂O₂ as 30 % solution (Merck, Darmstadt, Germany), was added to each aqueous citric acid solution of the different hydrogel precursors. The composition of the different formulations is shown in **Table 9**. All composites were prepared with a PLR of 2.5 g*mL⁻¹ in cuboid silicon molds (6*6*12 mm³) and placed for 4 h in a water bath (37 °C) to perform the setting and cross-linking reaction. The obtained samples were then kept hydrated in PBS. The values of the added polymers are always referred to the pure liquid phase. In the whole composite formulation, the organic phase amount can only be estimated based on the PLR of 2.5 g*mL⁻¹, which results in approximate final amounts of 4 wt%, 10 wt% and 20 wt% of the initial polymers in the composites. The concentrations of the hydrogel precursors referring to the liquid phase (10 wt%, 25 wt% and 50 wt%) will be used in the following context to designate the amount of organic phase in the composites.

Table 9:

Composition of the liquid solution and the solid phase used for preparation of the different batches.

		Liquid phase		
	Brushite reference	PEG-DMA _{lmw}	PEG-DMA _{hwm}	PEG-PLLA-DMA
Polymers (hydrogel precursors)	none			
			10 wt% / 25 wt% / 50 wt%	
H ₂ O ₂ -solution (30 wt%)	none			5 wt%
0.5 M citric acid solution	100 wt%		85 wt% / 70 wt% / 45 wt%	
		Solid phase		
	Brushite reference	Composite formulations		
β-TCP/MCPA-mixture (1:1)	100 wt%			95 wt%
Ascorbic acid	none			5 wt%

8.4.2.4 Phase coherence study of the brushite-PEG-based composites

Network structure of the hydrogels within the composites was analyzed *via* a demineralization study in EDTA solution to demonstrate that the hydrogel phase is continuous within the composites. 100 g of disodium ethylenediaminetetraacetic acid (EDTA-Na₂, Sigma Aldrich, Steinheim, Germany) were dissolved in demineralized water using a volumetric flask. A 40 wt% sodium hydroxide solution (NaOH; Sigma Aldrich, Steinheim, Germany) was produced for pH-adjustment and 25 mL were added to the suspension to dissolve EDTA. The pH-level was then

adjusted to 7.4 using NaOH (Merck, Darmstadt, Germany) and the total volume was completed to 500 mL using demineralized water. The composite samples were produced with three different concentrations (10 wt%, 25 wt%, 50 wt%) of the polymeric hydrogel precursors (see **8.4.2.3**). 5 mL EDTA-solution were added to a small petri dish and samples were stored at room temperature in the liquid with a daily change at the beginning and a several days-time interval at the end for a period of 15 days. Specimens were weighed and measured regarding their dimension change over the time and pictures were taken in order to illustrate the remaining hard core of inorganic phase in the specimen.

8.4.3 Dual setting system based on gelatin and brushite cement

8.4.3.1 Production of inorganic reference

The inorganic reference was produced by mixing 0.5 molar citric acid solution (produced out of citric acid monohydrate, Sigma Aldrich, Steinheim, Germany) in different PLRs ($PLR_1 = 1.5 \text{ g}\cdot\text{mL}^{-1}$, $PLR_2 = 2.0 \text{ g}\cdot\text{mL}^{-1}$; $PLR_3 = 2.5 \text{ g}\cdot\text{mL}^{-1}$) with an equimolar mixture of β -TCP (see **8.3.1**) and MCPA (Chemische Fabrik Budenheim, Budenheim, Germany) and 1 wt% genipin (Challenge Bioproducts, Yun-Lin Hsien, Taiwan) to compare it with composite materials. Pastes were transferred in silicon molds ($6\cdot6\cdot12 \text{ mm}^3$) and stored at 37 °C and 100 % humidity for 4 h. After demolding, specimens were stored in PBS (pH = 7.4).

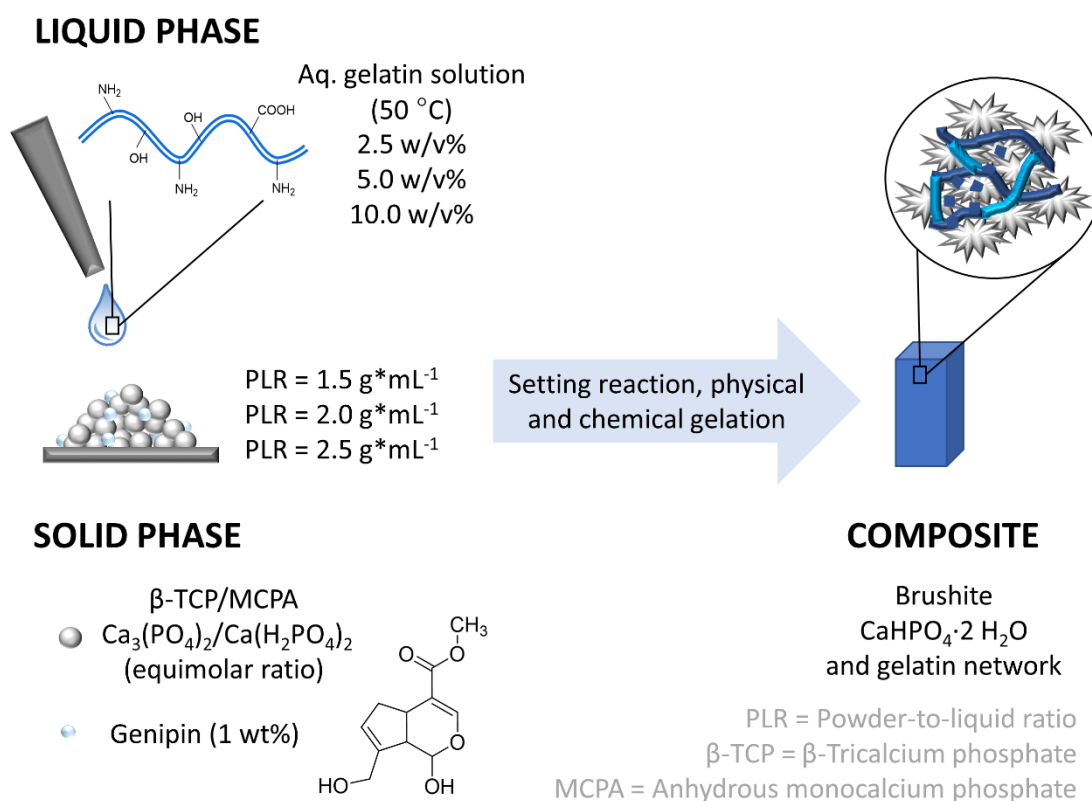
The reaction to DPCD is depicted in **Equation 16**. Also in this study, citric acid was used as setting retardant.

8.4.3.2 Production of dual set composite materials with gelatin and brushite cement

Composite materials were prepared by mixing a solid phase composed of equimolar amounts β -TCP (see **8.3.1**) and MCPA (Chemische Fabrik Budenheim, Budenheim, Germany) as well as 1 wt% genipin (Challenge Bioproducts, Yun-Lin Hsien, Taiwan) with different gelatin solutions on a glass plate. For this liquid phase, gelatin (Gelatin from porcine skin powder, gel strength ~ 300 g Bloom, Type A, Sigma Aldrich, Steinheim, Germany) was dissolved at 50 °C (oil bath) overnight

in three different concentrations (2.5 w/v%, 5.0 w/v% and 10.0 w/v%) in demineralized water while stirring at 200 rpm. PLRs were in the range of $1.5 \text{ g}\cdot\text{mL}^{-1}$ to $2.5 \text{ g}\cdot\text{mL}^{-1}$ with a step size of $0.5 \text{ g}\cdot\text{mL}^{-1}$. Samples were prepared using cubic silicon molds with a dimension of $6\cdot 6\cdot 12 \text{ mm}^3$. After storage at 37°C and 100 % humidity for 4 h, samples were demolded and placed in PBS. During this step, the setting reaction of the cement and the physical as well as chemical gelation of the biopolymer were performed. Color of the specimens turned from white to blue due to the reaction of amine groups of the gelatin with the natural cross-linker. This effect was obviously not observed for the pure brushite samples. The higher the amount of gelatin, the more intensive the blue color of the composite materials. Samples were transferred in 20 mL PBS and placed in a water bath at 37°C until analysis was performed.

The whole production procedure is illustrated in **Scheme 8**.



Scheme 8:

Production procedure of composite materials containing brushite cement and gelatin hydrogels. Different formulations were varied regarding PLRs and gelatin concentrations (2.5 w/v%, 5.0 w/v% and 10.0 w/v%).

8.5 Mechanical characterization of inorganic references and dual set composites

8.5.1 Compressive strength testing

Samples were characterized regarding compressive strength with the static mechanical testing machine Z010 (Zwick Roell, Ulm, Germany). Therefore, a load cell with a maximum force of 10 kN and a cross head speed of $1 \text{ mm} \cdot \text{min}^{-1}$ was used.

8.5.2 Evaluation of compressive strength upon degradation of PEG-brushite composite materials

For mechanical characterization upon degradation, the compressive strength of the composites was investigated at three different time points (1 d, 5 d, 8 d). The endpoint for the more brittle samples (brushite reference as well as PEG-DMA_{lmw}) was defined as 70 % force referred to the maximum detected force value. For the more elastic formulations (PEG-DMA_{hmw} and PEG-PLLA-DMA), the endpoint was defined as first optical cracks (burst of the surface) of the sample because they did not reach this percentage of reduction of the maximum force previous to a support collision. Additionally, the pH-value of the degradation solution was measured using a pH-meter (InoLab Level 1 WTW, Weilheim, Germany).

For production of PBS, the chemicals potassium chloride (KCl; Merck, Darmstadt, Germany; 0.2 g per 1000 mL), sodium chloride (NaCl; Sigma Aldrich, Steinheim, Germany; 8.0 g per 1000 mL), disodium hydrogenphosphate (Na₂HPO₄; Merck, Darmstadt, Germany; 1.11 g per 1000 mL) and potassium dihydrogenphosphate (KH₂PO₄; 0.2 g per 1000 mL) were dissolved in a volumetric flask and pH-level (InoLab Level 2 WTW, Weilheim, Germany) was adjusted with 0.1 M sodium hydroxide solution (NaOH; Merck, Darmstadt, Germany) to 7.4.

8.5.3 Evaluation of 3-point bending strength and toughness of PEG-brushite composite materials

The pastes of the dual set composites based on brushite cement and PEG-hydrogels with the highest amount of organic phase (50 wt% hydrogel precursor related to the liquid phase) as well as brushite reference (see **8.4.2.3** and **8.4.2.1**) were transferred into cuboid silicon rubber molds in order to prepare samples for 3-point bending strength testing (3*4*25 mm³) and characterized according to a procedure adapted from DIN EN ISO 7438 with an outer distance of 20 mm for the supports. Samples were tested using an axial bending with a 100 N load cell at a crosshead speed of 1 mm*min⁻¹ and a pre-load (despite the samples containing PEG-PLLA-DMA) of 0.1 N. Therefore, mechanical analysis was performed with the static mechanical testing machine Z010 (Zwick/Roell, Ulm, Germany) after storage of one day in PBS. The flexural strength was calculated according to **Equation 17** which is listed in **Table 10**. Additionally, toughness was determined by integrating the area under the load-displacement curves and dividing the values through the cross-sectional area of the specimen.

Table 10:

Calculated parameters of static and dynamic compressive strength testing with corresponding equations.

Parameter	Equation	Explanation	
Bending strength σ	$\varepsilon = \frac{3 * F_{max} * l}{2 * b * h^2}$	Flexural strength σ / MPa F_{max} = failure load / N l = distance between outer supports / mm b = sample width / mm h = sample height / mm Δh = way of sample deformation / mm	Equation 17

8.5.4 Mechanical characterization *via* 4-point bending testing of HEMA-apatite composite materials

For mechanical characterization of dual set composites containing polyHEMA and/or PEG-PLLA-based hydrogels incorporated in apatite cement, 4-point bending test was performed using the static mechanical testing machine Zwick/Roell Z010 (Zwick/Roell, Ulm, Germany). For testing of 4-point bending strength, a 2.5 kN load cell was used with a crosshead speed of 1 mm*min⁻¹. Samples were prepared in cuboid silicon rubber molds with a dimension of 3*4*45 mm³. Additional parameters were determined and calculated, respectively: toughness as area under load-displacement curves, elasticity as function of deformation according to **Equation 18** and E-modulus as function of 4-point bending test according to **Equation 19**. Here, a is the thickness and b the width of the specimen, respectively. Start and end point of the force for the E-modulus determination are abbreviated as X_l and X_h whereas dc is the difference of corresponding way of deformation. Furthermore, the spans of the set-up are defined as l_a (= 10 mm) and l_b (= 20 mm). The measure dL is the deformation at failure.

$$Elasticity / \% = \frac{4 * a * dL}{l_b^2} \quad \text{Equation 18}$$

$$E - modulus / GPa = \frac{3 * (l_a * (l_b)^2 * (X_h - X_l))}{4 * dc * b * a^3} \quad \text{Equation 19}$$

8.6 Biological testing

Cytocompatibility measurements were performed according to DIN EN ISO 10993-5 and 10993-12. For this analysis, disk-shaped samples were prepared ($n = 4$; $\varnothing = 15$ mm, $h = 2$ mm), washed in demineralized water, PBS and ethanol (VWR Chemicals, Ismaning, Germany) with afterwards sterilization *via* gamma-irradiation with 25 kGy. Gelatin powder was irradiated with UV-light (254 nm; UV lamp VL-4.LC, Vilber Lourmat Deutschland GmbH, Eberhardzell, Germany) prior to use. Additionally, positive control (death cells; Vekaplan KT poly(vinyl chloride) (PVC) disks (König GmbH, Wendelstein, Germany)) and negative control (living cells; growth on PS) were treated in the same way as all other samples. After incubation in medium for 48 hours (the amount of eluate was calculated according to the surface of the disks with $3 \text{ cm}^2 \cdot \text{mL}^{-1}$ for the samples and $1.25 \text{ cm}^2 \cdot \text{mL}^{-1}$ for the positive control), eluate was collected and used in further experiments pure (= 100 %) and diluted (1:1 = 50 % and 1:4 = 25 %).

Human osteoblastic cell line MG-63 (ATCC No. CRL-1427) was cultured in Dulbecco's modified Eagle's medium (Invitrogen Life Technologies, Karlsruhe, Germany) supplemented with 10 % fetal calf serum (Life Technologies, Karlsruhe, Germany), 2 % 4-(2-hydroxyethyl)-1-piperazineethanesulfonic acid (HEPES; Gibco™ HEPES buffer solution, Life Technologies Corporation, Staley Rd., Grand Island, USA) and 1 % penicillin and streptomycin (Invitrogen Life Technologies, Karlsruhe, Germany). Cells were seeded in quadruplicates in 24-well plates (Nunc, Wiesbaden, Germany) with an initial density of $50,000 \text{ cells} \cdot \text{mL}^{-1}$ per well. After adding the eluate to the cell culture for 48 h, MG-63 cell activity and cell number were examined by Water-soluble tetrazolium salt (WST)-test and PicoGreen Assay. For cell activity measurements, WST-1 reagent (dilution 1:10; Roche Diagnostic, Mannheim, Germany) was added to the cells and the supernatant was analyzed after color reaction using a spectrometer (Tecan SpectraFluor Plus, Tecan, Maennedorf, Switzerland) at a wavelength of 450 nm. Pico Green Assay was performed using Quant-iT™ PicoGreen™ dsDNA Assay Kit (Invitrogen by ThermoScientific, Life Technologies Corporation, Eugene, USA). Therefore, cells were lysed using an aqueous 0.5 wt% Thesit-solution (produced out of Thesit® for membrane research, Sigma Aldrich, Steinheim, Germany), frozen and afterwards

thawed when ready to perform quantification. As calibration was done by λ DNA standards using protocol for high range standard curve (1-1,000 ng*mL⁻¹), samples were pipetted in triplicates in a black 96-well plate (Life Technologies Corporation, Grand Island, USA). After addition of the fluorescent dye, fluorescence was measured with the same spectrometer as described above at a wavelength of 485 nm for excitation and 538 nm for emission. Cell activity (WST-1) was normalized to PS as reference whereas quantified amount of double stranded DNA (dsDNA) was specified as total DNA amount in ng*mL⁻¹.

Additionally, live-dead images were taken to analyze growth of MG-63 cells using the fluorescence microscope Axio Imager M1 (Carl Zeiss, Oberkochen, Germany). Living cells were fluorescently colored in green by calcein AM (Life technologies, Karlsruhe, Germany) and dead cells were stained in red by ethidium homodimer-1 (Sigma Aldrich, Steinheim, Germany).

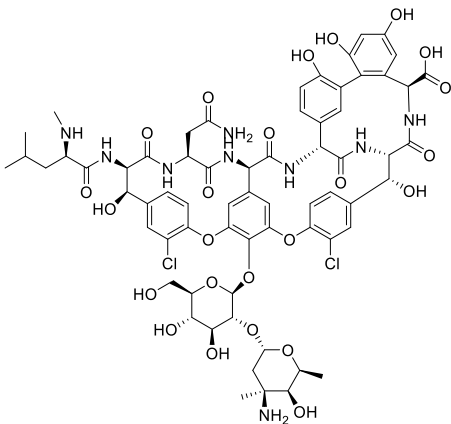
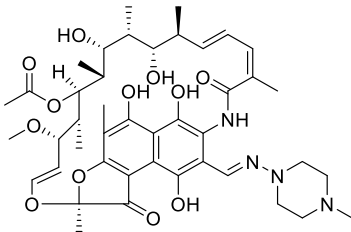
8.7 Drug release study

Drug release of two different antibiotic substances was tested for gelatin-CPC-composites. Vancomycin hydrochloride (Vancomycin CP 500 mg, Hikma Pharma GmbH, Gräfeling, Germany) and rifampicin sodium (Eremfat[®], Riemser Pharma GmbH, Greifswald, Insel Riems, Germany) were dissolved directly in the liquid phase of the inorganic reference as well as the gelatin solutions for the composites ($c = 5 \text{ mg} \cdot \text{mL}^{-1}$). Disk shaped specimens ($n = 3$; $\varnothing = 12 \text{ mm}$, $h = 2 \text{ mm}$) were produced as described in section **8.4.3.2**. After setting and gelation, they were placed in 2 mL PBS in 24-well plates at 37 °C (Incubator IG150, Jouan, Winchester, USA) under shaking conditions. Drug release was determined at different time points (1 h, 2 h, 4 h, 8 h, 1 d, 2 d, 3 d, 6 d, 8 d, 9 d, 10 d, 13 d, 20 d and 27 d) by taking an aliquot of 1 mL out of the solution and replacing it with the same amount of fresh PBS. At day 44, samples were ground and destroyed to liberate last remaining amounts of incorporated drug (set to 100 %, maximum release). Quantification of both antibiotics was performed *via* HPLC analysis (Shimadzu Deutschland GmbH, Duisburg, Germany; see **8.2.1.3**). The chosen method for determination of released vancomycin was adapted from De Jesús Valle *et al.* [304]. HPLC method of rifampicin was fit to an established protocol of Panchagnula *et al.* [305]. Calibration curves for the two drugs were measured in a concentration range of 5-1,000 $\mu\text{g} \cdot \text{mL}^{-1}$.

Table 11 gives an overview of the detailed analytical parameters for each method.

Table 11:

Overview of the adapted HPLC methods used for the quantification of vancomycin [304] and rifampicin [305] and the corresponding instrument parameters. Both measuring options were performed under isocratic conditions with a flow rate of $1 \text{ mL} \cdot \text{min}^{-1}$ and a C18-column for separation. Detection was carried out using a photodiode array detector.

	Vancomycin	Rifampicin
HPLC device	HPLC Shimadzu (LC-20AT) with autosampler (SIL-20AC)	
Column	Luna $5 \mu\text{m}$ C18(2) 100 \AA , LC Column $150 \times 4.6 \text{ mm}$	
Flow rate	$1 \text{ mL} \cdot \text{min}^{-1}$	
Oven temperature	$40 \text{ }^\circ\text{C}$	
Injection volume	$10 \mu\text{L}$	
Detector	Photodiode Array Detector (SPD-M20A)	
Detection wavelength	220 nm	254 nm
Mobile phase	<p>0.05 M Ammonium-dihydrogen phosphate ($\text{NH}_4\text{H}_2\text{PO}_4$) : ACN; $98:2 \text{ v/v}$</p> <p>$\text{pH} = 4.0$, adjusted with $2 \text{ M H}_3\text{PO}_4$</p>	<p>0.01 M Sodium phosphate tribasic dodecahydrate ($\text{Na}_3\text{PO}_4 \cdot 12 \text{ H}_2\text{O}$) : methanol; $65:35 \text{ v/v}$</p> <p>$\text{pH} = 5.2$, adjusted with $2 \text{ M H}_3\text{PO}_4$</p>
Chemical structure		
Molecular weight	$M_w = 1,449.265 \text{ g} \cdot \text{mol}^{-1}$	$M_w = 822.953 \text{ g} \cdot \text{mol}^{-1}$

8.8 Statistical analysis

Statistical evaluation of data was performed by two-way analysis of variance (ANOVA) with the statistical software package SigmaPlot 12.5 (Systat Software, Erkrath, Germany). To prove statistical significant differences of the individual groups, a post hoc Tukey test was used as a pairwise multiple comparison procedure. Significant differences between the represented groups are assigned with * ($p < 0.05$) and ** ($p < 0.001$).

References

1. Weiner, S. and H.D. Wagner, *The material bone: structure-mechanical function relations*. Annual Review of Materials Science, 1998. **28**(1): p. 271-298.
2. Rho, J.-Y., L. Kuhn-Spearing, and P. Zioupos, *Mechanical properties and the hierarchical structure of bone*. Medical engineering & physics, 1998. **20**(2): p. 92-102.
3. Athanasiou, K., et al., *Fundamentals of biomechanics in tissue engineering of bone*. Tissue engineering, 2000. **6**(4): p. 361-381.
4. Eliaz, N. and N. Metoki, *Calcium Phosphate Bioceramics: A Review of Their History, Structure, Properties, Coating Technologies and Biomedical Applications*. Materials, 2017. **10**(4): p. 334.
5. Gibson, L.J., *The mechanical behaviour of cancellous bone*. Journal of biomechanics, 1985. **18**(5): p. 317-328.
6. McKibbin, B., *The biology of fracture healing in long bones*. The Journal of bone and joint surgery. British volume, 1978. **60**(2): p. 150-162.
7. Currey, J.D., *Bones: structure and mechanics*. 2013: Princeton university press.
8. Hing, K.A., *Bone repair in the twenty-first century: biology, chemistry or engineering?* Philosophical Transactions of the Royal Society of London A: Mathematical, Physical and Engineering Sciences, 2004. **362**(1825): p. 2821-2850.
9. Fung, Y.-c., *Biomechanics: mechanical properties of living tissues*. 2013: Springer Science & Business Media.
10. Wang, M., *Developing bioactive composite materials for tissue replacement*. Biomaterials, 2003. **24**(13): p. 2133-2151.
11. Sheikh, Z., C. Sima, and M. Glogauer, *Bone replacement materials and techniques used for achieving vertical alveolar bone augmentation*. Materials, 2015. **8**(6): p. 2953-2993.
12. Kannan, S., et al., *Metallic implants-An approach for long term applications in bone related defects*. Corrosion reviews, 2002. **20**(4-5): p. 339-358.
13. Heide, H., E. Poeschel, and U. Roth, *Implantable bone replacement materials based on calcium phosphate ceramic material in a matrix and process for the production thereof*. 1982, Google Patents.
14. Nair, L.S. and C.T. Laurencin, *Biodegradable polymers as biomaterials*. Progress in polymer science, 2007. **32**(8-9): p. 762-798.
15. Rezwan, K., et al., *Biodegradable and bioactive porous polymer/inorganic composite scaffolds for bone tissue engineering*. Biomaterials, 2006. **27**(18): p. 3413-3431.
16. Woesz, A., et al., *Towards bone replacement materials from calcium phosphates via rapid prototyping and ceramic gelcasting*. Materials Science and Engineering: C, 2005. **25**(2): p. 181-186.
17. Kenny, S. and M. Buggy, *Bone cements and fillers: a review*. Journal of Materials Science: Materials in Medicine, 2003. **14**(11): p. 923-938.
18. Gkioni, K., et al., *Mineralization of hydrogels for bone regeneration*. Tissue Engineering Part B: Reviews, 2010. **16**(6): p. 577-585.
19. Rödel, M., et al., *7 - Bioceramics as drug delivery systems A2 - Thomas, Sabu*, in *Fundamental Biomaterials: Ceramics*, P. Balakrishnan and M.S. Sreekala, Editors. 2018, Woodhead Publishing. p. 153-194.

References

20. Wang, L. and G.H. Nancollas, *Calcium orthophosphates: crystallization and dissolution*. Chemical reviews, 2008. **108**(11): p. 4628-4669.
21. Kucko, N.W., et al., *Calcium Phosphate Bioceramics and Cements*, in *Principles of Regenerative Medicine*. 2019, Elsevier. p. 591-611.
22. Dorozhkin, S.V., *Calcium orthophosphates: applications in nature, biology, and medicine*. 2012: Pan Stanford.
23. Bohner, M., *Calcium orthophosphates in medicine: from ceramics to calcium phosphate cements*. Injury, 2000. **31**: p. D37-D47.
24. Bohner, M., *Physical and chemical aspects of calcium phosphates used in spinal surgery*. European Spine Journal, 2001. **10**(2): p. S114-S121.
25. Champion, E., *Sintering of calcium phosphate bioceramics*. Acta biomaterialia, 2013. **9**(4): p. 5855-5875.
26. Boanini, E., M. Gazzano, and A. Bigi, *Ionic substitutions in calcium phosphates synthesized at low temperature*. Acta biomaterialia, 2010. **6**(6): p. 1882-1894.
27. Epple, M., *Review of potential health risks associated with nanoscopic calcium phosphate*. Acta biomaterialia, 2018.
28. Chow, L.C., *Next generation calcium phosphate-based biomaterials*. Dental materials journal, 2009. **28**(1): p. 1-10.
29. Chow, L.C., *Calcium phosphate cements: chemistry, properties, and applications*. MRS Online Proceedings Library Archive, 1999. **599**.
30. Chow, L.C., *Development of self-setting calcium phosphate cements*. Journal of the Ceramic society of Japan, 1991. **99**(1154): p. 954-964.
31. Lu, J., et al., *The biodegradation mechanism of calcium phosphate biomaterials in bone*. Journal of Biomedical Materials Research: An Official Journal of The Society for Biomaterials, The Japanese Society for Biomaterials, and The Australian Society for Biomaterials and the Korean Society for Biomaterials, 2002. **63**(4): p. 408-412.
32. Liu, C. and H. He, *Developments and Applications of Calcium Phosphate Bone Cements*. 2018: Springer.
33. Brown, W.E. and L.C. Chow, *Dental resporative cement pastes*. 1985, Google Patents.
34. Fernández, E., et al., *Calcium phosphate bone cements for clinical applications. Part I: solution chemistry*. Journal of materials science: materials in medicine, 1999. **10**(3): p. 169-176.
35. Schnettler, R., et al., *Calcium phosphate-based bone substitutes*. European Journal of Trauma, 2004. **30**(4): p. 219-229.
36. Spies, C.K., et al., *Efficacy of Bone Source™ and Cementek™ in comparison with Endobon™ in critical size metaphyseal defects, using a minipig model*. Journal of Applied Biomaterials and Biomechanics, 2010. **8**(3): p. 175-185.
37. Zhang, J., et al., *Magnesium modification of a calcium phosphate cement alters bone marrow stromal cell behavior via an integrin-mediated mechanism*. Biomaterials, 2015. **53**: p. 251-264.
38. Thormann, U., et al., *Bone formation induced by strontium modified calcium phosphate cement in critical-size metaphyseal fracture defects in ovariectomized rats*. Biomaterials, 2013. **34**(34): p. 8589-8598.
39. Ewald, A., et al., *The effect of Cu (II)-loaded brushite scaffolds on growth and activity of osteoblastic cells*. Journal of Biomedical Materials Research Part A, 2012. **100**(9): p. 2392-2400.

40. Manchón, A., et al., *A new iron calcium phosphate material to improve the osteoconductive properties of a biodegradable ceramic: a study in rabbit calvaria*. *Biomedical Materials*, 2015. **10**(5): p. 055012.
41. Bohner, M., U. Gbureck, and J. Barralet, *Technological issues for the development of more efficient calcium phosphate bone cements: a critical assessment*. *Biomaterials*, 2005. **26**(33): p. 6423-6429.
42. Chow, L., *Calcium phosphate cements*, in *Octacalcium phosphate*. 2001, Karger Publishers. p. 148-163.
43. Tamimi, F., Z. Sheikh, and J. Barralet, *Dicalcium phosphate cements: Brushite and monetite*. *Acta biomaterialia*, 2012. **8**(2): p. 474-487.
44. Ginebra, M., et al., *Setting reaction and hardening of an apatitic calcium phosphate cement*. *Journal of dental research*, 1997. **76**(4): p. 905-912.
45. Ginebra, M.-P., et al., *Bioceramics and bone healing*. *EFORT Open Reviews*, 2018. **3**(5): p. 173-183.
46. O'Neill, R., et al., *Critical review: Injectability of calcium phosphate pastes and cements*. *Acta biomaterialia*, 2017. **50**: p. 1-19.
47. Lewis, G., *Injectable bone cements for use in vertebroplasty and kyphoplasty: State-of-the-art review*. *Journal of Biomedical Materials Research Part B: Applied Biomaterials: An Official Journal of The Society for Biomaterials, The Japanese Society for Biomaterials, and The Australian Society for Biomaterials and the Korean Society for Biomaterials*, 2006. **76**(2): p. 456-468.
48. Ramesh, N., S.C. Moratti, and G.J. Dias, *Hydroxyapatite–polymer biocomposites for bone regeneration: A review of current trends*. *Journal of Biomedical Materials Research Part B: Applied Biomaterials*, 2018. **106**(5): p. 2046-2057.
49. Ginebra, M.-P., T. Traykova, and J. Planell, *Calcium phosphate cements as bone drug delivery systems: a review*. *Journal of Controlled Release*, 2006. **113**(2): p. 102-110.
50. Takagi, S., L. Chow, and K. Ishikawa, *Formation of hydroxyapatite in new calcium phosphate cements*. *Biomaterials*, 1998. **19**(17): p. 1593-1599.
51. Ginebra, M.-P., et al., *Calcium phosphate cements as drug delivery materials*. *Advanced drug delivery reviews*, 2012. **64**(12): p. 1090-1110.
52. Tampieri, A., et al., *From wood to bone: multi-step process to convert wood hierarchical structures into biomimetic hydroxyapatite scaffolds for bone tissue engineering*. *Journal of Materials Chemistry*, 2009. **19**(28): p. 4973-4980.
53. Barralet, J., et al., *Cements from nanocrystalline hydroxyapatite*. *Journal of Materials Science: Materials in Medicine*, 2004. **15**(4): p. 407-411.
54. Liu, C., et al., *Mechanism of the hardening process for a hydroxyapatite cement*. *Journal of Biomedical Materials Research: An Official Journal of The Society for Biomaterials and The Japanese Society for Biomaterials*, 1997. **35**(1): p. 75-80.
55. Driessens, F., et al., *Formulation and setting times of some calcium orthophosphate cements: a pilot study*. *Journal of Materials Science: Materials in Medicine*, 1993. **4**(5): p. 503-508.
56. Owen, G., M. Dard, and H. Larjava, *Hydroxyapatite/beta-tricalcium phosphate biphasic ceramics as regenerative material for the repair of complex bone defects*. *Journal of Biomedical Materials Research Part B: Applied Biomaterials*, 2018. **106**(6): p. 2493-2512.

References

57. LeGeros, R.Z., *Calcium phosphate-based osteoinductive materials*. Chemical reviews, 2008. **108**(11): p. 4742-4753.
58. Munting, E., A. Mirtchi, and J. Lemaitre, *Bone repair of defects filled with a phosphocalcic hydraulic cement: an in vivo study*. Journal of Materials Science: Materials in Medicine, 1993. **4**(3): p. 337-344.
59. Apelt, D., et al., *In vivo behavior of three different injectable hydraulic calcium phosphate cements*. Biomaterials, 2004. **25**(7): p. 1439-1451.
60. Bohner, M. and U. Gbureck, *Thermal reactions of brushite cements*. Journal of Biomedical Materials Research Part B: Applied Biomaterials: An Official Journal of The Society for Biomaterials, The Japanese Society for Biomaterials, and The Australian Society for Biomaterials and the Korean Society for Biomaterials, 2008. **84**(2): p. 375-385.
61. Bohner, M., et al., *Effect of several additives and their admixtures on the physico-chemical properties of a calcium phosphate cement*. Journal of Materials Science: Materials in Medicine, 2000. **11**(2): p. 111-116.
62. Ginebra, M.P., et al., *Calcium phosphate cements as drug delivery materials*. Advanced Drug Delivery Reviews, 2012. **64**(12): p. 1090-1110.
63. Manzano, M., *Ceramics for Drug Delivery*. Bio-Ceramics with Clinical Applications, 2014: p. 343-382.
64. Reszka, A.A. and G.A. Rodan, *Bisphosphonate mechanism of action*. Current rheumatology reports, 2003. **5**(1): p. 65-74.
65. Scriba, G.K., *Bisphosphonate im Überblick*. Pharmazie in unserer Zeit, 2000. **29**(1): p. 50-56.
66. Åkesson, K., *New approaches to pharmacological treatment of osteoporosis*. Bulletin of the World Health Organization, 2003. **81**(9): p. 657-663.
67. Fazil, M., et al., *Bisphosphonates: therapeutics potential and recent advances in drug delivery*. Drug delivery, 2015. **22**(1): p. 1-9.
68. Panzavolta, S., et al., *Alendronate and Pamidronate calcium phosphate bone cements: setting properties and in vitro response of osteoblast and osteoclast cells*. Journal of inorganic biochemistry, 2009. **103**(1): p. 101-106.
69. Abrahamsen, B., *Adverse effects of bisphosphonates*. Calcified tissue international, 2010. **86**(6): p. 421-435.
70. Murphy, C.M., et al., *A collagen–hydroxyapatite scaffold allows for binding and co-delivery of recombinant bone morphogenetic proteins and bisphosphonates*. Acta biomaterialia, 2014. **10**(5): p. 2250-2258.
71. Verron, E., et al., *In vivo bone augmentation in an osteoporotic environment using bisphosphonate-loaded calcium deficient apatite*. Biomaterials, 2010. **31**(30): p. 7776-7784.
72. Gong, T., et al., *Osteogenic and anti-osteoporotic effects of risedronate-added calcium phosphate silicate cement*. Biomedical Materials, 2016. **11**(4): p. 045002.
73. Mosbahi, S., et al., *Risedronate adsorption on bioactive glass surface for applications as bone biomaterial*. Applied Surface Science, 2016. **367**: p. 205-213.
74. Boanini, E., et al., *Alendronate Functionalized Mesoporous Bioactive Glass Nanospheres*. Materials, 2016. **9**(3): p. 135.

75. Jones, D.A., et al., *Molecular cloning of human prostaglandin endoperoxide synthase type II and demonstration of expression in response to cytokines*. Journal of Biological Chemistry, 1993. **268**(12): p. 9049-9054.
76. Willoughby, D.A., A.R. Moore, and P.R. Colville-Nash, *COX-1, COX-2, and COX-3 and the future treatment of chronic inflammatory disease*. The Lancet, 2000. **355**(9204): p. 646-648.
77. Rome, L.H. and W. Lands, *Structural requirements for time-dependent inhibition of prostaglandin biosynthesis by anti-inflammatory drugs*. Proceedings of the National Academy of Sciences, 1975. **72**(12): p. 4863-4865.
78. Cashman, J.N., *The mechanisms of action of NSAIDs in analgesia*. Drugs, 1996. **52**(5): p. 13-23.
79. Patrignani, P., P. Filabozzi, and C. Patrono, *Selective cumulative inhibition of platelet thromboxane production by low-dose aspirin in healthy subjects*. Journal of Clinical Investigation, 1982. **69**(6): p. 1366.
80. Moja, L. 2017; Available from: https://en.wikipedia.org/wiki/WHO_Model_List_of_Essential_Medicines#/media/File:V1_40_years_Model_List_of_Essential_Medicines.001.png.
81. Ginebra, M., et al., *Mechanical and rheological improvement of a calcium phosphate cement by the addition of a polymeric drug*. Journal of Biomedical Materials Research Part A, 2001. **57**(1): p. 113-118.
82. Otsuka, M., et al., *A novel skeletal drug-delivery system using self-setting calcium phosphate cement. 4. Effects of the mixing solution volume on the drug-release rate of heterogeneous aspirin-loaded cement*. Journal of pharmaceutical sciences, 1994. **83**(2): p. 259-263.
83. Chevalier, E., et al., *Ibuprofen-loaded calcium phosphate granules: Combination of innovative characterization methods to relate mechanical strength to drug location*. Acta biomaterialia, 2010. **6**(1): p. 266-274.
84. Alexopoulou, M., et al., *Preparation, characterization and in vitro assessment of ibuprofen loaded calcium phosphate/gypsum bone cements*. Crystal Research and Technology, 2016. **51**(1): p. 41-48.
85. de Guevara-Fernández, S.L., C. Ragel, and M. Vallet-Regí, *Bioactive glass-polymer materials for controlled release of ibuprofen*. Biomaterials, 2003. **24**(22): p. 4037-4043.
86. Neut, D., et al., *Biomaterial-associated infection of gentamicin-loaded PMMA beads in orthopaedic revision surgery*. Journal of Antimicrobial Chemotherapy, 2001. **47**(6): p. 885-891.
87. Shinsako, K., et al., *Effects of bead size and polymerization in PMMA bone cement on vancomycin release*. Bio-medical materials and engineering, 2008. **18**(6): p. 377-385.
88. Schnieders, J., et al., *Controlled release of gentamicin from calcium phosphate—poly (lactic acid-co-glycolic acid) composite bone cement*. Biomaterials, 2006. **27**(23): p. 4239-4249.
89. Sunderkötter, C. and K. Becker, *Systemtherapie mit Antiinfektiva*. Der Hautarzt, 2014. **65**(2): p. 113-124.
90. Saleh, A.T., L.S. Ling, and R. Hussain, *Injectable magnesium-doped brushite cement for controlled drug release application*. Journal of Materials Science, 2016. **51**(16): p. 7427-7439.

References

91. Nairi, V., et al., *Adsorption and release of ampicillin antibiotic from ordered mesoporous silica*. Journal of Colloid and Interface Science, 2017. **497**: p. 217-225.
92. Schnieders, J., et al., *The effect of porosity on drug release kinetics from vancomycin microsphere/calcium phosphate cement composites*. Journal of Biomedical Materials Research Part B: Applied Biomaterials, 2011. **99**(2): p. 391-398.
93. Minelli, E.B., T. Della Bora, and A. Benini, *Different microbial biofilm formation on polymethylmethacrylate (PMMA) bone cement loaded with gentamicin and vancomycin*. Anaerobe, 2011. **17**(6): p. 380-383.
94. Garg, S., et al., *Antibacterial and anticancerous drug loading kinetics for (10-x) CuO-xZnO-20CaO-60SiO₂-10P₂O₅ (2 ≤ x ≤ 8) mesoporous bioactive glasses*. Journal of Materials Science: Materials in Medicine, 2017. **28**(1): p. 11.
95. Li, W., et al., *Preparation and characterization of PHBV microsphere/45S5 bioactive glass composite scaffolds with vancomycin releasing function*. Materials Science and Engineering: C, 2014. **41**: p. 320-328.
96. Frew, N., et al., *Comparison of the elution properties of commercially available gentamicin and bone cement containing vancomycin with 'home-made' preparations*. Bone Joint J, 2017. **99**(1): p. 73-77.
97. Nagarajan, R., *Glycopeptide antibiotics*. Vol. 63. 1994: CRC Press.
98. Alenezi, A., et al., *Controlled release of clarithromycin from PLGA microspheres enhances bone regeneration in rabbit calvaria defects*. Journal of Biomedical Materials Research Part B: Applied Biomaterials, 2017.
99. Trajano, V., et al., *Osteogenic activity of cyclodextrin-encapsulated doxycycline in a calcium phosphate PCL and PLGA composite*. Materials Science and Engineering: C, 2016. **64**: p. 370-375.
100. Canal, C., et al., *Regulating the antibiotic drug release from β-tricalcium phosphate ceramics by atmospheric plasma surface engineering*. Biomaterials Science, 2016. **4**(10): p. 1454-1461.
101. Gaynor, M. and A.S. Mankin, *Macrolide antibiotics: binding site, mechanism of action, resistance*. Current topics in medicinal chemistry, 2003. **3**(9): p. 949-960.
102. Meseguer-Olmo, L., et al., *A bioactive sol-gel glass implant for in vivo gentamicin release. Experimental model in Rabbit*. Journal of orthopaedic research, 2006. **24**(3): p. 454-460.
103. Marques, C.F., et al., *Insights on the properties of levofloxacin-adsorbed Sr- and Mg-doped calcium phosphate powders*. Journal of Materials Science: Materials in Medicine, 2016. **27**(7): p. 1-12.
104. Boulila, S., et al., *Antioxidative/oxidative effects and retarding osteoconductivity of ciprofloxacin-loaded porous polyvinyl alcohol/bioactive glass hybrid*. Medical & biological engineering & computing, 2017. **55**(1): p. 17-32.
105. Jana, S. and J. Deb, *Molecular understanding of aminoglycoside action and resistance*. Applied microbiology and biotechnology, 2006. **70**(2): p. 140-150.
106. Aldred, K.J., R.J. Kerns, and N. Osheroff, *Mechanism of quinolone action and resistance*. Biochemistry, 2014. **53**(10): p. 1565-1574.

107. Longley, D.B., D.P. Harkin, and P.G. Johnston, *5-fluorouracil: mechanisms of action and clinical strategies*. Nature Reviews Cancer, 2003. **3**(5): p. 330-338.
108. Chu, W., et al., *Calcium phosphate nanoparticles functionalized with alendronate-conjugated polyethylene glycol (PEG) for the treatment of bone metastasis*. International Journal of Pharmaceutics, 2017. **516**(1): p. 352-363.
109. Dasari, S. and P.B. Tchounwou, *Cisplatin in cancer therapy: molecular mechanisms of action*. European journal of pharmacology, 2014. **740**: p. 364-378.
110. Siddik, Z.H., *Cisplatin: mode of cytotoxic action and molecular basis of resistance*. Oncogene, 2003. **22**(47): p. 7265-7279.
111. Hess, U., et al., *Co-delivery of cisplatin and doxorubicin from calcium phosphate beads/matrix scaffolds for osteosarcoma therapy*. Materials Science and Engineering: C, 2017.
112. Farbod, K., et al., *Controlled Release of Chemotherapeutic Platinum-Bisphosphonate Complexes from Injectable Calcium Phosphate Cements*. Tissue Engineering Part A, 2016. **22**(9-10): p. 788-800.
113. Yancopoulos, G.D., et al., *Vascular-specific growth factors and blood vessel formation*. Nature, 2000. **407**(6801): p. 242-248.
114. Soker, S., M. Machado, and A. Atala, *Systems for therapeutic angiogenesis in tissue engineering*. World journal of urology, 2000. **18**(1): p. 10-18.
115. Schumacher, M., et al., *Calcium phosphate bone cement/mesoporous bioactive glass composites for controlled growth factor delivery*. Biomaterials Science, 2017. **5**(3): p. 578-588.
116. Akkineni, A.R., et al., *3D plotting of growth factor loaded calcium phosphate cement scaffolds*. Acta biomaterialia, 2015. **27**: p. 264-274.
117. Ahlfeld, T., et al., *Design and fabrication of complex scaffolds for bone defect healing: combined 3D plotting of a calcium phosphate cement and a growth factor-loaded hydrogel*. Annals of Biomedical Engineering, 2017. **45**(1): p. 224-236.
118. Ruhe, P.Q., et al., *In vivo release of rhBMP-2 loaded porous calcium phosphate cement pretreated with albumin*. Journal of Materials Science: Materials in Medicine, 2006. **17**(10): p. 919-927.
119. Ruhe, P.Q., et al., *Bone inductive properties of rhBMP-2 loaded porous calcium phosphate cement implants in cranial defects in rabbits*. Biomaterials, 2004. **25**(11): p. 2123-2132.
120. Ruhe, P.Q., et al., *Controlled release of rhBMP-2 loaded poly (dl-lactic-co-glycolic acid)/calcium phosphate cement composites in vivo*. Journal of Controlled Release, 2005. **106**(1): p. 162-171.
121. van de Watering, F.C., et al., *Differential loading methods for BMP-2 within injectable calcium phosphate cement*. Journal of controlled release, 2012. **164**(3): p. 283-290.
122. Buenger, D., F. Topuz, and J. Groll, *Hydrogels in sensing applications*. Progress in Polymer Science, 2012. **37**(12): p. 1678-1719.
123. Gibas, I. and H. Janik, *Synthetic polymer hydrogels for biomedical applications*. 2010.
124. Hoffman, A.S., *Hydrogels for biomedical applications*. Advanced drug delivery reviews, 2012. **64**: p. 18-23.

References

125. Xinming, L., et al., *Polymeric hydrogels for novel contact lens-based ophthalmic drug delivery systems: A review*. *Contact Lens and Anterior Eye*, 2008. **31**(2): p. 57-64.
126. Jungst, T., et al., *Strategies and molecular design criteria for 3D printable hydrogels*. *Chemical reviews*, 2015. **116**(3): p. 1496-1539.
127. Peppas, N., et al., *Hydrogels in pharmaceutical formulations*. *European journal of pharmaceutics and biopharmaceutics*, 2000. **50**(1): p. 27-46.
128. Ullah, F., et al., *Classification, processing and application of hydrogels: A review*. *Materials Science and Engineering: C*, 2015. **57**: p. 414-433.
129. Wichterle, O. and D. Lim, *Hydrophilic gels for biological use*. *Nature*, 1960. **185**(4706): p. 117.
130. Van Vlierberghe, S., P. Dubruel, and E. Schacht, *Biopolymer-based hydrogels as scaffolds for tissue engineering applications: a review*. *Biomacromolecules*, 2011. **12**(5): p. 1387-1408.
131. Groll, J., et al., *A definition of bioinks and their distinction from biomaterial inks*. *Biofabrication*, 2018.
132. Dubbin, K., et al., *Dual-Stage Crosslinking of a Gel-Phase Bioink Improves Cell Viability and Homogeneity for 3D Bioprinting*. *Advanced healthcare materials*, 2016. **5**(19): p. 2488-2492.
133. Bigi, A., et al., *Mechanical and thermal properties of gelatin films at different degrees of glutaraldehyde crosslinking*. *Biomaterials*, 2001. **22**(8): p. 763-768.
134. Buwalda, S.J., et al., *Hydrogels in a historical perspective: From simple networks to smart materials*. *Journal of controlled release*, 2014. **190**: p. 254-273.
135. Teßmar, J., F. Brandl, and A. Göpferich, *Hydrogels for tissue engineering*, in *Fundamentals of tissue engineering and regenerative medicine*. 2009, Springer. p. 495-517.
136. Gong, J.P., *Why are double network hydrogels so tough?* *Soft Matter*, 2010. **6**(12): p. 2583-2590.
137. Chen, Q., et al., *Fundamentals of double network hydrogels*. *Journal of Materials Chemistry B*, 2015. **3**(18): p. 3654-3676.
138. Gong, J.P., et al., *Double-network hydrogels with extremely high mechanical strength*. *Advanced materials*, 2003. **15**(14): p. 1155-1158.
139. Fratzl, P., *Collagen: structure and mechanics, an introduction*, in *Collagen*. 2008, Springer. p. 1-13.
140. GMIA-Members, *Gelatin Handbook*. 2012. p. 26.
141. Babel, W., *Gelatine—ein vielseitiges Biopolymer*. *Chemie in unserer Zeit*, 1996. **30**(2): p. 86-95.
142. Michon, C., et al., *Influence of thermal history on the stability of gelatin gels*. *International journal of biological macromolecules*, 1997. **20**(4): p. 259-264.
143. Rault, I., et al., *Evaluation of different chemical methods for cross-linking collagen gel, films and sponges*. *Journal of Materials Science: Materials in Medicine*, 1996. **7**(4): p. 215-221.
144. Tsai, C.C., et al., *In vitro evaluation of the genotoxicity of a naturally occurring crosslinking agent (genipin) for biologic tissue fixation*. *Journal of biomedical materials research*, 2000. **52**(1): p. 58-65.
145. Bertlein, S., et al., *Thio-Ene Clickable Gelatin: A Platform Bioink for Multiple 3D Biofabrication Technologies*. *Advanced Materials*, 2017.

146. Jaipan, P., A. Nguyen, and R.J. Narayan, *Gelatin-based hydrogels for biomedical applications*. MRS Communications, 2017. **7**(3): p. 416-426.
147. Tessmar, J.K. and A.M. Göpferich, *Customized PEG-derived copolymers for tissue-engineering applications*. Macromolecular Bioscience, 2007. **7**(1): p. 23-39.
148. Luxenhofer, R., et al., *Poly (2-oxazoline)s as Polymer Therapeutics*. Macromolecular rapid communications, 2012. **33**(19): p. 1613-1631.
149. Cohen, Y., et al., *Characterization of inhomogeneous polyacrylamide hydrogels*. Journal of Polymer Science Part B: Polymer Physics, 1992. **30**(9): p. 1055-1067.
150. Schmedlen, R.H., K.S. Masters, and J.L. West, *Photocrosslinkable polyvinyl alcohol hydrogels that can be modified with cell adhesion peptides for use in tissue engineering*. Biomaterials, 2002. **23**(22): p. 4325-4332.
151. Drury, J.L. and D.J. Mooney, *Hydrogels for tissue engineering: scaffold design variables and applications*. Biomaterials, 2003. **24**(24): p. 4337-4351.
152. Knop, K., et al., *Poly (ethylene glycol) in drug delivery: pros and cons as well as potential alternatives*. Angewandte chemie international edition, 2010. **49**(36): p. 6288-6308.
153. Goddard, J.M. and J. Hotchkiss, *Polymer surface modification for the attachment of bioactive compounds*. Progress in polymer science, 2007. **32**(7): p. 698-725.
154. Zhu, J., *Bioactive modification of poly (ethylene glycol) hydrogels for tissue engineering*. Biomaterials, 2010. **31**(17): p. 4639-4656.
155. Markovsky, E., et al., *Administration, distribution, metabolism and elimination of polymer therapeutics*. Journal of Controlled Release, 2012. **161**(2): p. 446-460.
156. Kim, Y.-H., *Der mikrobielle Abbau von Etherverbindungen unter besonderer Berücksichtigung von Aralkyl- und Alkylethern*. 1999.
157. Metters, A.T., C.N. Bowman, and K.S. Anseth, *A statistical kinetic model for the bulk degradation of PLA-b-PEG-b-PLA hydrogel networks*. The Journal of Physical Chemistry B, 2000. **104**(30): p. 7043-7049.
158. Nguyen, K.T. and J.L. West, *Photopolymerizable hydrogels for tissue engineering applications*. Biomaterials, 2002. **23**(22): p. 4307-4314.
159. Okay, O., *General properties of hydrogels*, in *Hydrogel sensors and actuators*. 2009, Springer. p. 1-14.
160. Koltzenburg, S., et al., *Polymere: Synthese, Eigenschaften und Anwendungen*. 2014: Springer.
161. Stille, J.K., *Step-growth polymerization*. 1981, ACS Publications.
162. Szwarc, M. and M. Van Beylen, *Ionic polymerization and living polymers*. 2012: Springer Science & Business Media.
163. Lu, L., et al., *The Formation Mechanism of Hydrogels*. Current stem cell research & therapy, 2017.
164. Matyjaszewski, K., et al., *Preparation of hyperbranched polyacrylates by atom transfer radical polymerization. 1. Acrylic AB* monomers in "living" radical polymerizations*. Macromolecules, 1997. **30**(17): p. 5192-5194.
165. Weis, M., et al., *Evaluation of Hydrogels Based on Oxidized Hyaluronic Acid for Bioprinting*. Gels, 2018. **4**(4): p. 82.
166. Stichler, S., et al., *Thiol-ene clickable poly (glycidol) hydrogels for biofabrication*. Annals of biomedical engineering, 2017. **45**(1): p. 273-285.

References

167. Brandl, F., et al., *Hydrogel-based drug delivery systems: comparison of drug diffusivity and release kinetics*. Journal of Controlled Release, 2010. **142**(2): p. 221-228.
168. Uhrich, K.E., et al., *Polymeric systems for controlled drug release*. Chemical reviews, 1999. **99**(11): p. 3181-3198.
169. Dhanasingh, A., *sP (EO-stat-PO)-glycosaminoglycans (GAGs) hybrid-hydrogels for medical applications*. 2011, Aachen, Techn. Hochsch., Diss., 2011.
170. Bauer, K.H., K.-H. Frömmling, and C. Führer, *Pharmazeutische Technologie*. Vol. 9. 2012: Wissenschaftliche Verlagsgesellschaft Stuttgart. 820.
171. Gupta, P., K. Vermani, and S. Garg, *Hydrogels: from controlled release to pH-responsive drug delivery*. Drug discovery today, 2002. **7**(10): p. 569-579.
172. Qiu, Y. and K. Park, *Environment-sensitive hydrogels for drug delivery*. Advanced drug delivery reviews, 2001. **53**(3): p. 321-339.
173. Drotleff, S., et al., *Biomimetic polymers in pharmaceutical and biomedical sciences*. European Journal of Pharmaceutics and Biopharmaceutics, 2004. **58**(2): p. 385-407.
174. Han, D.K. and J.A. Hubbell, *Lactide-based poly (ethylene glycol) polymer networks for scaffolds in tissue engineering*. Macromolecules, 1996. **29**(15): p. 5233-5235.
175. Dos Santos, L., et al., *Influence of polymeric additives on the mechanical properties of α -tricalcium phosphate cement*. Bone, 1999. **25**(2): p. 99S-102S.
176. Geffers, M., J. Groll, and U. Gbureck, *Reinforcement Strategies for Load-Bearing Calcium Phosphate Biocements*. Materials, 2015. **8**(5): p. 2700-2717.
177. Neumann, M. and M. Epple, *Composites of calcium phosphate and polymers as bone substitution materials*. European Journal of Trauma, 2006. **32**(2): p. 125-131.
178. Dos Santos, L.A., et al., *Dual-Setting Calcium Phosphate Cement Modified with Ammonium Polyacrylate*. Artificial organs, 2003. **27**(5): p. 412-418.
179. Christel, T., et al., *Dual setting α -tricalcium phosphate cements*. Journal of Materials Science: Materials in Medicine, 2013. **24**(3): p. 573-581.
180. Schamel, M., J. Groll, and U. Gbureck, *Simultaneous formation and mineralization of star-P (EO-stat-PO) hydrogels*. Materials Science and Engineering: C, 2017. **75**: p. 471-477.
181. Schamel, M., et al., *Intrinsic 3D Prestressing: A New Route for Increasing Strength and Improving Toughness of Hybrid Inorganic Biocements*. Advanced Materials, 2017. **29**(35).
182. Gorgieva, S. and V. Kokol, *Collagen-vs. gelatine-based biomaterials and their biocompatibility: review and perspectives*, in *Biomaterials applications for nanomedicine*. 2011, InTech.
183. Bigi, A., B. Bracci, and S. Panzavolta, *Effect of added gelatin on the properties of calcium phosphate cement*. Biomaterials, 2004. **25**(14): p. 2893-2899.
184. Azami, M., et al., *A porous hydroxyapatite/gelatin nanocomposite scaffold for bone tissue repair: in vitro and in vivo evaluation*. Journal of Biomaterials Science, Polymer Edition, 2012. **23**(18): p. 2353-2368.

185. Brückner, T., et al., *Novel bone wax based on poly (ethylene glycol)–calcium phosphate cement mixtures*. *Acta biomaterialia*, 2016. **33**: p. 252-263.
186. Habraken, W., J. Wolke, and J. Jansen, *Ceramic composites as matrices and scaffolds for drug delivery in tissue engineering*. *Advanced drug delivery reviews*, 2007. **59**(4): p. 234-248.
187. Geffers, M., et al., *Dual-setting brushite–silica gel cements*. *Acta biomaterialia*, 2015. **11**: p. 467-476.
188. Krüger, R. and J. Groll, *Fiber reinforced calcium phosphate cements–On the way to degradable load bearing bone substitutes?* *Biomaterials*, 2012. **33**(25): p. 5887-5900.
189. Boehm, A.V., et al., *The Mechanical Properties of Biocompatible Apatite Bone Cement Reinforced with Chemically Activated Carbon Fibers*. *Materials*, 2018. **11**(2): p. 192.
190. Sousa, A., K. Souza, and E. Sousa, *Mesoporous silica/apatite nanocomposite: special synthesis route to control local drug delivery*. *Acta Biomaterialia*, 2008. **4**(3): p. 671-679.
191. Rödel, M., et al., *Tough and Elastic α -Tricalcium Phosphate Cement Composites with Degradable PEG-Based Cross-Linker*. *Materials*, 2019. **12**(1): p. 53.
192. Wang, J., et al., *Double-Network Interpenetrating Bone Cement via in situ Hybridization Protocol*. *Advanced Functional Materials*, 2010. **20**(22): p. 3997-4011.
193. Rödel, M., et al., *Highly flexible and degradable dual setting systems based on PEG-hydrogels and brushite cement*. *Acta Biomaterialia*, 2018(79): p. 182-201.
194. Dalton, P.D., et al., *Structure and Properties of Urea-Crosslinked Star Poly [(ethylene oxide)-ran-(propylene oxide)] Hydrogels*. *Macromolecular bioscience*, 2008. **8**(10): p. 923-931.
195. Matsumoto, A., et al., *Mechanisms of silk fibroin sol– gel transitions*. *The Journal of Physical Chemistry B*, 2006. **110**(43): p. 21630-21638.
196. Ahmed, E.M., *Hydrogel: Preparation, characterization, and applications: A review*. *Journal of advanced research*, 2015. **6**(2): p. 105-121.
197. Montheard, J.-P., M. Chatzopoulos, and D. Chappard, *2-hydroxyethyl methacrylate (HEMA): chemical properties and applications in biomedical fields*. *Journal of Macromolecular Science, Part C: Polymer Reviews*, 1992. **32**(1): p. 1-34.
198. Olszta, M.J., et al., *Bone structure and formation: a new perspective*. *Materials Science and Engineering: R: Reports*, 2007. **58**(3): p. 77-116.
199. Barinov, S. and V. Komlev, *Calcium phosphate bone cements*. *Inorganic Materials*, 2011. **47**(13): p. 1470-1485.
200. Ginebra, M.-P., et al., *New processing approaches in calcium phosphate cements and their applications in regenerative medicine*. *Acta biomaterialia*, 2010. **6**(8): p. 2863-2873.
201. Clapper, J.D., et al., *Development and characterization of photopolymerizable biodegradable materials from PEG–PLA–PEG block macromonomers*. *Polymer*, 2007. **48**(22): p. 6554-6564.
202. Hurle, K., et al., *Reaction kinetics of dual setting α -tricalcium phosphate cements*. *Journal of Materials Science: Materials in Medicine*, 2016. **27**(1): p. 1.

References

203. Wensch, S., et al., *In vivo mechanisms of hydroxyapatite ceramic degradation by osteoclasts: fine structural microscopy*. Journal of Biomedical Materials Research Part A: An Official Journal of The Society for Biomaterials, The Japanese Society for Biomaterials, and The Australian Society for Biomaterials and the Korean Society for Biomaterials, 2003. **67**(3): p. 713-718.
204. Browning, M., et al., *Determination of the in vivo degradation mechanism of PEGDA hydrogels*. Journal of Biomedical Materials Research Part A, 2014. **102**(12): p. 4244-4251.
205. Felsenberg, D., *Struktur und Funktion des Knochens: Stützwerk aus Kollagen und Hydroxylapatit*. Pharmazie in unserer Zeit, 2001. **30**(6): p. 488-494.
206. Tozzi, G., et al., *Composite hydrogels for bone regeneration*. Materials, 2016. **9**(4): p. 267.
207. Khan, Y., et al., *Tissue engineering of bone: material and matrix considerations*. JBJS, 2008. **90**(Supplement_1): p. 36-42.
208. Giannoudis, P.V., H. Dinopoulos, and E. Tsiridis, *Bone substitutes: an update*. Injury, 2005. **36**(3): p. S20-S27.
209. Kneser, U., et al., *Tissue engineering of bone: the reconstructive surgeon's point of view*. Journal of cellular and molecular medicine, 2006. **10**(1): p. 7-19.
210. Johnson, A.J.W. and B.A. Herschler, *A review of the mechanical behavior of CaP and CaP/polymer composites for applications in bone replacement and repair*. Acta biomaterialia, 2011. **7**(1): p. 16-30.
211. Christ, S., et al., *Fiber reinforcement during 3D printing*. Materials Letters, 2015. **139**: p. 165-168.
212. Zhang, Y. and H.H. Xu, *Effects of synergistic reinforcement and absorbable fiber strength on hydroxyapatite bone cement*. Journal of Biomedical Materials Research Part A, 2005. **75**(4): p. 832-840.
213. Dos Santos, L.A., et al., *Fiber reinforced calcium phosphate cement*. Artificial organs, 2000. **24**(3): p. 212-216.
214. Konsta-Gdoutos, M.S., Z.S. Metaxa, and S.P. Shah, *Highly dispersed carbon nanotube reinforced cement based materials*. Cement and Concrete Research, 2010. **40**(7): p. 1052-1059.
215. Konsta-Gdoutos, M.S., Z.S. Metaxa, and S.P. Shah, *Multi-scale mechanical and fracture characteristics and early-age strain capacity of high performance carbon nanotube/cement nanocomposites*. Cement and Concrete Composites, 2010. **32**(2): p. 110-115.
216. Neumann, M., *Synthese und Charakterisierung von Calciumcarbonat-Phasen und Calciumphosphat-basierter Knochenersatzmaterialien*. 2009, Universität Duisburg-Essen, Fakultät für Chemie» Anorganische Chemie.
217. Tamimi, F., et al., *Brushite–collagen composites for bone regeneration*. Acta biomaterialia, 2008. **4**(5): p. 1315-1321.
218. Linhart, W., et al., *Resorbierbare Kalziumphosphatzemente*. Trauma und Berufskrankheit, 2004. **6**(4): p. 277-284.
219. Roy, M., et al., *Mechanical property and in vitro biocompatibility of brushite cement modified by polyethylene glycol*. Materials Science and Engineering: C, 2012. **32**(8): p. 2145-2152.

220. Engstrand, J., C. Persson, and H. Engqvist, *Influence of polymer addition on the mechanical properties of a premixed calcium phosphate cement*. *Biomatter*, 2013. **3**(4): p. e27249.
221. Mirtchi, A.A., J. Lemaître, and E. Hunting, *Calcium phosphate cements: action of setting regulators on the properties of the β -tricalcium phosphate-monocalcium phosphate cements*. *Biomaterials*, 1989. **10**(9): p. 634-638.
222. Matyjaszewski, K. and T.P. Davis, *Handbook of radical polymerization*. 2003: John Wiley & Sons.
223. Wang, J., et al., *Fabrication of injectable high strength hydrogel based on 4-arm star PEG for cartilage tissue engineering*. *Biomaterials*, 2017. **120**: p. 11-21.
224. Peppas, N.A., et al., *Poly (ethylene glycol)-containing hydrogels in drug delivery*. *Journal of controlled release*, 1999. **62**(1): p. 81-87.
225. Harris, J.M., *Poly (ethylene glycol) chemistry: biotechnical and biomedical applications*. 2013: Springer Science & Business Media.
226. Seliktar, D., *Designing cell-compatible hydrogels for biomedical applications*. *Science*, 2012. **336**(6085): p. 1124-1128.
227. Leenslag, J.W., et al., *Resorbable materials of poly (L-lactide): VII. In vivo and in vitro degradation*. *Biomaterials*, 1987. **8**(4): p. 311-314.
228. Hofmann, M.P., et al., *FTIR-monitoring of a fast setting brushite bone cement: effect of intermediate phases*. *Journal of Materials Chemistry*, 2006. **16**(31): p. 3199-3206.
229. Kanter, B., et al., *Control of in vivo mineral bone cement degradation*. *Acta biomaterialia*, 2014. **10**(7): p. 3279-3287.
230. Giocondi, J.L., et al., *Molecular mechanisms of crystallization impacting calcium phosphate cements*. *Philosophical Transactions of the Royal Society of London A: Mathematical, Physical and Engineering Sciences*, 2010. **368**(1917): p. 1937-1961.
231. Eriksson, R., T. Albrektsson, and B. Magnusson, *Assessment of bone viability after heat trauma: a histological, histochemical and vital microscopic study in the rabbit*. *Scandinavian journal of plastic and reconstructive surgery*, 1984. **18**(3): p. 261-268.
232. Deramond, H., N. Wright, and S. Belkoff, *Temperature elevation caused by bone cement polymerization during vertebroplasty*. *Bone*, 1999. **25**(2): p. 17S-21S.
233. Zhao, X., et al., *Reactive calcium-phosphate-containing poly (ester-co-ether) methacrylate bone adhesives: Chemical, mechanical and biological considerations*. *Acta biomaterialia*, 2010. **6**(3): p. 845-855.
234. Abou Neel, E.A., et al., *Viscoelastic and biological performance of low-modulus, reactive calcium phosphate-filled, degradable, polymeric bone adhesives*. *Acta Biomaterialia*, 2012. **8**(1): p. 313-320.
235. Engstrand, J., C. Persson, and H. Engqvist, *The effect of composition on mechanical properties of brushite cements*. *Journal of the mechanical behavior of biomedical materials*, 2014. **29**: p. 81-90.
236. Sheikh, Z., et al., *In vitro degradation and in vivo resorption of dicalcium phosphate cement based grafts*. *Acta biomaterialia*, 2015. **26**: p. 338-346.
237. Xu, H.H., et al., *Strong and macroporous calcium phosphate cement: effects of porosity and fiber reinforcement on mechanical properties*. *Journal of Biomedical Materials Research: An Official Journal of The Society for Biomaterials, The Japanese Society for Biomaterials, and The Australian*

References

- Society for Biomaterials and the Korean Society for Biomaterials, 2001. **57**(3): p. 457-466.
238. Lin-Gibson, S., et al., *Synthesis and characterization of PEG dimethacrylates and their hydrogels*. *Biomacromolecules*, 2004. **5**(4): p. 1280-1287.
239. Roberts, J.J. and S.J. Bryant, *Comparison of photopolymerizable thiol-ene PEG and acrylate-based PEG hydrogels for cartilage development*. *Biomaterials*, 2013. **34**(38): p. 9969-9979.
240. Luo, J., et al., *In Situ Synchrotron X-ray Diffraction Analysis of the Setting Process of Brushite Cement: Reaction and Crystal Growth*. *ACS applied materials & interfaces*, 2017. **9**(41): p. 36392-36399.
241. Killion, J.A., et al., *Compressive strength and bioactivity properties of photopolymerizable hybrid composite hydrogels for bone tissue engineering*. *International Journal of Polymeric Materials and Polymeric Biomaterials*, 2014. **63**(13): p. 641-650.
242. Wistlich, L., et al., *A bone glue with sustained adhesion under wet conditions*. *Advanced healthcare materials*, 2017. **6**(3).
243. Lu, M. and E.N. Hansen, *Hydrogen peroxide wound irrigation in orthopaedic surgery*. *Journal of bone and joint infection*, 2017. **2**(1): p. 3.
244. Rutala, W.A. and D.J. Weber, *Guideline for disinfection and sterilization in healthcare facilities, 2008*. 2008.
245. Flory, P.J., *Principles of polymer chemistry*. 1953: Cornell University Press.
246. Metters, A., K. Anseth, and C. Bowman, *Fundamental studies of a novel, biodegradable PEG-b-PLA hydrogel*. *Polymer*, 2000. **41**(11): p. 3993-4004.
247. Theiss, F., et al., *Biocompatibility and resorption of a brushite calcium phosphate cement*. *Biomaterials*, 2005. **26**(21): p. 4383-4394.
248. Grover, L., et al., *In vitro ageing of brushite calcium phosphate cement*. *Biomaterials*, 2003. **24**(23): p. 4133-4141.
249. Bohner, M., et al., *Compositional changes of a dicalcium phosphate dihydrate cement after implantation in sheep*. *Biomaterials*, 2003. **24**(20): p. 3463-3474.
250. Flautre, B., et al., *Influence of polymeric additives on the biological properties of brushite cements: an experimental study in rabbit*. *Journal of Biomedical Materials Research Part A: An Official Journal of The Society for Biomaterials, The Japanese Society for Biomaterials, and The Australian Society for Biomaterials and the Korean Society for Biomaterials*, 2003. **66**(2): p. 214-223.
251. Suzuki, O., *Octacalcium phosphate (OCP)-based bone substitute materials*. *Japanese Dental Science Review*, 2013. **49**(2): p. 58-71.
252. Mirtchi, A.A., J. Lemaitre, and N. Terao, *Calcium phosphate cements: Study of the β -tricalcium phosphate-monocalcium phosphate system*. *Biomaterials*, 1989. **10**(7): p. 475-480.
253. Cama, G., et al., *A novel method of forming micro-and macroporous monetite cements*. *Journal of Materials Chemistry B*, 2013. **1**(7): p. 958-969.
254. Voigt, R. and A. Fahr, *Pharmazeutische Technologie*. Vol. 11. 2010: Deutscher Apotheker Verlag Stuttgart. 768.
255. Speer, D.P., et al., *Biological effects of residual glutaraldehyde in glutaraldehyde-tanned collagen biomaterials*. *Journal of biomedical materials research*, 1980. **14**(6): p. 753-764.

256. Bigi, A., S. Panzavolta, and K. Rubini, *Setting mechanism of a biomimetic bone cement*. Chemistry of materials, 2004. **16**(19): p. 3740-3745.
257. Bigi, A., et al., *A biomimetic gelatin-calcium phosphate bone cement*. The International journal of artificial organs, 2004. **27**(8): p. 664-673.
258. Bigi, A., et al., *Alpha-tricalcium phosphate-gelatin composite cements*. Journal of Applied Biomaterials and Biomechanics, 2004. **2**(2): p. 81-87.
259. Kim, H.W., J.C. Knowles, and H.E. Kim, *Hydroxyapatite and gelatin composite foams processed via novel freeze-drying and crosslinking for use as temporary hard tissue scaffolds*. Journal of Biomedical Materials Research Part A: An Official Journal of The Society for Biomaterials, The Japanese Society for Biomaterials, and The Australian Society for Biomaterials and the Korean Society for Biomaterials, 2005. **72**(2): p. 136-145.
260. Mi, F.L., S.S. Shyu, and C.K. Peng, *Characterization of ring-opening polymerization of genipin and pH-dependent cross-linking reactions between chitosan and genipin*. Journal of Polymer Science Part A: Polymer Chemistry, 2005. **43**(10): p. 1985-2000.
261. Paik, Y.-S., et al., *Physical stability of the blue pigments formed from geniposide of gardenia fruits: effects of pH, temperature, and light*. Journal of agricultural and food chemistry, 2001. **49**(1): p. 430-432.
262. Kong, J. and S. Yu, *Fourier transform infrared spectroscopic analysis of protein secondary structures*. Acta biochimica et biophysica Sinica, 2007. **39**(8): p. 549-559.
263. Teti, G., et al., *Morphological evaluation of adhesion and proliferation of osteoblast like cells grown on gelatin/genipin scaffold*. Journal of Life Sciences, 2013. **7**(9): p. 965.
264. Giesche, H., *Mercury porosimetry: a general (practical) overview*. Particle & particle systems characterization, 2006. **23**(1): p. 9-19.
265. Perez, R.A., et al., *Porous hydroxyapatite and gelatin/hydroxyapatite microspheres obtained by calcium phosphate cement emulsion*. Journal of Biomedical Materials Research Part B: Applied Biomaterials, 2011. **97**(1): p. 156-166.
266. Habraken, W., et al., *Introduction of gelatin microspheres into an injectable calcium phosphate cement*. Journal of Biomedical Materials Research Part A: An Official Journal of The Society for Biomaterials, The Japanese Society for Biomaterials, and The Australian Society for Biomaterials and the Korean Society for Biomaterials, 2008. **87**(3): p. 643-655.
267. Yin, Y., et al., *Gelatin manipulation of latent macropores formation in brushite cement*. Journal of Materials Science: Materials in Medicine, 2003. **14**(3): p. 255-261.
268. Butler, M.F., Y.F. Ng, and P.D. Pudney, *Mechanism and kinetics of the crosslinking reaction between biopolymers containing primary amine groups and genipin*. Journal of Polymer Science Part A: Polymer Chemistry, 2003. **41**(24): p. 3941-3953.
269. Nickerson, M., et al., *Some physical and microstructural properties of genipin-crosslinked gelatin-maltodextrin hydrogels*. International journal of biological macromolecules, 2006. **38**(1): p. 40-44.
270. Rose, J.B., et al., *Gelatin-based materials in ocular tissue engineering*. Materials, 2014. **7**(4): p. 3106-3135.

References

271. Cama, G., et al., *Structural changes and biological responsiveness of an injectable and mouldable monetite bone graft generated by a facile synthetic method*. Journal of The Royal Society Interface, 2014. **11**(101): p. 20140727.
272. Rahbani, J., et al., *Characterization of internal structure of hydrated agar and gelatin matrices by cryo-SEM*. Electrophoresis, 2013. **34**(3): p. 405-408.
273. Van Vlierberghe, S., et al., *Correlation between cryogenic parameters and physico-chemical properties of porous gelatin cryogels*. Journal of Biomaterials Science, Polymer Edition, 2009. **20**(10): p. 1417-1438.
274. Armstrong, D.W., K.L. Rundlett, and J.R. Chen, *Evaluation of the macrocyclic antibiotic vancomycin as a chiral selector for capillary electrophoresis*. Chirality, 1994. **6**(6): p. 496-509.
275. Reynolds, P.E., *Structure, biochemistry and mechanism of action of glycopeptide antibiotics*. European Journal of Clinical Microbiology and Infectious Diseases, 1989. **8**(11): p. 943-950.
276. Walsh, C., *Opinion-anti-infectives: Where will new antibiotics come from?* Nature Reviews Microbiology, 2003. **1**(1): p. 65.
277. Unissa, A.N. and L.E. Hanna, *Molecular mechanisms of action, resistance, detection to the first-line anti tuberculosis drugs: Rifampicin and pyrazinamide in the post whole genome sequencing era*. Tuberculosis, 2017. **105**: p. 96-107.
278. Maderuelo, C., A. Zarzuelo, and J.M. Lanao, *Critical factors in the release of drugs from sustained release hydrophilic matrices*. Journal of Controlled Release, 2011. **154**(1): p. 2-19.
279. Talukdar, M.M., et al., *Comparative study on xanthan gum and hydroxypropylmethyl cellulose as matrices for controlled-release drug delivery I. Compaction and in vitro drug release behaviour*. International journal of pharmaceutics, 1996. **129**(1-2): p. 233-241.
280. Higuchi, T., *Mechanism of sustained-action medication. Theoretical analysis of rate of release of solid drugs dispersed in solid matrices*. Journal of pharmaceutical sciences, 1963. **52**(12): p. 1145-1149.
281. Singhvi, G. and M. Singh, *In-vitro drug release characterization models*. Int J Pharm Stud Res, 2011. **2**(1): p. 77-84.
282. Dash, S., et al., *Kinetic modeling on drug release from controlled drug delivery systems*. Acta Pol Pharm, 2010. **67**(3): p. 217-23.
283. Hofmann, M., et al., *High-strength resorbable brushite bone cement with controlled drug-releasing capabilities*. Acta biomaterialia, 2009. **5**(1): p. 43-49.
284. Espanol, M., et al., *Intrinsic porosity of calcium phosphate cements and its significance for drug delivery and tissue engineering applications*. Acta Biomaterialia, 2009. **5**(7): p. 2752-2762.
285. Zhou, J., et al., *The controlled release of vancomycin in gelatin/ β -TCP composite scaffolds*. Journal of biomedical materials research Part A, 2012. **100**(9): p. 2295-2301.
286. Young, S., et al., *Gelatin as a delivery vehicle for the controlled release of bioactive molecules*. Journal of controlled release, 2005. **109**(1-3): p. 256-274.
287. Yaylaoğlu, M., et al., *Development of a calcium phosphate-gelatin composite as a bone substitute and its use in drug release*. Biomaterials, 1999. **20**(8): p. 711-719.

288. Li, M., et al., *Calcium phosphate cement with BMP-2-loaded gelatin microspheres enhances bone healing in osteoporosis: a pilot study*. Clinical Orthopaedics and Related Research®, 2010. **468**(7): p. 1978-1985.
289. Ruoslahti, E., *RGD and other recognition sequences for integrins*. Annual review of cell and developmental biology, 1996. **12**(1): p. 697-715.
290. Yeo, Y., et al., *Photocrosslinkable hydrogel for myocyte cell culture and injection*. Journal of Biomedical Materials Research Part B: Applied Biomaterials: An Official Journal of The Society for Biomaterials, The Japanese Society for Biomaterials, and The Australian Society for Biomaterials and the Korean Society for Biomaterials, 2007. **81**(2): p. 312-322.
291. Perez, R.A., H.-W. Kim, and M.-P. Ginebra, *Polymeric additives to enhance the functional properties of calcium phosphate cements*. Journal of tissue engineering, 2012. **3**(1): p. 2041731412439555.
292. Mickiewicz, R.A., A.M. Mayes, and D. Knaack, *Polymer-calcium phosphate cement composites for bone substitutes*. Journal of Biomedical Materials Research: An Official Journal of The Society for Biomaterials, The Japanese Society for Biomaterials, and The Australian Society for Biomaterials and the Korean Society for Biomaterials, 2002. **61**(4): p. 581-592.
293. Klee, D. and H. Höcker, *Polymers for biomedical applications: improvement of the interface compatibility*, in *Biomedical Applications Polymer Blends*. 2000, Springer. p. 1-57.
294. Gbureck, U., et al., *Resorbable dicalcium phosphate bone substitutes prepared by 3D powder printing*. Advanced Functional Materials, 2007. **17**(18): p. 3940-3945.
295. Klammert, U., et al., *Cytocompatibility of brushite and monetite cell culture scaffolds made by three-dimensional powder printing*. Acta Biomaterialia, 2009. **5**(2): p. 727-734.
296. Mills, D.K., *The Role of Polymer Additives in Enhancing the Response of Calcium Phosphate Cement*, in *Orthopedic Biomaterials*. 2018, Springer. p. 345-379.
297. Kolambkar, Y.M., et al., *An alginate-based hybrid system for growth factor delivery in the functional repair of large bone defects*. Biomaterials, 2011. **32**(1): p. 65-74.
298. Rödel, M., et al., *Simultaneous structuring and mineralization of silk fibroin scaffolds*. Journal of tissue engineering, 2018. **9**: p. 1-16.
299. Christel, T., et al., *Chelate bonding mechanism in a novel magnesium phosphate bone cement*. Journal of the American Ceramic Society, 2015. **98**(3): p. 694-697.
300. Mestres, G. and M.-P. Ginebra, *Novel magnesium phosphate cements with high early strength and antibacterial properties*. Acta biomaterialia, 2011. **7**(4): p. 1853-1861.
301. Sawhney, A.S., C.P. Pathak, and J.A. Hubbell, *Bioerodible hydrogels based on photopolymerized poly (ethylene glycol)-co-poly (α -hydroxy acid) diacrylate macromers*. Macromolecules, 1993. **26**(4): p. 581-587.
302. Marie, A., F. Fournier, and J. Tabet, *Characterization of synthetic polymers by MALDI-TOF/MS: Investigation into new methods of sample target preparation and consequence on mass spectrum finger print*. Analytical chemistry, 2000. **72**(20): p. 5106-5114.

References

303. Abbadessa, A., et al., *A synthetic thermo-sensitive hydrogel for cartilage bioprinting and its biofunctionalization with polysaccharides*. *Biomacromolecules*, 2016.
304. de Jesús Valle, M.J., F.G. López, and A.S. Navarro, *Development and validation of an HPLC method for vancomycin and its application to a pharmacokinetic study*. *Journal of pharmaceutical and biomedical analysis*, 2008. **48**(3): p. 835-839.
305. Panchagnula, R., et al., *Determination of rifampicin and its main metabolite in plasma and urine in presence of pyrazinamide and isoniazid by HPLC method*. *Journal of pharmaceutical and biomedical analysis*, 1999. **18**(6): p. 1013-1020.

Acknowledgements / Danksagung

Zunächst möchte ich mich bei Prof. Dr. Jürgen Groll bedanken, der mir die Arbeit an seinem Lehrstuhl sowie die Teilnahme an Konferenzen ermöglicht hat. Vielen Dank für die Betreuung und die Gespräche während meiner Dissertation, die immer wieder Anstoß für einen neuen Blickwinkel gaben.

Ein besonderer Dank gilt meinen zwei Betreuern Prof. Dr. Uwe Gbureck sowie Dr. Jörg Teßmar. Beide hatten immer eine offene Tür und haben mich bei Fragestellungen jeglicher Art tatkräftig unterstützt. Dennoch hatte ich auch Freiraum, um eigene Strategien und Ideen auszuprobieren. Neben fachlichen Diskussionen haben wir aber auch über Geschichten eurer Kids oder alte FMZ-Stories vor meiner Zeit geplaudert. Nicht zu vergessen, die stete Hilfe von Jörg bei HPLC-, Computer- oder sonstigen Wehwehchen sowie die legendären Sommerpartys im Hause Gbureck.

Der Deutschen Forschungsgemeinschaft (DFG; GR 3232/3-1 und GB 1/20-1) danke ich für die Finanzierung meiner Forschungsprojekte und damit die Realisierung meiner Promotion. Zudem wurde durch das Projekt INST 1522/58-1 FUGG die Anschaffung des Rasterelektronenmikroskops an unserem Lehrstuhl und somit die Erstellung der in meiner Arbeit gezeigten Aufnahmen ermöglicht.

Im Zuge dessen möchte ich auch Judith Friedlein, Dr. Claus Moseke und vor allem Philipp Stahlhut meinen herzlichsten Dank aussprechen. Philipp, deine Geduld in der Einarbeitung am Gerät sowie dein unermüdlicher Einsatz, Cryo-Prozesse zu optimieren und stets das Beste aus einem Bild heraus zu holen, haben eine Zusammenarbeit sehr angenehm gemacht. Außerdem habe ich mich in eurem Büro und deinem „zweiten Wohnzimmer“ immer sehr wohl gefühlt.

Für die Hilfestellung bei biologischen Testungen danke ich meiner Bio-Post-Doc Dr. Tatjana Schilling sowie Dr. Andrea Ewald und Simone Werner.

Weiterhin wäre sämtliche Organisation wie Bestellungen und terminliche Koordination von Besprechungen durch Tanja Dambach und Birgit Langner-Bischof unmöglich gewesen. Hierfür vielen Dank!

Harald Hümpfer und Anton „Toni“ Hofmann ergeht ein besonderer Dank für die Rettung in verschiedensten Lebenslagen – sei es bei Herausforderungen mit dem Servicezentrum Medizin-Informatik (SMI), Anfertigung von eigens konzipierten Messgeometrien im Express-Verfahren oder kompetenter Hilfe bei platten Fahrradreifen. Auf euch beide ist wirklich immer Verlass!

Ebenso ein Plätzchen auf den letzten Seiten möchte ich Isabell Biermann widmen. Sie trägt schon seit geraumer Zeit den Titel der „guten Seele des Anorganik-Labors“ und so manche Messung und Bestellung wäre ohne ihre Hilfe und Unterstützung nicht möglich gewesen. Sie kümmert sich nicht nur um Sauberkeit und Ordnung im Labor, sondern steht auch immer mit Rat und Tat an der statischen Prüfmaschine zur Seite und plaudert öfters aus dem Nähkästchen.

Weiterhin möchte ich mich bei den ehemaligen „Zementies“ für die liebevolle Aufnahme in die Subgroup bedanken. Hier sind vor allem die Damen Dr. Theresa Brückner und Dr. Susanne Meininger zu nennen, von denen ich so einiges über Calciumphosphatzemente lernen konnte und die mit meinen Fragen zu mechanischer Testung und Berechnung diverser Messgrößen stets geduldig waren.

Was wäre die Zeit am FMZ ohne die ehemalige Kitchen Crew und jetzigen FMZ Oldies gewesen. Besonderer Dank geht an meine Freundinnen Julia Blöhbaum, Dr. Theresa Brückner, Dr. Susanne Feineis, Dr. Ana Sancho, Dr. Simone Schäfer, Good Cop Dr. Susanne Meininger und meine Apotheker-Kollegin Dr. Laura Wistlich. Wir haben so viel zusammen erlebt, dass es hier Seiten füllen würde – vom Weinfest in Homburg über den Kochabend in Kürnach bis hin zum legendären H*****-Treffen am Graf-Luckner-Weiher.

Meinen Genossen der Gruppe #2014, Willi Smolan und Julia Blöhbaum, möchte ich meinen ganz besonderen Dank für die Jahre am FMZ aussprechen. Wir haben so einiges miteinander durchgemacht, gelacht, erörtert, diskutiert und kulinarisch erprobt. Jeder braucht seine Homies während der Doktorarbeit – und ihr ward meine. It's over.

Was wäre das Leben ohne Musik – hier danke ich meinen Musikerkolleginnen und Kollegen der Blaskapelle Eisingen. Vielen Dank für die Aufnahme in euren Reihen

und die schöne gemeinsame Zeit auf Proben und Auftritten, die mich von so mancher Herausforderung meiner Doktorarbeit abgelenkt haben. Besonders möchte ich meine liebgewonnene Freundin Simone Becker erwähnen, die immer ein offenes Ohr für sämtliche Anliegen hat und stets eine Lösung parat hält. Außerdem danke ich meinen Saxophon-Buddies Carmen Bayer und Fritz Kiesel, ohne die jede Probe nur halb so lustig ist.

Meinen Eltern Waltraud und Willy Rödel sowie meiner allerliebsten Schwester Christina gebührt das größte und herzlichste Dankeschön – was wäre ich ohne euch und eure Hilfe und Unterstützung in sämtlichen Lebenslagen. Danke für alles, Mama, Papa und Tina!

Everything happens for a reason.